Developments In Iron Ore Sintering Using A Laboratory Scaled Development Platform

Prifysgol Abertawe
Swansea University

Tariq Al-Haji

Department of Engineering
Swansea University

This Thesis is submitted for the degree of
Engineering Doctorate

Tariq Al-Haji

March 2022

DECLARATIONS

This work has not previously been accepted in substance for any degree and is not being currently submitted in candidature for any degree.

Signed .....T. Al-Haji..... (candidate)

Dated .....31/03/2022.....

This thesis is the result of my own investigations, except where otherwise stated. Other sources are acknowledged by footnotes giving explicit references. A bibliography is appended.

Signed .....T. Al-Haji..... (candidate)

Dated .....31/03/2022.....

I hereby give consent for my thesis, if accepted, to be available for photocopying and for inter-library loan, and for the title and summary to be made available to outside organisations.

Signed .....T. Al-Haji..... (candidate)

Dated .....31/03/2022.....

The University's ethical procedures have been followed and, where appropriate, that ethical approval has been granted.

Signed .....T. Al-Haji..... (candidate)

Dated .....31/03.2022.....

Abstract

Iron ore sintering is the pre-treatment process of agglomerating fine grained iron ores into a coarse grained solid porous burden, suitable for the blast furnace. Iron ore sinter is the primary source of a blast furnace's burden and as such plays a critical role in the steel making process. A small-scale pilot line sinter pot was commissioned and validated for the proposed research. Findings suggested that altering blend chemical composition, granulation properties, bed permeability and flame front characteristics were the most important parameters in optimising the process. Research conducted in this paper suggested that varying these parameters impacted the iron ore sintering process and quality of the sinter produced. Thus, this work package focused on how these parameters could be varied in order to maximise productivity and quality. The work package also focused on various fuel particle size distributions as well as ratios and found that this also plays a critical role in influencing process parameters as well as the quality of sinter produced. It was found that by controlling the particle size of fuel, process stability increased. This paper also focused on novel additions to a sintering blend, which could be up-scaled and implemented to industry, ensuring the iron and steel making industry is heading towards a more circular economy. It was found that by micro-pelletizing fine iron ores, permeability was increased and thus productivity improved. It was also found that the chemical composition of by-products such as used Mag-C refractory brick used in lining vessels at the BOS plant could be utilised by crushing and incorporating into raw sinter blends, offsetting purchased materials. Quality parameters of the produced sinter during investigations included sinter strength, reducibility, chemical composition, optical microscopy and phase mineralogy. Process parameters such as sintering time, temperature, flow rates, cooling rates and flame front characteristics were also monitored through out to make precise and accurate conclusions.

Acknowledgements

I would like to acknowledge and thank the following institutions and people for supporting both myself and the work package outlined within this thesis. The research conducted would not be possible without the support from Tata Steel Europe, Swansea University and M2A. A distinctive thank you goes to my academic supervisor Professor Cameron Pleydell-Pearce and my industrial supervisor Dr Peter Barnes for their ongoing support. Thank you to Dr Kevyn Bevan, Dr Chris Melvin and Ryan Davies for their technical support. Finally, immense appreciation and a special thank you to my family and partner for their continuous personal support throughout this project.

List of Figures

List of Tables

Contents

1 Introduction

This thesis and associated research project aims to provide novel solutions to the problem of sustainability within the production process of iron ore sintering. Sintering provides a process to widen the menu of possible raw materials to include fines, concentrates and gives the ability to recycle by-products. In the past, sintering was a minor process to enhance usage of low quality material but now sintering has grown into the primary means of preparing a quality and cost optimised raw materials feed. The aims of this project is to commission and validate a pilot line sintering facility in which novel research can be conducted on. The testing rig would be one of its kind and the only operational pilot line sintering facility in the United Kingdom. The planned outcome of this project is to help move the sintering process to a more circular economy by developing alternative sinter blend parameters and compositions that sit with Tata Steel's desire to reduce its environmental impact without compromising its production quality.

This thesis must address several case studies that are specific to the project to provide a desired outcome. The aim of this project was to validate a pilot scale sintering rig to elucidate the mechanisms of sintering and to understand to what extent how representative it is of the production plant. The platform was then used to demonstrate capability for making actual production decisions with the following case studies:

1. What are the areas identified through literature in which there is space for further research within the sintering process?
2. How does the particle size distribution, and varying ratios of anthracite to coke breeze influence the iron ore sintering process?
3. Can the sintering process and quality output be sustained at current levels through the inclusion of more environmentally sustainable additions?
4. Through what means is it possible to increase sintering productivity without negatively impacting the process or output quality?

1.1 Background

Port Talbot Steelworks is an integrated iron and steel production plant located on the coast of South Wales in Neath Port Talbot and is currently owned and operated by Tata Steel

Europe. This steelworks is one of two significant sites within the United Kingdom. It is one of the largest in Europe, directly employing over 4,000 people and capable of producing nearly 5 million tonnes of steel slab per year. Raw materials can not be added straight to a blast furnace due to the nature if its particle size and chemistry. Instead, it is sintered together at a sinter plant first. Iron ore sintering is an essential, pre-treatment process of agglomerating fine grained, raw iron ore material into a coarse grained burden suitable for blast furnace operations. A sinter plant is capable of producing up to 600 tonnes of sinter per hour and is a 24 hour operation. Over 70% of the furnace's burden is comprised of sinter. Thus, blast furnace operations and productivity rely heavily on the quality and production of iron ore sinter. Therefor, optimising the sintering process and quality of sinter is of utmost importance when trying to achieve a more sustainable future within the iron and steel industry.

1.2 Problem

Even though the sintering iron ore is a critical part of the steel making process, a sinter Plant is built to be the dustbin of a Steelworks. Sinter Plants are there to reprocess Steel making wastes, reducing environmental impacts of the steel industry through avoidance of landfill and storage of waste and hazardous materials. Due to this, a sinter plant can be the most polluting of the iron and steel making processes. Thus, optimisation of the process will aid the sinter plant's ability to use more by-products and support circular economy. It is vital to ensure sinter of good quality, in substantial amounts, to a blast furnace which meet a specific criteria that comprises of strict chemical composition, strength and reduciblility. Iron ore sinter which fails to meet the strict criteria and quality indices to that of the blast furnace's requirements can have catastrophic and costly consequences, especially as the blast furnace is currently the most efficient and productive methods of producing virgin iron. Poor sinter could influence the structural integrity of a blast furnace and also the quality of steel produced further down the production line. Producing poor sinter in itself has negative environmental impacts. Main environmental concern is the carbon footprint and poor sinter quality can result in the blast furnace needing to consume more fuel. The demand to ensure sinter specification as well as keeping to strict environmental regulations can lead to difficulties within the sintering process. Another occurring aspect which causes difficulties within the sinter plant is that the raw material market is constantly changing. Thus, not only optimising the sintering process but optimising the materials going into the sinter plant can also play an important key role in maintaining productivity without

increasing environmental impacts. The thermodynamic and kinetic concepts of flame front characteristics within the sinter bed during the process fundamentally drives the process reactions and can directly impact the sintering process and quality of the sinter produced. A clear understanding of flame front characteristics within the sintering process when altering operating parameters as well as input material will deepen our understanding and help tackle the demands a sinter plant can be faced with. This optimisation of iron ore sintering should be accomplished in order to further support and reach a more sustainable circular economy within the iron and steel industry.

1.3 Aims and Scope

The scope of this project is to commission and validate a pilot line sinter furnace known as a 'sinter pot'. Once commissioned, the small scale sinter furnace would be deployed to investigate several research avenues of the iron sintering process without impeding production at the sinter plant. This will be achieved through interpretation of the data collected via close control of blend composition, process parameters and the analysis of the sintered product. The pilot line sinter furnace would be deployed with aims to:

- Understand the process parameters and limitations of the sinter pot and how closely it mimics the macro process.
- Investigate how the particle size distribution and ratios of using different fuels such as anthracite coal and coke breeze can influence the sintering process and quality of sinter.
- Investigate how micro-pellets can be utilised to increase productivity without introducing any negative impacts.
- Investigate novel additions to a sintering blend, with aims of directing the research towards a more sustainable circular economy iron and steel making industry.

2 Literature review

This section aims to give a brief overview of the iron ore sintering process as well as identifying promising literature that revolves around iron ore sintering optimisation, especially where pilot line sinter pots are deployed for the investigation. This section also aims to identify promising literature which can be built on further or that require further investigations to build on various concepts.

2.1 Iron Steel making

At the very first instance, raw materials such as iron ores must be mined from the ground. Once mined, careful control of the materials must be taken. This includes carefully monitoring chemical composition, particle size distribution and moisture. The raw materials, being a selection of iron ores, coke breeze and limestone are all layered into potential blends. By-products known as reverts are also introduced to the blend at this point. Reverts are by-products of the iron and steel making process that have a percentage of iron in that can be recycled. [1] The blends are then mixed and granulated in a granulation drum, where careful control of the moisture level is taken. [2] The mixture is then sintered at a sinter plant to produce a porous iron rich sponge, which is an ideal burden for charging the blast furnace. The sintered product is then transported to the top of the blast furnace, along with iron ore pellets, coke and limestone. The raw mixture is met by a blast of hot air coming in from the bottom. A reduction reaction takes place and molten iron can be collected from the bottom. [3] This molten iron is then transported on to make steel, via the basic oxygen steel making process. Within the basic oxygen furnace, the molten iron is combined with varying amounts of scrap steel, an injection is introduced to the vessel and 99% pure oxygen is blown into it, causing temperatures to increase to 1700°C resulting in oxidation of the impurities and the carbon content decreasing by 90% to produce liquid steel. The liquid steel is then refined by secondary steel-making processes depending on the grade of steel required. The liquid steel is then moved on to a continuous casting process. The molten steel is transported via ladle and is lifted by crane on to a rotating turret. Steel flows out of the ladle at a controlled rate into a water-cooled casting machine where the it is met with several rollers and waters sprays which results in solid steel slab. [4]

2.2 Iron ore sintering procedure

Raw materials can be broken down into iron ores, fuel and fluxes. Prior to sintering, the fine raw materials are layered into blends in a blending yard and then transported to a granulation drum. In the granulation drum, moisture is added to promote agglomeration in granulation. The blend is granulated to increase bed permeability. [2] Once granulated, the mixture is dropped onto several conveyor belts and transported to a roll feeder where it is deposited onto a travelling grate known as the strand. The roll feeder is there to provide even distribution of the blend onto the grate/strand, ensuring a specific bed height. A layer of sinter, which is known as the hearth layer, is layered on the bottom of the strand before the blend falls on to it. This is to prevent the sinter mix being fused to the steel grate during sintering. A strand can vary in size but are generally 100m in length, 4m wide and 1m deep. Most sinter plants have the capacity to produce 500 tonne of sinter every hour, however, blast furnace operations usually dictate how much sinter is needed to be produced. The initial part of the strand is covered with an ignition hood. As the grate moves and the blend passes underneath the hood, the combination of the fuel enriched blend and the burners from the hood ignites the top of the blend, starting the sintering process. As the blend is ignited, a number of wind mains positioned underneath the strand create a suction, drawing air through the mixture along the strand. This allows the combusting top layer of the blend, known as the flame front, to be pulled downwards. Once the flame front has reached the bottom of the blend, the flame front is diminished through the hearth layer into a gas and exited via the wind main. Sinter plant operators will try and ensure the flame front will get to the bottom of the blend by the time it reaches the end of the strand. This is to maximise efficiency, production and reduce environmental impact. At the end of the strand, once the flamefront has passed the hearth layer and sintering has finished, the sinter is dropped a number of meters and crushed into smaller pieces. The sinter is then screened and left to cool. Sinter produced that is screened to less than 5 mm in size is categorised as return fines that are returned to the beginning of process to be recycled. The rest of the sinter is classed as product sinter and is sent to the blast furnace. [5]

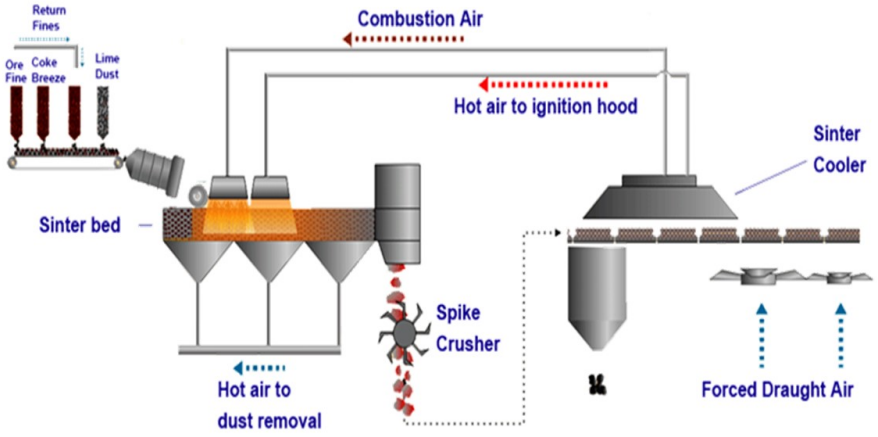

Figure 1: Sintering plant process flow diagram [6]

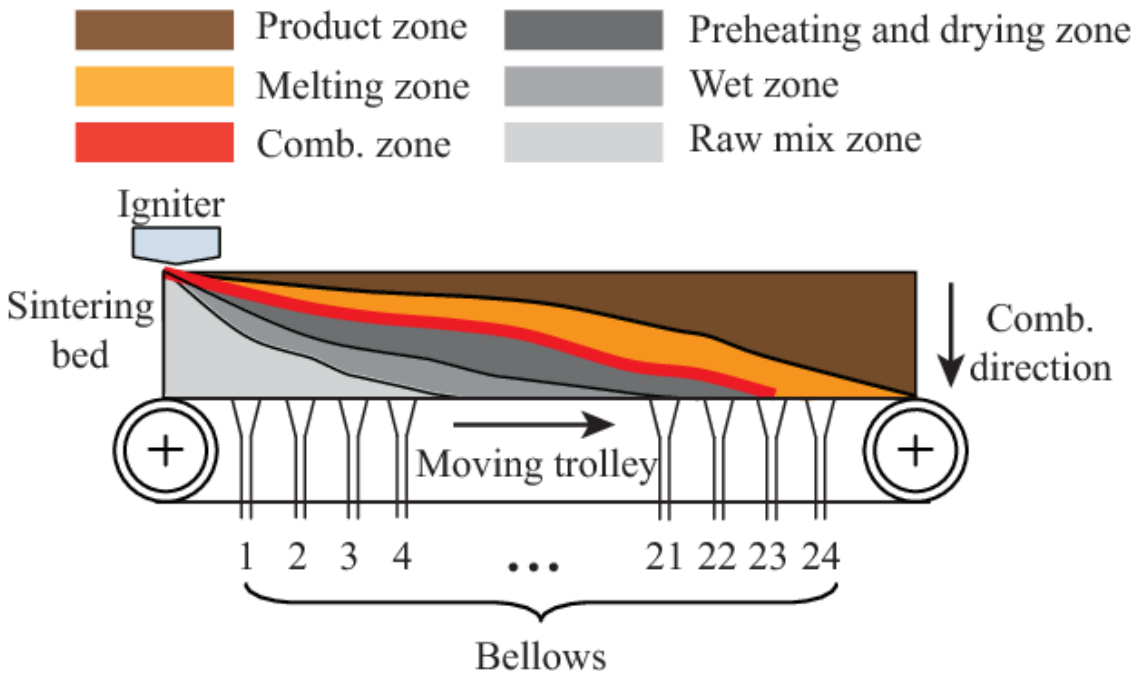

Figure 2: Sintering longitudinal cross section of sinter strand [7]

The final product is an iron rich, porous burden, tailored in properties to maximise efficiency and productivity for blast furnace operations. Sintering is necessary to convert fine raw materials into a semi molten mass that solidifies into porous pieces with the size

and strength characteristics desired by the blast furnace. Iron ore sintering therefor improves the permeability of the burden being put into the blast furnace, promoting the reduction process. High quality sinter has high reducability that can allow the intensity of the blast furnace operation to be reduced, as well as reduces the amount of coke demand, in turn making the blast furnace more productive and cost efficient. The sinter plant is also an effective way to utilise waste products and recycled material giving it key environmental advantages over other parts of the steel making process.

2.3 Raw materials

Raw materials include iron ores, fluxes and fuel. The individual constituents vary across steel making plants but the fundamental aim is always the same. All material needs to be within a specific chemical composition and all input material needs to be within a specific particle size and distribution region. [2] Iron ores can include concentrate, and a standard sinter feed as well as various mined ores with minimal processing. Fluxes can include Limestone, Magstone, Dunnite and Oilvine. Fuel is mainly Coke breeze but can include Anthracite.

2.3.1 Iron ores

Iron ores are brought into a sinter plant from all parts of the world. Iron ores are raw materials mined from the ground. The specific chemical composition is mainly driven by hematite (Fe_2O_3), geothite (a-FeOOH) and magnetite (Fe_3O_4). As of 2012, extraction of iron ore was mainly dealt with by BHP Billiton Ltd. (Australia) 176 Mt, Rio, Tinto (Australia and Canada) 199 Mt, Fortescue Metals Group (Australia) 63.7 Mt, Vale S. A. (Brasil) 320 Mt. In the worldwide market, western Europe and north America have been responsible for a large uptake of high quality dense hematite ore. Over the years, rich iron ore mines have been depleted due to demand and so much attention has been brought into the use of low grade iron ores [2]. Particle size of the iron ore material needs to be within range suitable for normal sinter plant operating operating conditions. Iron ore particle size should be no larger than 5mm but this varies. Thus both particle size of the iron ores as well as chemical composition plays an important role in optimising the iron ore sintering process. More recent research suggests that both high quality and low quality ores have increased in price over the years [8]. This indicates the demand for good quality ores have increased alongside the increase in the price.

2.3.2 Fluxes

The flux in sintering blends play an important role in the chemical reactions taking place at high temperatures during sintering. The flux is essential in sintering as it helps with agglomeration but more importantly promotes the generation of the liquid phase in the flamefront [9]. Fluxes play an important role in basicity and can influence sinter quality properties. Basicity is the CaO content over Si content and can have a direct impact on quality indices of the sinter produced for the blast furnace. Basicity has been known to influence sinter strength and RDI [10]. Reduction Degradation Index is a physical test subjecting the sinter to reducing environments using CO and N_2 at a temperature of 500C. Studies have been conducted showing the correlation between finished sinter and sinter strength and figures 3-4 show how basicity can have an impact sinter strength and reduction degradation index. Higuchi et al 2006 found an optimum basicity range of 1.5-2.0 along with a decrease in Al_2O_3 and increase in FeO, improved sinter reducability at high temperature [11]. It is clear that on increasing basicity, both RDI and sinter strength is improved. Fan et al, 2012 also investigated these impacts and found that on increasing basicity from 0.6 up to 2.22, a reducability improvement was evident and similar results were found for RDI [12]. Separate experiments were conducted by Savelev et a, 1981 at the chusovoi metallurgical plant and reported that varying basicity in the iron portion of the blast furnace charge could increase productivity and reduce coke rate [13]. Studies conducted by umadevi et al 2014 showed that when increasing basicity with high and low alumina sinter, results also show an improvement in RDI but productivity is decreased [14].

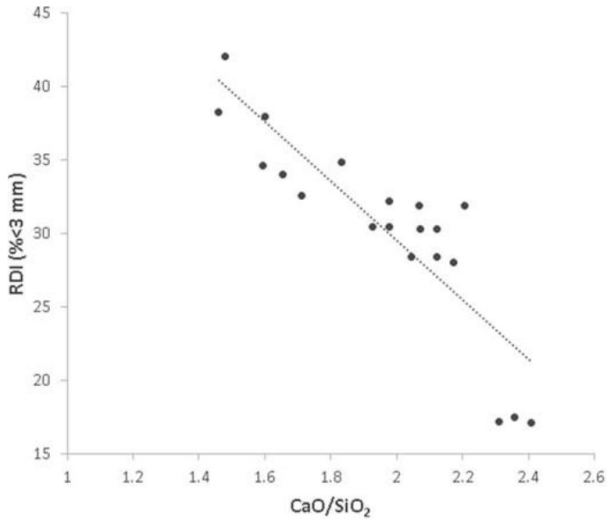

Figure 3: Relationship between sinter basicity and sinter RDI [10]

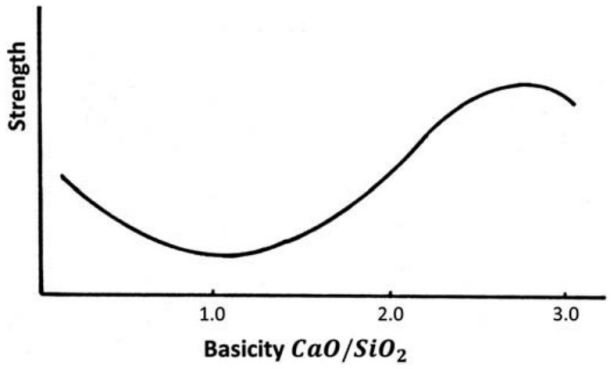

Figure 4: Relationship between sinter basicity and strength [10]

Three main fluxes are limestone, magstone and olivine. Limestone comprises of a high amount of CaO. Limestone promotes the solid phase reaction in iron ore sintering as the decomposition of calcium carbonate reduces the potential of oxygen in fumes, this results in a reduced reaction time and heating rate. In the flamefront, the decomposition of the carbonates can result in a decrease on thermal capacity. The addition of Ca2+ ions to the

liquid phase (flamefront) results in the increase of potential oxygen and therefore calcium ferrites and silicates are favored instead of wustite and magentite. These calcium and ferric silicate have thermal expansion coefficients and melting points which can be detrimental to strength as they are susceptible to internal stresses [10]. In terms of microstructure, Bolukas et al 2013 found that a higher basicity results in hematite nucleus encompassed by acicular ferrites. He also concluded that in the presence of iron oxides the CaO forms compounds which promotes primary melt formation. These compounds are Fe_2O_3·CaO at 1205°C and FeO·CaO at 1120C. Primary melt formation needs to be minimal if strong sinter is desired. In the presence of iron oxides the SiO forms compounds being FeO·SiO_2 at 1180C, 2FeO·SiO_2 at 1205°C and FeO·SiO_2·CaO at 1223°C [15]. Other studies found that when silica and basicity are increased, it promotes the assimilation reaction between particles within the liquid-solid phase. Primary melt formation (flamefront temperature) is decreased on increasing Si. On increasing Si, hematite content does not change. [16]

2.3.3 Fuel

Combustion is the driving mechanism behind iron ore sintering. If it wasn't for the fuel within the blend composition, the blend would not ignite under the ignition hood and therefor the process would not be possible. Ideal fuel characteristics are high calorific value, low volatile matter and uniform combustion characteristics. Fuel used in iron ore sintering is coke breeze. Coke breeze is a by product of the coke plant preparing coke for the blast furnace. It is basically fine breeze, usually less than 3mm. Breeze is the desired choice due to its unique combustion properties combined with its mechanical and structural properties. Impurities are low due to being driven off by the process undertaken at the coke ovens which is also desired by the sinter plant. [17]. The continuous consumption of coal and its carbon footprint has been of growing concern in the steel industry for many years [18]. As carbon is used as the reducing agent in converting iron ores into metallic iron, it is necessary to use. Research has been undertaken in how the carbon content can be substituted. Biomass has been researched regularly [19], [20], [21] to see if it can be used as a replacement. Even though it had been proven that biomass could be partially substituted, industrial application was minimal as substantial amounts of biomass would be needed to achieve the calorific value coke breeze can achieve. [21]. Anthracite coal has been looked into as a replacement coal due to it having similar combustion characteristics. Due to the increase in coke demand, anthracite had been used in many sinter plants. overtime, as the anthracite content has increased, more problems have surfaced. Studies show that anthracite usually

has a volatile matter which burns off into the gas flow and so this could be the reason it has proven problematic in sinter plants, especially with regards to emissions. Research suggests that anthracite up to 3mm in particle size has lower porosity, higher density and a slower combustion rate than that of coke breeze of the same size [22].

2.3.4 Reverts

Reverts consist of any material being produced as a waste-product of a process that falls within the steel industry. This can include by-products from plants such as the blast furnace or BOS plant. In order for the revert to be beneficial for the sinter plant, the revert must be high in Fe and not be detrimental to the sintering process. Compositions with high amounts of C, MgO and Al_2O_3 can also be beneficial for the sinter plant as it can be used as a trim to alter chemistry of final sinter as well as lowering the fuel rate. Reverts used in sinter plants can include blast furnace dust, BOS slag, Mill scale and generally all types of spillages that have desired composition. Blast furnace waste-products [23] can be split into light and heavy particle size fractions. Heavy fraction of flue dust taken from the top of furnace, captured in water to assist in minimising emissions, whereas light dust fractions is captured dry. Both have similar compositions of around 35% carbon and 25% iron. BOS slag can also be separated into 2 categories and can be used as a coarse aggregate in the transport sector [24]. Primary slag which is sold on and revert slag which is processed before it is recycled. Mill scale can contain 80% iron. Using reverts usually comes with additional problems, such as mill scale comes with a high amount of oil and so must be segregated. Blast furnace dust is rich in zinc and chlorides which can be detrimental to the sinter plant as well as blast furnace. Studies show that some reverts can be used in concrete making [25]. Millscale has been proven to influence phase formation, in particular hematite and SFCA formation [26].

2.4 Raw material granulation

Iron ore sintering performance can be optimised by sufficient granulation. The principle of granulation is to increase bed permeability [27] by reducing the amount of fines by layering them onto coarser particles. In order to achieve sufficient granulation a number of aspects need to be considered. Particle size distribution, flow characteristics and moisture are the main drivers behind good granulation. Granulation is the layering of ultra-fines that coat the surface of nuclear particles, which is followed by the layering of intermediate size particles that is embedded in a matrix of fines [28]. The particle size distribution and the ratio of the adhesive fines (below 0.25mm), nucleus (above 1mm) and non-adhesive fines (between

0.25-1mm) needs to be within a correct ratio for optimal granulation [29]. Studies suggest that keeping non adhesive fines to a minimum is optimal. Obtaining the correct type of flow withing the drum is important to promote agglomeration. Types of flow can be seen in figure 6 [30]. Filling degree, rotation per minute and drum dimensions have key aspects in flow characteristics. Optimal granulation is achievable with a rolling/cascading flow. A filling degree of 20% is usually adequate to achieve sufficient flow characteristics. If the filling degree and drum dimension was kept constant and the RPM increased, flow would go from cascading, to cataracting to centrifuging. This is due to the increase in frictional forces between the drum and the mixture which over come the granulating force in the sinter mix [28]. Rolling occurs when there is a steady discharge of particles rolling back onto the mixture surface in the drum. This can be seen in figure 5 and 6. As seen in figure 5, moisture is the main driving agent responsible for the forces agglomerating the particles to each other. Moisture is distributed in a uniform atomised fashion to the top of the surface layer of the mixture at one end of the granulation drum. As the granulation drum rotates and mixture is granulated, the moisture is distributed through out. Sufficient moisture for granulation and sintering is 6-7% but alternative studies found that a moisture level between 7-8% is most optimum for permeability [31]. At sufficient moisture, adhering particles layer onto the surfaces of nuclear particles and intermediate particles [29]. Porosity of the particles contribute to factors which vary the water retention capabilities . The more porous the particle the higher the moisture retention thus additional water needed for effective granulation [32]. The addition of moisture results in increased tension capillary forces between adhering/non adhering and nuclei particles bonding them together. As more moisture is added, void spaces within the mixture are filled, increasing tension forces that bonds the particles together. Bonding mechanisms are capillary forces within liquid bridges. Surface tension is holding the particles together by the cohesive forces formed by the liquid bridges. As the liquid increases surface area it therefor increases surface tension. Too much moisture can be detrimental to granulation. The point at which all the voids are filled with moisture will lead to breakdown of the structure turning the mixture into a slurry. [33]

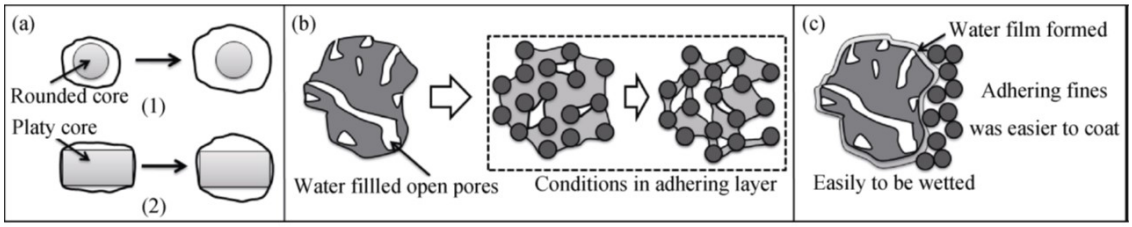

Figure 5: Iron ore granulation characteristics [29]

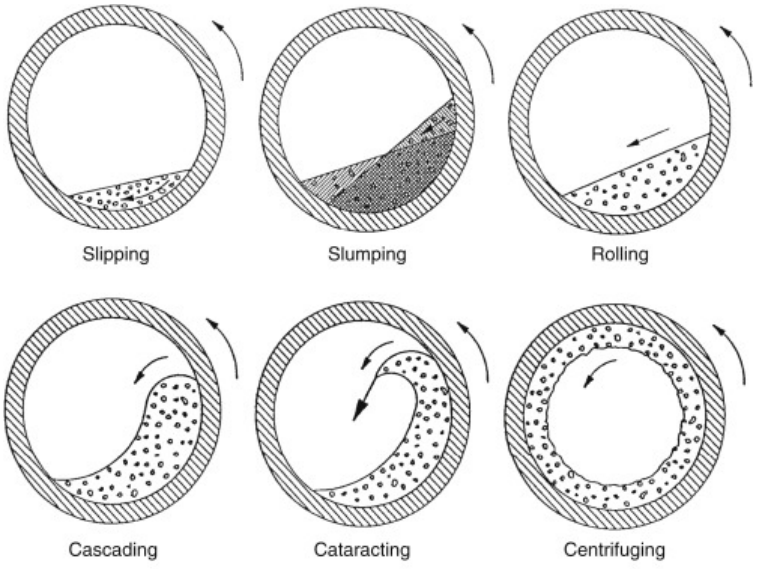

Mode	Fr($=\omega^2 R/g$) at $\phi = 35^\circ$
1. Slipping	$Fr < 1.0 \times 10^{-5}$
2. Slumping	$1.0 \times 10^{-5} < Fr < 0.3 \times 10^{-3}$
3. Rolling	$0.5 \times 10^{-3} < Fr < 0.2 \times 10^{-1}$
4. Cascading	$0.4 \times 10^{-1} < Fr < 0.8 \times 10^{-1}$
5. Cataracting	$0.9 \times 10^{1} < Fr < 1$
6. Centrifuging	$Fr > 1.0$

Figure 6: Flow characteristics within a granulation drum [30]

2.5 Sintering mechanism

During granulation, fine ore, limestone and coke adhere to core iron/coke particles of around 1-5mm in size. During heating, the oxides go through a phase transition and diffusion occurs at the interface in between the adhered fines and nucleus grain boundaries and a semi-liquid phase of Fe-Ca-O is produced. On cooling, the calcium ferrites precipitates and a network of pores is a result which is Fe_2O_3 nucleus grains embedded by calcium ferrites [34]. Masoa came up with a phase diagram for for quasi-binay CaO-Fe_2O_3 system and an illustration of the sintering reactions on heating and cooling. This can be seen in figure 8.

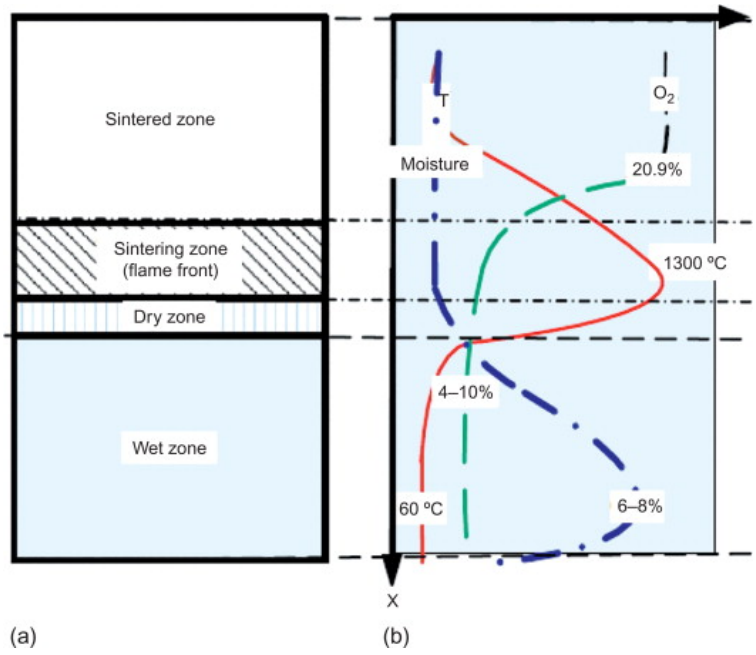

Figure 7: Different sintering zones of a bed [35]

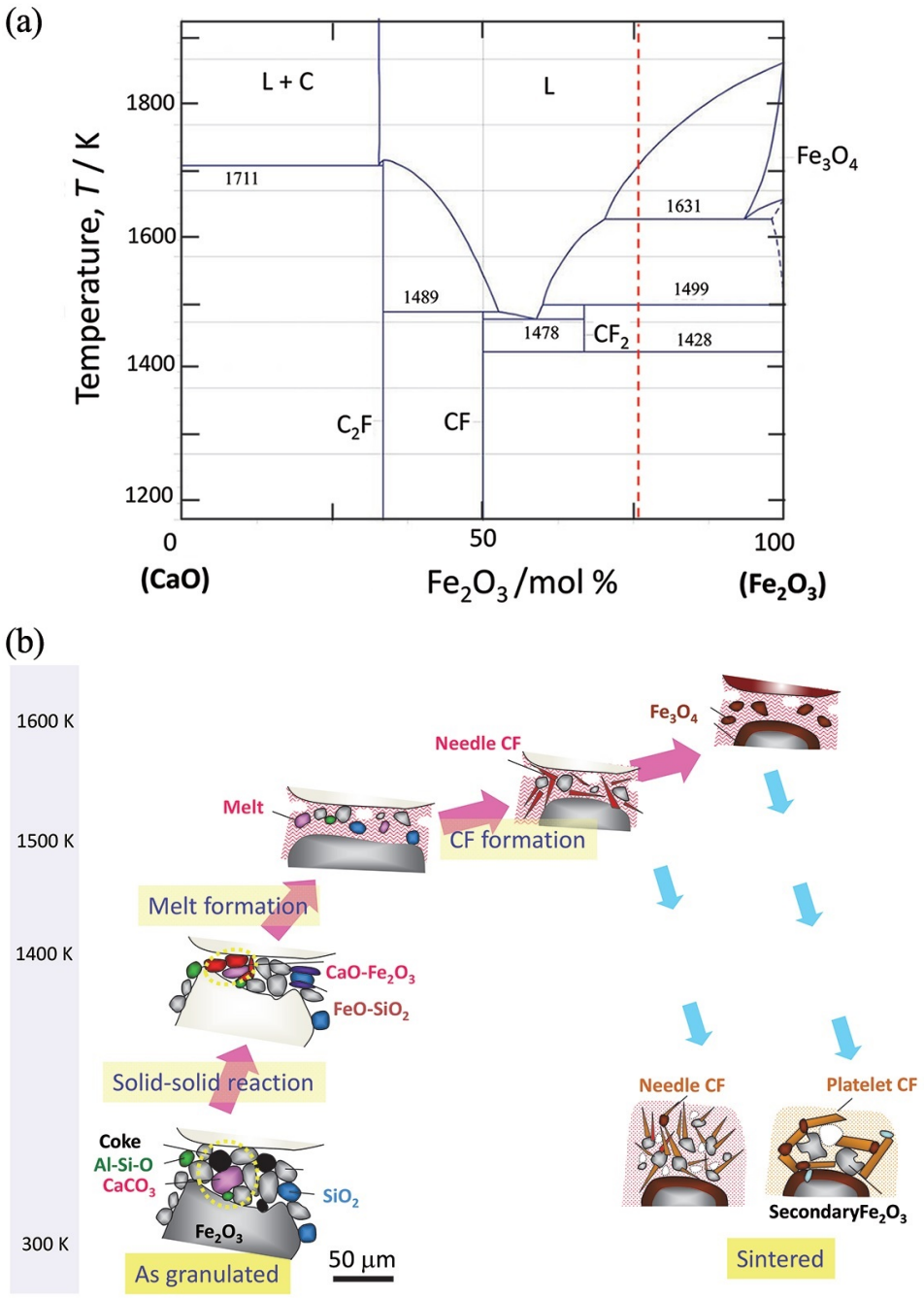

Figure 8: Iron ore sinter phase diagram [34]

The main driving factors behind sintering are bonding forces. Sintering is a thermal treatment bonding fine individual particles, coalescing into a porous solid structure. The two main bonding forces driving the sintering process is fusion bonding and diffusion bonding.

- Fusion bonding: considered the complete or partial formation of crystalline components

embedded in a glassy melt matrix

- Diffusion bonding: considered as the phenomenon of re-crystalisation and crystal growth of hematite and magnetite [36].

Figure 7 shows the different zones occurring at any given point during the sintering process. Each zone represents a different physical and chemical reaction taken place. In the preheating and drying zone - the the moisture being driven off due to the high temperatures in the neighbouring combustion zone. The combustion zone, is where the flame front is established. Temperatures are above 1100°C in order for a flame front to be established. This is where the thermal decomposition of carbonates and sulphate occurs, as well as the formation reduction reaction of hematite and magnetite. Studies suggest that a wet zone exists which neighbours the dry zone. This can be also be seen in figure 7 and is where moisture has condensed as a result of the downward pressure. Convective heat drives the flame front downwards via the continuous negative pressure applied. Once the sintered zone occupies all zones the sintering process has complete. In reality moisture content can control the size of the zones present i.e. if the moisture content in the granulated mix is increased, the wet zone would also increase. In theory, too much moisture in the granulated mix would result in in-adequate bed permeability which is likely to cause unstable flame front characteristics resulting in reduced and erratic flame front temperatures. This is due to there being too much moisture to evaporate or burn off, lowering the overall temperature of the system. In essence, too much energy is needed to evaporate all of the moisture away.

2.6 Sinter structure

Sinter is a complex, heterogeneous, multi-phase, solid mixture containing both poly-crystalline and amorphous material. A range of oxidation states may be present as well as structural in-homogeneity existing on a dimensional scale from microns to millimetres. The main phases and structures are mentioned below:

- **Hematite** - Hematite, chemical formula Fe_2O_3 is the most important ore of iron. Even though magnetite is easier to process and contains more iron, hematite is used more as it is widely available and more abundant. Hematite is mainly mined from China, Australia, India, US, South Africa and Russia [37]. In iron ore sintering it can be classified as primary and secondary hematite. Primary hematite is from the original mixture, un-sintered. Secondary hematite comes from the crystallisation of the molten phase via oxidation of magnetite crystals in the liquid phase or synthesised by

oxidation in the solid phase. Hematite in it's raw state can be seen in the micrograph below.

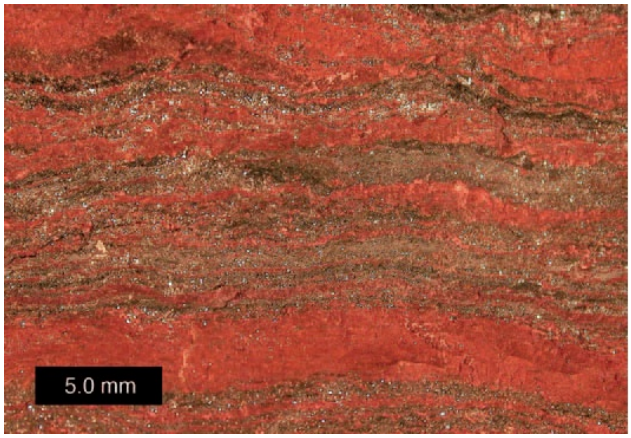

Figure 9: Unprocessed hematite micrograph [38]

- **Magnetite** - Chemical formula of magnetite is Fe_3O_4 and is ferrimagnetic unlike hematite. In iron ore sintering, magnetite appears in areas of poorly sintered areas or crystallised during the melt formation. Studies have been conducted on pilot scale plants investigating the impacts of a magnetite rich blend compared to a hematite rich blend. It has been considered that the energy requirements for sintering can be slightly lower for a magnetite rich blend as the chemical energy released from exothermic reactions of the fine concentrate partially preheats the bed ahead of the flame front [39]. This would allow slightly less fuel being needed. Figure 10 shows sintering performance and sinter quality of the sinter produced from the investigations. It can be seen that even though less solid fuel is needed, productivity, reducability and yield favours the hematite rich blend.

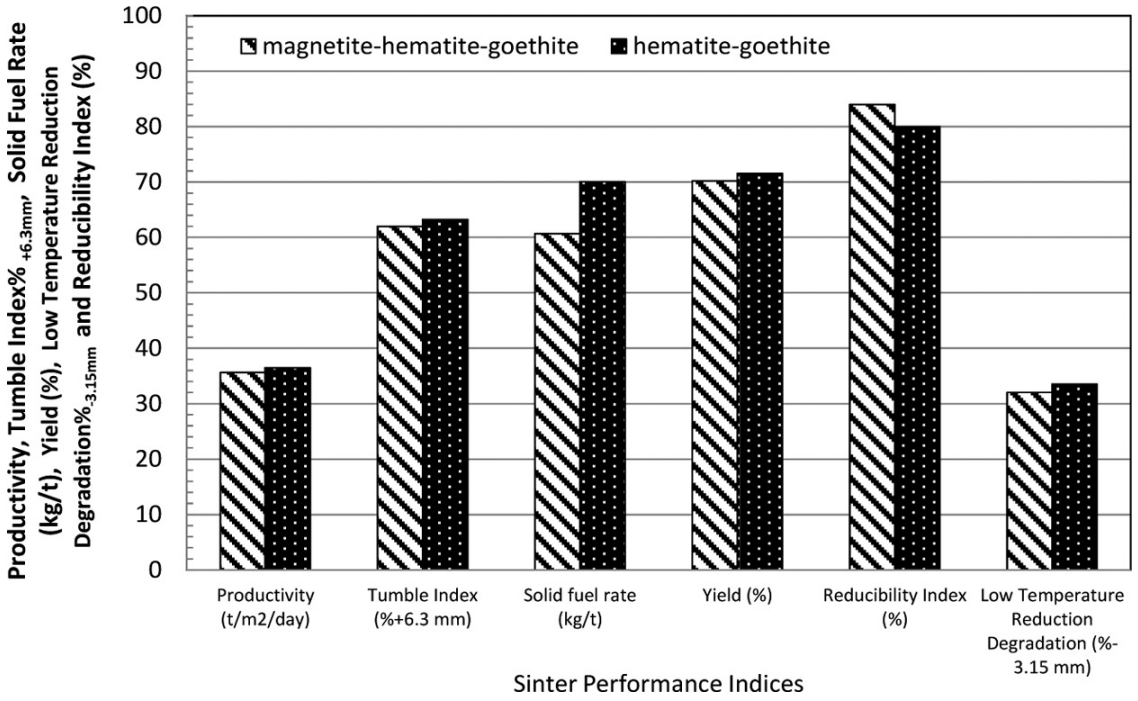

Figure 10: Sinter performance and sinter quality of magnetite rich blend vs hematite rich blend [39]

- **Wustite** - Wustite (FeO) in its natural mineral form is grey with a reflective green tint. Formation of wustite in sintering is caused by the precipitation from the melt in low potential oxygen and usually linked to over fuelling or reduction of magnetite in its solid phase. Studies suggest that during reduction, the surface structure of wustite becomes porous but not as porous as when hematite is reduced to iron [40]. Figures 11 and 12 emphasises this point [41]. A non porous structure can lead to deterioration in reducability performance.

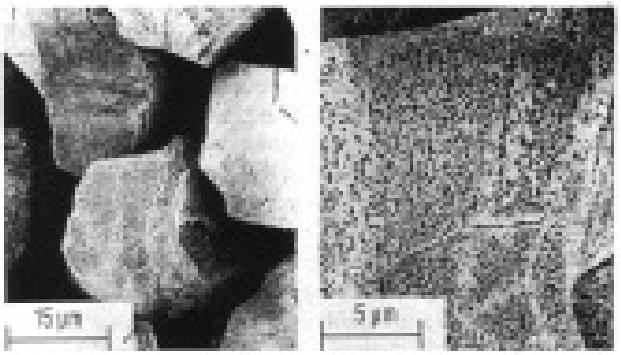

Figure 11: Micrograph of hematite reduced to wustite [41]

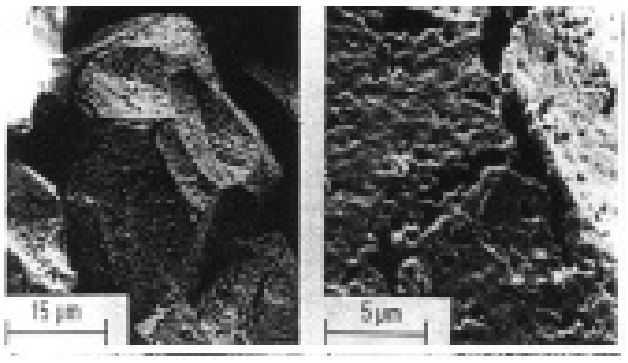

Figure 12: Micrograph of hematite reduced to porous iron [39]

- **Calcium ferrites** - These are formed at the grain boundaries of iron oxides that react with slag components rich in CaO with SiO_2 and Al_2O_3. Calcium ferrite can be the most desirable liquid phase. It is desirable due to its binding properties which contributes to strength and reducability of the sintered product [42]. Studies show that calcium ferrite generation has a maximum generation amount at a temperature of 1275°C for hematite and limonite whereas for specularite and magnetite 1250°C was the optimum for maximum calcium ferrite generation. Investigations also showed that increasing partial oxygen content in airflow benefits calcium ferrite formation [43]. Figure 13 points out calcium ferrites within the microstructure taken with an electron microscope [44].

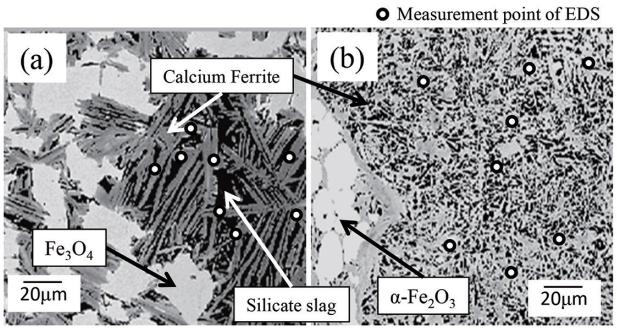

Figure 13: Structure of calcium ferrite [44]

- **Silicates** - Considered a multi-component of continuous solid solutions of calcium ferrites which make up silico-ferrites of calcium and aluminium known as SFCA [44]. Formed due to the reaction among molten calcium ferrite and silica. [10].

2.6.1 Sinter mineralogy and microstructure

Apart from input material, flamefront characteristics play an important part in sinter mineralogy. In sinter, the iron rich minerals are fused together in a matrix of complex calcium rich, ferrite phases and calcium silicates. The calcium rich phases contain Alumina and silica. Figure 14 shows a typical sinter mix pre (a) and post (b) sintered.

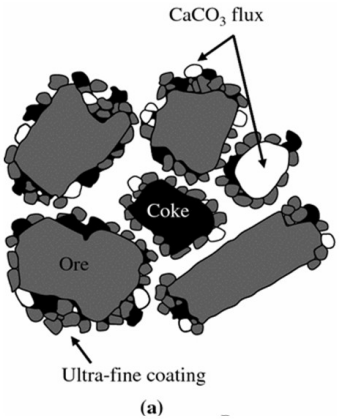

Figure 14: Structure of blended mix prior to ignition [45]

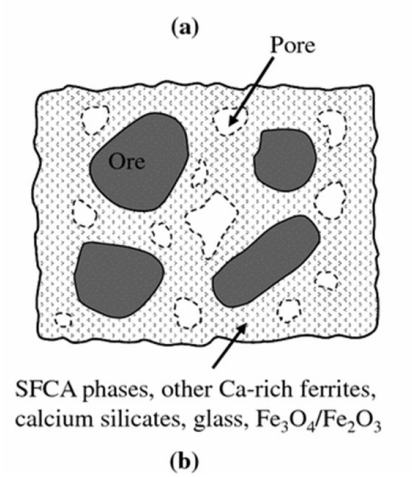

Figure 15: Structure of sintered iron ore [45]

Studies suggest that SFCA's are most desirable for low reduction degradation index and good mechanical strength. There are two types of SFCAs [45]. First type is low-Fe form which appears prismatic or columnar in morphology. The second being high-Fe form known as SFCA-I which appears accicular or needle like morphology. Research suggests that texture of SFCA-I results in superior properties of strength and reducability. Sinter containing large amounts of prismatic SFCA which is associated with glass is of lower quality. Research [46] also suggests that a third apparent member of the SFCA homologous series known as SFCA-II which is an intermediate of the crystal structure of SFCA and SFCA-I. Research indicates that as long as the temperature remained below 1300°C, SFCA-I could only be present. This was also true when temperature was above 1300°C for minimal amount of time. If the temperature was above 1300°C for a long period of time (ie thick flame front) then SFCA-I would transform to Fe_2O_3 or Fe_3O_4 in a calcium silicate-rich melt. On cooling, oxidation occurs and the Fe_3O_4 reacts with the melt and oxygen by picking up Ca and Al which results in the formation of SFCA and secondary Fe_2O_3 [45]. The different types of SFCA formation can be seen in the microstructures below in figures 16, 17, and 18.

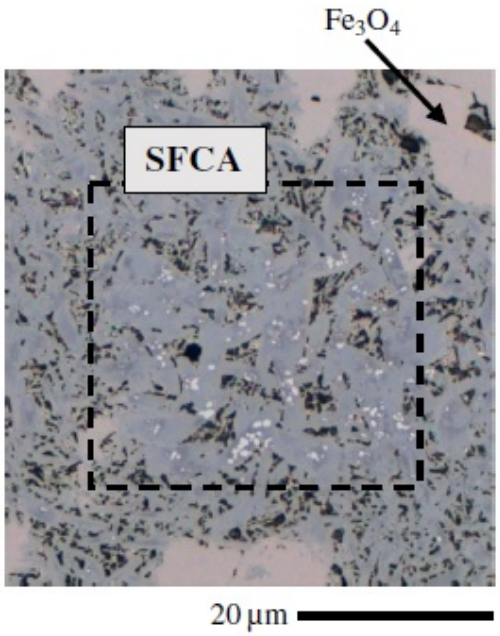

Figure 16: Microstructure of SFCA formation [47]

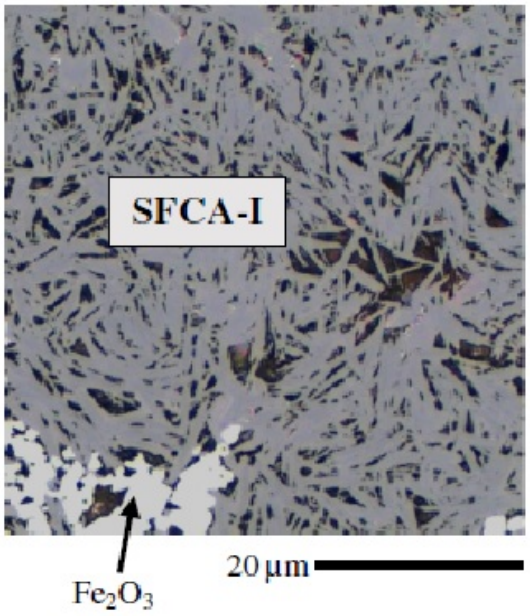

Figure 17: Microstructure of SFCA1 formation [47]

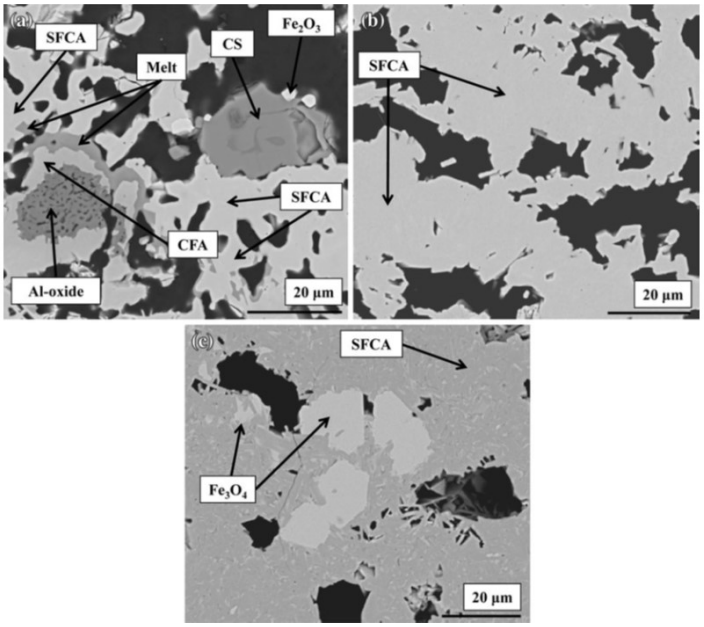

Figure 18: Microstructure of typical sinter

Webster [45] proved that:

- During heating in the range 25°C to 1350°C, SFCA-I formation was associated with the reaction of Fe_2O_3, C2F, and SiO_2. SFCA initially formed by the reaction of CF, CFA-phase, and SiO_2, and its initial formation was associated with the formation of CS and a melt phase.

- During cooling in the range 1350°C to 25°C, the first phase to crystallise by reaction between Fe_3O_4 and the melt was a Fe-rich SFCA phase of composition similar to SFCA-I, which also has an unknown structure. At a lower temperature, this Fe-rich phase reacted with the melt to form SFCA, which persisted down to 25°C

- During heating, increasing Al_2O_3 concentration (1) increased the temperature range over which SFCA-I was stable before the formation of SFCA and (2) stabilised SFCA to higher temperature. During cooling, increasing Al_2O_3 (1) increased the temperature at which crystallisation of the Fe-rich SFCA phase occurred, (2) increased the temperature at which crystallisation of SFCA occurred, and (3) suppressed the formation of Fe_2O_3 to lower temperatures.

This corresponds with the current literature available and [45] shows the complexity of these phases formed. The complexity of the phases mentioned resulted in webster conducting

more studies on what influences SFCA formation and found that basicity greatly impacts the type of SFCA formation. He found that increasing basicity from 2.48 to 4.94 increased the temperature range by 100°C for SFCA-1 formation. He also experimented and found that on increasing basicity from 2.48 to 4.94, it increased overall percentage of SFCA-1 from 18 wt pct to 25 wt pct respectively. It is worth noting here that the mechanism of SFCA formation did not change on increasing basicity. This can be seen on investigating figure 19, 20 and 21 below where webster used an in-situ S-XRD which was able to mimic atypical sintering thermal profile on several mixtures with increasing basicity and performed phase quantitative analysis during heating. [47]

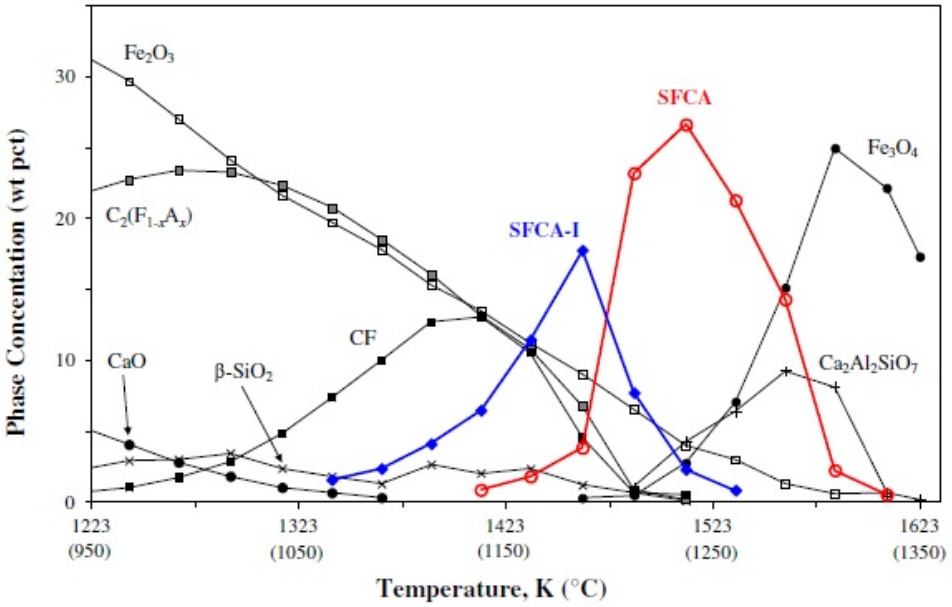

Figure 19: Thermal profile of SFCA formation with basicity at 2.48

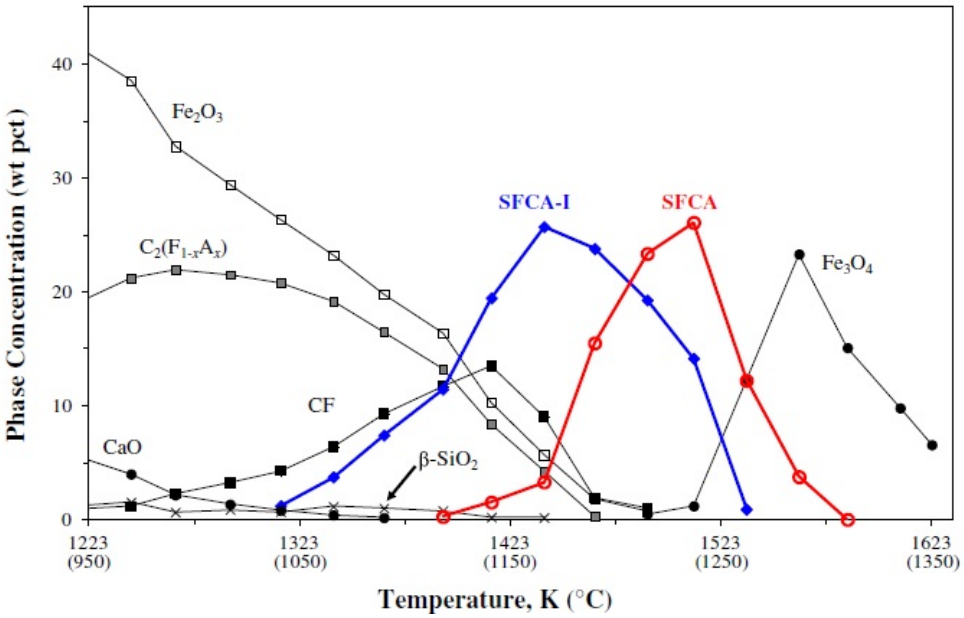

Figure 20: Thermal profile of SFCA formation with basicity at 3.96

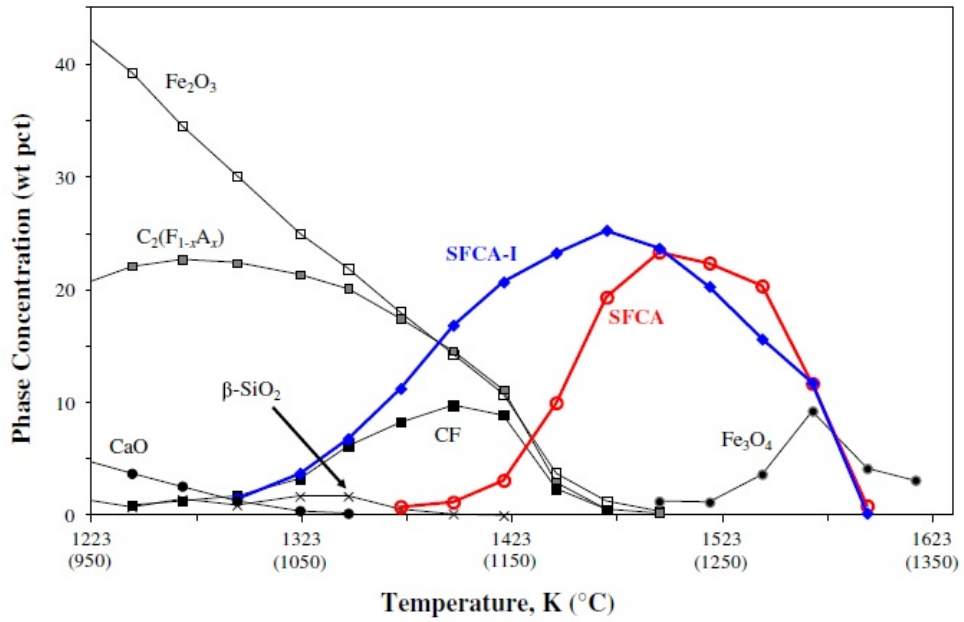

Figure 21: Thermal profile of SFCA formation with basicity at 4.94

2.7 Quality indices and varying affects

Many factors influence iron ore sintering. The following section goes through the various quality indices and how they can impact the sintering process and quality of sinter.

2.7.1 Mechanical properties

Tumble index is the cold strength of finished sinter. This is important as transportation and handling can cause a certain amount of structural stress and sinter needs to be able to withstand drops from height. Good cold strength is dependent on the strength of the bonding matrix components as well as close control over iron ore composition. [48] Studies suggest that sinter porosity can be related to reducability. Studies found that as the surface area (porosity) decreased the reducability decreased. Pores needed to be at least 0.01microns to allow gas to access pores and allow the reduction reactions to take place. Anything above 1-5 microns had the tendency to latch on to micro-pores which also resulted in in reduction in reducability. [49]

2.7.2 Reducing properties

Reducability index testing gives an indication of how efficient the sinter is at transferring oxygen during the reduction reaction process within the blast furnace. An increase in FeO results in a decrease in reducability. This is a result of the FeO reacting with SiO_2 and as a result forms fayalite which is difficult to reduce. Reduction reaction of the mineral phases in decreasing order is:

- $Fe_2O_3 > CaO._2Fe_2O_3 > CaO.Fe_2O_3 > 2CaO.Fe_2O_3 > Fe_3O_4$

The hematite and magnetie is initially reduced to wustite from hematite. The FeO then homogeneously reduced with wustite and from magnetite the following reduction process takes place:

- $Fe_3O_4 \rightarrow$ FeO $\rightarrow$ Fe.

It can also be noted that SFCA reducibility can be related to morphology, porosity and the presence of a glass coating. [50] The Reduction Degradation Index of sinter can be related to basicity (see figure 3) and is a measure of sinter strength after undergoing partial reduction in a furnace to give indication of degradation characteristics. The sample is sized and weighed into several size fractions before and after the test to give a value.

2.7.3 Chemical properties

FeO content can be an indicator of thermal properties within the sintering process. It has been studied that FeO is related to RDI in that RDI value is decreased (improved) by 8 for an increase of every 2% in FeO [51]. Studies also found that too much of an increase in FeO also results in a decrease in rebucibility. [52] It was found this caused permeability issues within the blast furnace which in turn influenced coke rate and productivity. FeO is directly related to magnetite content and its reported that productivity and strength is at its optimum when FeO content of 8-10% are achieved. This is due to the efficient permeability and temperature reached. [53] RDI decreases with increasing FeO due to the reduced amount of hematite within the sinter matrix. The hematite also causes a decrease in sinter reducibiltiy due to the decrease of accicular calcium and ferrite phases and increase in magnetite and columnar ferritic phase. Al_2O_3 can impact sinter quality. It has been studied that RDI is related to Al_2O_3 content in sinter, however, research has been contradictory [10]. When [54] studied the impacts of Al_2O_3 whilst keeping MgO and SiO constant a general deterioration in chemical and physical properties was observed. It has been studied that MgO content within sinter has a direct impact on its RDI value. This can be seen in figure 22. MgO is important in blast furnace productivity and is added directly as Dolomite or through sinter composition. In general, MgO stabilises hematite content, improving RDI. The increase in MgO also increased the amount of spinal and glassy phase. [54] Even though RDI improved, SFCA phase percentage decreased and consequently reducability. It is understood that the impact of MgO on RDI is not clear as there are contradictory results. [10]

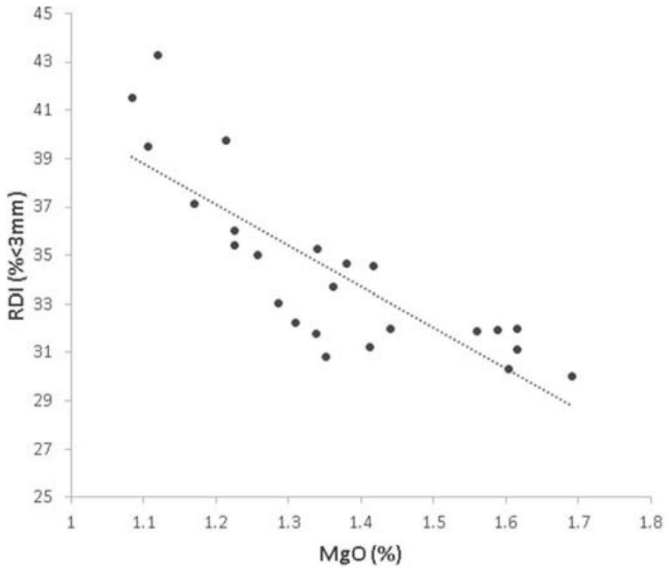

Figure 22: Relationship between MgO Vs RDI [10]

Alkali content in sinter is governed by blast furnace operations and should be limited due to its detrimental impact to the blast furnace. Studies suggest that the addition of alkali as well as chlorine favours the reduction of hematite to magnetite due to catalytic aspects of the alkali. Chlorine is detrimental to the sinter plant as well as sinter due to it being deposited onto the sinter surface restricting its efficiency in the blast furnace. As mentioned previously, basicity can influence sinter strength as can be seen in figure 4. It has been studied that sinter reducability is also increased on increasing basicity from 0.6 to 2.22. [10]

2.8 Factors impacting Iron Ore Sintering

2.8.1 Granulation

Poor granulation characteristics results in a non granulated blend, in which the average granule size is not sufficient for sintering. This results in the sinter bed being to compact. As mentioned previously, optimised granulation is performed when optimum flow characteristics is achieved. This is when a cascading and rolling motion is present within the granulation drum. In order to achieve cascading and rolling a correct filling degree needs to be present with regards to the blend within the drum and drum dimensions. A sufficient amount of nuclei to adhering particles should also be present. Too many adhering particles can lead to a balling effect which although may increase average granule size, they are usually compacted

under the pressure when suction is applied. Too many nuclei particles result it there not being enough adhering particles which lead to nuclei particles with no fine particles adhered to it, lowering the average granule particle size. [2]

2.8.2 Moisture

Moisture has a direct impact on the sintering process. Too much moisture can cause the granulation mix to turn into a slurry making it not possible for sintering. Studies found that, through varying moisture, flame front speed could be increased from 23.9 to 27.8mm/min which resulted in sinter productivity increasing whilst maintaining sinter strength. Increasing moisture further started to have a detrimental impact on the process [55].

2.8.3 Permeability

A well granulated blend will have high permeability. High permeability generally results in faster flame front speed which can increase productivity. High permeability is a result of optimised granulation characteristics. Poor permeability results in a high packing factor within the bed resulting in the flame front not being able to propagate due to the lack of pores and oxygen able to pass through the bed.

2.8.4 Flow rate

The lower the flow rate through the bed results in the lower amount of downward force available to pull the flamefront downwards. An increase in flowrate therefor increases flamerfront speed and therfor productivity. Flow rate can be impeded by poor permeability of the sinter mixture.

2.8.5 Flame front speed

As mentioned, flame front speed can govern the process. A faster front speed promotes productivity to a point but also promotes an accicular SFCA microstructure. Columnar SFCA was evident when slower flame front speeds are applied. As mentioned previously, this can influence final sinter properties. Figure 23 below shows the microstructures of sinter at different moisture levels and flame front speeds.

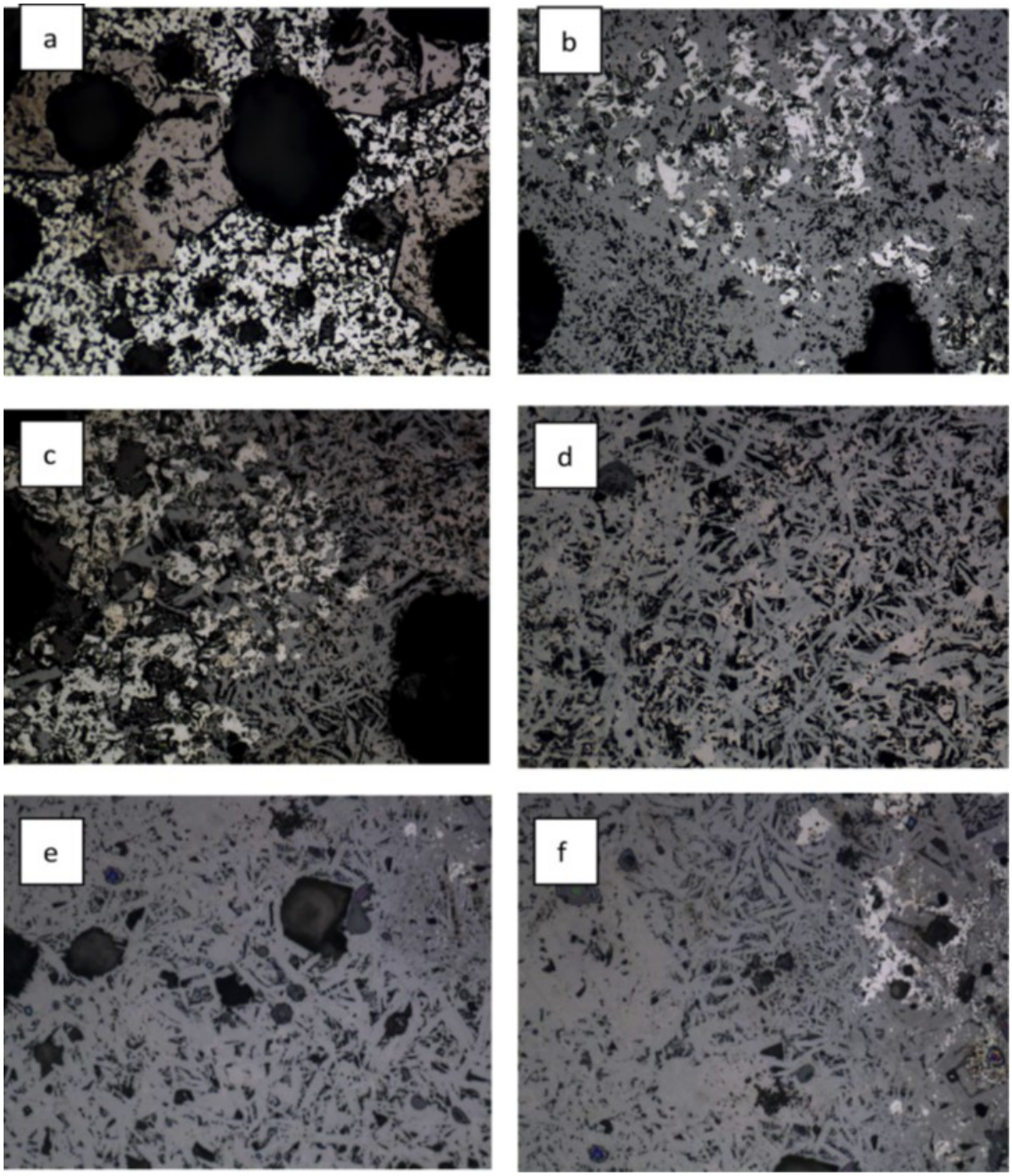

Figure 23: Microstructure characteristics when increasing moisture and flame front speed [55]

Due to the nature of experiments and to 'challenge' the investigation,thwe following can be said; the impact of increasing flame front speed is a result of varying moisture and so the influence of the increasing flame front speed could be that of the moisture addition. If moisture addition can be kept constant through out the flame front speed increase, the true

impacts of flame front speed could possibly be discovered. [55]

2.8.6 Various sinter pot dimensions used in research

Exploring the iron ore sintering process by utilising pilot line sinter pots have been used for decades. Each sinter pot can provide the researcher with different information depending on the pot dimensions and what analytical equipment is set up with the pot. Some sinter pots have the ability to capture emissions and dust particulates and therefor directly look at emission related issues. These are generally quite small and the sinter produced can be of poor quality. An example of a small sinter pot can have a diameter of 50mm and a length of 400mm. Issues can arise with using such small dimensions. Particle size needs to be compacted due to the nature of the pot. Edge affect is increased and so heat loss in increased and an increased pressure drop is usually required to maintain a stable process [56].

A slightly larger sinter pot has been used for research conducted on the emissions of iron ore sintering. This research was conducted on a sinter pot with similar diameter to the sinter pot deployed in this project. However, length is decreased significantly to 170mm which is capable of producing sinter in 2kg batches [57]. When using such short sinter pots, limitations include issues such as not allowing enough time and space for the flame front to establish itself. This in turn would result in an increased percentage of poor quality sinter being produced in relation to the total quantity of sinter produced. Larger pilot line sinter pots exist as well, with a 250mm diameter with a depth of 800mm [58]. This could produce sinter in 75kg batches. Another large sinter pot was deployed to investigate the effects of chloride on sinter emissions. The pot is capable of producing sinter in 80kg batches with a 370mm diameter and a depth of 500mm [59]. The advantage of using a larger pilot line sinter pot is that it produces a substantial amount of sinter. Large amounts of sinter can be directly analysed in the same manner to that of what sinter plants do, especially with regards to cold strength and tumble index which requires around 15kg of sinter in a particular size fraction. The disadvantages of such large pilot line facilities is that it is very labour intensive. Another disadvantage to a large sinter pot is that an increased amount of variation can be included with respects to flame front characteristics as only a small area is analysed by each thermocouple.

A sinter pot with dimensions of 100mm diameter and 550mm in length seemed to be a reasonable medium across all the sinter pots being used to conduct research. It's decent length of 550mm by-passes the fact the poor quality sinter is made at the top of the sinter

pot and so the majority of the produced product is of good quality. This was achieved due to the flame front having enough time and distance to establish itself. It also allows for for 5 embedded thermocouples to be used which can closely monitor flame front characteristics and the diameter of the pot helps minimise variation of the flame front. These dimensions allow for a pot that can produce sinter in batches of around 7kg. It is adequate enough to produce sinter of good quality to be subjected to reduction degradation index testing which is an important sinter quality parameter. Further more, mechanical strength could be tested which could give indication of cold strength. For example, subjecting the sinter to a mechanical vibration and analysing the resulting size fractions. Additionally, using a sinter pot with these dimensions does not require as much of a labour intensive approach when compared to a sinter pot capable of producing 70kg+ of iron sinter. Such quantities would require gantry cranes to lift such heavy loads. Given the above description, it was concluded that a sinter pot with a diameter of 100mm and length of 550mm was adequate and ideal for analysing, investigating and optimising the iron ore sintering process.

2.9 Conclusion

The current literature focuses predominantly on the impact of variation in composition in the input materials on the iron ore sintering process and the quality of the sintered product. Research suggests that careful control over input material as well as process parameters can increase sinter productivity. In terms of process, flame front characteristics seem to play an important role in the kinetics and can effect phase formation. This could lead to further investigations to enhance control over the kinetics of iron ore sintering. This paper also suggests that particle size distribution is an important factor in granulation, which has a knock on impact to sintering performance. In this respect, a better understanding of particle size influence of individual ores, fuel and fluxes could be useful to increase control over sinter quality indices. Reverts are having more importance in iron ore sintering as the capabilities to recycle these materials increase. This leaves the potential to investigate novel additions in iron ore sintering and how this impacts sinter performance and sinter quality. As a result of the literature review, the following hypotheses will be addressed.

1. It is apparent particle size plays an important role in iron ore sintering, however, it is not well understood how the particle size distribution and ratios of anthracite coal to coke breeze have impacted the iron ore sintering process. The expectations of this research is that the particle size distribution and ratios of anthracite coal to coke breeze,

can negatively, as well as positively, impact the thermodynamics and kinetics of the iron ore sintering process, and therefor, sinter quality.

2. To have proved that specific novel additions to a blend can be tailored to create a more circular economy in iron and steel making without impeding the process nor quality of sinter, by utilising the chemical composition of used products through-out the various process plants, which are destined for landfill.

3. To have optimised productivity through increasing bed permeability by increasing flame front speed during the sintering process without having any negative implications on the process or sintered product. Micro-pellets of fine iron ore raw materials can increase bed permeability through increased granule size within the bed but can sometimes lead to poor quality sinter. Directly reduced iron fines can be fed into the sinter plant and have highly advantageous chemistry for sintering but can sometimes be problematic due to the nature of its small particle size. Thus, increasing the granule size of the directly reduced iron fines could increase bed permeability, in turn, increasing flame front propagation speed and hence increase productivity - without having any negative consequences.

3 Design of Experiments

This chapter focuses on the experimental methodology, commissioning and validation of the small scale pilot line sinter pot in the new sinter pot laboratory. Initial laboratory operations of the project included gathering of equipment, setting up the laboratory and the design of a manual and safe working procedure. Secondly, this section also set out to investigate optimal set points for the sinter pot. Thirdly, the repeat-ability of the sinter pot process was looked at in great detail and lastly, a small validation of the sinter quality when using the blend taken from the sinter plant. This included a series of tests to investigate optimal granulation time, speed and moisture content for optimal flow rates. A series of tests to investigate optimal pressure drop for a stable process. It also included a number of tests using a blend from the sinter plant and processing it in the sinter pot and comparing sinter quality to that of the sinter plant's. It must be noted here that work conducted on the sinter pot for research purposes was kept in line with priorities for sinter plant production testing. As such, resources like materials, consumables and time spent on the sinter pot was restricted and limited according to sinter plant activities.

3.1 Methodology

This section set out to clearly state the methodology for the next chapters set out in this thesis. Unless stated otherwise and although most experiments will have a small experimental procedure section, the remaining chapters will adhere to the following experimental procedure, formula sheet as well as post analysis procedure. All table data which includes process parameters recorded to computer panel as seen in table 6 above will be placed in the appendices from here on. This is due to the information already being available from thermal profiles. All thermal profiles and graphs will be placed in chapters accordingly.

3.1.1 Optical Microscopy and Electron Dispersive X-ray Spectroscopy

Electron dispersive x-ray spectroscopy, also known as EDS, is a type of analysis that concentrates on the surface of the subject being analysed. It is used in combination with scanning electron microscopy. The technique uses electron beams which hits the sample. This excites an electron in an inner shell that causes the formation of an electron hole in the electronic structure of the element and photon (X-Ray) emission associated with an electron from an outer shell 'falling' to fill that hole. The intensity of the photon can be correlated to the size of the atom and a spectrum of intensity can be used to determine the composition of the

interaction volume of the beam with the sample. [60] .

It was decided that optical microscopy would be required to analyse the sinter produced within this work package. The following section aims to correlate the optical microscopy analysis of sinter to its EDS analysis. This was achieved via analytical Correlative Light to Electron Microscopy (CLEM) whereby a stage comprising 3 reference points was used in both the light microscope and electron microscope to analyse identical fields in both modalities using 3 point sample registration. This analysis method was required in order validate the qualitative analysis when describing the microstructures going forward. Figure 24 below shows the light microscopy image of two different sinter samples produced in slightly different manners. A was produced with a 6% fuel rate and B was produced with a 4% fuel rate. The images in figure 25 below are the EDS images of the respective sinter samples. Figure 26 shows their electron dispersive X-ray spectrum associated with the images.

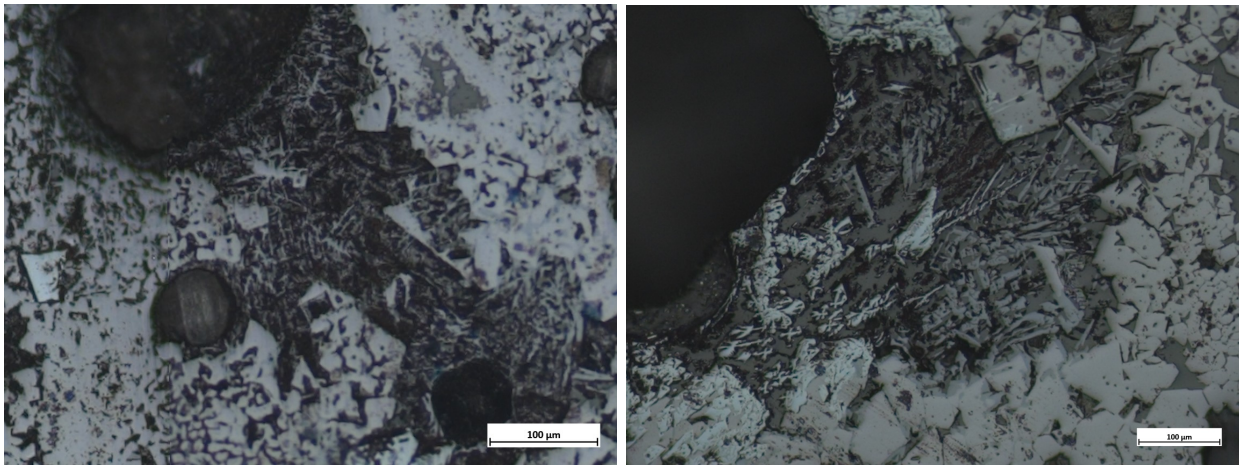

(a) Light microscopy of sinter A

(b) Light microscopy of sinter B

Figure 24: Microstructures of sinter produced with A) 4% and B) 6% fuel

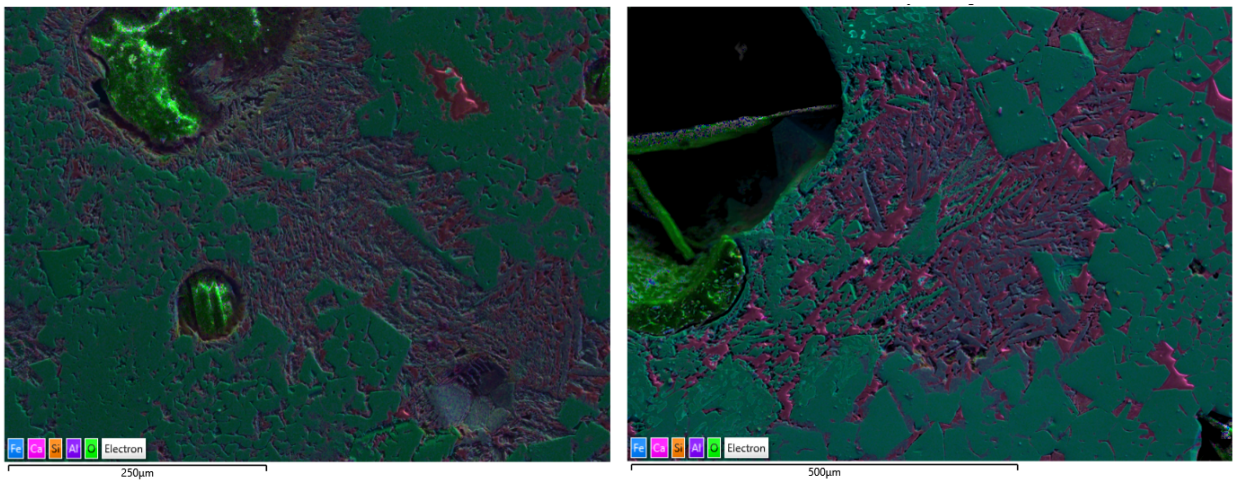

(a) Layered EDS image of sinter A

(b) Layered EDS image of sinter B

Figure 25: EDS layered images of sinter produced with A) 4% and B) 6% fuel

When analysing the microstructures above, 2 things are apparent. The first is that both exhibit plate-like hematite and magnetite structures with accicular needle like SFCA's. The second is that these structures seem quite refined when looking at A, whereas the structures in B appear coarser in appearance. This holds true as when fuelling with 6% fuel, the sinter is subjected to higher temperatures for a longer period of time, resulting in more time for reactions and phase transformations to occur as opposed to when fuelling at a 4% rate.

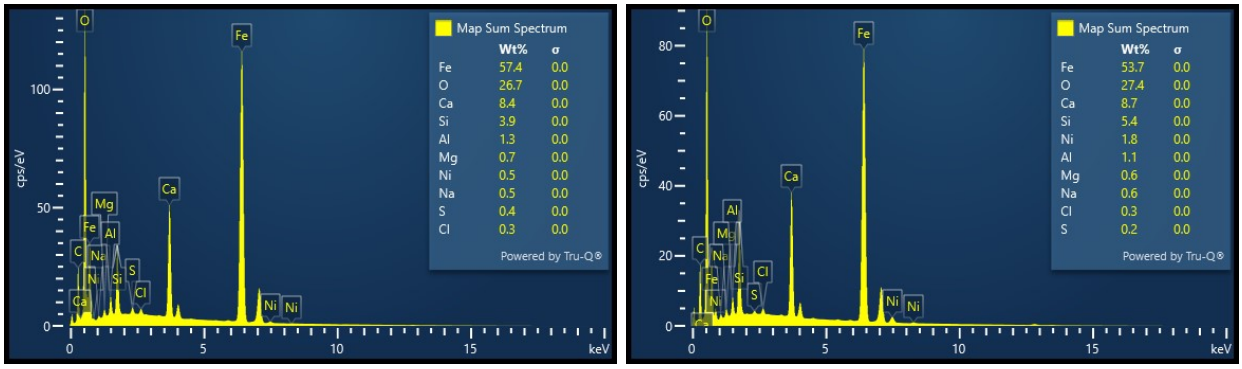

(a) Layered EDS image of sinter A

(b) Layered EDS image of sinter B

Figure 26: EDS analysis of sinter produced with A) 4% and B) 6% fuel

The spectra above tells us that there is iron and oxygen present, these are the iron oxides. These being the hematite and magnetite described above. There are also amounts of Ca, Si and Al. These are evident as the silico-ferrites of calcium and aluminium. There are also

trace amounts of Ni, Mg, Na, Cl and S but this can be expected when referring to input composition. The spectra also tell us there is slightly more Fe in image A. This was evident as more hematite and magnetite visible in image A.

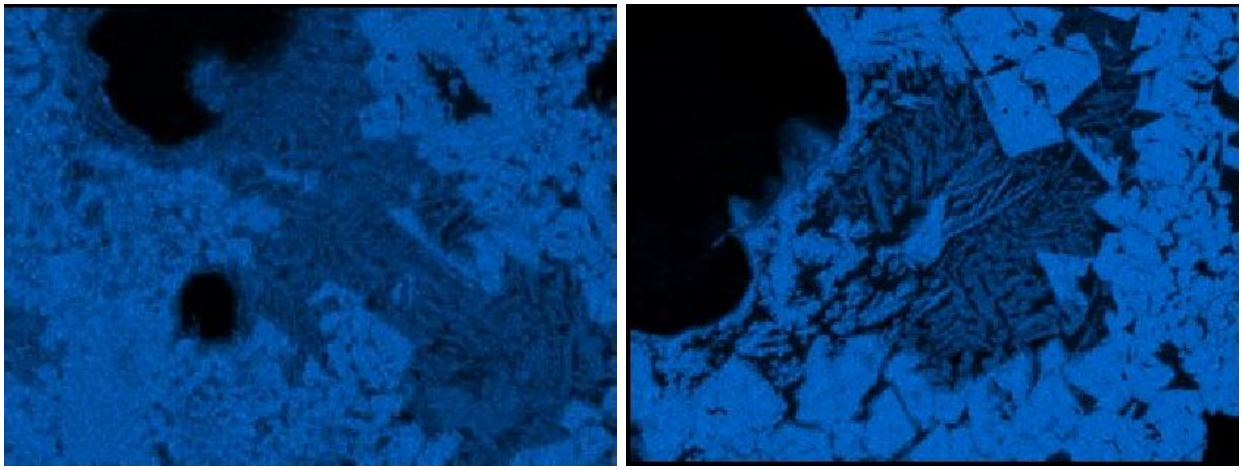

(a) EDS Fe image of sinter A

(b) EDS Fe image of sinter B

Figure 27: EDS analysis of sinter produced with A) 4% and B) 6% fuel

This is especially visible when separating the Fe analysed image out of the EDS layered image. This can be seen in figure 27 above It's clear that there is more blue visible in image A as opposed to image B, it must be noted that this was the case due to the pore in image A being smaller than the pore in image B and not due to there being more Fe in the sample. However, when looking at the contrast and brightness of the blue colour in the images, there is a difference. This could give indication of hemetite or magnetitie, however, on inspection it is easier to differentiate between the two via optical microscopy due to the reflective characteristics of hematite vs magnetite. This indicates that The spectra also tells us there is more Mg in image A than in image B. This can not be seen in the light microscopy images in figure 24. This is one advantage of EDS analysis that light microscopy does not give. The Mg is clearly picked up when separating the layered images into their individual analysis and this can be seen in figure 28. This is also true for certain elements as can be seen later on in the chapters when analysing for Cl and Na.

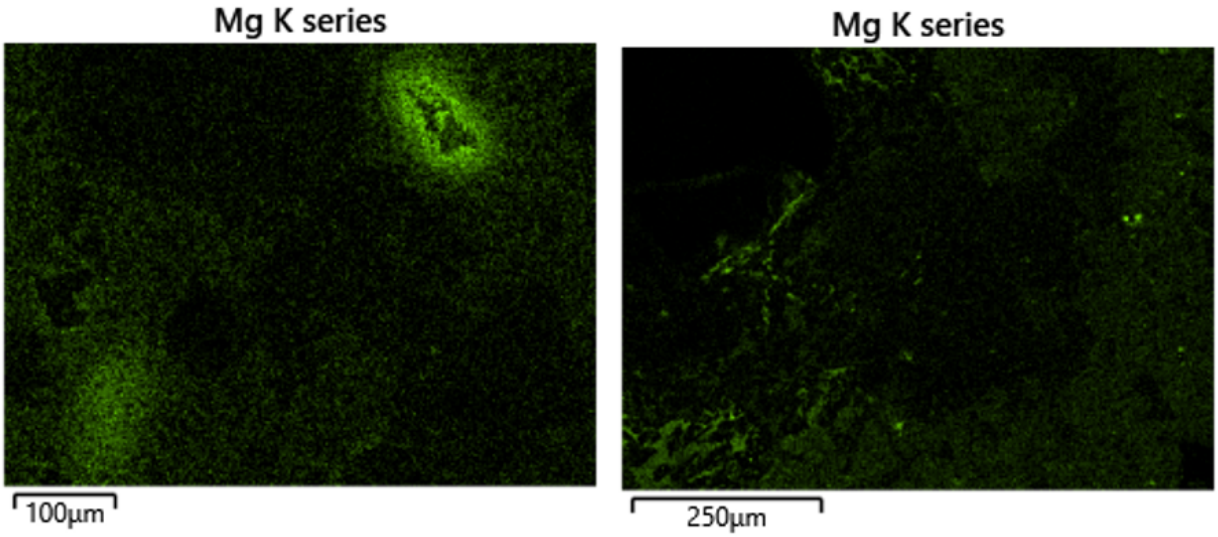

(a) EDS Fe image of sinter A

(b) EDS Fe image of sinter B

Figure 28: EDS analysis of sinter produced with A) 4% and B) 6% fuel

3.1.2 Summary of EDS validation

i) The EDS analysis clearly maps out different elemental compositions and can pick up on certain aspects that light microscopy can not. For example, Mg, Cl and Na cannot be seen when using light microscopy but is picked up when using EDS. However, for main constituents such as hematite, Magetitie and SFCA's, light microscopy is able to pick out the differences. For hematite and magnetite, this is due to a number of different iron oxides being present making it difficult to differentiate between the contrasts, however a qualitative description can be made. For SFCA's, there is little to be gained from the EDS analysis apart from when there are high concentrations of Si and Al, O and Ca.

ii) The EDS analysis can give qualitative descriptions and supports the light microscopy analysis giving confidence when characterising the sinter microstructures via light microscopy and EDS analysis in the remainder of this work package

iii) Even though EDS analysis is a powerful tool, it does not quantify how much of each phase is present, but a qualitative interpretation can be made.

3.1.3 Experimental Procedure - Thermogravimetric Analysis

Thermogravimetric analysis was used in order to understand and obtain information on combustion characteristics. Full detail of equipment used can be found in the appendix. Combustion characteristics of the fuels used within this study is of fundamental importance when analysing and describing the process of sintering during the pilot line testing set out in this thesis. The combustion characteristics of material input into the process will hopefully give insight into some of the process characteristics observed. Thermal characteristics wan be obtained such as change in enthalpy, ash percentage and combustion time for analysis. Operating procedure was as follows:

The furnace temperature is increased to 110°C at a rate of 20C/min and held isothermally for 15 minutes. This ensured that any weight loss experienced is a direct impact of the moisture in the coal. The temperature is then increased to 950°C at a rate of 40C/min and held isothermally for 25 minutes. Any weight loss occurring in this isotherm region is a direct result of the loss of volatile matter. The previous two steps are performed in a nitrogen atmosphere. For the third part, the atmosphere is then changed to oxygen. This creates an environment suitable for combustion. Once complete combustion of coal has occurred, the residue is taken as the ash. The following method was used:
Both fuels were characterised using various analysis techniques. Shape and surface characterisation were done using the optical microscopy. Combustion characteristics were analysed using a thermogravimetric analyser. Method for TGA testing was as follows:

i) Hold for 1.0min at 30°C

ii) Hold for 1.0min at 30°C

iii) Heat from 30.00°C to 110°C at 20°C/min

iv) Hold for 15.00 minutes at 110°C

v) Heat from 110°C to 950°C AT 40.00c/min

vi) Hold for 25min at 950°C

vii) Switch from nitrogen to air at 30.0ml/min

viii) Hold for 40.0min at 950°C

3.1.4 Experimental Procedure - Sintering

A pilot line sinter facility was deployed for this investigation. The sinter pot is one of its kind and the only operating sinter pot in the UK. It can produce sinter in 6.5kg batches. process parameters are recorded to a computer interface where set points are input which control the pressure drop. Once the sinter is discharged it is screened using ISO standard equipment which falls in line with normal sintering operations at the sinter plant. The produced sinter is then taken for post analysis which also falls inline with normal operations at the sinter plant. Sinter pot dimensions can be seen in figure 59 below. All blends were made up under laboratory conditions. This was done to achieve homogeneous mixture in terms of the blend composition and particle size distribution. This gives the ability to control particle size as the blends from the sinter plant are operated at a much larger scale, thus having a larger particle size. This is especially true when wanting to sinter in 6.5kg batches with a sinter pot that has a diameter of 100mm.

The raw materials were dried and screened to sub 5.00 mm. Fuel was dried and screen to sub 3.0 mm, flux was dried and screened to sub 3.00 mm. It was important to start off with a dry blend so optimal granulation could take place via close control of moisture addition. The dry blend was mixed in cement mixer for 2 minutes. This was done to ensure homogeneity throughout the different constituents within the pre-sintered blend prior to granulation. The blend was then ready for granulation. The blend was granulated for 5 minutes which is relatively representative of sinter plant operation. Initial investigation proved a granulation time of 5 minutes was optimal for bed permeability. 1100ml of moisture is added during the initial part of granulation known as mixing. Once moisture had been deposited into the drum, the blend was allowed to granulate for 5 minutes. At the plant, initial section is mixing where moisture is added and second section is granulation. This was done as it was representative of the granulation drum in the sinter plant which would take the granulated blend moisture to a reading to 6-6.5% depending on moisture retention capabilities. After granulation the blend was split into two representative samples using riffle box. The riffle box was used in order to achieve two granulated blends representative of each other. Pot was then filled with 400g of hearth layer sized between 10-16mm. Hearth layer was used to ensure the blend would not sinter the to grate at the bottom of the pot and is also represented of the sinter plant operation.

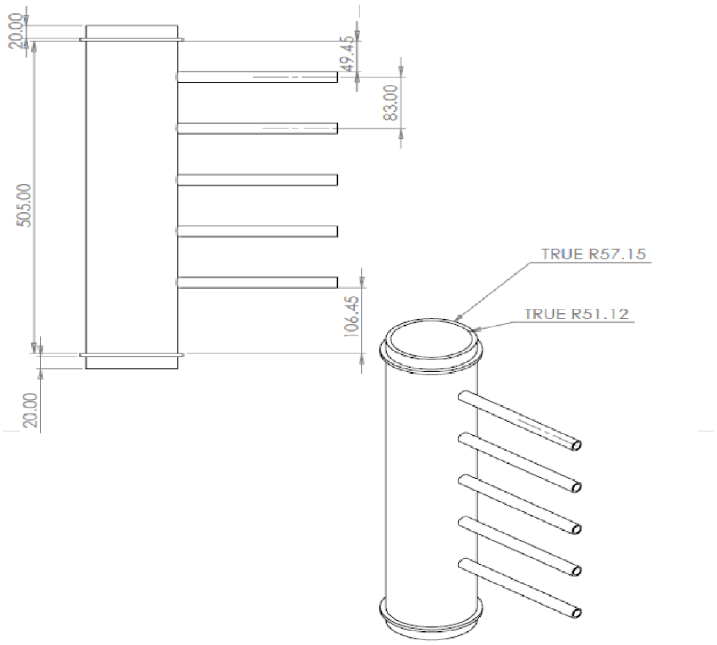

Figure 29: Sinter pot dimensions

The blend was then ready to be charged to the sinter pot. The blend was charged into sinter pot scoop by scoop alternating 90 in direction each time. This was done to avoid preferential packing. Preferential packing could lead to larger particles dominating one side of the pot, which would lead to one side of the pot being more permeable than the other. Having a sinter pot blend within the pot being more permeable down one side would result in process issues such as the flame front speed being drawn downwards at faster rate at one side of the pot compared to other. All tests had an ignition time of 1 minute. This was done as initial investigations proved this was sufficient time to get the first thermocouple to reach adequate sintering temperatures. The sinter pot set points for pressure drop was set at 100mBar suction. This was done to achieve adequate suction through the bed and falls in line with normal sinter plant procedures. Prior to ignition, flow rate was measured which gives indication of bed permeability before sintering operation. Before the tests were conducted and before any blends were made up, each blend constituent was subjected to chemical analysis via x-ray fluorescence. This data was used accordingly to make up the sinter blend. Ores and fluxes were adjusted to maintain sinter quality levels. It must be noted

here that iron ores used in the experiments were classified for sensitive information purposes.

Post analysis on the sintered products included subjecting the sinter to 1-minute mechanical vibration and then screened into size fractions. This was done to give sinter yield in specific size fractions and to give an indication of cold strength. Cold strength could only be analysed when running a series of tests within an experiment and comparing between each test when looking for a trend. Sinter in the size fraction of 16-20mm was then subjected to reduction degradation index testing. This was done to give indication on reducibility of the sintered product. This also complied with normal sinter plant operations. X-ray fluorescence was deployed on a small amount of sinter in the size fraction of 16-20mm. This was done to give chemical composition data on the produced sinter so correlations could be determined between sintering process, chemical composition and the reducibility of the produced sinter.

Please note: Sinter pot tests were conducted at 7% fuel

3.1.5 Experimental set points

i) Moisture measured to: 6.5%

ii) Granulation filling degree: 18%

iii) Granulation time: 5 minutes

iv) Burner set time: 1 minute

v) Pressure drop: 100mBar

Please note: Information as to why these were chosen can be seen above

3.1.6 Process Parameters Recorded and Calculated During Operation

i) **Average cold and hot flow**

This was calculated as flow rates could give indication of bed permeability pre and post ignition.

ii) **Temperature Profile**

This was calculated as the temperature profile could give indication on process stability and uniformity between tests and gives the user the ability to further calculate flame front characteristics.

iii) **Sintering time**

This was calculated as sintering time could give indication on process productivity.

iv) **Flame front speed**

Distance between each thermocouple is known (70mm). Time when each thermocouple peaks is known. If mid-point of flame front is assumed to be peak temperature of thermocouple then flame front speed can be calculated. I.e. one peak to the next. Formula S = D/T S = speed, T = peak time D = distance between each thermocouple. Flame front speed was an important parameter to monitor as it gave information on the thermodynamics and kinetics of the process. The thermodynamics and kinetic is the driving phenomena that runs the sintering process and thus correlates with sinter quality.

v) **Flame front thickness**

This was calculated as flame front thickness could give indication on time spent above 1100°C and should correlate with sintering time.

vi) **Cooling rates**

This was calculated as cooling rates could possibly correlate with sinter quality especially sinter morphology. Cooling rate from maximum sintering temperature to 1100°C could be defined as flame front cooling rate as a flame front is established at 1100°C. Cooling rates from 1100°C to 600°C could be defined as sinter cooling rate.

3.1.7 Post Analysis Procedure

i) Process summary

ii) Sinter yield in size fractions after 1-minute mechanical vibration.

iii) Reduction degradation index analysis

iv) X-ray fluorescence analysis

v) Optical microscopy

Please note: Information as to why these were chosen can be seen above

3.1.8 Formula Sheet

i) **Sintering time**

Taken from the moment thermocouple 1 reaches 40°C (i.e. burner head is on) to the moment off gas thermocouple 1 peaks (i.e. burn through point). Sintering time is an important parameter to monitor as it could relate to productivity of the process.

ii) **Average cold flow**

Average of values taken from flow meter attached to top of sinter pot. Measurements taken when desired pressure drop is reached and averaged over a period of 5 minutes prior to ignition. Average flow rate prior to ignition is an important parameter to monitor as it relates to bed permeability which can relate to several process parameters such as flame front speed and sintering time. It also gives indication of how well the blend was granulated and if the chosen blend was too fine to sinter.

iii) **Average hot flow**

Average of values taken from flow meter attached to top of sinter pot post ignition. Measurements taken from the moment thermocouple 2 reaches its maximum to the point where thermocouple 4 reaches its maximum value. Average flow rate after ignition was an important parameter to monitor as it gives indication of how permeable the bed is during sintering. It can also relate to several process parameters such as the different flame front characteristics as well as sintering time.

iv) **Sintered airflow**

Average of values taken from flow meter attached to the top of the sinter pot. Measurements taken from the burn through for 5 minutes and averaged. This parameter was monitored to give indication of how porous the produced sinter was as it measure the total flow through the sinter was complete.

v) **Flame front speed**

Flamefront speed is an important parameter to monitor as it can give information on the thermodynamics and kinetics of the process. Flame front speed can also give indication on time spent above 1100°C and should correlate with sintering time. It is worked out by the following. Distance between each thermocouple = 70mm. Mid point of flame front assumed to be peak temperature of thermocouple. Time taken for each thermocouple to reach peach temperature is known. Thus, flame front speed can be worked out between each thermocouple. Flamefront speed FFS = D distance / T time.

vi) **Flame front thickness**

Flame front is established at 1100°C and time (T1a) this occurs is recorded. Peak thermocouple temperature = mid-point of flame front and time (T1b) is recorded. Speed between two thermocouples given by formula above. Flame front thickness is a distance so flame front thickness D = flame front speed S x time taken from flame front establishing (1100C) to hit peak temperature (mid-point). Flame front thickness was an important parameter to monitor as it allowed the user to monitor how long the sinter was subjected to temperatures above 1100°C which could then be related to sinter quality. I.e. D = S * T mm = (mm/s) * (T1b-T1a)

vii) **Cooling rate**

Defined as the rate in which the sinter cools from its maximum sintering temperature down to 600°C. Peak temperature monitored and time (T1b) is recorded. Point at which sinter cools down to 600°C is monitored and time (T1c) is recorded. Cooling rate also recorded from peak temperature to 1100°C and 100°C. Cooling rate was monitored to see if there was any correlation between the sinter quality and cooling rates of the sinter as phase formation is highly dependent on cooling rates of the product. Cooling rate from maximum temperature to 1100C can be defined as flame front cooling rate. Cooling rates from 1100°C to 600°C can be defined as sinter cooling rate. Cooling rate = (maximum peak temperature – 600) / (T1c-T1b)

3.1.9 Reproducibility

i) **Sintering tests**

The sinter pot test is a robust experimental analysis proven in the repeatability and validation study of this project. The data from the validation was used to determine what was considered to be measurable variation within the data for each of the subsequent experimental investigations undertaken. It must be clear that due to the industrial demands of the project, there were limitations at hand such as resource, time on kit, material availability and working around a schedule that supported the production plant. However, during the repeatability and validation study, the data acquired was sufficient to make up the standard deviation of process parameters and the standard error that the sinter pot produces. All tests were repeated and standard error explicitly stated within the text, with error bars on charts where applicable.

ii) **Optical microscopy and EDS Analysis**

Each batch of sinter was optically analysed. Over 6 physical sinter samples analysed per test and over 15 locations analysed per sinter sample in order to ensure representative samples. EDS analysis was done over numerous areas to ensure representative features were analysed. Due to the representative optical microscopy, this analysis followed suit.

iii) **TGA Analysis**

When identifying thermal characteristics of the fuel presented in this project, the analysis was run x5 times per particles size in increments of 1mm as well as characterising less than 0.5mm and 0.5-1mm. It was also decided to run the analysis on different particle sizes of the fuel as well as different masses to understand and ensure representative analysis was undertaken.

3.2 Commissioning

This section will focus on the commissioning of the project. This includes laboratory set up, design of the manual, various COSHH/risk assessments and a safe working procedure (official SOP can be found in the appendix 1). This section aims to give a brief overview of all the equipment needed to produce and analyse iron ore sinter. It discusses both the importance and relevance of all the equipment needed.

3.2.1 Laboratory configuration

The laboratory set up can be seen in figure 30 below. Pipework infrastructure was designed to mimic plant operations at a laboratory scale. A granulation drum was designed to provide control over granulation characteristics and average granule size of sinter raw mixture. Everything in the laboratory is needed to produce iron ore sinter. This includes raw materials, moisture meter, hearth layer, granulation drum, gas rig, sinter pot rig, ignition burner, flow meter and a computer panel. There are several zones within the lab. These are: the granulation zone, the desk zone, the gas alarm zone, storage zone, computer system zone, sinter pot zone and gas rig zone. Each zone has its own safety precautions and step-by-step guidance in the user manual which can be found in the appendices.

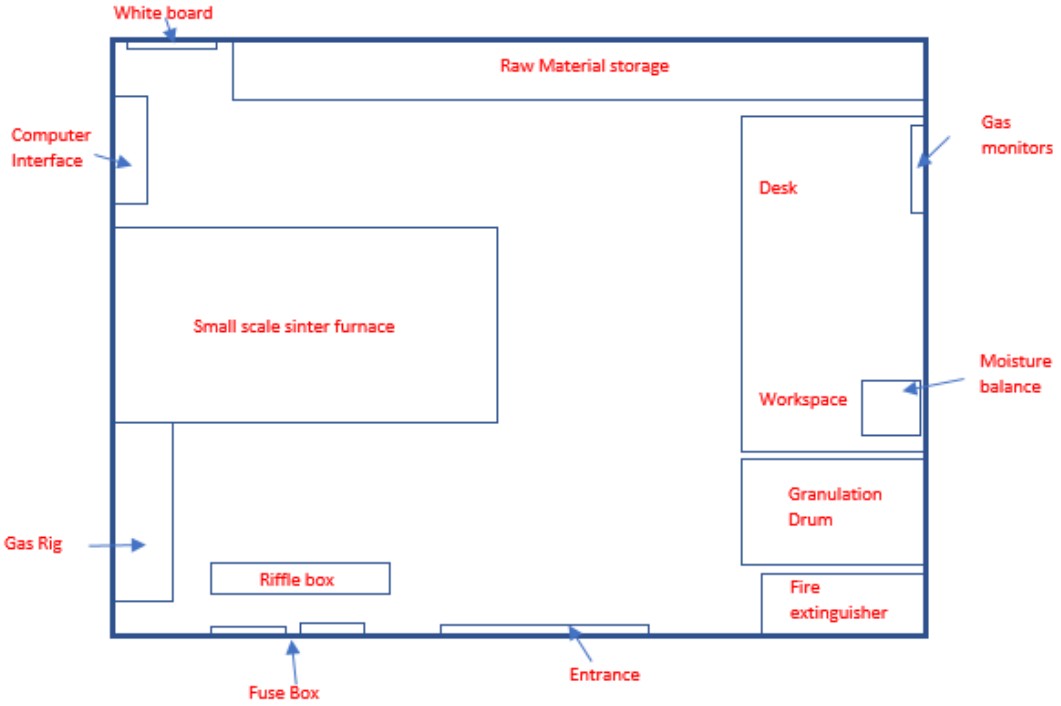

Figure 30: Laboratory configuration

As mentioned earlier, everything you need to make iron ore sinter has been put into the sinter pot lab. The following will outline what these are, how they are used and why it is used to make iron ore sinter. This includes raw materials, such as iron ores, fluxes and fuels, a moisture balance, a granulation drum, a riffle box, a dual system sinter pot, computer panel and discharge barrel.

- **Raw materials** - Raw materials are stored in the lab as well as a recently commissioned storage facility close by. Raw materials include iron ores, such as concentrates and other ores rich in hematite. Fluxes such as limestone, olivine and magstone. Fuels such as coke breeze and anthracite. It was decided that material that would be used to make up a blend would be dried and screened before being used - known as material preparation. This was done to achieve optimum granulation and wetting, as well as having a homogeneous blend before granulation.

- **Moisture balance** - A moisture balance was needed to accurately measure the blend moisture percentage at different stages of the process. As mentioned previously, moisture is an essential component in granulation. It was decided that an atomised spray was best to use as it deposits liquid covering a large surface area.

- **Blend mixer** - a cement mixer is located in a different lab due to dust generation. This is to mix the blend prior to granulation to obtain a completely homogeneous mixture.
- **Granulation drum** - Granulation drum is needed to granulate a material and increase its mean particle size. This is to increase the permeability of the blend as required.
- **Riffle box** - The riffle box is used to split a sample into two. The riffle box plays a unique and important role in the process where it splits a granulated blend into two representative samples. This allows for a repeated test with the exactly the same granulation conditions.
- **Dual Sinter pot rig** - the sinter pot is located in the middle of the laboratory. It is a dual system so one pot can be prepped whilst the other is operational.
- **Computer panel** - The computer interacts with the sinter pot rig and allows the user to alter set point for the experiment. Set points include desired pressure drop during the process. It also allows the user to record and monitor the process via thermocouples
- **Discharge barrel** - Allows for the sinter to be discharged in a repeatable and safe manner.

3.2.2 Manual and procedure design

The following section will go into how the experimental apparatus are used in detail and explain their importance to the process as well as focusing on raw material and blend preparation, sintering process, and post analysis.

- **Mixing and sieving** - The mixing of material is important, specifically getting the correct particle size distribution for a homogeneous mixture. It is important to dry all materials to around 0.2% moisture prior to mixing and sieving to avoid granulation during mixing. It is also important to sieve materials to the correct particle size before mixing. This is done to optimise the productivity of the granulation and sintering process. Particles greater than 1mm are defined as nuclei. Particles smaller than 0.25mm are defined as adhering or layering particles. Particles in the size range of 0.25-1mm act as intermediate particles where they either act as a nuclei or adhering particle, or neither. Therefor, it is sometimes good practice to keep this fraction to a minimum. Information on this can be found in chapter 2 as well as the available literature [61].

- **Granulation** - As previously mentioned, there is a need to granulate the mixture before it is charged into the sinter furnace. Granulation involves the coating of fine particles onto coarser particles to increase the average granule size of the mixture via liquid bridges. The objective of granulation is to create a homogeneous permeable mixture. The high porosity and permeability level of a bed helps draw the flame front downwards when sintering. Higher moisture up to a point helps particles to adhere to one another through the creation of liquid bridges during granulation. In industry, around 6.5% moisture is known to be the optimum moisture content for granulation and sintering. Information on this can be found in the literature mentioned earlier in chapter 2 and a small set of experiments was carried out to find the optimal moisture content in terms of flow and permeability and results complemented the literature. This report can be found in a later section of this chapter. The blend is mixed in the granulation drum whilst a known amount of moisture is added via spray can in an atomised fashion. It was calculated that, if the pre-granulated blend had a moisture content of between 0-0.2% then 1.1 liter of liquid should be added to achieve a total granulated moisture content of between 6.2-6.5%. The granulation drum was design so it could hold 16kg of mixture with 18/20% filling degree to obtain the correct flow characteristics mentioned earlier in the literature review. As the pot can hold 7kg of granulated mixture, a 16kg granulated mixture could be split with a riffle box into two representative 7kg mixtures which leaves an extra 1kg per test that could be analysed if needed. It was decided upon a small set of experiments that the best RPM for optimum flow characteristics being cascading/rolling motion was 20 rotations per minute given the dimensions of the drum. The dimensions of the granulation drum had a radius of 180mm and a length of 400mm. Please see report on flow optimisation below for further information on flow characteristics. The sinter plant granulation drum also uses the same filling degree, however, the sinter plant's granulation drum is part mixer and part granulation and is continuous whereas the lab-scale granulation drum is solely for granulation. For this reason it was decided to mix for 2 minutes and granulate for 5 minutes once moisture has been added, replicating plant conditions in terms of time spent in the drum/mixer. Figure 31 below shows the granulation drum placed in the lab. Once granulated it was decided to split the granulated mixture into two representative samples. This was to allow the user to conduct a repeat test with identical granulation flow characteristics.

Figure 31: Granulation drum

- **Sintering** - As previously mentioned, the sinter pot rig design was a dual rig. This allowed for one pot to be operational whilst the other could be prepared. This allowed for rapid testing when needed. Figure 32 shows the dual sinter pot design

Figure 32: Sinter pot dual system

The small-scale sinter furnace is 100 mm in diameter and around 500 mm in length and was designed to accommodate a 7kg blend and produces around 6.5kg of iron ore sinter with the remainder accounted for by oxidation losses and combustion. A photo of the sinter pot can be seen in figure 32 above and exact dimensions can be seen be seen in figure 33 below.

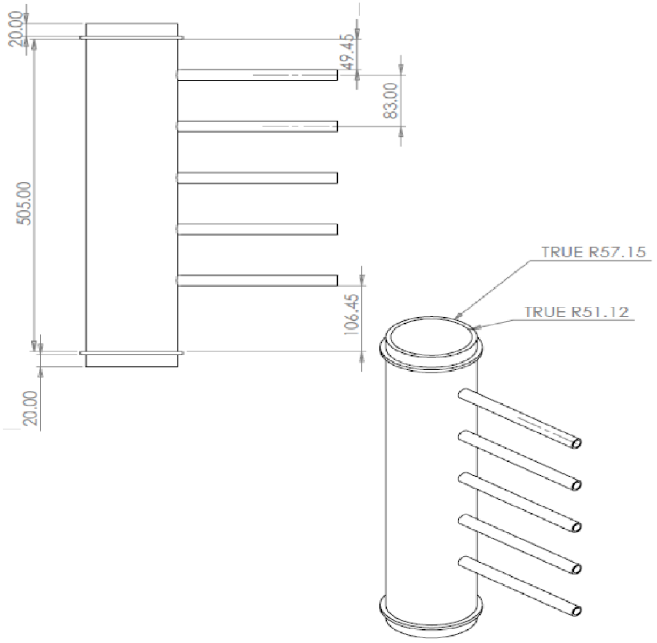

Figure 33: Sinter pot dimensions

There are 2 furnaces connected on an axial with the concept of running one furnace while preparing the other. This also gives the ability to get quick results and rapid testing. There is a ceramic insulation case that should be clamped to the sinter pot to ensure minimal heat loss. The pot was designed to accommodate 7 thermocouples in total, with the potential of an eighth. 5 type R thermocouples can be embedded into the furnace via steel tubing, to monitor temperature and flame front characteristics. Type R thermocouples were used to deal with the high temperatures exhibited during sintering. There are 2 type K thermocouples placed within the centre of the exhaust pipework to monitor waste gas temperatures. There are 5 steel tubes protruding out of the furnace for the type R thermocouples to slot into with rubber plugs ensuring

a seal. It was decided to place the thermocouples into the sinter pot after the pot had been charged. This was done to minimise unwanted cavities when the blend falls onto the ceramic sleeves, as it may not completely fill the space underneath. The off-gas thermocouples are fixed directly underneath the furnace and another further down (1m) the pipework. A flow meter was designed to be fastened on to the top of the furnace to record flow rates prior to and after ignition. This is to give indication of bed permeability. It was decided that a cold flow rate measurement across the bed prior to ignition would be of value. This gives indication of bed permeability which is crucial for productive iron ore sintering.

Figure 34: Ignition of sinter pot

A burner head and gas rig were designed to ensure robust, uniform ignition. The burner head is 100mm in diameter with 25 small jet holes. The top of the sinter bed, directly after ignition can be seen in figure 34. A combination of compressed air and natural gas was used in the gas rig to fire up the burner head. The sinter furnace is connected to an extraction system via pipework including a butterfly rotork servo-valve which is connected to the computer panel. The conditions for each test are controlled by a PID feedback system and a computer interface which communicates between the sinter furnace, servo-valve and the control system. This computer system logs process

parameters and displays a live readout. The computer interface also allows the user to choose parameter set points for the process, in particular the pressure-drop across the bed that the extraction system produces. This set up allows for the furnace to run at a given pressure-drop desired by the user. Once the set point has been input into the computer system, the computer interface sends signals to the butterfly servo-valve which in turn will open and close accordingly to maintain that set point. Before charging the pot with the granulated blend, a hearth layer is introduced. The hearth layer is there to ensure the new sinter fuses to the hearth layer and not the steel mesh at the bottom of the pot. It was also decided that when charging the pot it must be done in a controlled and repeatable manner. The pot should be charged in alternating directions in order to navigate away from preferential packing. This was mentioned in the literature review earlier in chapter 2. A preferentially packed pot could alter the propagation route of the flame-front i.e bigger particles along one side of the pot would allow the flame-front to descend downwards faster than the other side of the pot that was packed with smaller particles. One minute of ignition was deemed a sufficient ignition period after successful trials. It was also decided to over fuel the pot in order to achieve the high temperatures needed for iron ore sintering and to accommodate for the substantial heat loss due to the small dimensions of the design. The discharging of the sinter pot must also be controlled and repeatable. With this in mind, a discharge barrel should be placed under the pot when discharging and minimal mechanical noise must be present when dislodging the sinter from the pot once turned upside down. Once the pot has been charged and thermocouples positioned, the system is set up. Finally, suction can be applied and once desired pressure drop is reached, the top of the pot can be ignited for one minute and then the sintering process is allowed to commence. During the process, data can be monitored via the control system which displays live data. Live data includes flow rates, pressure drop, embedded thermocouple temperatures as well as off gas thermocouple temperatures. The live data is recorded and can be exported for further analysis.

- **Post analysis** - It was decided that once the sinter cake had been discharged, a sinter yield value would be of use to give an indication of how much sinter is being produced as well as giving some indication on cold strength. Once discharged, the sinter cake is transported to a mechanical sieve. The mechanical sieve applies a strong vibration which breaks the sinter apart where it then falls through a number of screens at different size fractions. This gives an indication of yield as well as a qualitative cold

strength between a series of tests. Sinter in the size fraction of between 16-20 mm would be subjected to X-ray fluorescence to monitor chemical composition. This was decided as it is follows the procedure of that of the sinter plant. Furthermore, it was decided that reduction degradation testing would be done on this size fraction as well. As mentioned, these measures were decided as it is the same procedure taken by routine inspections of sinter produced by the production plant to ensure no quality issues. X-Ray Diffraction should be deployed in order to investigate phase mineralogy of the sintered cake. This should be incorporated into the analysis further down the testing line.

3.2.3 Safe Operating Procedure

Safe operating procedure was produced in compliance with Tata Steel regulations and standards and was published internally. This can be found in the appendices.

3.3 Process Optimisation

This section investigates what the optimal parameters of the small-scale sinter pot are and sets out to clarify what parameters will be relied on to undergo accurate analysis in the following technical chapters.

3.3.1 Optimal Moisture, Granulation Time and Granulation Speed

The following section goes through a series of experiments investigating optimal granulation parameters in terms of granulation time, drum speed and blend moisture for optimum bed permeability when using the recently commissioned sinter pot.

Introduction

Granulation speed is important in obtaining a good granulated mixture with increased average granule size. It is essential in producing correct flow characteristics within the granulation drum. A fine balance between rolling and cascading flow motion is desired. Moisture is the driving mechanism in agglomerating these particles together during granulation via liquid bridges. Granulation time is important as there will be a moment in time as to when all adhered particles have agglomerated to a nuclei. Hence why it is important to take into consideration the granulation speed, granulation time and moisture when choosing optimal parameters. It is worth noting here that the filling degree of the drum was maintained at 18% in the following experiments in order to some what represent plant conditions. Please see literature review in chapter 2.4 for more information on flow characteristics in granulation.

Experimental plan

Tests were carried out using the recently commissioned sinter pot and a granulation drum. Please refer back to section on commissioning for granulation drum and sinter pot dimensions The granulation drum has 10 speed settings going from the slowest (1) to the fastest (10). Please refer to earlier section for specific RPM per speed setting. The butterfly-valve was fixed for these experiments. Extraction fan was allowed to run for 30 seconds before readings were recorded over a 2 minute period. Flow rate and pressure drops were recorded at 5 second intervals. The blend used in experiments can be seen in the table below and chemistry of the blend was kept constant through out all experiments. It must be noted

here that for the purpose of this study, the butterfly-rotork valve remained open at 100% to ensure accurate flow rates according to blend properties. 400g of hearth layer was used and same hearth layer used through out this experiment. The blend was then introduced and charged to the pot via the standardised charging method. The blend was then levelled off at the top of the sinter pot with a ruler to avoid any additional packing. Once charged, flow meter was then locked into place. Suction was then applied at 100% and data recorded for a 2 minute per test at 5 second intervals. Once flow rate had been recorded, the sinter pot was unlocked and the blend discarded. Please note: The blend was taken from plant and allowed to dry. Please see following for experiment variables.

i) Granulation time

For this phase of experiments, granulation speed and moisture content were kept the constant through-out. Moisture reading was kept at 4.4%. Granulation speed kept at 20 rpm through-out. Moisture readings were taken at intervals through out to ensure no major changes. Each test subjected to granulation for a set amount of time as desired. There were 10 cold flow permeability tests in total with additional repeats. Starting from 1 minute and increasing in 1 minute intervals per test up to 10 minutes.

ii) Granulation speed

For this phase of experiments, granulation time and moisture content were kept the constant through-out. Moisture reading was kept at 4.4%. Granulation time kept at 5 minutes. Moisture readings were taken at intervals through out to ensure no major changes. Each test was subjected to a different granulation speed. Granulation drum had 10 different speed settings starting from 1 and ending at 10. Please see earlier section for speed setting rpm.

iii) Granulation moisture

For this phase of experiments, granulation time and speed were kept constant through-out. Granulation speed kept at 20 rpm and granulation time kept at 5 minutes. Moisture readings were taken at intervals through out to ensure desired moisture content is correct. Each test was subjected to a different moisture content. Starting from 2.43% moisture up to 8.6% moisture. Moisture was increased in increments of 0.8%-1% and 7 tests done in total, with additional repeats. Moisture balance was used to ensure correct moisture. Moisture was added using standardised atomised spray. It can be noted here that once desired moisture was deposited into drum, granulation for 5 minutes would then begin.

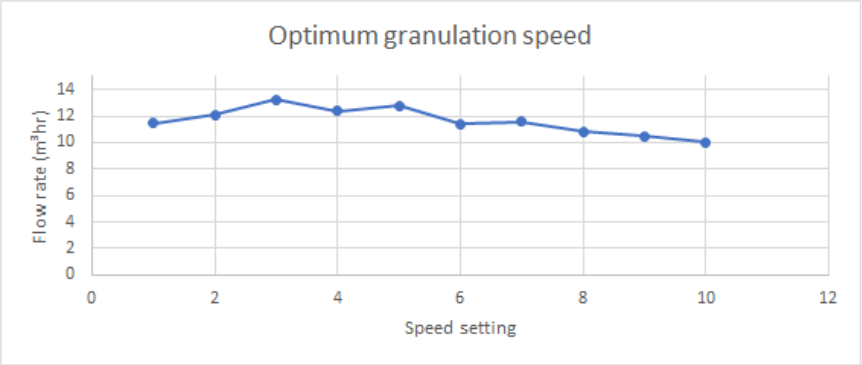

Figure 35: Impact of granulation speed on bed permeability

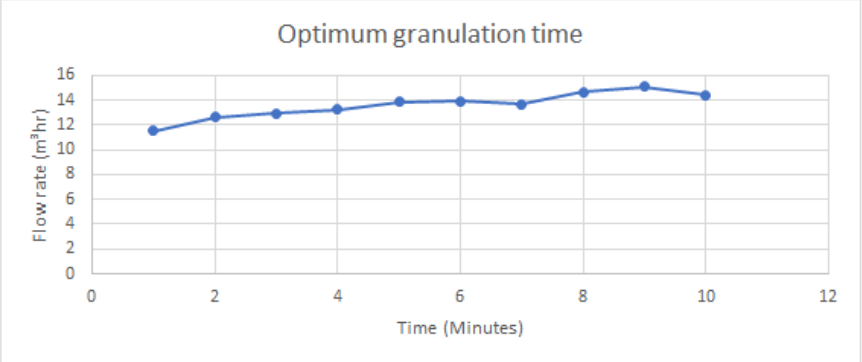

Figure 36: Impact of granulation time on bed permeability

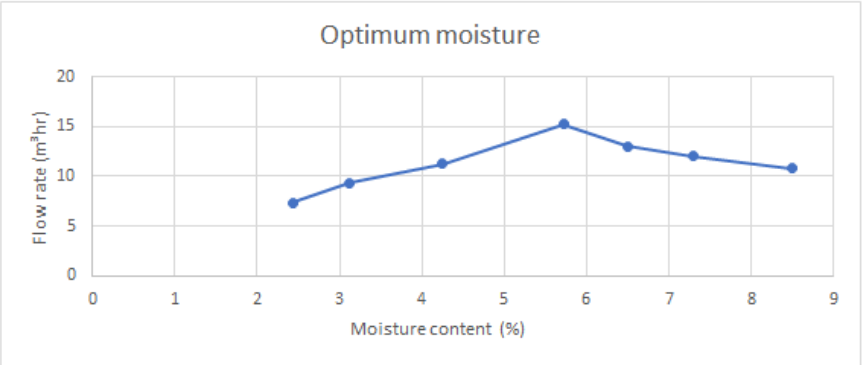

Figure 37: Impact of moisture addition on bed permeability

Discussion and Conclusion

Figure 35 shows a graph of increasing granulation speed and flow rate. Flow rate was used to give an indication of permeability trends. It was evident that on increasing granulation speed, bed permeability increased up to a point and then started to decrease. This indicated that for flow characteristics of rolling and cascading were evident for the blend with maximum flow rates evident. This occurred at a speed level of 4 which is 20 rpm, given a filling degree of 18% and a moisture level of 4.4%. This indicated that a granulation rotating speed of 20rpm, given the dimensions of the granulation drum, was most optimal in producing the maximum flow rate through the bed. Maximum flow rate was indicative of maximum permeability. Optimal granulation speed resulted in maximum granule size which was not impeded by the pressure drop. When analysing figure 36, it was evident that average flow rate through the bed increased with increasing granulation time. However, this started to decrease after 7 to 9 minutes of granulation. This was due a balling effect when granulation time surpassed 7 minutes. Balling is where too many adhering fines are agglomerated together which collapse under pressure. This was also evident from the decrease in the graph as the balling started to collapse under the large pressures which in turn actually decreases flow rate and thus permeability. it must be noted here that even though this trend does not fall off the edge of a cliff after 9 minutes, it was deemed optimum due to the time constraints of the procedure. Going forward, 5 minutes will be taken as sufficient granulation time to be somewhat representative of the production plant's granulation drum. When analysing figure 37, it was evident that bed permeability increased as moisture levels increased up to around 6% and the started to decrease. This coincides with the moisture content set point usually maintained at a sinter plant. It can be noted here when moisture levels were above

8.5%, the blend turned into a sludge and so was not operable. To conclude, it was clear that optimal moisture content for granulation and bed permeability was around 6% when using a maximum flow rate through sinter pot as an indicator of maximum bed permeability.

Going forward, the following will be used. A moisture reading of 6-6.6% is recommended. A granulation speed of 20rpm given granulation drum dimensions and filling degree used. A granulation time of 5 minutes but total time would equal around 7 minutes once all moisture had been added.

3.3.2 Optimal pressure drop

This section aims to investigate optimal pressure drop for operating the small-scale sinter pot with least variation and maximum stability.

Introduction

The pressure drop across the sintering bed is of vital importance in flame front propagation. Adequate suction i.e pressure drop, allows the flame front to propagate downwards in a stable and uniform manner, creating the correct conditions for ideal sintering to take place. A low pressure drop, in theory, would produce low suction and therefor only allow the flame front to descend downwards with a decreased speed as appose to when using a higher pressure drop. This study was initiated to find the sinter furnace's optimal pressure drop with regards to the process/ and to see what influence this has on process parameters and in particular flame front characteristics. Reduction degradation index testing and chemical analysis of the produced sinter was also analysed.

Experimental Procedure

The experimental plan followed the same outline as stated in the above sections. The main discrepancy in experimental parameters was the different pressure drops applied. For more information on experimental design please see commissioning section. A total of 10 tests were conducted using the same blend and same parameters across all tests apart from altering the set point for pressure drop per test. All tests consisted of the same blend with identical chemical composition. All ores were dried and screened to sub 5.00 mm. Fuel was dried and screened to sub 3.0 mm, flux was dried and screened to sub 3.00 mm. The dry blend was then mixed in the cement mixer for 2 minutes to obtain a homogeneous mix. The blend was

granulated for 5 minutes where 1.1l of moisture was added to bring blend moisture reading to 6-6.5%. After granulation the blend was split into two representative samples using the riffle box. The sinter pot was filled with 400g of hearth layer sized between 10-16mm. The blend was then charged into sinter pot scoop by scoop alternating 90 degrees in direction each time to avoid preferential packing. All tests had an ignition time of 1 minute. All tests were repeated. Each blend contained the following constituents:

Table 1: Blend composition

Blend material	kg	%
Sinter Fines	1.94	
sinter feed A	1.55	
Sinter feed B	1.74	
sinter feed C	2.74	
Sinter feed D	4.94	
Limestone	2.19	
Coke breeze	0.90	

Please note: Sinter pot tests were conducted at 7% fuel

A) **First Experiment:**

x2 pot test with a standard blend at 50mbar

B) **Second Experiment:**

x2 pot test with a standard blend at 75mbar

C) **Third Experiment:**

x2 pot test with a standard blend at 100mbar

D) **Fourth Experiment:**

x2 pot test with a standard blend at 125mbar

E) **Fifth Experiment:**

x2 pot test with a standard blend at 150mbar

Please note: Please see formula sheet for calculated parameters and experimental design for sinter pot dimensions.

Post analysis: Complies with sinter production plant policy

Results

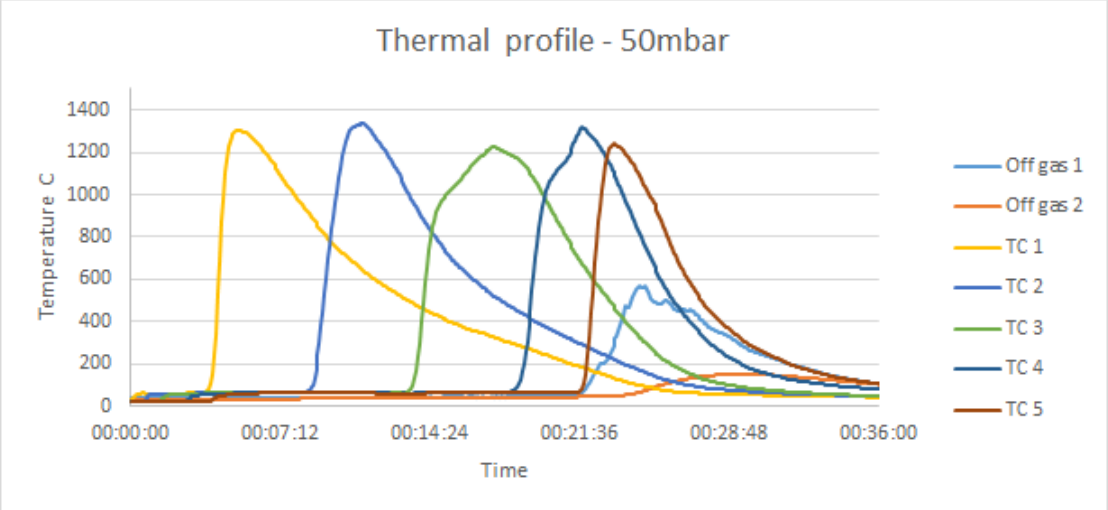

Figure 38: Process optimisation - Thermal profile 50mbar

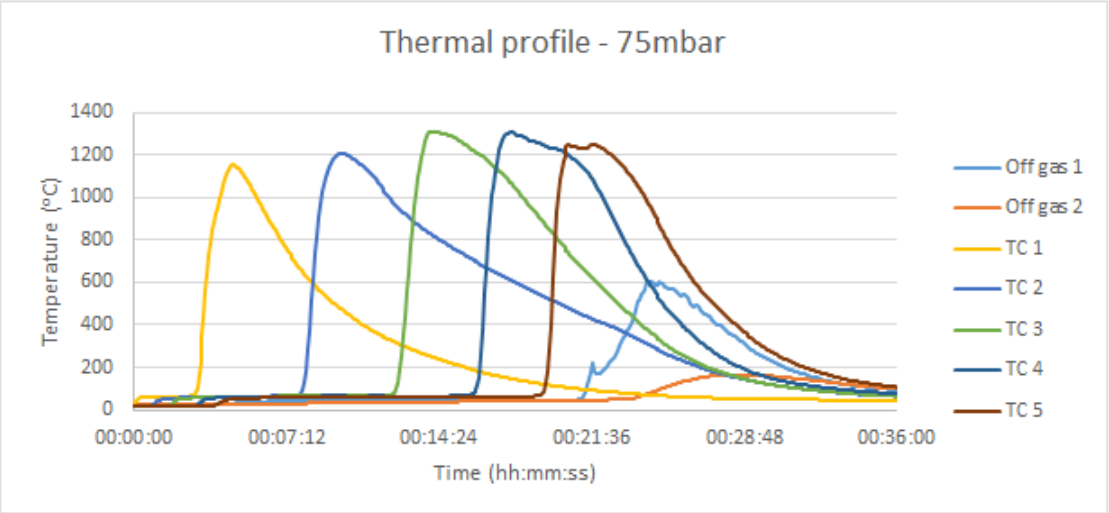

Figure 39: Process optimisation - Thermal profile 75mbar

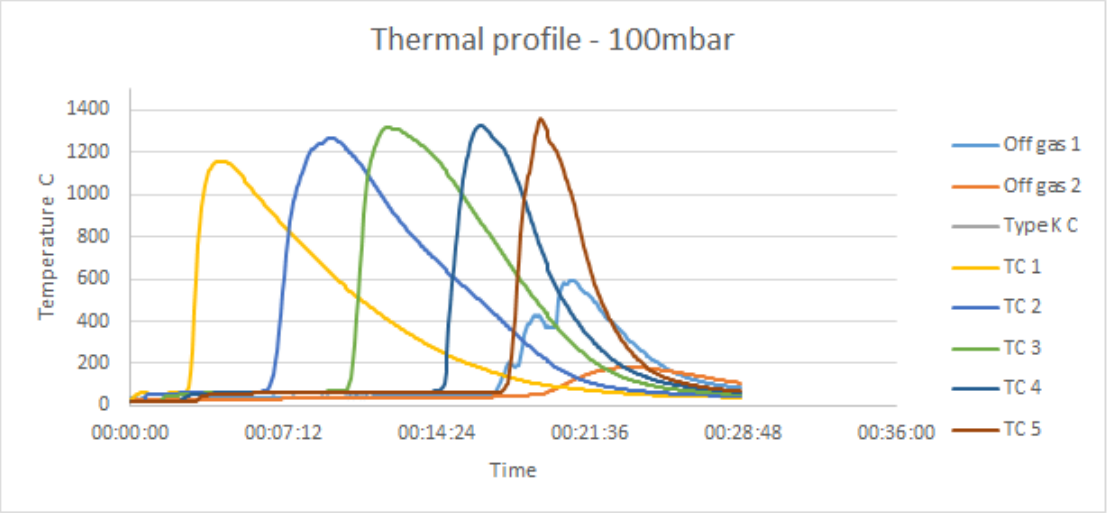

Figure 40: Process optimisation - Thermal profile 100mbar

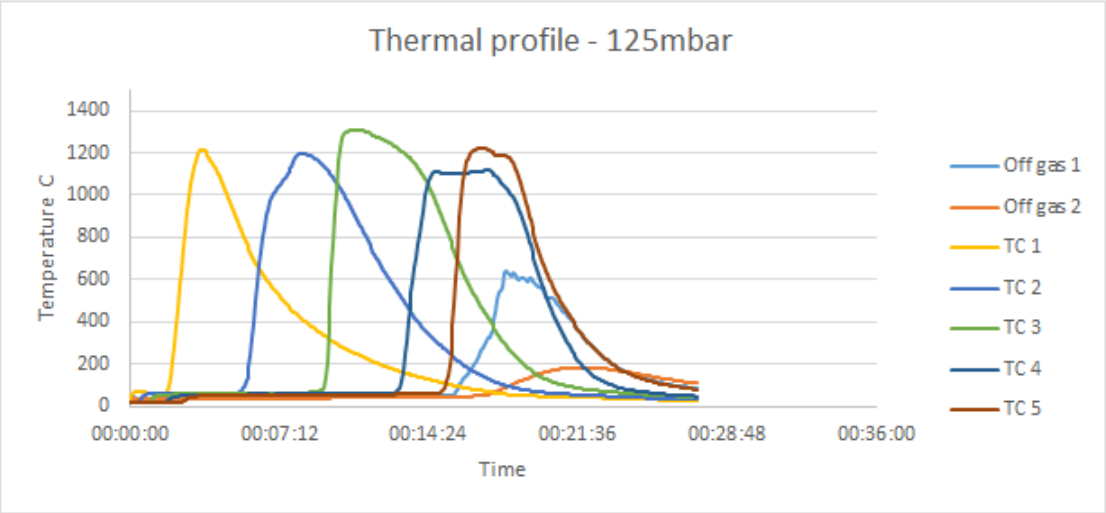

Figure 41: Process optimisation - Thermal profile 125mbar

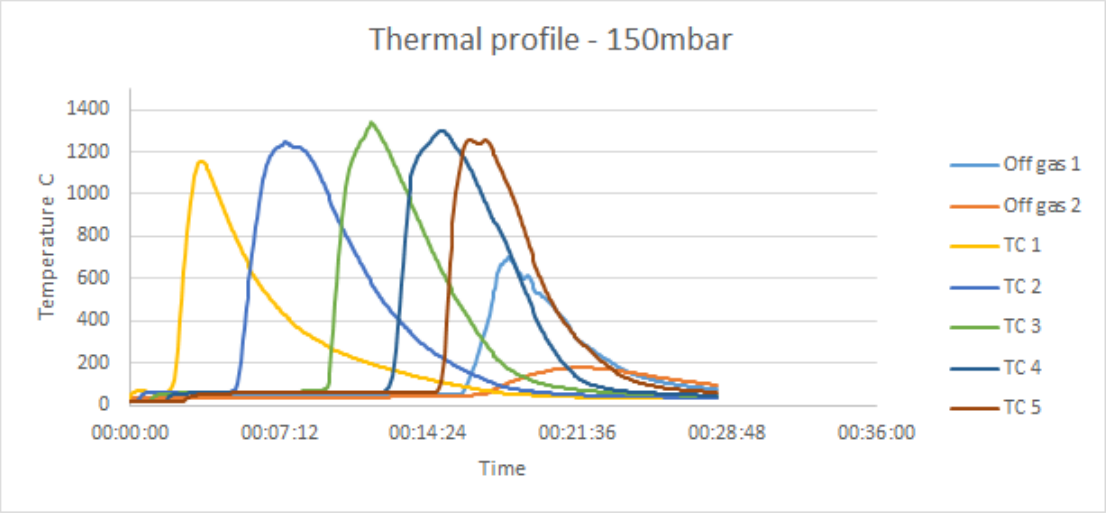

Figure 42: Process optimisation - Thermal profile 150mbar

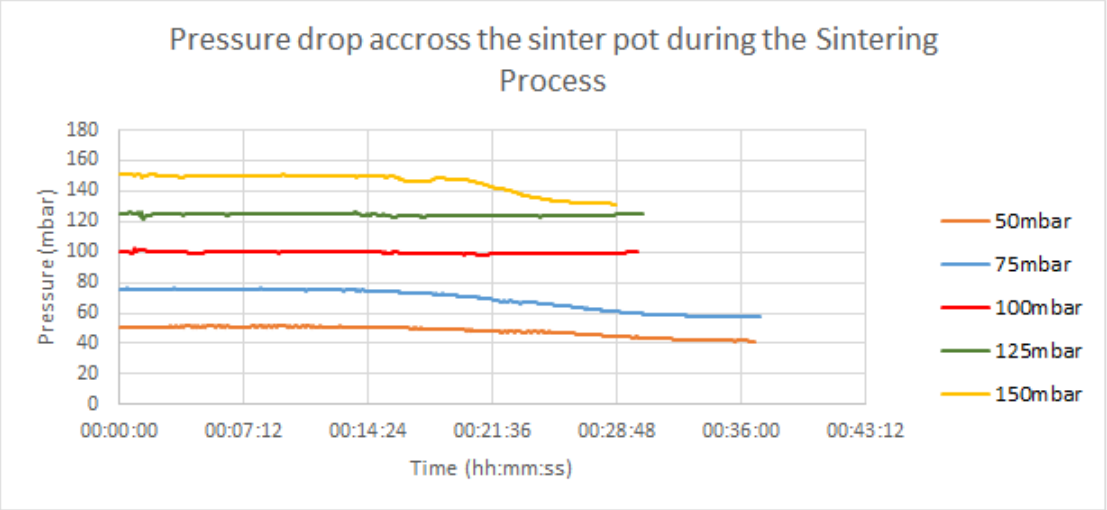

Figure 43: Process optimisation - Pressure drop across all experiments

Figures 38 to 42 show the thermal profiles from the experiments. On analysing the thermal profiles from 50mbar to 150mbar sinter pot tests, the following points can be made. At 50mbar of suction it was evident that each thermocouple trace starts to rise and peaks in a sequential manner, this indicated that the flame front travelled from the top of the sinter pot to the bottom in an orderly and uniform fashion. Each trace peaked one after the other also indicating a stable process. Off gas 1 and off gas 2 rise and peaked after all embedded thermocouples which indicated the flame front being diminished into a gas stream at the bottom of the bed. This is also true when repeating the test at 75mbar, 100mbar, 125mbar and 150mbar, all thermal profiles indicate stable and uniform flame front travel. However, on initial observation of all the thermal profiles, peaks seem to widen and increase in broadness but further analysis is required. Figure 43 shows the pressure drop across the bed for each test. It can be observed that when running at 100mbar and 125mbar, suction remains the same through out where as when using a higher or lower pressure drop, the system struggled to maintain a constant flow and drops off. On first impressions it seemed to drop off around the time as when the flame front is at the end of the process or even diminishing but further analysis required. Please see discussion below for further analysis.

Table 2: Process parameters for pressure drop study

Parameters	50mbar	75mbar	100mbar	125mbar	150mbar	Units
Pressure drop	100	100	100	100	100	mbar
Ignition time	01:00:00	01:00:00	01:00:00	01:00:00	01:00:00	m s
Cold permeability flow rate	8.24	8.43	9.52	10.07	9.93	M3 hr
Hot Permeability flow rate	6.07	6.39	7.16	8.14	8.18	M3 hr
Sintering time	00:24:35	00:24:20	00:20:45	00:18:10	00:18:25	hr:mn:s
Max sintering temp	1334.81	1311.17	1359.93	1309.71	1338.05	C
Peak temperatures						
Thermocouple 1	1303.60	1150.99	1157.57	1217.14	1156.46	C
Thermocouple 2	1334.81	1209.66	1269.26	1196.92	1245.28	C
Thermocouple 3	1223.60	1311.17	1316.08	1309.71	1338.05	C
Thermocouple 4	1316.24	1308.61	1327.76	1120.56	1300.93	C
Thermocouple 5	1239.80	1249.70	1359.93	1223.78	1256.63	C
Max off gas temp 1	567.82	604.76	593.32	636.83	700.95	C
Max off gas temp 2	150.81	165.04	181.62	183.03	178.73	C
Sintered airflow	28.08	31.11	63.31	56.91	50.08	M3 hr
Time above 1000C						
Thermocouple 1	03:25:00	01:40:00	02:30:00	01:50:00	01:20:00	mn:s
Thermocouple 2	03:35:00	03:10:00	04:00:00	03:30:00	03:15:00	mn:s
Thermocouple 3	04:40:00	05:05:00	04:30:00	04:40:00	03:00:00	mn:s
Thermocouple 4	03:45:00	05:15:00	02:50:00	04:05:00	03:30:00	mn:s
Thermocouple 5	02:20:00	04:05:00	02:15:00	03:00:00	02:45:00	mn:s

Table 3: Process parameters for pressure drop study

Parameters	50mbar	75mbar	100mbar	125mbar	150mbar	Units
Flame front speed						
TC1-2	0.23	0.23	0.22	0.25	0.29	mm/s
TC2-3	0.27	0.27	0.42	0.47	0.28	mm/s
TC3-4	0.32	0.32	0.27	0.18	0.34	mm/s
TC4-5	0.30	0.30	0.42	x	0.58	mm/s
Flame front width						
TC1-2	7.78	4.59	6.67	6.14	4.29	mm
TC2-3	11.97	10.77	33.94	18.67	15.40	mm
TC3-4	21.96	12.73	14.81	7.18	22.20	mm
TC4-5	58.33	13.70	19.09	n/a	49.58	mm
Cooling rate (Max-1100C°)						
TC1	5.86	18.37	9.29	12.34	8.56	°C/S
TC2	7.00	6.77	6.37	6.63	6.15	°C/S
TC3	5.67	3.47	4.21	3.46	9.23	°C/S
TC4	7.54	3.15	7.66	26.03	3.69	°C/S
TC5	8.53	5.91	10.13	5.42	10.94	°C/S
Cooling rate (1100°C – 600°C)						
TC1	1.79	2.56	1.82	3.57	5.26	°C/S
TC2	2.33	1.23	2.00	2.94	3.57	°C/S
TC3	2.78	1.92	2.50	4.00	3.70	°C/S
TC4	3.70	3.03	4.55	3.57	14.29	°C/S
TC5	3.57	2.78	6.25	5.26	4.55	°C/S

Discussion and Analysis

When analysing the data further, several calculated parameters can be established. On initial inspection of the thermal profiles it was mentioned that the profile traces seemed to widen as the pressure drop reduced. This can be clarified when looking at the total time taken for each test to complete. This can be seen in table 2 and 3 above and in the graph in figure 45 (b). This is backed up when looking at the average cold flow and hot flow in figure 44. As expected, it can be seen that as we increase the pressure drop set point of the system, we increase the flow rate across the bed. It is worth noting here, there was not much variation in maximum sintering temperature and only a subtle, if any, trend was found, this can be seen in figure 45 (a). However, when analysing the off gas thermocouple temperatures in figure 46 in can be seen that as we increase the pressure drop, an increase in off-gas temperatures is evident. This could be a conduction effect as at increased gas velocities there is less time for the gas to cool before reaching the off gas thermocouples.

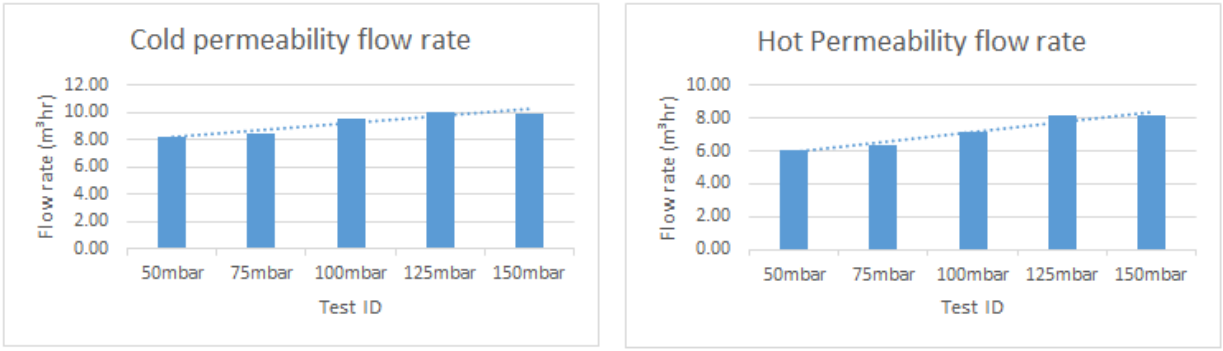

(a) Average cold flow rate across bed before ignition

(b) average hot flow rate across bed during sintering

Figure 44: Process optimisation - Average cold and hot flow

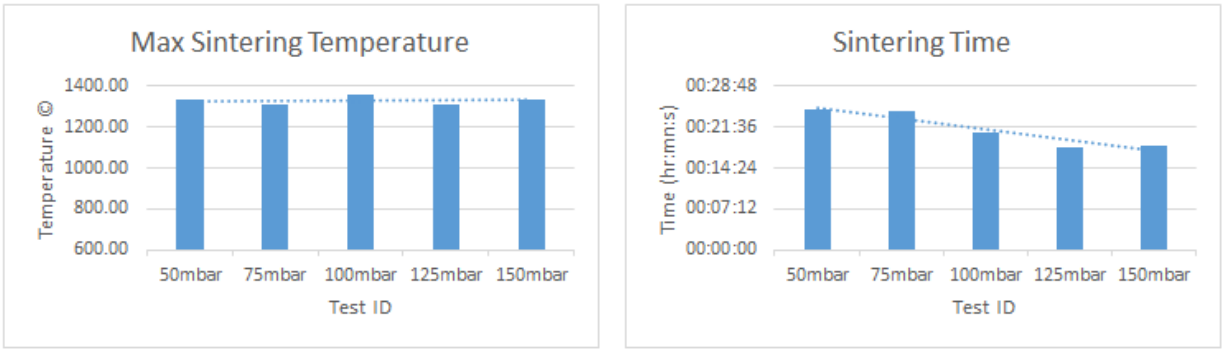

(a) Maximum sintering temperature

(b) Sintering time

Figure 45: Process optimisation - Sintering temperature and sintering time

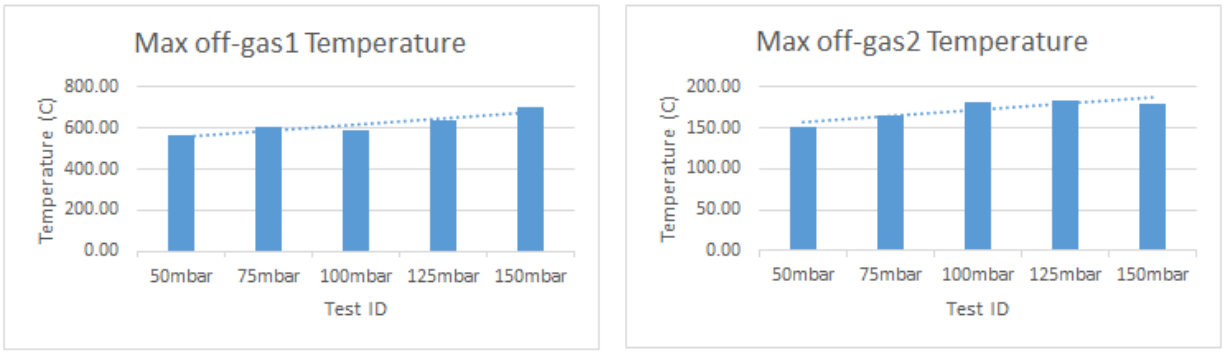

(a) Maximum off-gas1 temperatures

(b) Maximum off-gas2 temperatures

Figure 46: Process optimisation - Off gas temperatures

The analysis above established that the average flow rate increases and sintering time decreases as we increase the pressure drop set point i.e suction. Further analysis of flame front characteristics would be useful in understanding what occurs to the flame front when using a low or high pressure drop set point. Analysis of flame front characteristics can be seen in figures 47 and 48 below. Please see formula sheet for calculations.

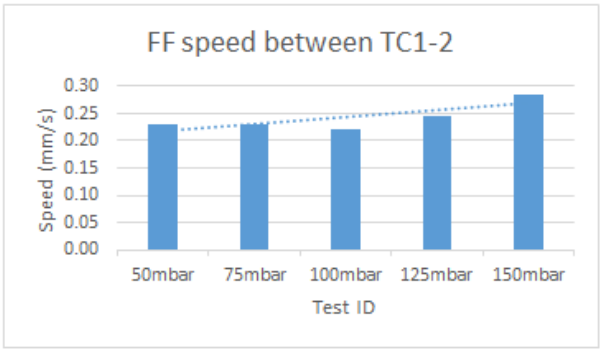

(a) Flame front speed

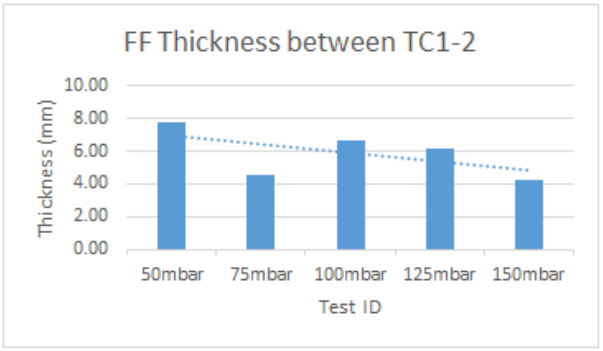

(b) Maximum off-gas2 temperatures

Figure 47: Process optimisation - Flame front characteristics

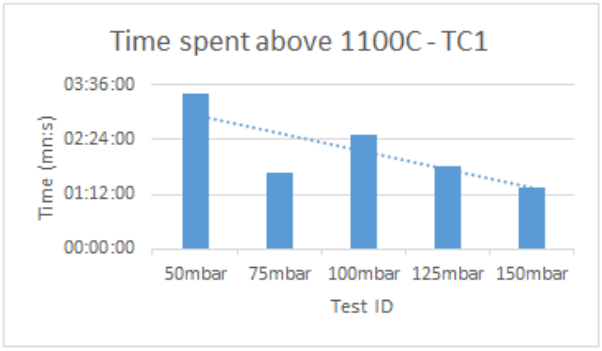

(a) Flame front speed

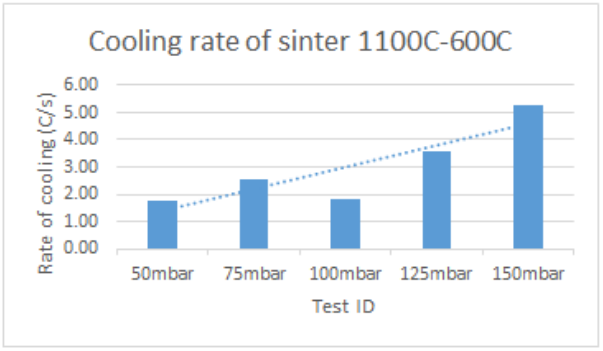

(b) Flame front thickness

Figure 48: Process optimisation - Additional characteristics

Figures 47 and 4 shows flame front characteristics, more specifically, flame front speed and flame front thickness. When analysing the graphs it can be said with reasonable confidence that there is a trend evident. When looking at figure 47 (a), it seems that as we increase the pressure drop per test, flame front speed is increased. This correlated with increased flow rate and sintering time. This occurs due to the additional oxygen in the system and additional flow rate experienced within the system due to the increased pressure drop. When analysing figure 47 (b) it can be seen that as the pressure drop is increased per test, flame front thickness decreased. This was potentially due to 2 reasons, the increased flow rate didn't allow the flame front to be held above 1100°C for a long period of time as it is being drawn down at an increased rate, or, due to the increased flow rate resulting in an increased amount of oxygen in the system, essentially fuelling the flame front whereby it increases the rate of oxidation reaction between the coke breeze and oxygen. This statement can be back

up by looking at figure 48 (a) as it can be seen that the time spent above 1100°C decreases as the pressure drop is increased per test. It should be noted here that when analysing the cooling rates of the sinter from 1100°C-600°C, as expected, cooling rates were increased per test as the pressure drop increased per test; due to the increased flow rate as a result of the increased pressure drop. It should be noted here for future reference that cooling rates may have influence on micro structural properties and morphology of the sinter and would be useful to subject sinter from each test to optical microscopy. Unfortunately this was not done for this particular experiment due to time constraints and sinter availability as reduction degradation testing and chemical analysis was undertaken instead. Before subjecting the sinter to the above analysis; the sinter was subjected to 1 minute of mechanical vibration to produce a sinter yield per test. This can be seen in figure 49 below.

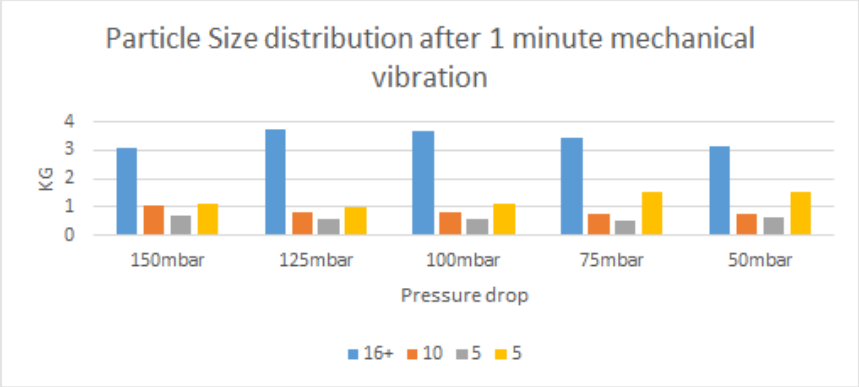

Figure 49: PSD of sinter per test after 1 minute of mechanical vibration

Figure 49 shows the particle size distribution of sinter per test after 1 minute of mechanical vibration. On first inspection, it was evident that there was not much variation between tests. However, on closer inspection it can be seen that sinter in the size fraction of below 5mm (return fines) per test was increased slightly as the pressure drop reduced per test. This can be seen in figure 50 where a slight trend is evident.

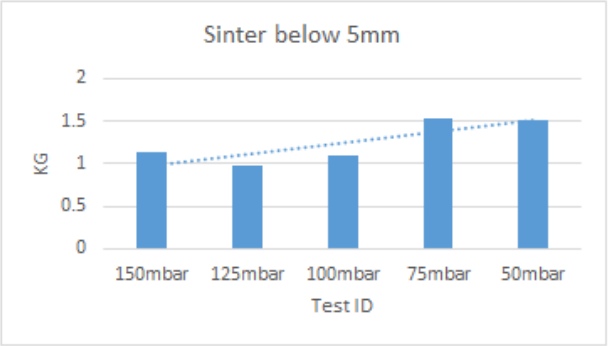

Figure 50: Process optimisation - Return fines analysis

Once the sinter had been subjected to 1 minute mechanical vibration to obtain a yield in size fractions, sinter from each test was subjected to reduction degradation index testing and chemical analysis. Chemical analysis was performed on sinter via XRF. This can be seen in table 4 below and RDI can be seen in figure 51.

Table 4: Chemical analysis of sinter per test

XRF	50mbar	75mbar	100mbar	125mbar	150mbar
SiO_2	5.83	5.36	5.51	5.64	5.49
Al_2O_3	1.06	1.1	1.04	1.06	1.09
TiO2	0.08	0.08	0.08	0.08	0.08
CaO	10.91	10.92	10.83	10.61	10.24
MgO	0.77	0.62	0.83	0.72	0.64
Fe	57.3	58.18	58.77	57.96	57.91
Fe_2O_3	69.91	72.84	71.72	72.14	73.14
FeO	10.82	9.31	11.08	10.67	8.7
P	0.028	0.027	0.029	0.029	0.029
Mn	0.14	0.14	0.18	0.13	0.13
Basicity	1.87	2.04	1.97	1.88	1.87
RDI	21.73	36.6	37.5	33.8	40.4

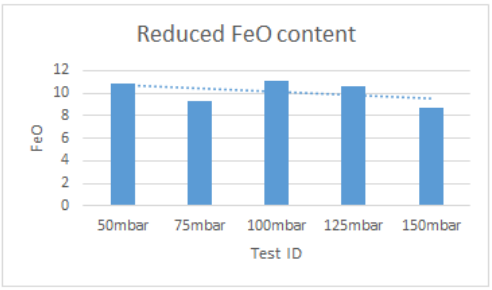

(a) Reduced FeO of sinter per test

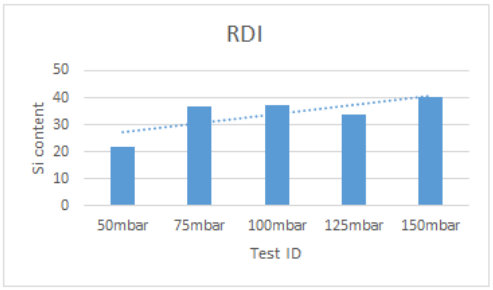

(b) Reduction degradation index per test

Figure 51: Process optimisation - Additional chemistry characteristics

When investigating table 4, it is clear that there is minimal variation in chemistry of the sinter produce per test. However, on closer inspection, it is worth noting here that there could be a small trend in FeO. This can be seen in figure 51 (a) where it seems that the amount of FeO relatively decreases as the pressure drop is increased. The decrease in the amount of FeO could be due to the fact that the sinter is not subjected to the high temperature flame front properties for a long enough period, as can be seen in figures 47 and 48. It must be noted that this is minimal and there should be more conclusive evidence before concluding on this matter. FeO has been known to vary with temperature. An increased sintering temperature allows for the rate of reduction and oxidation reactions to be increased and occurs more violently. [62] It is worth noting here that basicity of the sinter per test does not vary substantially and chemistry of sintered products are all in line with standard sinter plant quality indices. On analysing the data in figure 51 (b) on reduction degradation index testing, it can be seen that there is substantial variation in RDI values which indicates reducibility of the sintered product is influenced when using alternative pressure drops. It looked to be that on increasing the pressure drop, RDI values increased but trend is not conclusive as per the trend in FeO.

Conclusion

i) It was evident from the thermal profiles that flame front propagation was stable through out the experiments. However, Flame front speed increased as the pressure drop increased as a result of an increased flow rate through the sinter bed. Flame front thickness generally decreased as the pressure drop increased as a result of increased oxidation rates between fuel and oxygen due to the increased flow rate.

ii) It is also evident from the thermal profiles that maximum sintering temperature does not vary much, however, off gas temperatures are increased when using an increased pressure drop.

iii) It was evident that sintering time is decreased when increasing pressure drop set point.

iv) The amount of time the sinter was subjected to temperatures above 1100°C decreased when increasing the pressure drop.

v) Cooling rate of sinter is increased when increasing the pressure drop across the bed. It should be noted that further potential investigation on phase mineralogy would be useful in finding out if cooling rate has an impact.

vi) Sinter yield had minimal variation, however, return fines are slightly increased when decreasing suction rates ie pressure drop.

vii) Chemical analysis of sinter had little variation when increasing pressure drop, however, FeO content may be decrease as pressure drop is increased. Further investigation required to draw conclusions.

viii) Reduction degradation index values seemed to increase as pressure drop is increased.

3.3.3 Repeat-ability

This sections aimed to investigate the repeat-ability of the process and variation within the produced product when using the recently commissioned sinter pot. It aimed to investigate what variation there is between tests and impose a standard deviation per test parameter when analysing the process as well as quality of sinter.

Introduction

This section set out to test the robustness of the newly designed manual and safe operating procedure as well as determining the variation per test. It will allow for in depth analysis into the iron ore sintering process in terms of flame front propagation and sinter quality. Another objective to this set of experiments was to see how representative the sinter produced from the pot compared to sinter produced from the plant when making up a blend under ideal laboratory conditions. This was achieved via analysis of the process parameters recorded as well as chemical analysis and reducibility of the sinter via x-ray fluorescence and reduction degradation index testing. It was decided that a basic blend would be used for this set of experiments. The blend was chosen with nuclei to layering ratio (NTLR) in mind as well as chemical composition. This was achieved using an edited sinter plant blend model used for sinter plant activities. Simplicity was kept in mind when choosing a blend and thus the blend only consisted of 3 iron ores, a fuel and a flux. The iron ores chosen for this study are sinter feed A, sinter feed B and sinter feed C. Fuel being coke breeze and flux being limestone. The chosen blend can be seen in table below. It can be noted here a fuel

rate of 7% was chosen to ensure sintering temperature range could be reached for efficient sintering. This is 7% of the total iron ores within the blend. All iron ores were collected from the blending plant and stockyards prior to it being transferred to the sinter plant. The iron ores collected were dried to 0/0.2% moisture and screened to 5.0mm. The fuel and flux were also dried and particle size would be kept below 3.00mm. The individual dry iron ores were weighed out along with fuel and flux according to the table below. The weighed constituents were then deposited into a cement mixer and mixed for 2 minutes to achieve homogeneous mixture. The mixture was then deposited back into the bucket ready for the granulation drum. Process parameters such as granulation time, pressure drop set point and ignition time were kept as close to operational sinter plant standards as possible and are outlined in the methodology. Post analysis protocols were conducted in compliance with sinter plant operational standards.

Experimental Procedure

Experimental plan - Validation included 8 full sinter pot tests to investigate repeat-ability and accuracy. The blend composition remained the same throughout all 8 tests and is outlined below. Process parameters all remained the same throughout all 8 tests and are outlined below. Analysis techniques remained the same throughout all 8 tests and are also outlined below.

Material preparation - The small scale sinter pot holds 7kg of blend. The blend was made in 16kg batches, which is enough for 2 tests with 2kg left over for granulated blend analysis. Individual iron ores, flux and fuels were weighed out and mixed together for 2 minutes in a cement mixer to obtain homogeneous mixture. The blend was then deposited into granulation drum and turned on at 20 RPM. 1.1lite of water was added via atomised spray nozzle which takes around 3 minutes. The moistened blend is then allowed to granulate for a further 5 minutes. Once granulated the blend is split into 2 representative samples using a riffle box. Once split into two trays, moisture is checked and ensured to be between 6 and 6.5%. The trays are then transported to the sinter pot ready for charging.

Table 5: Blend composition

Blend material	kg	%
Sinter Fines	1.935	15.0
sinter feed A	2.258	17.5
sinter feed B	6.129	47.5
sinter feed C	2.581	20
Limestone	2.194	17.0
Fuel	0.903	7.0

Charging and sintering - After the blend was split using the riffle box. 400 grams of sinter from the production plant between 10-15mm was charged into the pot to act as the hearth layer. The blend was then charged into the furnace, scoop by scoop, in alternating direction of the charge by 90 degrees each scoop. Once charged, the top of the pot was levelled off without impeding the packing factor of the charged bed. Thermocouples with ceramic protection sleeves were then inserted into the sinter pot via the steel tubes (see earlier section). Insulation was then clamped around the sinter pot and flow meter positioned. Extraction fan was then turned on to achieve desired pressure drop of 100mbar. Once achieved, data is recorded for 5 minutes to obtain a cold flow permeability value. Once complete, the flow meter is replaced with the burner head and the top of the bed was ignited for 1 minute to allow for initial combustion. Flow meter is then fastened back into place and the sintering process allowed to complete.

Post analysis - The process was monitored via the computer panel and data recorded in 5 second intervals through out. Once all thermocouples had peaked and dropped to below 100C, the process was complete and the sinter cake discharged safely. Once discharged into the discharge zone, sinter cake was taken for post analysis. This included subjecting each sinter cake to one minute of mechanical vibration and screened into size fractions to give indication of sinter yield. Post analysis also included analysing the process parameters recorded via computer interface. This included temperature profiles and average flow rates, sintering time, flame front speed, maximum sintering temperature and so on. 300 grams of sinter cake between 20-25mm was taken and subjected to reduction degradation index test-

ing and 30 grams taken for x-ray fluorescence testing chemical composition. Sinter cake was also sectioned from thermocouple spots in case phase identification using X-ray diffraction techniques was desired.

Process parameter set points:

i) Fuel rate kept at 7%

ii) Moisture controlled to 6.2-6.5%

iii) Granulation time controlled to 5 minutes

iv) Ignition period controlled to 1 minute

v) Pressure drop set point maintained at 100mbar

Results and Discussion

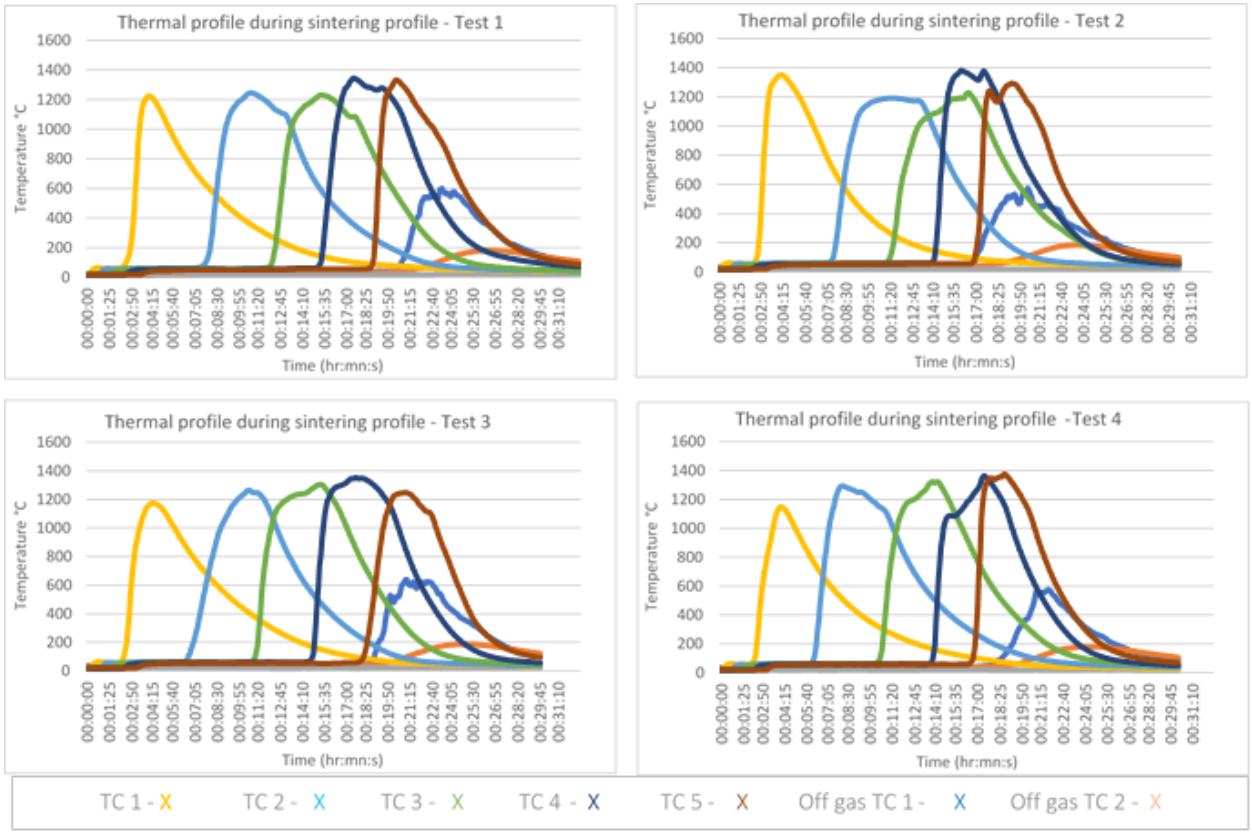

Figure 52: Thermal profiles for repeat-ability Test 1 - 4

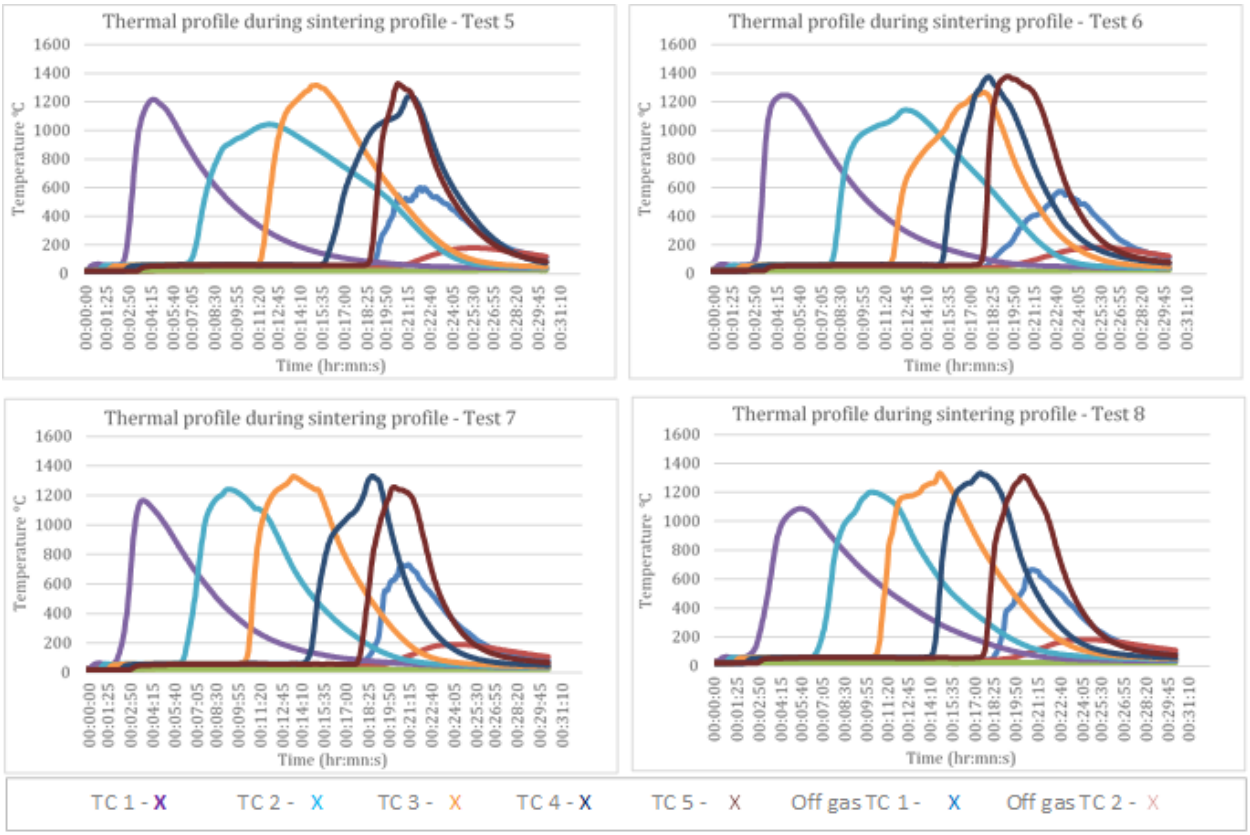

Figure 53: Thermal profiles for repeat-ability Test 4 - 8

Figures 52 and 53 show the thermal profiles for the sinter pot tests conducted. The legend is applicable for all graphs. Temperature on the y-axis and time on the x-axis. All sinter pot tests are initiated from 00:00:00 and burner head is applied at the same time for each test. TC1-5 are embedded thermocouples and off gas TC1-2 are the thermocouples placed in the pipework below the sinter pot in the wind-main. On analysing the thermal profiles, it was evident from visual appearance that all temperature profiles were relatively uniform and exhibited the similar characteristics. most importantly, TC 1-5 traces start to rise one after the other and drop in a sequential manner. This indicated a stable process as the flame front travelled in a stable manner, passing each thermocouple without any additional flame fronts reigniting or the flame front breaking apart. Off gas TC 1 and 2 also rise and drop in a sequential manner and peak after all embedded TC1-5 traces. This indicated that the flame front passed the last embedded thermocouple and then diminished into the gas stream after it passed the hearth layer. The peak point of the off gas TC 1 trace is the 'burn through point' and this indicated the sintering process has finished. It was decided that sintering time would be taken from the moment TC1 recognises the burner head being applied (TC1

> 50°C), to the burn through point (peak point in off gas TC1). It was evident from table 6 and figure 54 (a) that all tests finished between 00:20:15 and 00:23:15 with a standard deviation of 1 minute and 6 seconds. Maximum sintering temperature recorded over all tests was 1381°C and the lowest maximum sintering temperature was 1326°C. Standard deviation can be seen in the table below and on initial observation it was evident that all experiments exhibited minimal variation.

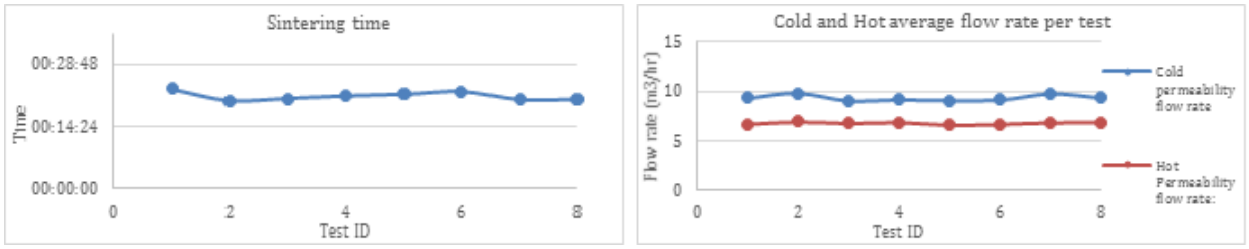

Figure 54: Repeatability - Sintering time and average cold/hot flow rate per test

On analysing table, 6 average cold flow rates per test had a repeat-ability standard deviation of 0.26m3/hr, with all of them being in the 9-9.8 m3/hr region. Standard deviation for average hot flow rate had standard deviation of only 0.12m3/hr, with all averages in the 6.7-7 m3/hr region, this showed minimal variation. Embedded thermocouples TC1-2 had a standard deviation of less than 80°C across all 8 tests and below 50°C for embedded thermocouples TC3, TC4 and TC5. This was suitable variation per test. Maximum temperature recorded by the off gas thermocouple 1 was 730°C and minimum recorded was 573°C. This had a standard deviation of 55C. Maximum temperature recorded by off gas thermocouple TC2 was 53°C and lowest was 45°C with a standard deviation of 3.7. All standard deviation would be incorporated as error margins for future tests.

Table 6: Process parameters recorded from repeatability study

	Test 1	Test 2	Test 3	Test 4	Test 5	Test 6	Test 7	Test 8	StDev
Cold flow rate	9.32	9.77	9.10	9.19	9.13	9.17	9.73	9.34	0.26
Hot flow rate	6.73	6.99	6.83	6.93	6.66	6.74	6.90	6.92	0.12
Sintering time	00:23:15	00:20:15	00:20:50	00:21:30	00:21:55	00:22:40	00:20:30	00:20:35	00:01:06
Max sintering temp	1345.44	1381.35	1352.51	1375.89	1326.69	1376.61	1330.41	1332.78	22.53
Thermocouple 1	1224.68	1350.57	1172.91	1148.11	1214.91	1245.60	1165.42	1087.45	78.25
Thermocouple 2	1245.19	1191.22	1263.15	1294.35	1041.83	1142.65	1240.20	1201.94	80.07
Thermocouple 3	1231.15	1228.80	1305.89	1323.44	1314.76	1266.23	1328.37	1332.78	43.17
Thermocouple 4	1345.44	1381.35	1352.51	1364.23	1238.15	1375.20	1330.41	1332.53	45.11
Thermocouple 5	1331.33	1294.37	1246.40	1375.89	1326.69	1376.61	1257.39	1311.60	48.36
Max off gas TC 1	601.46	575.31	641.62	577.77	601.58	573.77	731.54	665.90	55.56
Max off gas TC 2	181.20	184.67	186.25	180.14	179.23	181.91	190.82	182.85	3.78
Sintered air flow	45.90	51.86	53.10	50.80	50.83	51.58	53.43	50.07	2.34

Post Analysis and Discussion

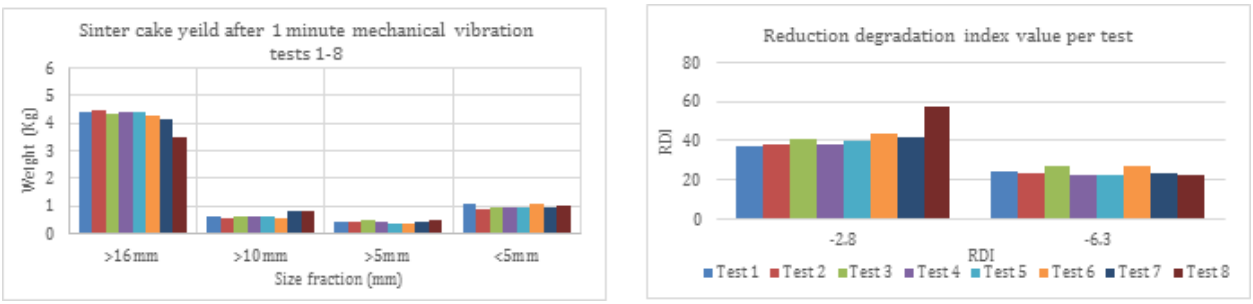

Figure 55: Repeatability - Sinter PSD and RDI

As mentioned earlier, after the sinter had been discharged, the sinter cake was subjected to 1 minute of mechanical vibration and screened into size fractions. This can be seen in figure 55 (a). Return fines are defined as all particles below 5mm. This size fraction would be recycled back to the start of the sintering process at a sinter plant and hence the term 'return fines'. Average percentage of sinter produced above 16 mm in diameter was 66% with a standard deviation of less than 5%. Average percentage of sinter produced between 10 - 16 mm was 10% with a standard deviation of less than 2%. Average sinter produced between 5 – 10 mm was 6.5% with a standard deviation of 0.5%. Average percentage of

return fines was 15.8% with a standard deviation of less than 2%. The low variation in size fractions was the initial indication that all sinter is of similar quality as the PSD testing gives indication of cold strength when comparing a series of tests within an experiment. For a more accurate indication of sinter quality, chemical analysis and reduction degradation index testing was performed. Sinter in the size region between 16-20mm was subjected to RDI testing for every test. RDI values can be seen in figure 55 (b). Average 6.3 RDI reading over all 8 sinter cakes was 24 with a standard deviation of less than 2. Average 2.8 RDI reading was 42 with a standard deviation of less than 7. All RDI results were in the suitable range as per normal sinter plant operations. It is worth noting here that standard deviation across all tests would decrease to 2 if test 8 was not included. It is also worth noting here that test 8 produced the lowest amount of sinter above 16 mm and also produced the highest -2.8 RDI result. This could be a potential indication that test 8 produced slightly weaker sinter in terms of cold strength. It is also worth noting here that the temperature profile for test 8 had a maximum TC 1 temperature of 1087°C, 110°C lower than the maximum TC 1 average temperature. The temperature difference explains why the sintered product in test 8 produced the least amount of sinter +16mm. If TC1 did not reach adequate temperature for sintering then this would result that section of the sinter pot being of poor sinter quality as assimilation could not occur at the low temperature.

Table 7: Sinter composition

	Test 1	Test 2	Test 3	Test 4	Test 5	Test 6	Test 7	Test 8	StDev
SiO_2	3.96	4	3.91	3.99	3.93	3.94	3.91	3.79	0.07
Al_2O_3	1.2	1.13	1.17	1.16	1.16	1.27	1.33	1.07	0.08
TiO2	0.09	0.09	0.09	0.1	0.09	0.1	0.1	0.09	0
CaO	9.75	10.08	9.58	9.28	9.6	9.83	10.25	9.53	0.31
MgO	0.56	0.71	0.55	0.48	0.53	0.56	0.56	0.59	0.07
P	0.05	0.04	0.04	0.05	0.05	0.05	0.05	0.05	0
Mn	0.2	0.19	0.18	0.18	0.18	0.22	0.24	0.18	0.02
Fe	55.78	59.13	58.74	59.1	57.54	58.99	61.33	59.08	1.57
Fe_2O_3	70.74	73.81	70.85	76.76	75.39	73.2	74.32	75.03	2.12
FeO	8.12	9.66	11.82	6.97	6.2	10.03	12.03	8.5	2.12
CaO/SiO_2	2.46	2.52	2.45	2.33	2.44	2.49	2.62	2.51	0.08
RDI -2.8	37.51	38.42	40.95	37.79	39.97	43.27	41.47	57.74	6.61
RDI -6.3	24.17	23.12	27.18	22.62	22.93	26.76	23.64	22.78	1.81

Figure 56: Repeatability - FeO and basicity

Table 7 above shows the chemical content and RDI data from the 8 sinter pot tests. As mentioned earlier, less than 25 grams of sinter in the size region of 16-20mm was subjected to XRF analysis to determine chemical composition of the sintered product. It can be noted here that for all chemical components had a standard deviation of less than 2 across all 8 tests. All chemical readings were in an acceptable range as per normal sinter plant operations. The maximum Fe content was 61.33 and lowest was 57.54, the maximum content of Fe_2O_3 was 76.76 and lowest was 70.74 and the maximum FeO content was 12.03 and lowest reading was 6.2 across all 8 sinter pot tests. Highest variation was seen in the Fe content and this could be due to the slight variation in sintering temperatures across 8 sinter pot tests. It is worth noting here that even though Fe had exhibited the highest variation, all variation is within the normal limit for sinter plant operations. Basicity is very important in iron ore sintering. Maximum SiO_2 reading over 8 sinter pot tests was 4.00 and lowest was 3.79. SiO_2 content over all 8 tests had a standard deviation of 0.07. Maximum CaO content over 8 sinter pot tests was 10.25 and lowest reading was 9.28. CaO content had a standard deviation of 0.31 across all 8-sinter pot test. CaO/SiO_2 ratios across all 8 sinter pot tests had a standard deviation of 0.08. Highest CaO/SiO_2 ratio was 2.62 and lowest was 2.33. It is worth noting here that all other chemical constituents were in a range for normal sinter plant operations with minimal variation.

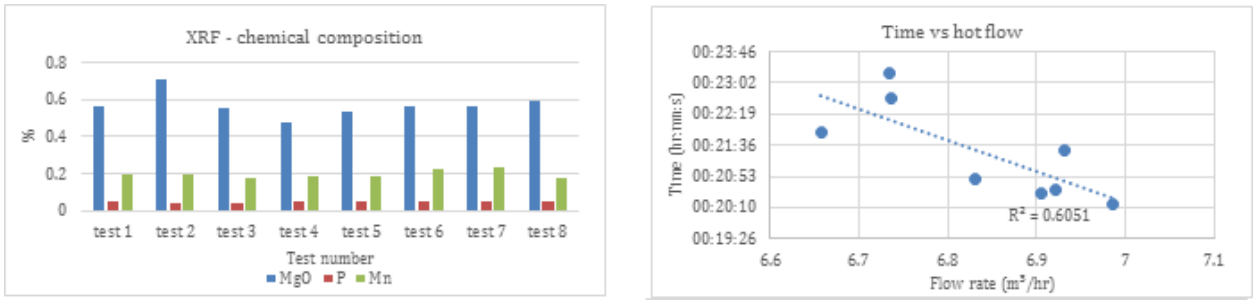

Figure 57: Repeatability - chemical composition and sintering time vs flowrate

Figure 56 shows iron content and basicity across all 8 tests respectively. Figure 57 (a) shows the chemical content of MgO, P and Mn for each sinter pot test. It can be noted here that there was a small increase in MgO for test 2. The average MgO content is 0.57 with a standard deviation of 0.07. P and Mn were also very consistent with a standard deviation of 0.05 and 0.19 respectively. Figure 57 (b) shows the variation of sintering time against average variation in hot flow rates. Albeit with minimum variation in the process, it was evident from the trend line and R2 value that as average hot flow increased, sintering time decreased. This was promising to witness in terms of reliability in that the process is working as it should and the data is outputting correctly. As one would expect, albeit with minimal fluctuation, if hot flow rate is increased then it can be expected that sintering time would decrease.

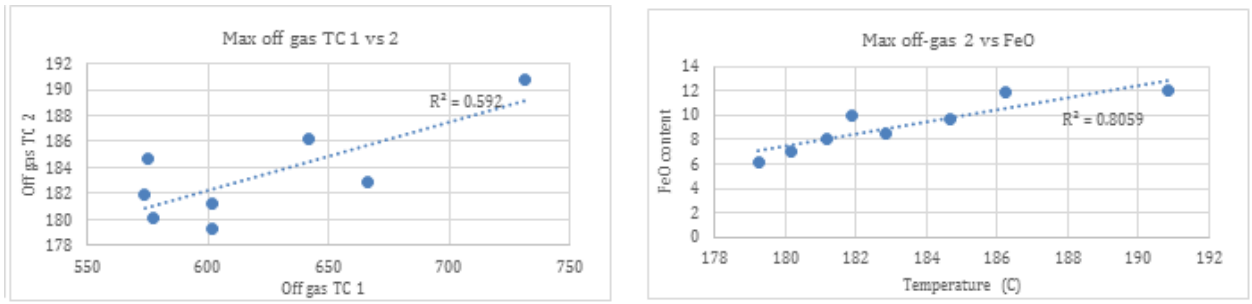

Figure 58: Repeatability - Off gas (a) and FeO (b)

Figure 58 (a) showed maximum off gas TC1 temperatures against maximum off gas TC 2 temperatures. It was evident from the trend line and r2 value that generally, as TC1 increased, max off gas TC2 increased. This was another encouraging yet obvious trend to have witnessed throughout the 8 sinter pot tests as we would expect this trend to occur. Figures 58 (b) showed FeO content against the max off gas TC 2 for all 8 sinter pot tests. FeO

content is on the y-axis and the temperature for the max off-gas TC 2 readings on the X-axis. The graph showed a trend line with R2 value indicating a strong correlation. Correlation showed that with the increase in maximum off gas TC 2 temperatures an increase in FeO content was evident. This was not picked up in the literature and is worth investigating further for future work.

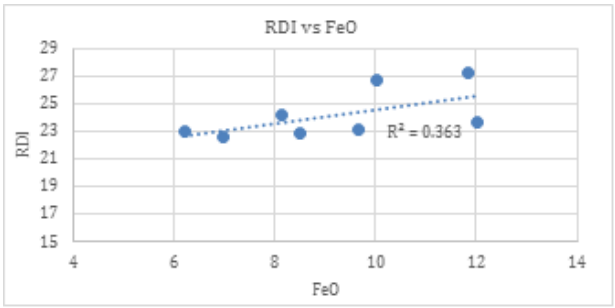

Figure 59: Repeatability - RDI vs FeO

Figure 59 showed a graph of RDI against FeO content in sinter produced. There was a possible correlation between RDI and FeO content. Even though the trend line was not as strong as previous correlations this may be worth further investigating. Trend indicated RDI value increased with increasing FeO content.

Conclusions

The results and discussion in the above investigation looked into the repeat ability and variation of the small-scale sinter pot. It was set out to prove that the testing rig and safe working procedure was repeatable and accurate. By close analysis of the repeat-ability and accuracy of the process and quality of sinter over 8 full sinter pot tests with identical process parameters and blend, this paper can conclude that:

i) The sinter pot test rig is a robust set up and can successfully sinter mixtures of iron ores, flux and fuel into a good quality sinter similar to that of the quality of sinter produced at the sinter plant.

ii) The sinter pot rig can run the same parameters with very minimal variation in process each time.

iii) The sinter pot process produces very similar temperature profiles when tested with identical blend composition and process parameters.

iv) All 8 tests finished within 1.5 minutes of each other.

v) All 8 sinter pot tests produced sinter with minimal variation and a chemical composition acceptable for normal sinter plant operations.

vi) Variation of sintering process in terms of process parameters such as sintering time, average cold and hot flow, and maximum sintering temperatures were minimal.

vii) Variation of sinter quality in terms of chemical composition and RDI values were minimal and all were in an acceptable range for normal sinter plant operations.

viii) Correlations were evident between average hot flow rate and sintering time.

ix) Correlations were evident between maximum off-gas TC temperature and maximum off gas TC 2 temperatures.

x) Correlations were evident between maximum off-gas TC 2 temperature and FEO content.

xi) All correlations must be taken in the context of the deliberately low variation in the variables

xii) Overall, variation in sintering process and sinter quality produced was minimal and the variation will make up the standard error bars for future work.

3.3.4 Validation - Comparing Sinter Quality

This section set out to investigate the variation in comparing sinter quality when using the small scale sinter pot when using a blend pre-made from the sinter plant.

Introduction

It was decided to validate the pilot line sinter pot via close comparison of the sinter it could produce against the sinter produced from the sinter plant when using a blend taken from the sinter plant. Main objective for this investigation was to compare sinter produced and not process parameters. However, some parameters are mentioned. The blend was taken from the sinter plant at the roll feeder which had already been granulated and prepped for sintering. The blend was taken from this point to achieve identical blend composition and granulation characteristics as to that of the sinter plant's.

Experimental Procedure

Experimental plan follows the same outline as stated in the methodology unless otherwise stated below. The main discrepancy in experimental parameters in this experiment was that the pressure drop was set to 80mbar and that the blend used was collected from the roll feeder at the sinter plant. For more information on experimental parameters please see commissioning and methodology section. The main purpose of these particular experiments was to investigate similarities in sinter quality when using the pilot line sinter pot and comparing to the quality of the sinter produced at the plant. 8 tests in total were conducted keeping the blend and process set point constant across all tests. Sinter pot was charged with 400g of hearth layer sized between 10-16mm. The blend was then charged into sinter pot scoop by scoop alternating 90° in direction each time to avoid preferential packing. All tests had an ignition time of 1 minute. Please see formula sheet for equations used in calculated parameters, experimental design for methodology and sinter pot dimensions.

The blend taken from the sinter plant at roll feeder and the blend constituents will remain confidential for this investigation.

Experiment:

x8 pot test with the blend collected from roll feeder at sinter plant, tested at 80mbar.

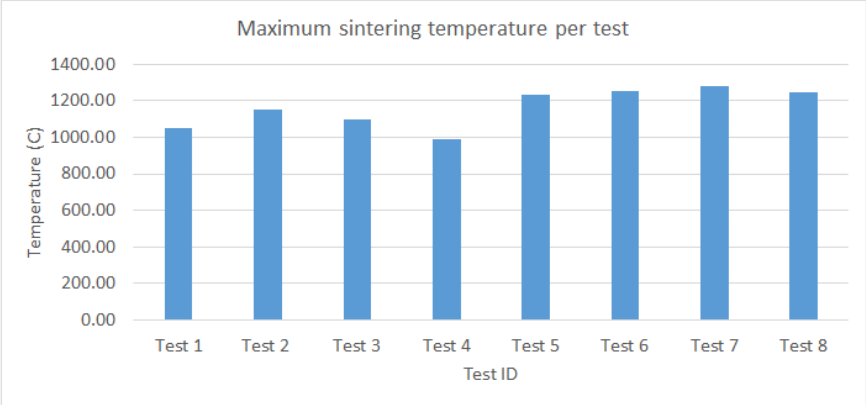

Figure 60: Validation - Sintering temperatures

Figure 60 shows the maximum sintering temperature reached for the 8 tests conducted. On analysing the figure, it can be seen that all but one test reached above 1000C. It can be noted that there was slight variation between maximum temperatures reached. This could be due to the variation in particle size and the decreased homogeneity in the blend composition due to it not being prepared under laboratory conditions. variation was expected due to the reasons mentioned above. However, the majority of tests reached adequate sintering temperatures so sinter quality could be analysed.

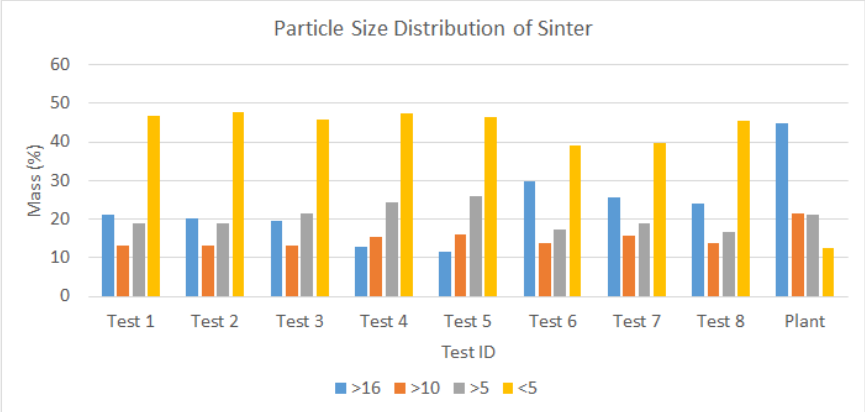

Figure 61: Validation - Particle size distribution of sinter produced compared to plant operation

Figure 61 shows particle size distribution of sinter produced from all 8 tests and compared to a plant operation when using the same blend. It was evident that there was substantial variation in return fines and sinter above 16mm in size when comparing the 8 tests to plant operations. This could be expected due to the decreased amount of fuel used at the sinter plant as compared to whats needed inside the sinter pot. This could also be due to the dimensions of the pot as compared to the large strand at the sinter plant with regards to heat loss and edge effect. However, there was minimal variation between the sinter produced in the size fraction of less than 5mm and 10mm. It can be recommended here that if it was possible to increase fuel rate without compromising the blend composition, it would be an advantageous study to check if sinter psd could be more representative to that produced by the plant.

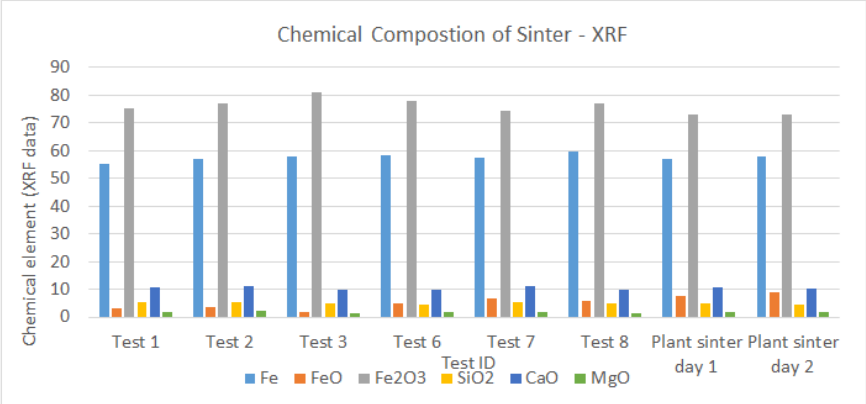

Figure 62: XRF data from 6 conducted tests compared to plant operation

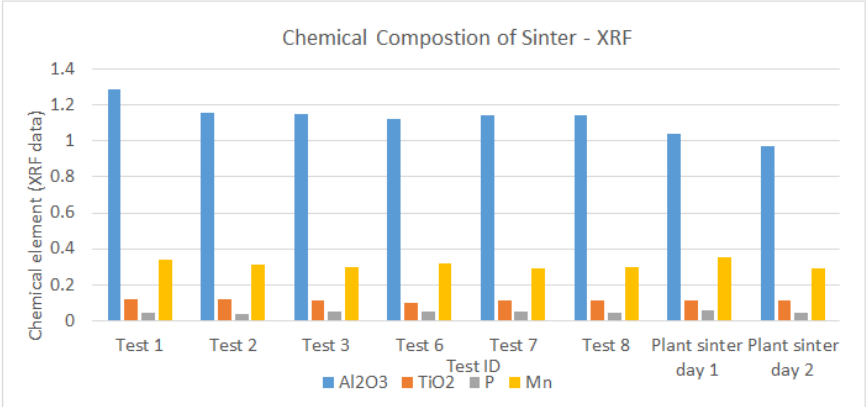

Figure 63: XRF data from 6 conducted tests compared to plant operation

Figures 62 and 63 shows the XRF data when the sinter produced from 6 of the 8 tests were subjected to chemical composition analysis. It can be seen that there was minimal variation in chemical composition of the sinter produced via the pilot line sinter pot compared to the sinter plant. Slight variation can be expected due to the decreased homogeneity of the blend when compared to a blend being made up in a laboratory specifically for the sinter pot. The slight variation can be seen in Fe_2O_3 and slight variation can be seen in content when comparing sinter produced from the pilot line sinter pot compared to the sinter plant. However, all variation lies within suitable range for normal sinter plant operations.

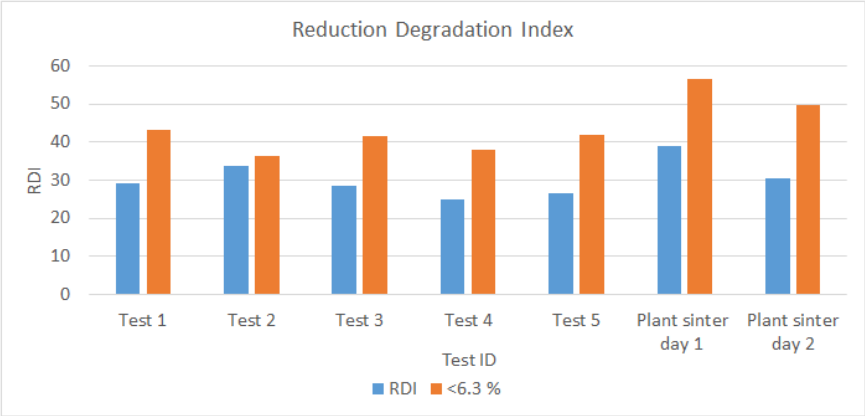

Figure 64: RDI values for sinter produced compared to plant operation

Figure 64 shows reduction degradation index values of the sintered product from 5 of the 8 tests conducted on the sinter pot. Data is compared to RDI values for the sintered product at the sinter plant. It was evident that there was slight variation when comparing RDI values of sinter produced at the plant. However, the sinter produced in the pilot line pot obtained increased reducibility characteristics. It must be noted here that the RDI value for the sinter produced by the pilot line sinter pot had minimal variation and all produced good RDI values. All variation was within suitable sinter plant operations.

Conclusion

i) It can be concluded that all 8 tests produced relatively adequate sintering temperatures. variation between pot sinter and plant sinter could be due to the decreased homogeneity of the blend composition at the plant as well as the increased fuel rate required in the pot.

ii) Particle size distribution of the sintered products from the pilot line sinter pot varied from that of the sinter plant. This was expected due to the small dimensions of the pot compared to that of the strand.

iii) It was evident that chemical composition of the sintered products had minimal variation when compared to that of the sinter produced at the plant when using the same blend.

iv) It was evident that sinter produced via the sinter pot produced improved RDI characteristics when compared to that of the sinter plant's. All variation was within suitable limits to that of the standard sinter plat operations.

v) It can be concluded that although sintering process conditions may vary when taking the blend from a roll feeder, chemical composition and sinter RDI fell within range of suitable sinter plant operations.

vi) Due to the above conclusions, it would be best to create blends under experimental laboratory conditions due to the variation in process when using a plant blend. However, quality of sinter produced is somewhat representative of the quality of the sinter produced via sinter plant.

3.3.5 Process optimisation summary

i) The sinter pot test rig is a robust set up and can successfully sinter mixtures of iron ores,flux and fuel into a good quality sinter similar to that the quality of sinter produced at the sinter plant.

ii) The sinter pot is 100mm in diameter and 500mm deep and is capable of producing sinter in 6.5kg batches in quick succession without impeding the production plant with similar process characteristics.

iii) Optimum and practical pre sinter capabilities and limitations include ability to control moisture up to 8%, granulation speed up to 55rpm, granulation time is set at 5 minutes which is relatively representative of the production granulation drum.

iv) Sinter pot is capable of running with a pressure drop of 50mbar up to 150mbar with strong correlations in recorded process parameters. It is worth noting here it was most practical and optimal to run between 100mbar and 125mbar.

v) In terms of repeatability, variation within the sintering process and quality of sintered product exhibited minimal variation where the standard deviation will make up the acceptable variation on future work.

vi) When comparing the process and quality of sinter to that of the sinter plants then following comments could be made; The process followed similar characteristics of the sinter plant process in terms of sintering fundamentals, however, has its limitation such as the scale difference and batch sequence process of the pot. The quality of sinter produced is comparable and falls in spec to that of the sinter produced at the sinter plant with some limitations.

4 Effect of Blend Composition on Sintering Process

This section focused on the initial experimental work conducted on the sinter pot. The pilot line sinter pot was deployed to investigate the addition of several raw ferrous materials to a blend. This was done to gain an enhanced knowledge on what occurs in the sintering process when adding different ferrous materials to a blend and to focus on process characteristics using the unique sinter pot design. Investigation was set out as not enough information is in the domain on what occurs to the sintering process when these materials were added or increased to a blend. Information could also be fed back to the production plant enhancing their ability to make quick decisive decisions when faced with different challenges.

4.1 Sinter feed A

The main iron ore minerals are hematite, magnetite and geothite. The main gangue minerals are quartz and chert with various silicates, carbonates and hydrates. In modern practice, iron ores must contain around 60wt-%Fe if they are the be used iron making. Sinter feed A is a geothitic-hematite ore. Characteristics can be seen in figure 65 below.

Mineral	Chemistry	Wt-%Fe (pure)	Density	Comments
Hematite	α-Fe_2O_3	70	5·25	Often contains inclusions of quartz, rutile, magnetite, etc., affecting properties
Magnetite	Fe_3O_4	72	5·20	Often contains small amounts of other cations in solid solution (s.s). Ferromagnetic
Maghemite	γ-Fe_2O_3			Uncommon, ferromagnetic
Goethite & limonite	α-FeOOH	62	4·3	Often contains some Al & P
Fe bearing silicates (e.g. grunerite, chlorite, minnesotaite)	Fe,Al,Mg, Ca silicates	Up to 35	3–3·5	Potential loss of Fe to tailings. Includes asbestiform minerals
Quartz & chert	SiO_2	....	2·65	Most common gangue
Kaolinite	$Al_2Si_2O_5(OH)_4$	....	2·6	Common gangue
Gibbsite	$Al(OH)_3$	....	2·4	Significant gangue in some ores
Apatite	$Ca_5(PO_4)_3(OH,F,Cl)$	....	3·2	Main P-bearing mineral in primary ores

Figure 65: Hematite, magnetite, geothite characteristics

It can be seen that geothite ores often contain some Al and P. It is virtually non-magnetic and has variable microtexture with internal porosity. Geothite can appear finely crystalline, soft and clay (limonitic) like and vitreous in appearance with variation in its metallurgical

behaviour. [63] The ore was subjected to chemical analysis via XRF. Please see below for this ore's chemical composition. It can be seen that the Fe content in the XRF analysis lines up with the information in figure 65.

Table 8: Sinter feed A composition

XRF	Ore A
SiO_2	5.14
Al_2O_3	1.87
TiO_2	0.09
CaO	0.01
MgO	0.01
Fe	62.75
Fe_2O_3	85.91
FeO	3.44
P	0.071
Mn	0.09

4.1.1 Introduction

Sinter feed A was obtained from the sinter plant stockyards and processed for sinter pot investigations. See earlier chapter for information on material preparation. It was decided that the data acquired from the sinter pot on investigating the impacts of increasing Sinter feed A to a blend would be useful as little information available in the domain on how this particular ore reacts during sintering and if any trends or correlations can be drawn from the data during the process. Information could also be fed back to the raw materials production team as well as sinter plant technical team to allow decisions to be made on how much of the ore should be used. It must be noted decisions weren't made solely on the information given by the pot, but to strengthen and validate various decisions.

4.1.2 Experimental Plan

Four sinter blends were produced under laboratory conditions, see material preparation in chapter 3 for more detail. Blend A contained 0% Sinter feed A, Blend 2 contained 8.5% Sinter feed A, blend 3 contained 16% Sinter feed A and blend 4 contained 25% Sinter feed A. Four sinter pot tests were conducted, not including repeats. Please see chapter 3 section 3.7 for experimental procedure, formula sheet and post analysis procedure. Blends contained the following:

Table 9: Blend composition

Material	Blend A	Blend B	Blend C	Blend D	Units
Sinter feed C	3.29	3.29	3.29	3.29	Kg
Sinter feed D	4.387	3.742	3.097	2.452	Kg
Sinter feed A	0	1.097	2.194	3.29	kg
Sinter fines	1.935	1.935	1.935	1.935	Kg
Sinter feed E	3.29	2.839	2.387	1.935	Kg
Limestone	2.194	2.194	2.194	2.194	Kg
Coke breeze	0.903	0.903	0.903	0.903	Kg

Please note: Sinter pot tests were conducted at 7% fuel

A) **First Experiment:**

x2 pot test with blend A at 100mbar

B) **Second Experiment:**

x2 pot test with blend B at 100mbar

C) **Third Experiment:**

x2 pot test with blend C at 100mbar

D) **Fourth Experiment:**

x2 pot test with blend D at 100mbar

4.1.3 Results

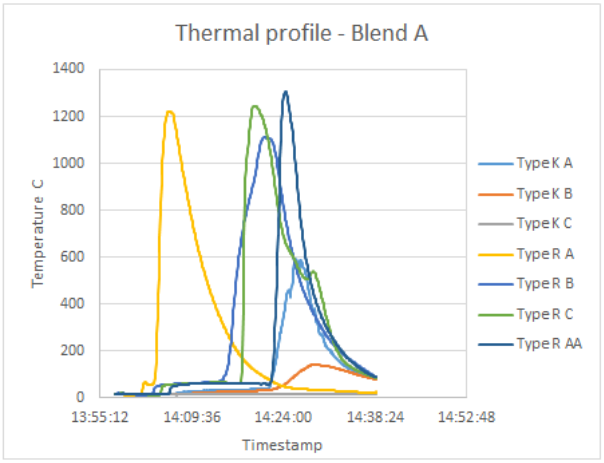

(a) Thermal profile from blend A

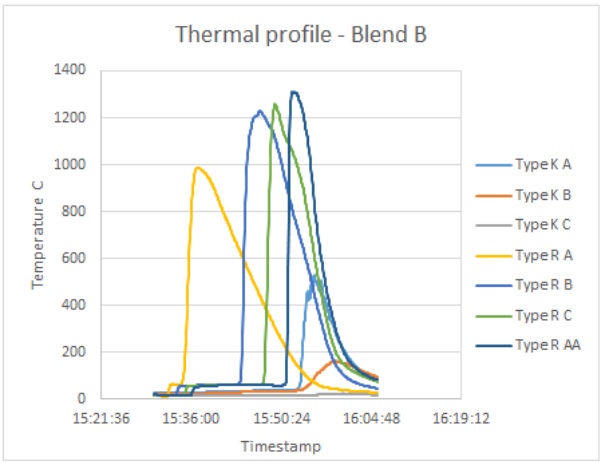

(b) Thermal profile from blend B

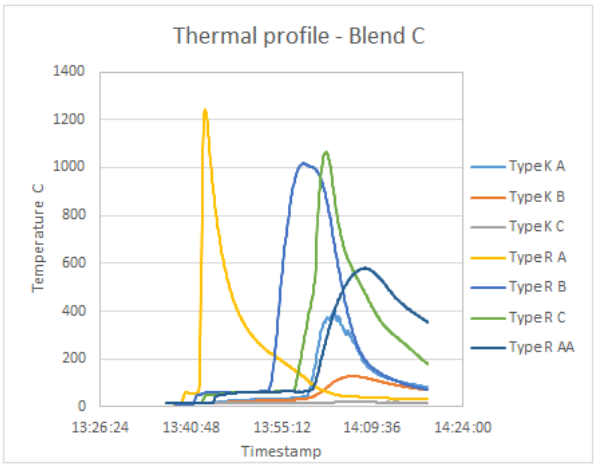

(c) Thermal profile from blend C

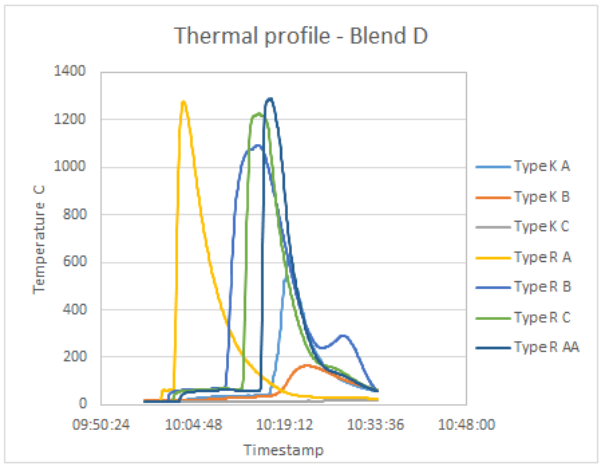

(d) Thermal profile from blend D

Figure 66: Thermal profiles from Sinter feed A study

As you can see from the thermal profiles in figure 66 above, the process is unstable. The thermocouple traces progress in a non uniform manner and some thermocouples do not reach high enough temperatures. This indicates the flame front passes the thermocouples in an erratic behaviour with some sections not reaching adequate sintering temperatures. It can also be seen that sometimes the off gas temperatures peak before the last embedded thermocouple which could be cause for concern. It should be noted here as this was early stages in the project that a suitable blend was difficult to establish. Even though instabilities were seen in flame front propagation. Sinter was produced and therefor analysed.

4.1.4 Post Analysis and Discussion

It has been said that the thermal profile in figure 66 exhibits an unstable process. A stable process would see each of the thermocouple trace peak one after another. The thermal profile in figure 66 (b) shows the most uniform and stable profile. Each thermocouple starts to increase and peaks in a sequential manner which indicates stable and uniform flame front travel. The thermal profiles in figures 66 (c) show the most erratic behaviour. Embedded thermocouple 4 (type R AA) starts to rise and peak after the off gas thermocouple which is cause for concern as this indicates part of the blend re-heating or re-igniting causing a potential second flame front to pass the bottom of the pot after the first. The thermal profile in figure 66 (d) is relatively stable apart from the second peak in thermocouple 4 after the off gas peaks. All thermocouples start to rise and peak one after another indicating uniform flame front propagation apart from the second peak as mentioned. This could be due to incomplete or delayed combustion where it re-ignites later down the line. It must be noted here that the computer panel only records for total of 35 minutes and so some profiles cut off before all thermocouples descend to below 100C. This issue was resurrected later in the project.

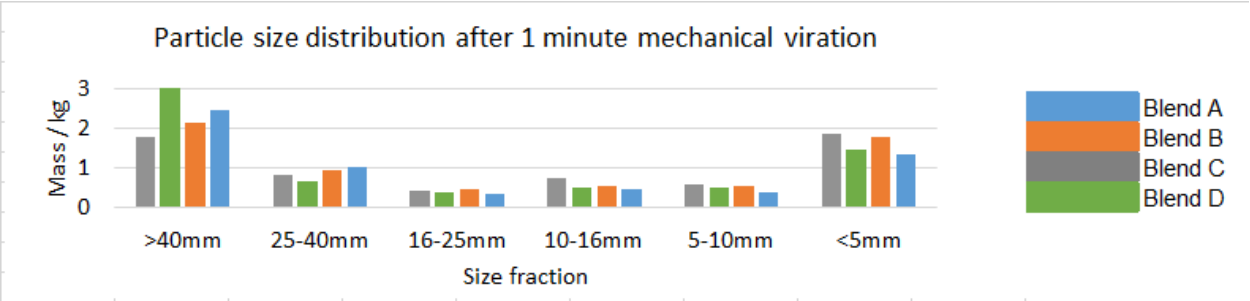

Figure 67: Particle size distribution after 1 minute mechanical vibration

The sinter from each test was subjected to 1 minute of mechanical vibration and then screened into different size fractions. This can be seen in figure 67 above. No correlation or trend was evident from the particle size distribution between the tests. It must be noted here that from the validation work package this was the weakest link compared to routine production.

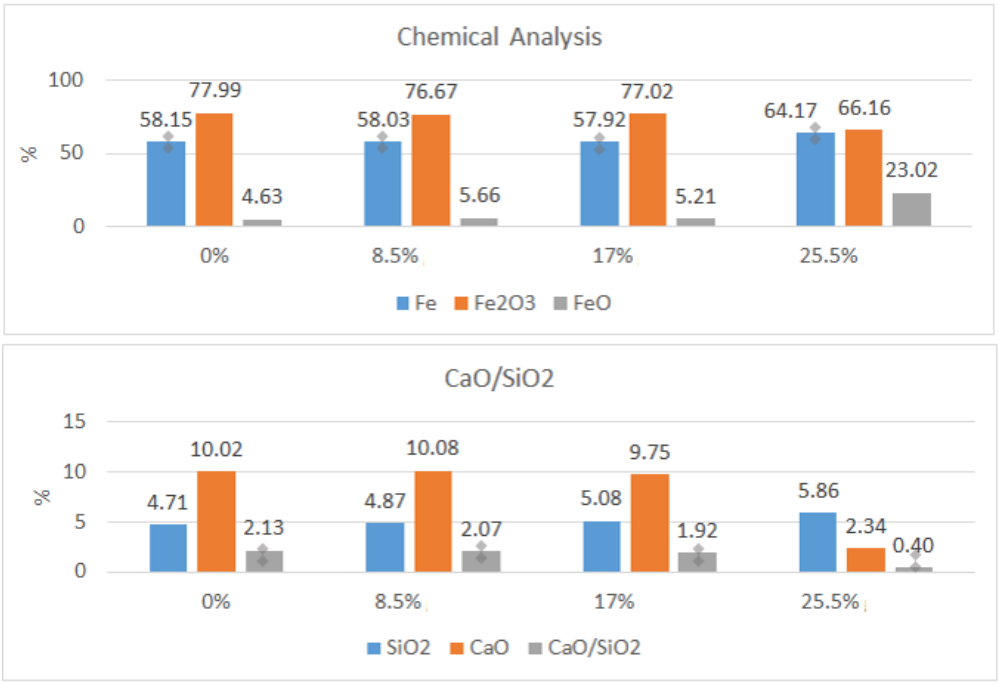

Figure 68: Chemical analysis of sinter from sinter feed A study

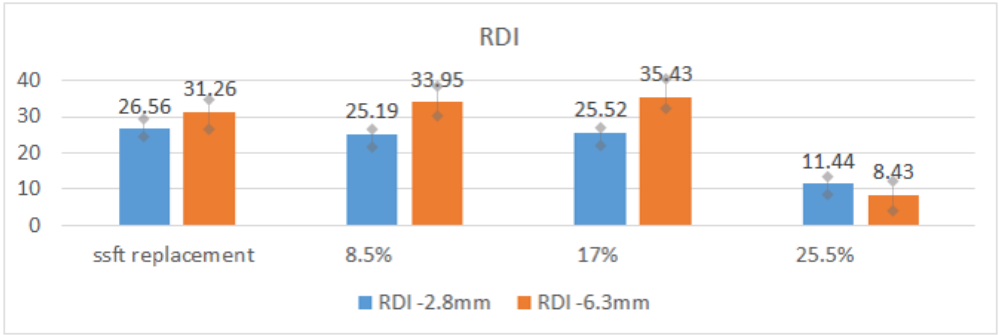

Figure 69: Reduction degradation index from sinter feed A study

Figures 68 and 69 shows some of the post analysis completed. Post analysis followed the same procedure of that of the sinter production plant. sinter in the size range of 16-

20mm was subjected to chemical analysis as well as reduction degradation index testing. On inspection of figure 68 (a), it was seen that there was minimal variation for basicity of sinter. Both in which are important for sinter quality and are in suitable range per sinter plant operations. It must be noted here that there is variation for chemical analysis in sinter produced from blend D. On the analysis of figure 69 the same trend can be seen. All RDI values are within a suitable sinter plant operations apart from Blend D.

Optical microscopy from sinter feed A study

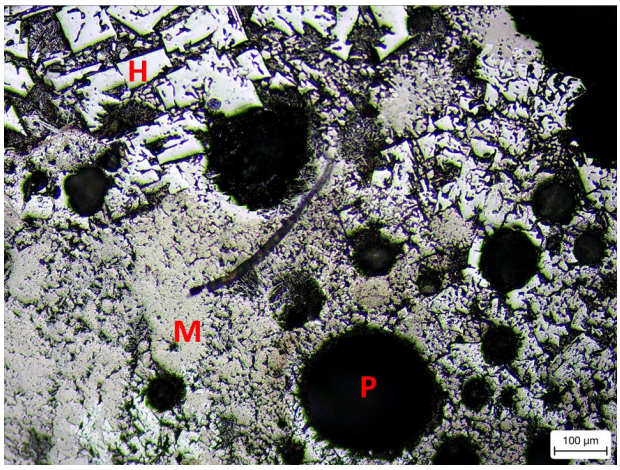

(a) 8% Siner feed A x10

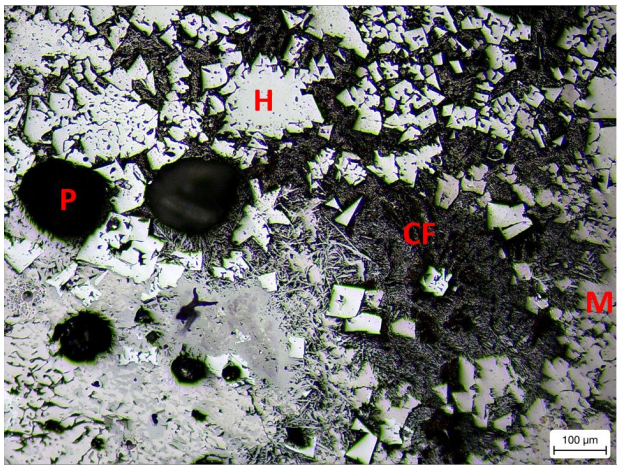

(b) 17% Siner feed A x10

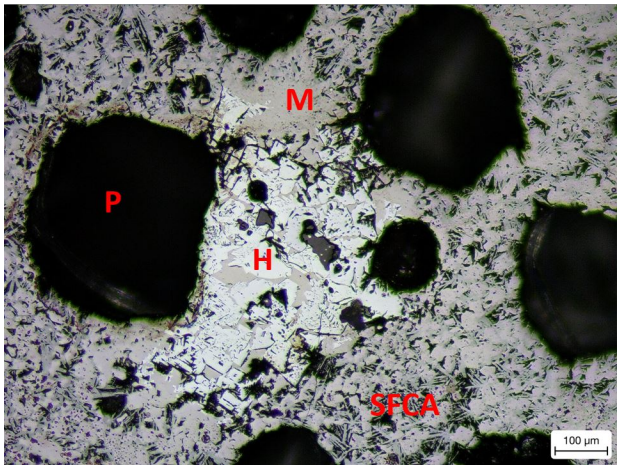

(c) 25% Siner feed A x10

Figure 70: Optical images of sinter from Sinter feed A investigation. H-hematite, M-magnetite, CF-calcium ferrite.

As previously mentioned, sinter in the size fraction between 16-20mm was taken for post analysis. It was decided that some sinter would be subjected to optical microscopy to investigate if Sinter feed A addition had any impact on the micro structures formed. The microstructures can be seen in figure 70. It must be noted that sinter from the sinter pot test conducted with 0% Sinter feed A could not be subjected to optical analysis as all the sinter had gone through reduction degradation index analysis. In figure 70 A the image shows the microstructure of sinter with 8% Sinter feed A at x10 magnification. Figure 70 (B) shows the microstructure of sinter with 17% Sinter feed A addition at x10 magnification. Figure 70 (C) shows the microstructure sinter with 25.5% Sinter feed A at 10x magnification. From

analysing the literature and visual observation it can be said that the block-like features are hematite with the slightly darker constituents being magnetite and all embedded in a matrix of SCFA's. As Sinter feed A content is increased, it can be seen that the hematite, magnetite and SFCA structure maintains the block-type and needle like features. This needs to be clarified with EDS chemical analysis. It must be noted that during optical microscopy analysis, some change in features in the sinter with 25.5% sinter was evident and this could correlate with the high FeO content in the sinter evident from the XRF chemical analysis. It must also be noted that basicity is evident as lower with higher Si levels and lower and CaO levels. This could also possibly correlate with the substantial decrease in RDI value for the sinter produced with 25.5 Sinter feed A as well as producing more sinter above 40mm in size. However, due to the high variation exhibited in the thermal characteristics within the process, variation in micro-structures should be expected.

4.1.5 Conclusion

i) It was evident from visual appearance that granule size after granulation was improved. Further studies to investigate granule size after granulation on increasing Sinter feed A is recommended.

ii) Sintering time decreased up to a point when Sinter feed A content was increased

iii) It was evident that return fines decreased as the Sinter feed A content increased.

iv) There was minimal variation between chemical compositions of sintered products between tests apart from when Sinter feed A had increased to 25.5%.

v) Variation in chemical composition in sinter when using 25.5% correlated with the substantially low value of RDI when using the amount of Sinter feed A. It must be noted here that this could be temperature related as this was the only test that observed temperature above 1200°C across all thermocouples.

vi) It is recommended that further investigation should be complete before making any conclusions on this investigation due to the erratic and unstable profile observed across all of the tests.

vii) Main purpose of including this batch of tests within the project thesis was to give indication on unstable flame front characteristics as compared to the majority of stable tests to come in future chapters

4.2 DRI content

Directly reduced iron ore pellets are produced via a pelletization process ready to be directly charged into the blast furnace. These are called DRI pellets. A by-product of this pelletizing process are fine particles of DRI. These are called DRI fines. Commercialisation of DRI began in the last 1960's and by mid-1970's over 100 designs were established combining different reactors and reducing agents. DRI processes can now be classified according to the kind and source of reducing gas or type of reactor used. [64]

Property	Direct reduced iron (DRI) values
Density	1.5–4.0 g/cm^3
Bulk density	1.5–1.9 ton/m^3
Specific surface area (Porosity)	0.5–4.0 m^2/g
Crushing strength	50–110 kg/cm^2
Degree of metallization	90–95% (average 91–93%)
% Metallic iron	~85%

Figure 71: DRI properties

DRI is what is used and explored in this section. Properties can be found in figure 71 above. It can be seen that density, crushing strength and porosity can vary substantially. [65] The DRI used in this investigation was subjected to chemical analysis and this can be seen in table 10 below.

Table 10: DRI composition

XRF	Ore B
SiO_2	3.21
Al_2O_3	0.89
TiO_2	0.12
CaO	1.08
MgO	0.02
Fe	66.56
Fe_2O_3	53.39
FeO	37.58
P	0.049
Mn	0.09

4.2.1 Introduction

This section looks into how DRI influences the iron ore sintering process when increasing the amount in a blend. All other parameters to be kept constant. All process parameters kept the same as the previous sinter feed A investigation. DRI was chosen to investigate as it had industrial relevance specific to the production sinter plant as well as having scientific value.

4.2.2 Experimental plan

Four sinter blends were produced under laboratory conditions, see material preparation in earlier section for more detail. Blend A contained 0% DRI, Blend 2 contained 10% DRI, blend 3 contained 20% DRI and blend 4 contained 30% DRI. Please see chapter 3 section 3.7 for experimental procedure, formula sheet and post analysis procedure. Blends contained the following:

Table 11: Blend composition

Material	Baseblend 0%	10% DRI	20% DRI	30% DRI	units
Sinter Fines	1.94	1.94	1.94	1.94	kg
Sinter feed E	4.94	4.61	4.29	3.97	kg
Sinter feed A	1.10	1.10	1.10	1.10	kg
Sinter feed D	4.94	3.97	3.00	2.03	kg
DRI	0.00	1.29	2.58	3.87	kg
Limestone	2.19	2.19	2.19	2.19	kg
Coke Breeze	0.90	0.90	0.90	0.90	kg

Please note: Sinter pot tests were conducted at 7% fuel

A) **First Experiment:**

x2 pot test with blend A at 100mbar with 0% DRI

B) **Second Experiment:**

x2 pot test with blend B at 100mbar with 10% DRI

C) **Third Experiment:**

x2 pot test with blend C at 100mbar with 20% DRI

D) **Fourth Experiment:**

x2 pot test with blend D at 100mbar with 30% DRI

4.2.3 Results

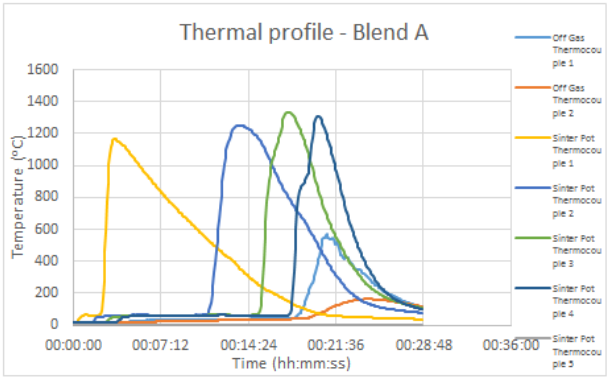

(a) Thermal profile from blend A

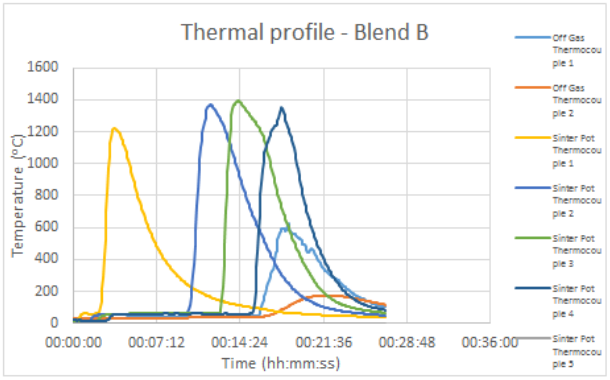

(b) Thermal profile from blend B

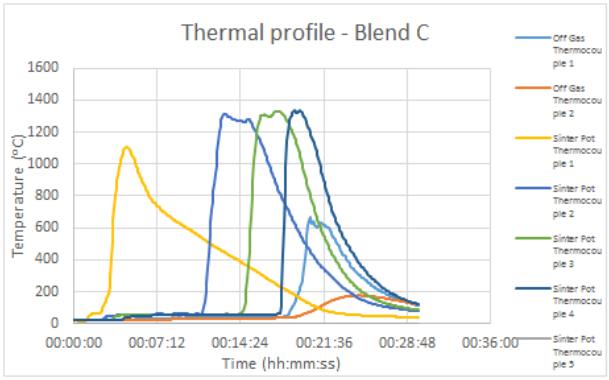

(c) Thermal profile from blend C

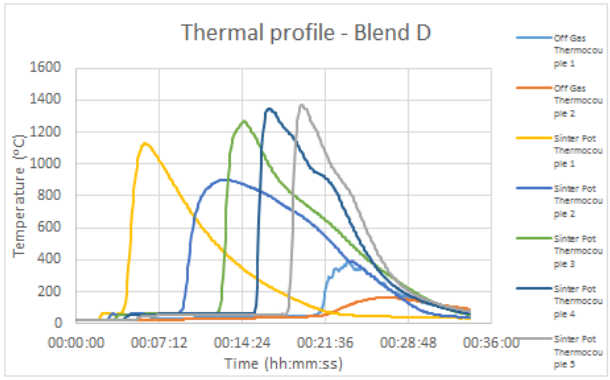

(d) Thermal profile from blend D

Figure 72: Thermal profiles from DRI study

4.2.4 Post analysis and Discussion

On the analysis of thermal profiles in figure 72, the following comments can be made. The thermal profile in figure 72 (a) shows a relatively uniform profile. All apart from thermocouple 1 reach suitable sintering temperatures but this can be expected as thermocouple 1 is placed close to the top of the bed so a set amount of time is needed for the flame front to establish itself. It must be noted here that there is a large space between thermocouple 1 (type R A and type R B) as there is usually a thermocouple placed in slot 2 (see chapter 3 on sinter pot for more detail on location) but due to practical thermocouple issues, thermocouple slot 2 was not used and hence the space. This issue is resurrected later in the project. All other thermocouples reach sintering temperature and start to rise and peak one after another. All embedded thermocouples rise and peak before the off gas thermocouples. All this translates to uniform flame front propagation and a stable process. The flame front

descends downwards in a uniform and repeatable manner. The same trends and correlations can be drawn from the profiles in figure 72 a, b and c. However, some variation in maximum temperatures reached and sintering time was evident and mentioned below.

Table 12: Process parameters for increasing DRI study

Parameters	0% DRI	10% DRI	20% DRI	30% DRI
Avg cold flow rate	8.90	10.30	7.88	8.11
Avg Hot flow rate	6.26	7.00	6.03	6.18
Sintering time	00:20:30	00:18:20	00:19:25	00:19:25
Sintering temperature	1334.06	1394.27	1335.18	1348.59
Peak temperatures				
TC 1	1164.01	1220.12	1107.52	1191.64
TC 2	1249.74	1368.29	1315.31	1348.59
TC 3	1334.06	1394.27	1328.88	1347.82
TC 4	1306.94	1352.59	1335.18	1328.28

On analysing the figures in the table above, it was evident that on the addition of DRI, cold and hot flow increased but exhibit a steady decrease when DRI was increased further. This correlated with sintering time as an increased average hot flow rate resulted in an increased flame front speed and overall sintering time. All tests produced adequate sintering temperatures for iron ore sintering and for agglomeration to occur. However, there was variation in sintering temperature which was observed. This could be due to the fact that DRI has different metallic iron contents as well as moisture retention capabilities and so could result in the flame front front to descend slightly quicker. Moisture retention of ores that are used should be calculated and tabulated for further reference.

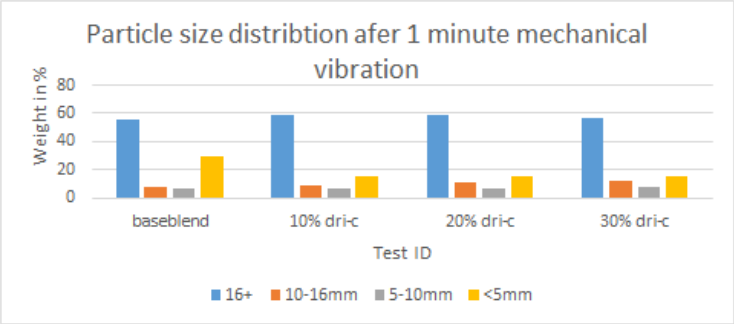

Figure 73: Particle size distribution after 1 minute mechanical vibration for DRI study

The sinter from each test was subjected to 1 minute of mechanical vibration. This can be seen in figure 73. No correlation or trend was evident from the particle size distribution between the tests and there was very little variation in size of sintered product between all tests. However, it must be noted that the blend with no DRI produced more return fines than when DRI is is used.

Table 13: XRF data

XRF	Base blend 0%	10% DRI	20% DRI	30% DRI
SiO_2	4.93	5.02	5.05	5.09
Al_2O_3	1.34	1.23	1.26	1.19
TiO_2	0.098	0.096	0.093	0.091
CaO	9.18	9.28	9.66	10.1
MgO	0.49	0.51	0.72	0.6
Fe	57.56	58.6	57.71	58.64
Fe_2O_3	75.47	73.22	72.35	71.47
FeO	6.15	9.51	9.15	10.83
P	0.044	0.041	0.045	0.045
Mn	0.23	0.19	0.2	0.16
CaO/SiO_2	1.86	1.85	1.91	1.98
RDI -2.8mm	29.43	31.14	31.29	29.86
RDI -6.3mm	36.17	39.45	37.28	37.61

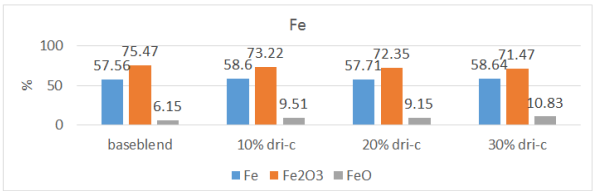

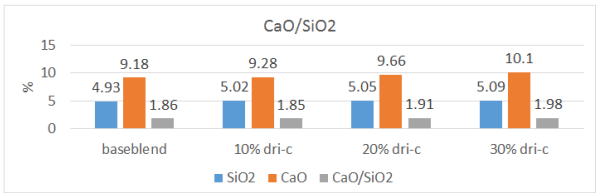

Figure 74: Chemical analysis of sinter DRI

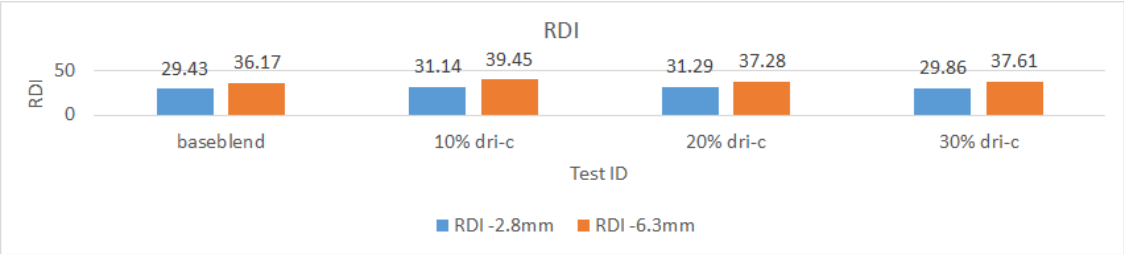

Figure 75: Reduction degradation index for DRI test

On analysing figures 74-75, it showed that there was minimal variation in chemical composition. Thus, minimal variation in the basicity of the sintered products. Chemical composition and basicity were in suitable range per sinter plant operations. It must be noted here that there was a slight trend in Fe_2O_3 across the tests. It was seen that as the DRI was increased, Fe_2O_3 decreased. All RDI values were within suitable sinter plant operations.

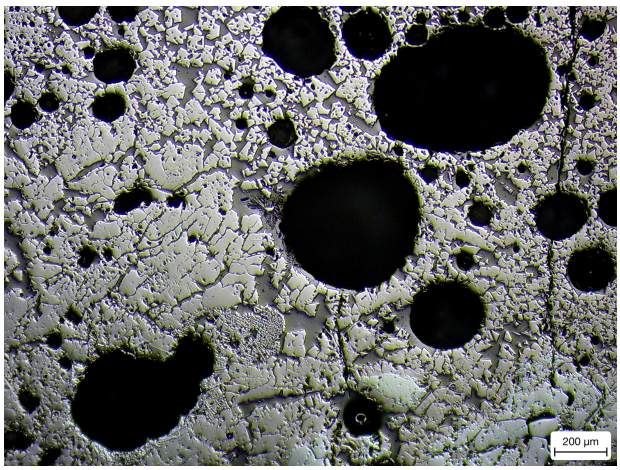

(a) 0 DRI X5

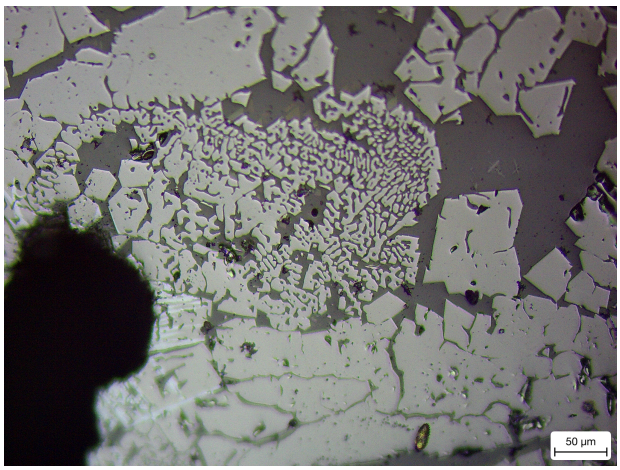

(b) 0 DRI x20

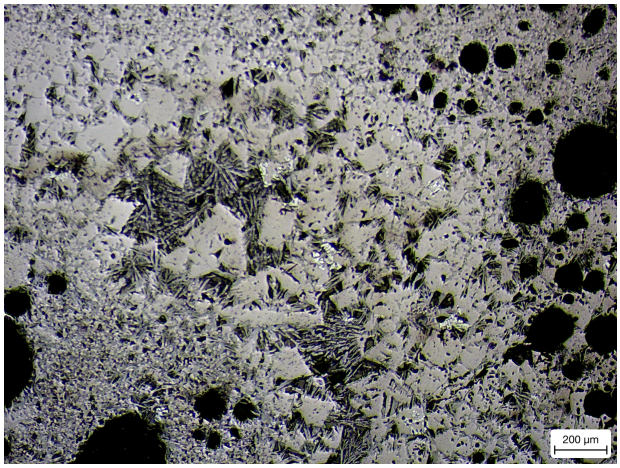

(c) 10% DRI X5

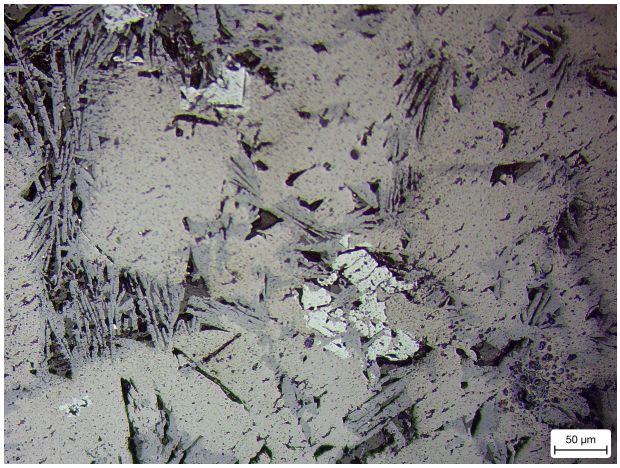

(d) 10% DRI x20

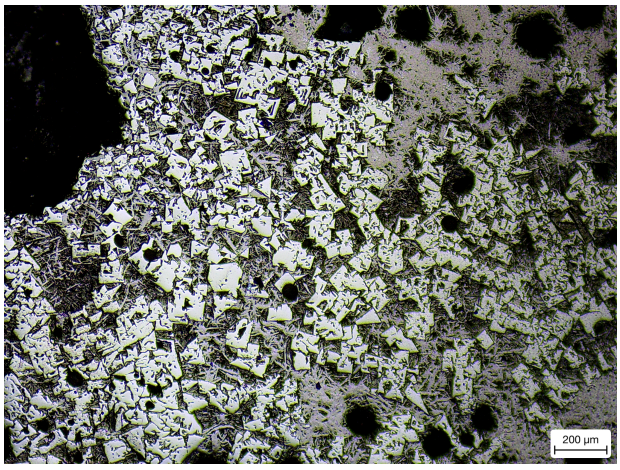

(e) 20% DRI X5

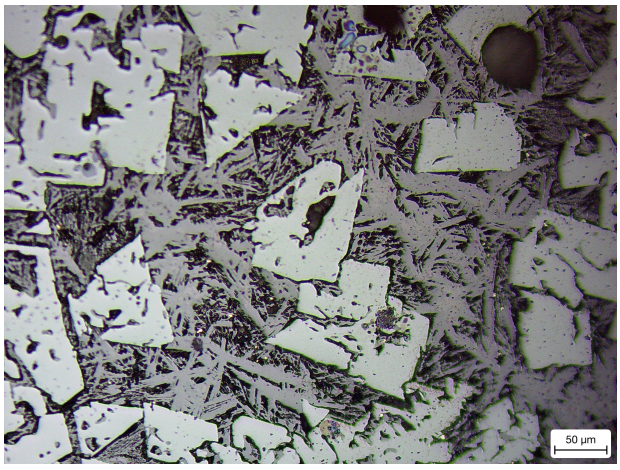

(f) 20% DRI x20

Figure 76: Optical microscopy of the sintered product across all tests from the DRI investigations.

Optical microscopy

Sinter from this investigation was subjected to optical microscopy to gain a better understanding if there were any impacts on the microstructure of the sinter when increasing DRI content. Figure 76 shows the optical microscopy images. On analysis of the micro structures it can be noted that on increasing DRI content in the sinter, hematite content is increased. It can also be noted that it seems like the structure goes from a dendritic structure when using no DRI and on increasing DRI, a more block type structure is evident with needle like SFCA's.

4.2.5 Conclusion

i) On increasing DRI content, thermal profiles exhibited uniform and stable processes which indicated stable and uniform flame front propagation.

ii) Sintering time was within 2 minutes of each other across all tests with no trend evident but correlated with average flow rates through the bed

iii) It should be noted here that the return fines of the sintered product was increased when no DRI was included in the blend.

iv) Chemical composition of sintered products across all tests had minimal variation. However, there was a slight trend was exhibited in the Fe_2O_3 when DRI was increased.

v) Reduction degradation was not affected when DRI content was increased.

4.3 Sinter feed B

Sinter feed B is a hematite ore mined in Canada. Often contains inclusions of quartz, rutile megnetite which influences properties. [63] Whilst the amount of other cations in solid solution hematite is low, it does contain microscopic amount of magnetite. Textures of hematite can be found in the table below.

1.	Coarsely crystalline, dense single crystals
2.	Equidimensional, somewhat rounded crystals
3.	Martitic, with a lamellar texture
4.	Martitic, with an interlocking, recrystallised texture
5.	Interlocking, hypidiomorphic with some indications of martitisation
6.	Microplaty, with a length-to-breadth ratio of < 5:1, often boat-shaped
7.	Flaky, often with a length-to-breadth ratio of > 5:1, frequently foliated
8.	Finely crystalline with small flakes, typically < 5 µm in size
9.	Ultrafine microcrystalline with the individual crystals hardly visible
10.	Ochreous, porous material

Figure 77: Hematite textures

It can be seen that hematite ores are coarsely crystalline and can appear flakey. Properties of texture can vary with varying amount of other inclusions. The Sinter feed B used in this study was subjected to chemical analysis via XRF and this can be seen in the table below.

Table 14: Sinter feed B composition

XRF	Sinter feed B
SiO_2	5.51
Al_2O_3	1.04
TiO_2	0.071
CaO	0.086
MgO	0.008
Fe	62.35
Fe_2O_3	88.42
FeO	0.67
P	0.022
Mn	0.086

4.3.1 Introduction

This section concentrates on Sinter feed B. It investigates how this ore can influence the iron ore sintering process. This particular ore was chosen as it had relevant industrial application with some scientific value. Sinter feed B was considered a good sintering ore by the technical team but it wasn't decided how much of the ore can be used without impeding the process and quality of sinter.

4.3.2 Experimental plan

There were 7 sinter pot tests conducted in this study. Blend A did not contain any Sinter feed B and blend B contained 5% Sinter feed B. The remaining tests then observed Sinter feed B level increase in increments of 10% up to Blend G. Please see chapter 3 section 3.7 for experimental procedure, formula sheet and post analysis procedure. Blends contained the following seen in table 11:

Table 15: Blend composition for Sinter feed B investigation

	0%Sinter feed B	5%Sinter feed B	15%Sinter feed B	25%Sinter feed B	35%Sinter feed B	45%Sinter feed B	55%Sinter feed B
Sinter Fines	1.94	1.94	1.94	1.94	1.94	1.94	1.94
Sinter feed E	4.45	4.13	3.45	2.74	2.19	1.55	0.90
Sinter feed D	3.77	3.55	3.13	2.74	2.19	1.74	1.29
Sinter feed C	2.74	2.74	2.74	2.74	2.74	2.74	2.74
Sinter feed B	0.00	0.55	1.65	2.74	3.84	4.94	6.03
Limestone	2.19	2.19	2.19	2.19	2.19	2.19	2.19
Coke Breeze	0.90	0.90	0.90	0.90	0.90	0.90	0.90

Please note: Sinter pot tests were conducted at 7% fuel

A) **First Experiment:**

x2 pot test with blend A at 100mbar with 0% Sinter feed B

B) **Second Experiment:**

x2 pot test with blend B at 100mbar with 5% Sinter feed B

C) **Third Experiment:**

x2 pot test with blend C at 100mbar with 15% Sinter feed B

D) **Fourth Experiment:**

x2 pot test with blend D at 100mbar with 25% Sinter feed B

E) **Fifth Experiment:**

x2 pot test with blend D at 100mbar with 35% Sinter feed B

F) **Sixth Experiment:**

x2 pot test with blend D at 100mbar with 45% Sinter feed B

G) **Seventh Experiment:**

x2 pot test with blend D at 100mbar with 55% Sinter feed B

4.3.3 Results

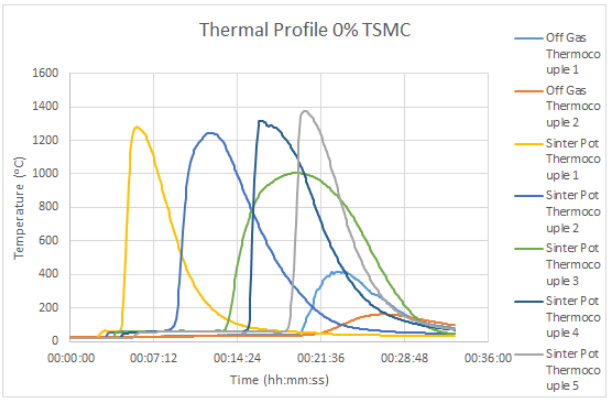

(a) Thermal profile from 0% Sinter feed B test

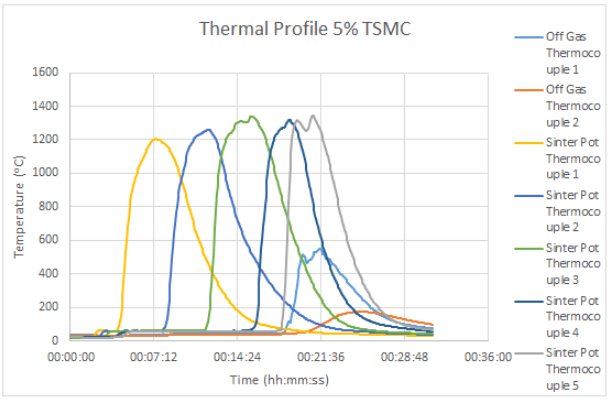

(b) Thermal profile from 5% Sinter feed B test

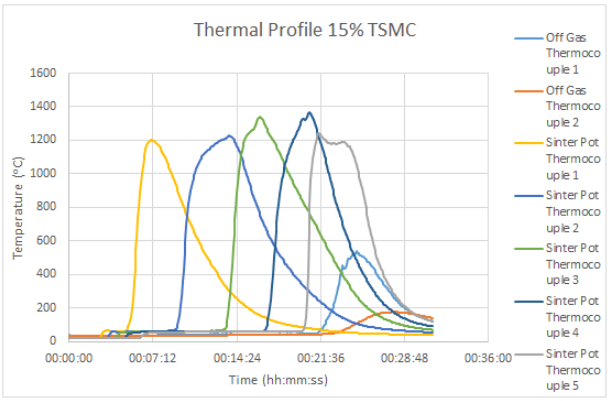

(c) Thermal profile from 15% Sinter feed B test

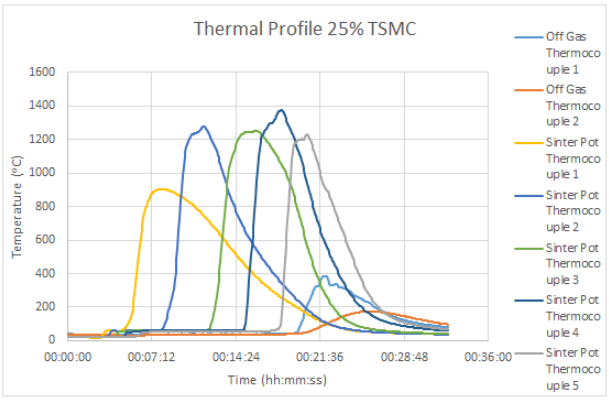

(d) Thermal profile from 25% Sinter feed B test

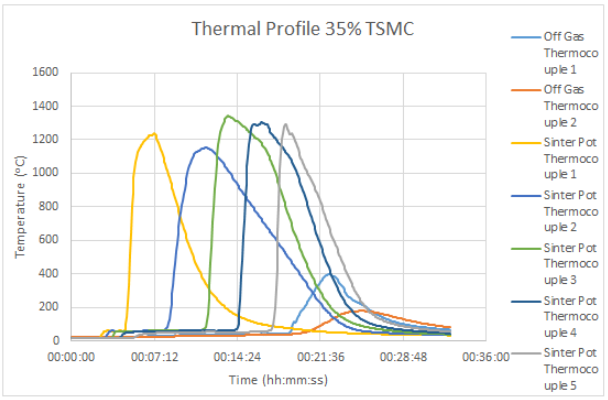

(e) Thermal profile from 35% Sinter feed B test

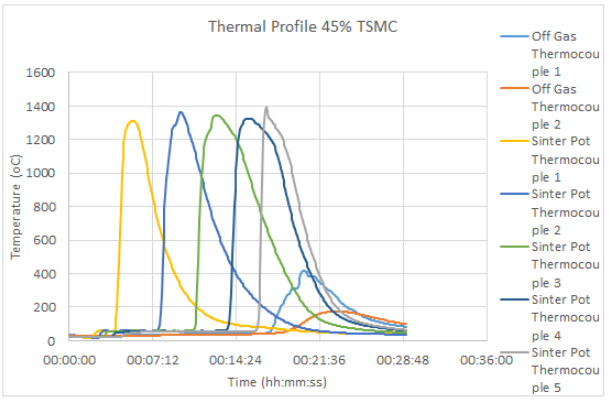

(f) Thermal profile from 45% Sinter feed B test

Figure 78: Thermal profiles from Sinter feed B study

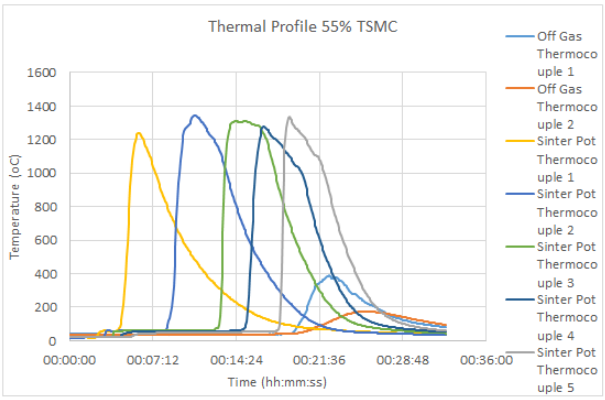

(a) Thermal profile from 55% Sinter feed B test

Figure 79: Thermal profiles from Sinter feed B study

On analysing the thermal profiles in figures 78 and 79 the following can be said; All thermal profiles exhibit relatively similar characteristics apart from TC3 and TC 1 in 0% Sinter feed B and 25% Sinter feed B profiles respectively. This could be due to incorrect thermocouple positioning. All traces start to increase where they should, starting to rise one after another. All traces peak where they should, peaking one after another. Tables below contain process parameters recorded during the tests as well as some averages. The information below also contain calculated flame front characteristics. Please see formula sheet for more information on calculations.

4.3.4 Post Analysis and Discussion

The characteristics that the temperature profiles exhibited indicated that the flame front propagated in a relatively uniform and stable manner across all tests. Off gas temperatures started to rise after all embedded thermocouples also indicating a stable and uniform process. This indicated that once the flame front had passed the bottom of the sinter pot, no extra material re-ignited nor did a second flame front seem evident. This remained true as Sinter feed B content increased.

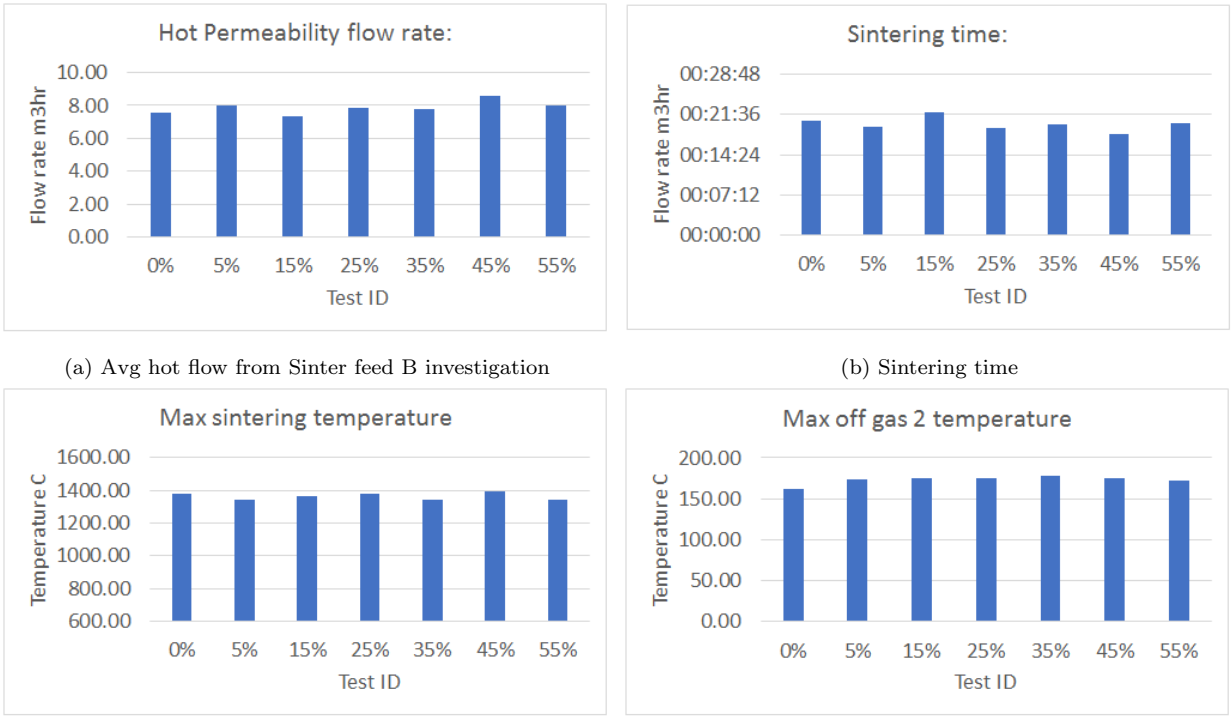

(a) Avg hot flow from Sinter feed B investigation

(b) Sintering time

(c) Sintering temperature

(d) Off gas temperatures

Figure 80: Calculated parameters from Sinter feed B study

On analysing figure 80 (a) no trends were visible when looking at the average flow rate through the bed after ignition. When analysing sintering time, it was evident that all tests had a sintering time of within 2 minutes of each with no significant trend. However, a slight trend might be observed on sintering time being decreased as sinter feed B was increased but not substantial enough to call it a true trend. On analysing the maximum sintering temperatures across all tests, it could be seen that maximum sintering temperature across all tests were within 50°C of each other. All within suitable sintering conditions but offering no trend in process characteristics on the increase of Sinter feed B. When analysing figure 80 (c) it must be noted that the off-gas temperature was 10°C lower when no Sinter feed B was included in the blend, as appose to when it was included into the blend.

Table 16: XRF of sinter for Sinter feed B investigation

	0%Sinter feed B	5%Sinter feed B	15%Sinter feed B	25%Sinter feed B	35%Sinter feed B	45%Sinter feed B	55%Sinter feed B
SiO_2	5	5.08	4.92	4.94	5.09	5.04	5.26
Al_2O_3	1.22	1.06	1.17	1.08	1.15	1.41	1.23
TiO_2	0.098	0.096	0.092	0.091	0.09	0.1	0.1
CaO	9.95	10.84	9.19	9.57	9.51	9.8	9.67
MgO	0.42	0.46	0.42	0.45	0.43	0.68	0.56
Fe	57.82	58.46	59.62	58.9	59.02	57.7	58.95
Fe_2O_3	71.91	69.13	71.72	79.99	79.03	69.03	75.67
FeO	9.69	13.01	12.17	3.81	4.83	12.12	7.76
P	0.061	0.044	0.044	0.039	0.038	0.042	0.038
Mn	0.19	0.14	0.14	0.16	0.13	0.16	0.13

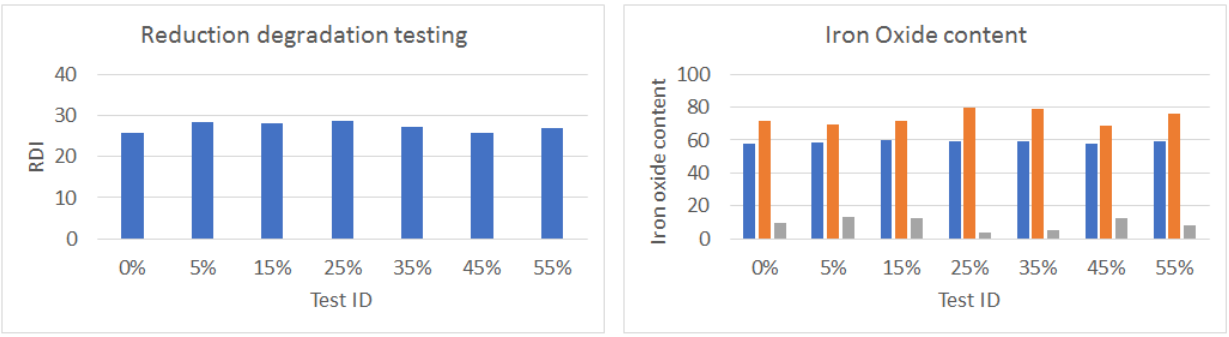

(a) RDI from Sinter feed B investigation

(b) Fe content

Figure 81: Chemical analysis and reduction degradation index testing for DRI study

As mentioned in the experimental design, sinter was taken for chemical analysis as well as reduction degradation index testing. No sinter yield took place. RDI and Fe content can be seen in figure 81 and a full XRF chemical composition analysis can be seen in table 16 on each of the finished sintered products. There was minimal variation in chemical composition between sinter products apart from some variation in FeO content. It must be noted here that during the process of sintering for blend that contained 25% Sinter feed B, it took longer for a flame front to be established. There was minimal variation within the RDI tests and all within a suitable range for acceptable production plant sinter. It must be noted here however that RDI value for 0 %Sinter feed B was one of the lowest out of all 8 tests and so had the best RDI characteristics.

4.3.5 Conclusion

i) It was evident from the thermal profiles observed that when sintering with Sinter feed B a uniform and stable process was evident. No process issues occurred when taking Sinter feed B content up to 55%

ii) Sintering time was within 2 minutes of each other across all tests with no trend evident

iii) Chemical composition of sintered products across all tests had minimal variation. However, FeO was slightly lower for that of the 25% Sinter feed B sintered product but this could be a result of process instability as it took longer for the flame front to establish itself. No trend was observed when Sinter feed B was increased further.

iv) Reduction degradation was not affected when Sinter feed B content was increased. However, RDI was improved when using no Sinter feed B.

4.4 Sinter feed C content

4.4.1 Introduction

Sinter feed C is a hematite concentrate. Concentrates are an important constituent in the composition of a sinter mix. They are usually produced at a pelletizing plant where the iron ores are crushed and then beneficiated where gangue material is removed [66]. Concentrates can have a chemical composition that can contain up 70% Fe, which is ideal for sintering. This can be seen in the chemical analysis of sinter feed C below. However, the small particle size of concentrate can sometimes bring about problems when trying to create adequate nuclei to layering ratios to achieve optimum granulation characteristics for optimum sintering. However, when used in correct quantities it can increase adhering particles to a point where it promotes the layering of nuclei which increases permeability. The following experiments set out to achieve an understanding of how these concentrates can impact the sintering process via the pilot line sinter furnace. The sinter feed C in this study was subjected to chemical analysis via XRF ant this can be seen in the table below.

Table 17: Sinter feed C composition

XRF	Ore D
SiO_2	4.34
Al_2O_3	0.03
TiO_2	0.05
CaO	0.44
MgO	0.42
Fe	65.58
Fe_2O_3	79.59
FeO	12.76
P	0.007
Mn	0.14

4.4.2 Experimental procedure

There were 4 sinter pot tests conducted in this study including repeats. Blend A only contained 4% sinter feed C. Blend B contained 40% concentrates including the addition of 32% sinter feed C. Please note that a small percentage of sinter feed F was used to balance chemistry. Please see chapter 3 for sinter pot dimensions and full methodology. Please see chapter 3 section 3.7 for experimental procedure, formula sheet and post analysis procedure. Blends contained the following:

Table 18: Blend composition

Material	Blend A	Blend B	units
Sinter feed C	0.000	4.129	Kg
Sinter Fines	2.581	2.581	Kg
Sinter feed E	0.516	0.826	Kg
Sinter feed F	0.000	0.206	Kg
Sinter feed B	9.806	5.161	Kg
Limestone	2.194	2.194	Kg
Coke Breeze	0.903	0.903	kg

Please note: Sinter pot tests were conducted at 7% fuel at 75mbar.

A) **First Experiment:**

x2 pot test with blend A at 100mbar

B) **Second Experiment:**

x2 pot test with blend B at 100mbar

4.4.3 Results

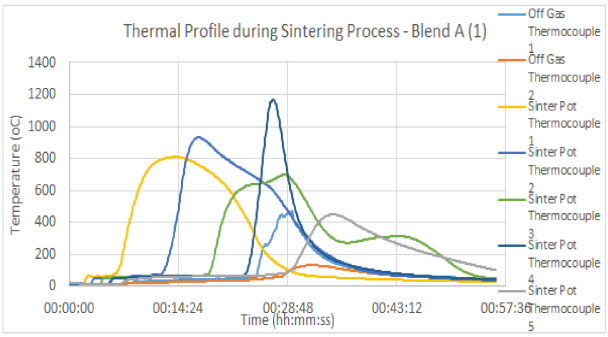

(a) Thermal profile from 0% sinter feed C test

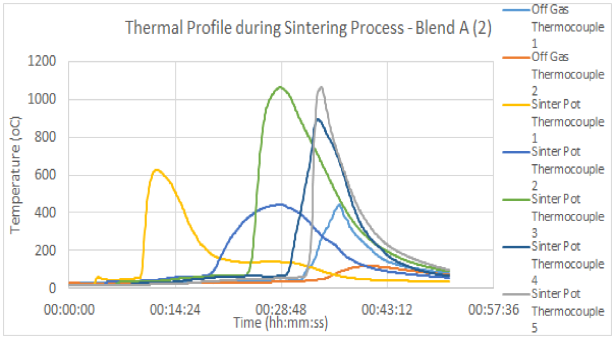

(b) Thermal profile from 0% sinter feed C test

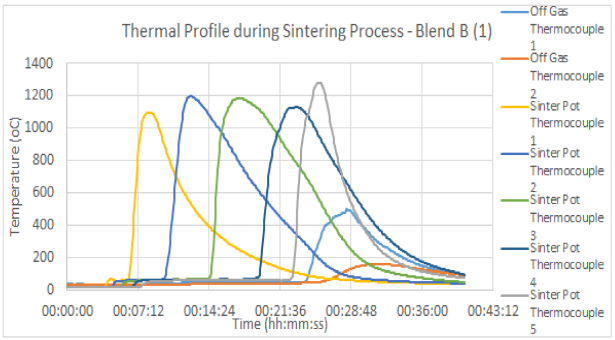

(c) Thermal profile from 32% sinter feed C test

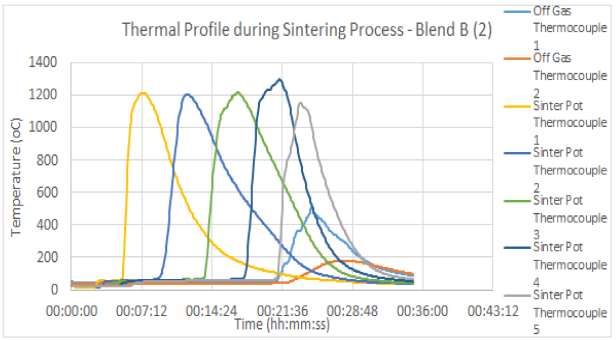

(d) Thermal profile from 32% sinter feed C test

Figure 82: Thermal profiles from sinter feed C study

4.4.4 Analysis and Discussion

On inspecting the thermal profiles in figure 82 a-d, the following can be said; When looking at the thermal profiles of the sintering tests conducted with blend A, it was evident that the thermal traces appeared in a non uniform manner. Thermocouple traces started to rise one after another, however, did not peak one after another. This indicated that the flame front propagated downwards through the bed in an erratic manner. Some of the thermocouple traces did not reach adequate sintering temperatures and so the flame front could have been partially broken up as it descended downwards. It is also worth noting that the last embedded thermocouple started to rise after the off gas thermocouple, which adds to the erratic and non uniform manner of the flame front propagation. This indicated that parts of the sinter cake started to reignite after the initial flame front passed the bottom of the bed, further indicating an erratic, unstable process. The graphs below indicate differences in the process when using a small amount of concentrates compared to a large amount.

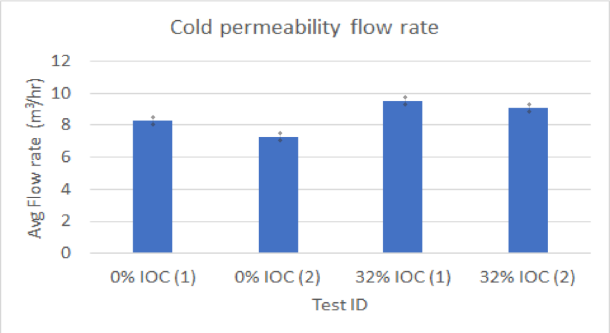

(a) Average cold flow per test

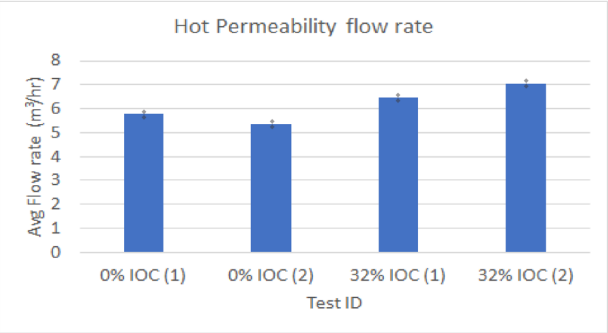

(b) Average hot flow per test

Figure 83: Flow rates calculated for sinter feed C investigations

When flow rates were analysed in figure 83 (a) and (b), it was clear that when using concentrates it produced an increase in bed permeability which was evident from the average cold flow rate. This could be due to the increased amount of adhering particles able to layer around the nucleus which in turn increased bed permeability. Having more nucleus than adhering resulted in a smaller average granule size after granulation. Further in depth investigations on granule size after granulation should be performed in order to clarify this statement. It can be seen that the bed permeability increase was also maintained after ignition. This indicated a higher permeable flame front as it descended downwards through out the bed. This, in theory, would increase flame front speed as well as sintering time.

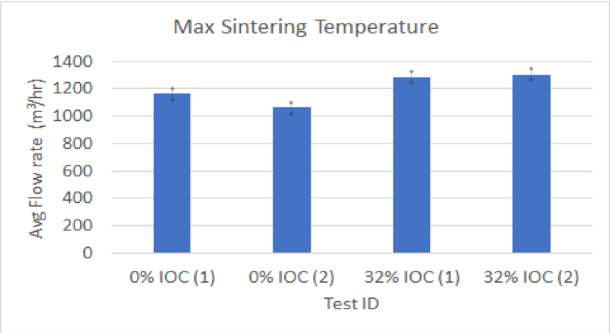

(a) Maximum sintering temperature per test

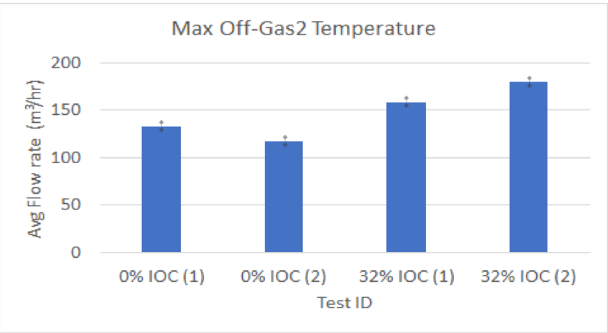

(b) Maximum off gas TC temperature per test

Figure 84: Calculated parameters for sinter feed C investigations

Figure 84 (a) and (b) shows the maximum temperature reached within the sinter pot per test and the maximum temperature reach in the off gas thermocouples in the wind-main directly below the sinter pot. It could be seen that due to the uniform and erratic flame

flame front behaviour, temperatures only reached a maximum of 1180°C when using blend A. However, when sintering with blend A, including repeats, only 1 thermocouple increased over 1100C. When sintering with blend B it was evident that all thermocouples apart from one, reached over 1100°C. It is worth noting here that the 1 thermocouple not passing 1100°C was only 3°C short. This indicated that a well established flame front was evident when using blend B. However, a well established flame front was not evident when using Blend A. This is clarified and can be seen in figure 87 (a). When looking at the off gas temperatures, blend B producing higher values. This was expected due to the low sintering temperatures exhibited when using Blend A.

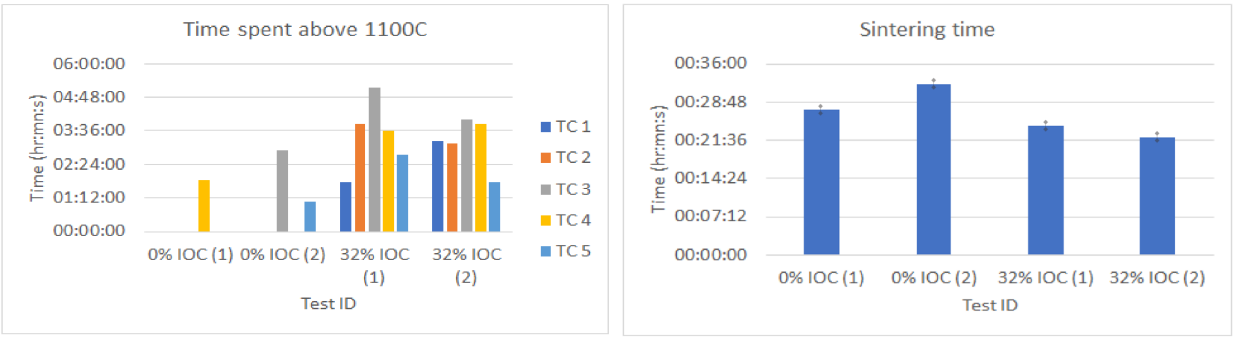

(a) Time spent above 1100C

(b) Sintering time

Figure 85: Calculated parameters for sinter feed C investigations

Figure 85 (a) and (b) shows the time spent above 1100°C per test as well as over all sintering time per test, respectively. On analysing (b) it can be seen that sintering time was decreased when using blend B. This correlated with the data in figure 85 when looking at average cold flow rates through the bed before and after ignition and was due to the increased bed permeability.

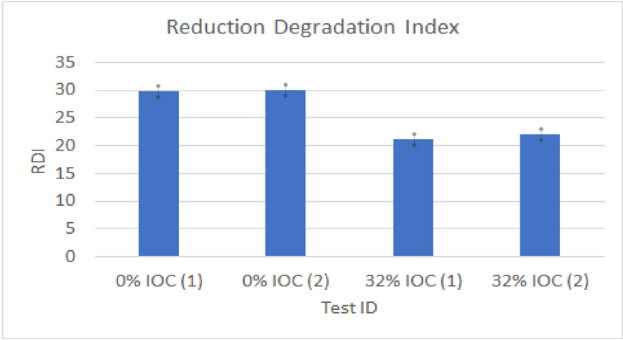

Figure 86: Reduction Degradation Index for sinter feed C investigation

The sintered cake from each initial test was evaluated for RDI strength via the standardised reduction degradation index testing. Unfortunately a sinter yield was not calculated for this set of experiments. However, sinter in the size fraction of 16-20mm was subjected for reduction degradation testing. This can be seen in figure 86 above. It could be observed that the RDI value is substantially lower (improved) when using blend B. This was due to the adequate sintering temperatures observed when sintering with blend B as appose to A. This indicates that the fines within the blend gave stability to the process.

4.4.5 Conclusion

i) It was evident from the thermal profiles observed that when sintering with blend A that had a very low amount of concentrates and no sinter feed C, the process was erratic and low sintering temperatures were observed. However, when sintering with a high amount of concentrates which included sinter feed C, a uniform thermal profile was witnessed. This indicated stable flame front propagation and hence a stable process.

ii) Sintering time was improved when using concentrates and this could be due to the increased granule size after granulation, which improved bed permeability, thus increasing flame speed and hence decreasing sintering time.

iii) RDI strength via reduction degradation testing improved when using a large amount of concentrates. this was due to the adequate sintering temperatures observed in the process when compared to the sintering temperatures observed when using a low amount of concentrates i.e blend A.

iv) Further investigation should be performed to investigate the granule size after granulation to confirm this was the reason of the increased bed permeability.

5 Fuel Sources And Particle Size Distribution

This chapter focused on optimising the fuel source in the sinter pot. The following will attempt to explain how the fuel was optimised to maximise efficiency and productivity and to gain an understanding of the fundamental concepts occurring during iron ore sintering when altering various fuel parameters. Optimisation was investigated with regards to breeze percentage content, particle size distribution, alternative fuels and fuel combinations. Particle size distribution of different fuel ratios of anthracite to breeze was extensively investigated due to the little research in the domain on the topic and to build on the research already available on particle size and ratios. Although anthracite and breeze additions have been been researched in the past, particle size distribution was not investigated with the close process control and quality analysis. The fuels used were characterised using thermo-gravimetric analysis and various optical microscopy techniques. Furthermore, recent research suggests that all experimental work completed using alternative fuels such as anthracite have been on a fuel particle size of less than 3mm in diameter. Anthracite will in fact have a much larger average particle size when being used in a sinter plant. This section also intended to obtain an understanding of the sintering process when fuelling the small-scale sinter furnace with a larger fuel particle size up to 5.00mm.

5.1 Fuel characterisation

Coke breeze and anthracite have been used in the iron ore sintering industry for many years. Anthracite is being increasingly used in industry due to reasons such as the shortage of coke breeze and price tag of anthracite. Many sintering plants use anthracite in small percentages to help lower costs and some have reported anthracite usage up to 90%. The issue is that there is not enough scientific information out there for relatively new control operators to make rapid informed decisions on a daily basis without having to rely on experience. The rapid informed decision making should be based on facts and data. Recent research tells us how anthracite can perform in a small-scale sinter furnace in terms of sintering speed and sinter yield. Recent studies suggests a lack of flame front characteristic knowledge when using anthracite. Furthermore, it is unknown what happens to the flame front characteristics when increasing anthracite particle size as well as combining both anthracite with coke breeze in different ratios. In this section, an attempt to characterise the fuel used in the sinter plant has been done. It is important to understand the characteristics of the fuels in terms of thermal properties as well as their micro structures as this can have a direct impact on flame

front propagation during iron ore sintering. Fuels include coke breeze, anthracite A and anthracite B.

5.1.1 Thermogravimetric analysis

This section concentrates on characterising the thermal properties of coke breeze and anthracite. The thermogravimetiric experimental procedure was as follows:
The furnace temperature is increased to 110°C at a rate of 20C/min and held isothermally for 15 minutes. This ensured that any weight loss experienced is a direct impact of the moisture in the coal. The temperature is then increased to 950°C at a rate of 40C/min and held isothermally for 25 minutes. Any weight loss occurring in this isotherm region is a direct result of the loss of volatile matter. The previous two steps are performed in a nitrogen atmosphere. For the third part, the atmosphere is then changed to oxygen. This creates an environment suitable for combustion. Once complete combustion of coal has occurred, the residue is taken as the ash. The following method was used:
Both fuels were characterised using various analysis techniques. Shape and surface characterisation were done using the optical microscopy. Combustion characteristics were analysed using a thermogravimetric analyser. Method for TGA testing was as follows:

i) Hold for 1.0min at 30°C

ii) Hold for 1.0min at 30°C

iii) Heat from 30.00°C to 110°C at 20°C/min

iv) Hold for 15.00 minutes at 110°C

v) Heat from 110°C to 950°C AT 40.00c/min

vi) Hold for 25min at 950°C

vii) Switch from nitrogen to air at 30.0ml/min

viii) Hold for 40.0min at 950°C

Thermal characteristics were obtained such as change in enthalpy, ash percentage and combustion time for analysis.

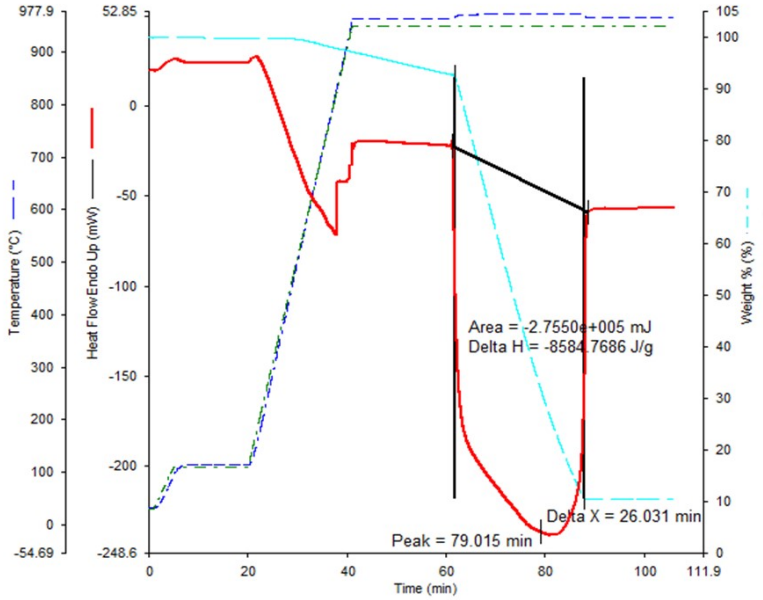

Figure 87: Thermogravimetric analysis of Breeze particles

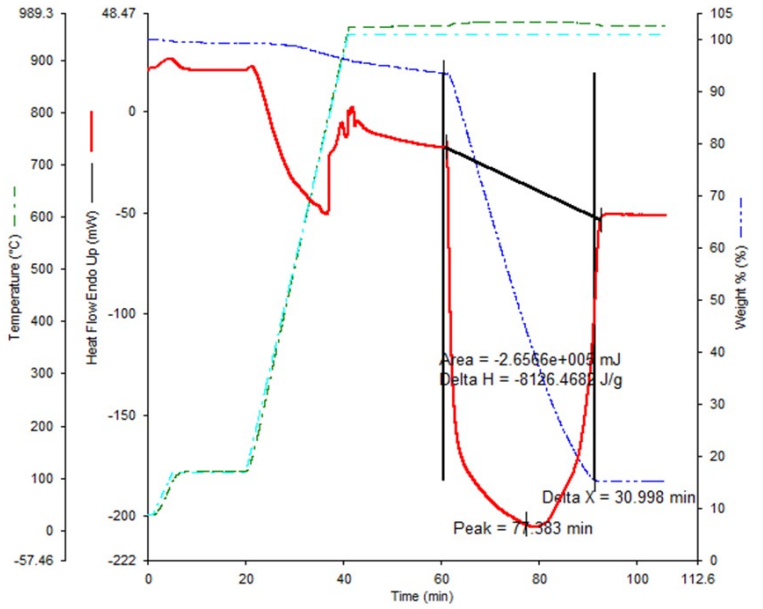

Figure 88: Thermogravimetric analysis of Anthracite particles

On investigating the thermogravimetric graphs in figure 87 and 99, under constant gas flow of oxygen at 950°C coke breeze takes 26.9 minutes for complete combustion. After combustion coke breeze had 10.5% mass remaining, this can be classed as ash content. It

was also evident that coke breeze had an energy release of 216.7mW. During combustion, coke breeze sample reached a temperature of 974.05°C. In comparison, anthracite took 31.1 minutes for complete combustion. After combustion anthracite had 15.2% mass remaining, this can be classed as ash content. It was also evident that anthracite had an energy release of 187.3mW. During combustion, anthracite sample reached a temperature of 972.71°C. The sample temperature was increased to 950°C in nitrogen and so everything driven off here was either moisture and or volatile matter. It must be noted here sample weights were identical. Further analysis can be deployed in future work to investigate this volatile matter. Recent research suggests that anthracite has a higher volatile content than coke breeze [22]. The results indicate that coke breeze reaches a higher combustion temperature, and releases more energy at an increased rate than anthracite.

5.1.2 Optical Microscopy

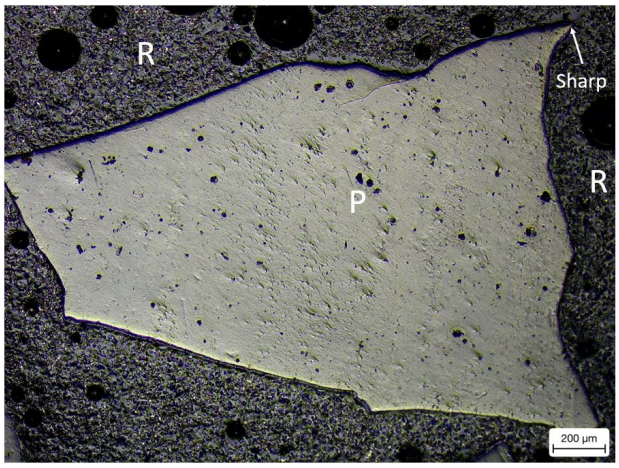

(a) Welsh anthracite

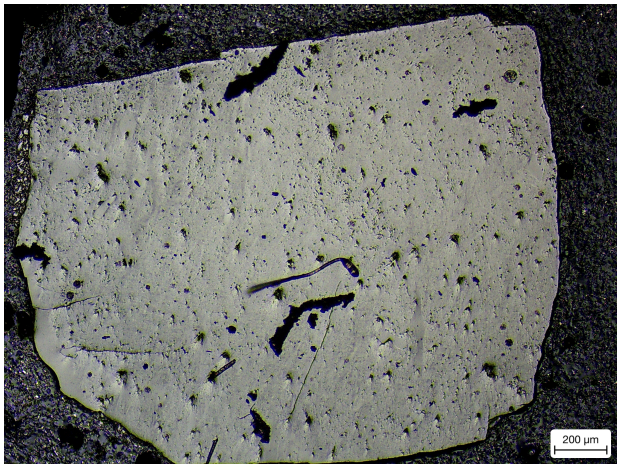

(b) Russian anthracite

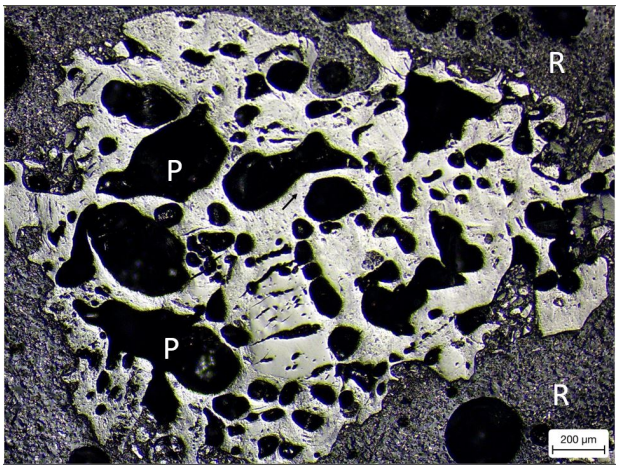

(c) Coke breeze

Figure 89: Microstructures of different fuels used. R - Resin, P - Pore

Figure 89 shows the microstructures of the various fuels used in this chapter. Fuel in the size fraction of between 2-3mm was mounted in resin and polished for optical microscopy. It was evident from analysing the microstructures that coke breeze was more round in shape compared to the anthracite samples which appeared very irregular. Anthracite A exhibited sharp angular corners where anthracite B exhibited less sharp angular corners. This could impact moisture retention capabilities as well as granulation characteristics and therefor bed permeability as it would increase the difficulty for adhering particles to agglomerate to the sharp corners. Coke breeze also exhibited a substantial increase in total pores compared to the anthracite samples. It must be noted these microstructure characteristics were evident in

the majority of samples analysed across the board. It can be noted here that microstructure characteristics correlated with flow rates measured prior to ignition when comparing bed permeability when using coke breeze as opposed to anthracite. This can be seen in figure 90 below.

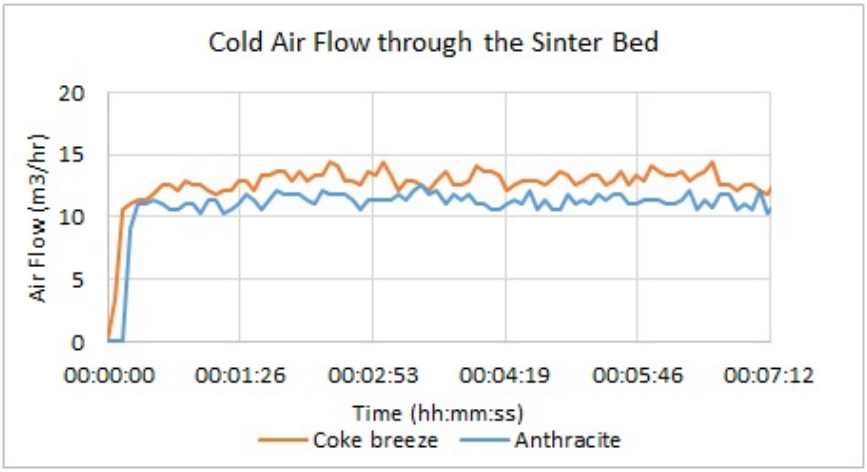

Figure 90: Comparing flow rates across bed prior to ignition with different fuels

Future work using Anthracite

It must be noted here that anthracite A was only used in the optimum particle size study in this chapter. After this study, anthracite B was used through out for the particle size distribution as well as ratio study. The reason for this was logistical and that origin of anthracite A had depleted, and was no longer available to use. It must also be noted here that anthracite B was investigated in more detail due to it having significant industrial impact and was readily available. It can be said that the differences in anthracite A and B was noted above during the characterisation of fuels and this was minimal. This allowed for investigating the impact of particle size, particle size distribution and varying ratios of anthracite in sintering to be made.

5.2 Coke Breeze Optimal Particle Size Versus Anthracite

5.2.1 Introduction

This section of the chapter will concentrate on investigating what particle size of fuel is optimal for use in the sinter pot. An optimal particle size region is generally understood for sinter plants but it is the case that the information and data acquired from sinter plants are usually kept internal. The sinter pot was deployed for this investigation in hopes to gain an understanding of the process and product when altering fuel particle size. An optimal particle size for the pot was also investigated. Fuel used for investigation was coke breeze and anthracite. The experimental procedure was as follows:

5.2.2 Experimental Procedure

Before any sinter pot tests were conducted, a chemical analysis and a sizing analysis was performed on the coke breeze and anthracite and then incorporated into a blend model. Breeze and anthracite was sized into separate size fractions of 0-1mm, 1-2mm, 2-3mm and 3-4mm. 8 sinter pot tests were conducted for this experiment. Please see chapter 3 section 3.7 for experimental procedure, formula sheet and post analysis procedure. Blends contained the following:

Table 19: Blend composition

Material	Blend A - kg	Percentage
Sinter Fines	1.935	15.0
Sinter feed A	2.742	21.5
Sinter feed B	2.742	21.5
Sinter feed C	2.742	21.5
Sinter feed D	2.742	21.5
Limestone	2.194	17.0
Fuel	0.903	7.0

Please note: sinter pot tests were conducted at 7% fuel

A) **First Experiment:**

Test 1 - Typical ore blend fuelled with coke breeze with particle size 0-1 mm

Test 2 - Typical ore blend fuelled with coke breeze with particle size 1-2 mm

Test 3 - Typical ore blend fuelled with coke breeze with particle size 2-3 mm

Test 4 - Typical ore blend fuelled with coke breeze with particle size 3-4 mm

B) **Second Experiment:**

Test 5 - Typical ore blend fuelled with W Anthracite with particle size 0-1 mm

Test 6 - Typical ore blend fuelled with W Anthracite with particle size 1-2 mm

Test 7 - Typical ore blend fuelled with W Anthracite with particle size 2-3 mm

Test 8 - Typical ore blend fuelled with W Anthracite with particle size 3-4 mm

5.2.3 Results

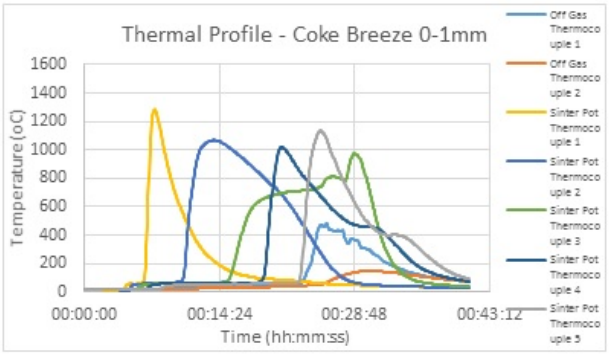

(a) Thermal profile from test with 0-1mm breeze

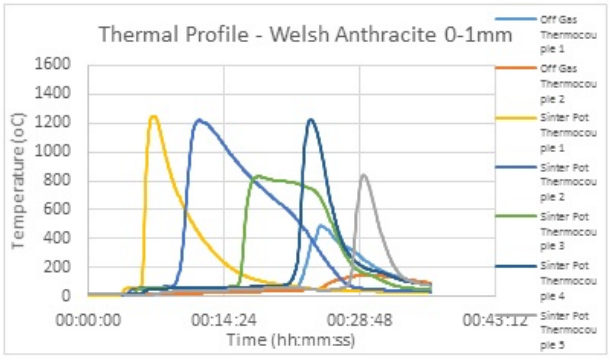

(b) Thermal profile from test with 0-1mm anthracite

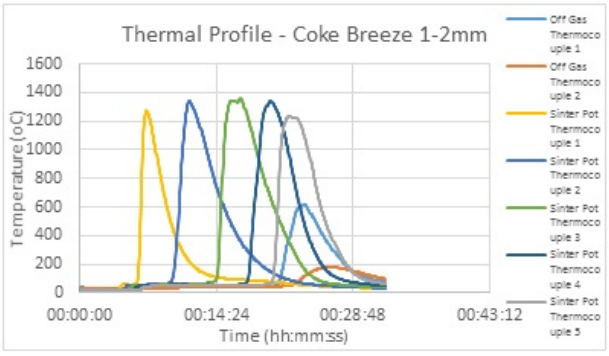

(c) Thermal profile from test with 1-2mm breeze

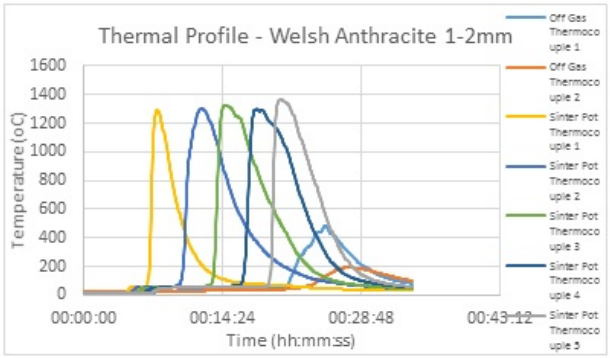

(d) Thermal profile from test with 1-2mm anthracite

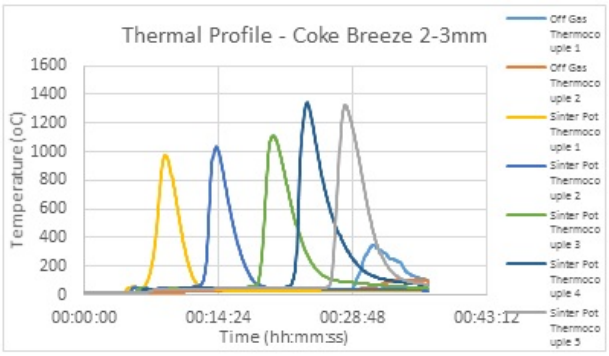

(e) Thermal profile from test with 2-3mm breeze

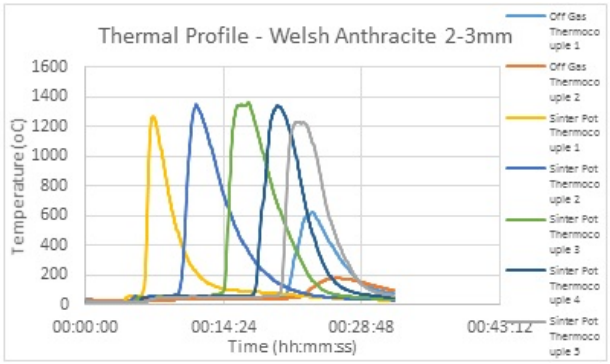

(f) Thermal profile from test with 2-3mm anthracite

Figure 91: Thermal profiles from fuel particle size study

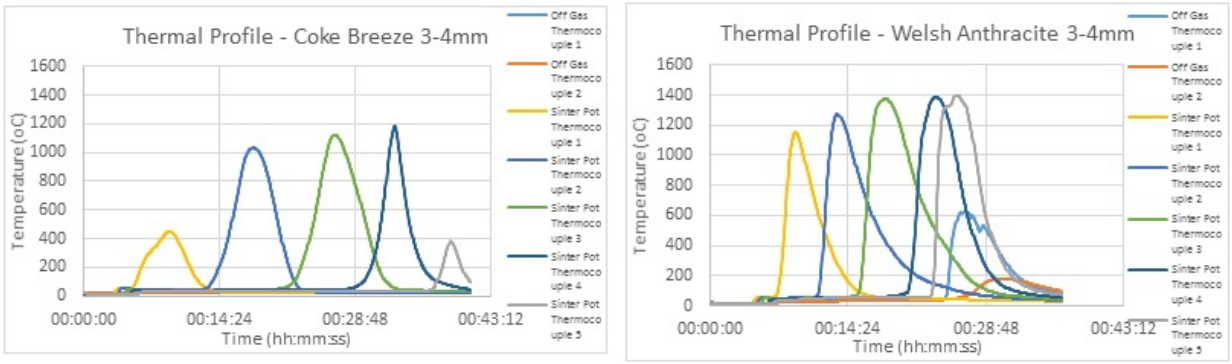

(a) Thermal profile from test with 3-4mm breeze

(b) Thermal profile from test with 3-4mm anthracite

Figure 92: Thermal profiles from fuel particle size study

5.2.4 Analysis and Discussion

Coke breeze vs Welsh anthracite at 0-1 mm

i. It was evident from comparing thermal profiles that when fuelling the sinter pot with coke breeze or anthracite at a very fine particle size of 0-1mm an unstable erratic flame front is produced. This is evident from analysing the thermal profiles for this particle size range. It is clear that each trace does not form/peak sequentially one after another and it is also clear that sintering temperatures are not being reached consistently. It can also be seen that the off gas 1 traces for both thermal profiles start to rise before the last embedded thermocouple thus the flame front has broken apart, with different sections of the flame front reaching the bottom at different times. It is evident of an unstable process and this is backed up by the amount of sinter made during these tests as well as RDI results and this can be seen in table 20.

Coke breeze Vs Welsh anthracite at 1-2 mm

ii. Figure 91 C-D shows the thermal profiles for sinter pot tests fuelled with coke breeze or anthracite at increased particle sizes of 1-2mm. When comparing the profiles when fuelled with anthracite as opposed to coke breeze in the size range of 1-2mm it is clear that both of the processes are stable. When comparing profiles of all size ranges, it was apparent that this was the ideal size range in terms of stability. This is evident from the thermal profiles as each trace peaks and drops sequentially, indicting the flame front passing each embedded thermocouple one after another, indicating no break ups. Flame front temperatures at each embedded thermocouple are in the correct sintering temperature range. Off gas thermocouple temperatures peak one after another and both peak after all embedded

thermocouples, proving that the flame front travelled in a stable consistent manner. This is the first indication that anthracite B may have promising results.

Coke breeze Vs Welsh anthracite at 2-3 mm

iii. When analysing the thermal profiles for the sinter pot tests fuelled with anthracite or coke breeze in the size range of 2-3mm, it was clear that for the coke breeze fuelled test, the flame front does not reach ideal sintering temperatures apart from the last 2 embedded thermocouples, evident from the graph. The thermal profile also indicates that the flame front is thinner and slower. This is evident from analysing flame front characteristics. When looking at the profile fuelled with anthracite at a size range of 2-3mm, the profile shows stable characteristics. Sintering temperatures are being maintained by all thermocouples and each trace peaks and drops sequentially, indicating that stable flame front travel. This is the first indication that anthracite B may have better sintering characteristics than that of coke breeze as it still produces ideal sintering characteristics at a high particle size as opposed to what coke breeze fuelled tests can produce at this size range.

Coke breeze Vs Welsh anthracite at 3-4 mm

iv. The statements above are emphasised even further when analysing the thermal profiles for anthracite or coke breeze at the size range of 3-4mm. It can be seen that for the coke breeze fuelled test at this size range that the flame front temperature does not reach ideal sintering temperature across all thermocouples and basically no sinter was made. By the time the flame front got to the 4th thermocouple it had died out dropping to below 400C. When this thermal profile is compared to the anthracite fuelled profile it's evident that the anthracite fuelled test at a particle size range of 3-4 still produces a relatively stable process. All thermocouple traces peak and drop sequentially. All thermocouples reach ideal sintering temperatures and off gas thermocouple traces peak after embedded thermocouples.

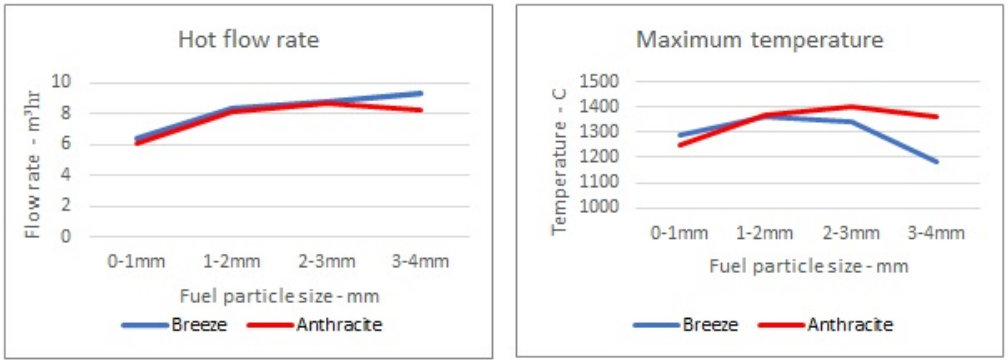

(a) Average hot flow rate comparison

(b) Maximum temperature comparison

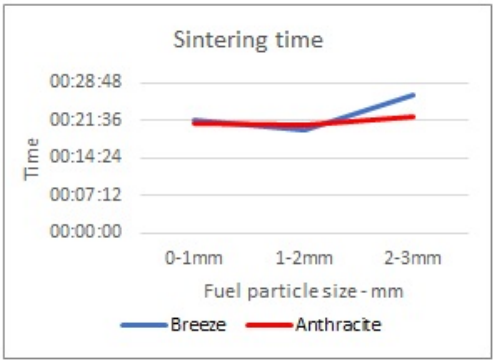

(c) Sintering time comparison

Figure 93: Comparison of process parameters from fuel particle size study

On analysing the data, it was evident that as fuel particle size in increased, the average cold and hot flow rate is increased, This indicated an increase in bed permeability. From looking at figure 93, it was clear that both anthracite and coke breeze have similar trends when increasing particle size in terms of sintering time. However, it must be noted here that the only stable thermal process for the coke breeze fuelled test was in the 1-2mm particle size region. It was also clear that sintering time for the anthracite (1-2mm) fuelled tests was slightly faster than that of the coke breeze fuelled tests at the same particle size range. It should also be noted here that sintering time generally decreased as particle size increased for the anthracite fuelled tests but continued to produce sinter. The sinter produced was still of good quality and this was evident from table 20. This was not the case for coke breeze fuelled tests. It was also evident that anthracite produced an increased maximum sintering temperature per test than the coke breeze fuelled tests apart from when fuelling with a size range between 0-1mm. Even then the process was unstable so it was difficult to draw any accurate conclusion. Sintered flow rates give indication of porosity of sinter. When analysing the sintered flow rates, it was clear that when fuelling with coke breeze,

low sintered flow rates were evident apart from when using particles in the 1-2mm range. However, when fuelling with anthracite, sintered air flow rate were high for all tests apart from when fuelling with a very small particle size. This indicated that sinter was produced with adequate porosity. This was further backed up when subjecting the sintered product to 1-minute mechanical vibration and sieving into size fractions which can be seen in figure 96 below.

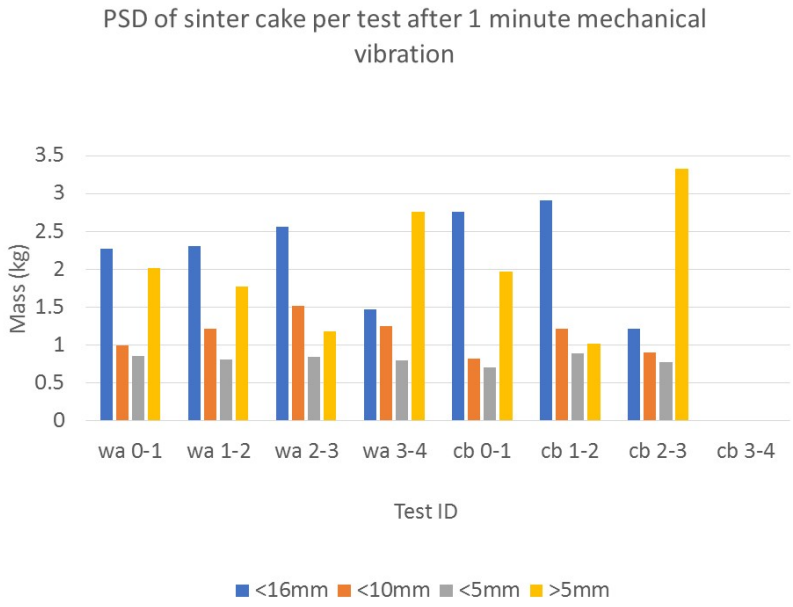

Figure 94: Sinter yield from fuel particle size study

Table 20: XRF of sintered product from fuel particle size study

	wa 0-1	wa 1-2	wa 2-3	wa 3-4	cb 0-1	cb 1-2	cb 2-3
RDI	50.62	9.89	31.84	33.99		29.7	44.31
SiO_2	5.46	5.29	5.16	4.74	5.29	5.07	5.67
Al_2O_3	1.32	0.99	0.96	0.93	1.16	1.19	1.21
TiO_2	0.12	0.11	0.08	0.1	0.13	0.11	0.14
CaO	10.36	10.02	9.92	9.61	10.01	9.98 9.63	
MgO	0.6	0.59	0.53	0.45	0.57	0.55	0.81
Fe	58.09	59.18	59.88	58.69	58.08	59.07	58.09
Fe_2O_3	75.57	72.55	77.49	75.45	74.57	76.36	75.83
FeO	6.74	10.86	7.32	7.62	7.63	7.29	6.51
P	0.038	0.038	0.037	0.037	0.036	0.037	0.039
Mn	0.15	0.16	0.15	0.16	0.15	0.17	0.16
CaO/SiO_2	1.897436	1.89414	1.922481	2.027426	1.89225	1.968442	1.698413
Al_2O_3/SiO_2	0.241758	0.187146	0.186047	0.196203	0.219282	0.234714	0.213404

As mentioned, sinter produced in the size region between 16-20mm was subjected to chemical analysis. This can be seen in table 15 above. When comparing chemical composition of sinter made when fuelled with particles between 1-2mm, it was clear that minimal variation was evident. It is worth noting here that there was variation in FeO content within the produced sinter when fuelling with coke breeze and anthracite particles between 1-2mm. This could be due to the higher temperatures reached when using anthracite. However, variation could be expected due to the variation in thermal characteristics between tests. It is worth noting here that basicity remained in a suitable range for sinter plant conditions as well as all other composition.

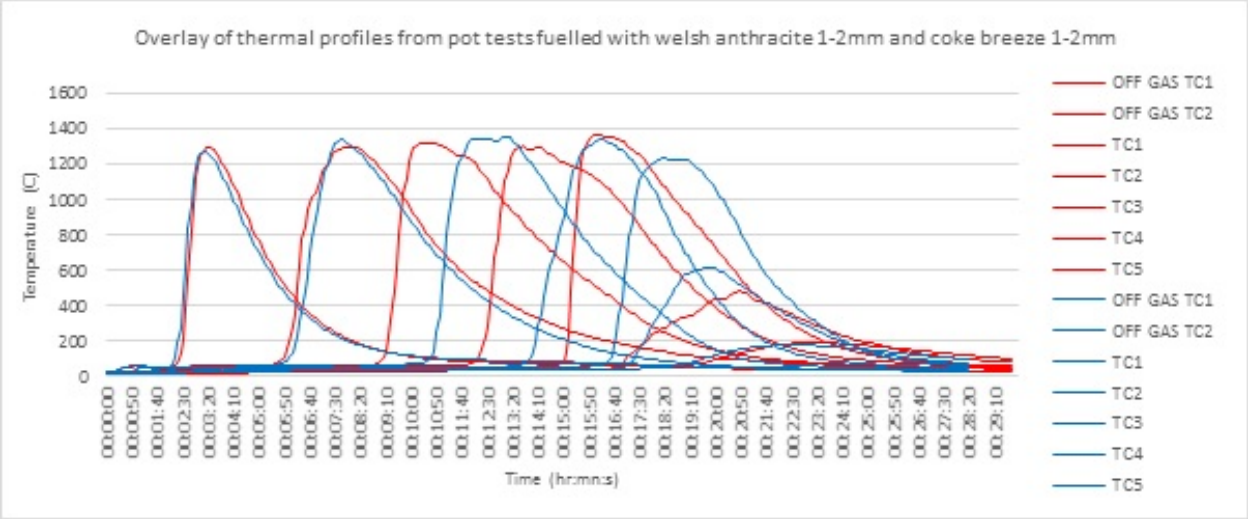

Figure 95: Overlay of thermal profile from tests conducted with 1-2mm anthracite(red) and 1-2mm breeze(blue)

As mentioned earlier, the only two comparable tests are the pot tests fuelled with coke breeze particles between 1-2mm and the pot tests fuelled with anthracite particles between 1-2mm. Flame front speed, thickness and cooling rates can be compared between the two fuels as well as comparing the sintered product of these tests. The only reasonable conclusion that can be drawn from analysing the other anthracite and coke breeze fuelled tests is that anthracite continues to produce a stable process as we increase fuel particle size whereas coke breeze becomes unstable relatively quickly. As a result of this, the following analysis concentrates on the characteristic differences between process parameters and sintered products between the tests fuelled with anthracite and coke breeze particles between 1-2mm. Figure 95 shows an overlay of the thermal profile traces from test fuelled with Welsh anthracite particles between 1-2mm. The blue trace represents the breeze fuelled test and the red trace represents the anthracite fuelled test. Both data sets are overlaid so that ignition starts at the same point. TC1 and 2 traces are almost identical apart from that the cooling curve seems to have a higher gradient and takes more time to cool. It was also clear that the anthracite trace for TC 2 starts to peak just before the coke breeze fuelled test. This was emphasised when comparing TC3 for anthracite and coke breeze where it is even clearer that the anthracite trace starts to peak around a minute before the coke breeze fuelled trace and then cools at a slower rate. This is also true when comparing TC 4's and TC5's traces. Even though the anthracite TC 5 trace peaks before the coke breeze fuelled TC 5 trace, both off gas TC 1 traces start to peak at the same time However, the anthracite fuelled trace takes

longer to peak indicating a slightly longer sintering time. It was also evident that there was minimal variation in maximum temperatures reached per thermocouple. Maximum temperature reached by embedded thermocouple was 1369°C by the anthracite fuelled test and only 10°C higher than the maximum temperature reached by the coke breeze fuelled test. It should be noted, even though the maximum sintering temperature reached was higher for anthracite fuelled test, all other thermocouples within the test were consistently lower than the thermocouples in the coke breeze fuelled tests. It was also evident that for the coke breeze fuelled test, the flame front thickness generally increased the further it progresses down the pot. It seemed that the anthracite fuelled test had a flame front that generally followed the same trend apart from between TC2-3, where thickness was relatively large compared to the breeze fuelled test. The same trend was exhibited for flame front speed which was evident in figure 96 below. It was evident that the anthracite fuelled flame front speed increased between thermocouple 2 and 3.

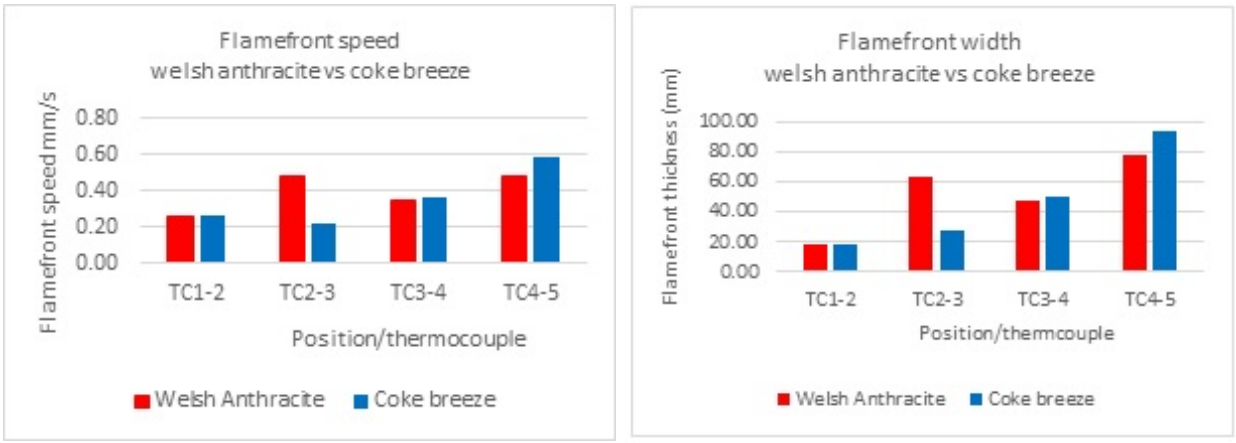

(a) Flame front speed from anthracite vs breeze 1-2mm

(b) Flame front width from anthracite vs breeze 1-2mm

Figure 96: Comparing flame front characteristics for tests fuelled with 1-2mm fuel particles

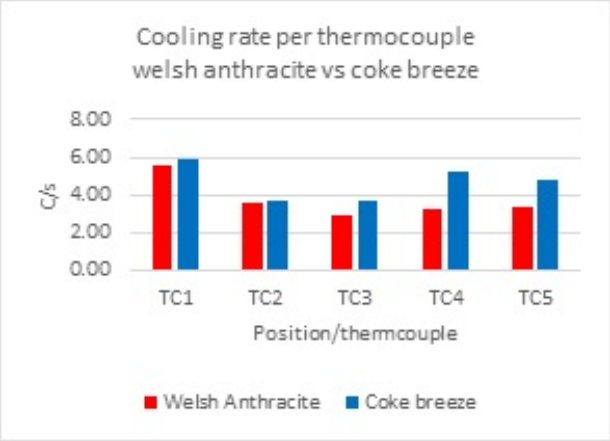

(a) Cooling rate from anthracite vs breeze 1-2mm

Figure 97: Cooling rates for tests fuelled with 1-2mm fuel particles

Optical microscopy

Figure 97 shows the microstructures of the sinter produced from the tests conducted with breeze and anthracite particles between 1-2mm. A and B shows microstructures of sinter produced when fuelled with particles of breeze and anthracite at 0-1mm. C and D shows microstructures of sinter produced when fuelled with particles of breeze and anthracite at 1-2mm. On analysis of the microstructures it was evident that both A and B had hematite and magnetite with SFCA's in the form of globular block like structures. Where as, C and D exhibit more needle like SFCA's. This was due to the adequate sintering temperatures reached when fuelling with particles at 1-2mm. There were no major microstructural differences when fuelling with breeze as opposed to anthracite. However, this shows the importance of fuelling with the correct particle size as it can have a direct impact on the sintering temperatures. Therefor, the difference in sintering temperatures can impact the morphology and thus the structural formation of the hematite and SFCA's. As stated in the literature review, when higher temperatures are reached, SCFA-1 formation is favoured over SFCA. More investigations should be performed on whether the duration spent at high temperatures could have an impact on the formation of the SFCA's. The main take away from the optical microscopy is that fuelling with breeze or anthracite doesn't vary the formation of the phases, however, particle size plays a more important role.

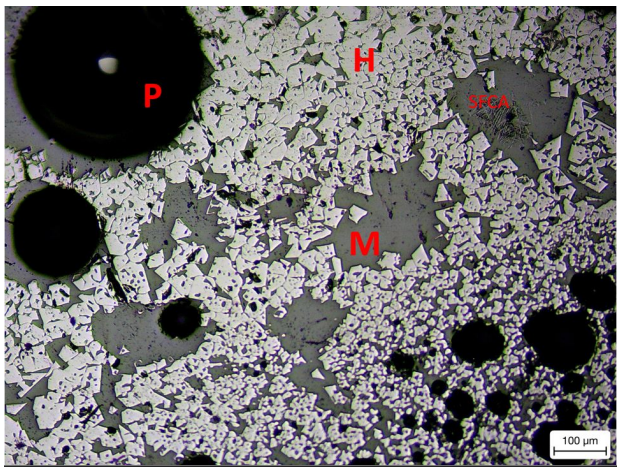

(a) sinter fuelled with breeze 0-1mm

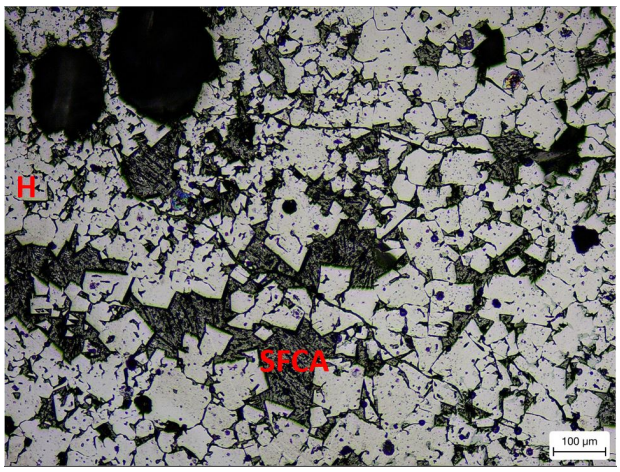

(b) Sinter fuelled with anthracite 0-1mm

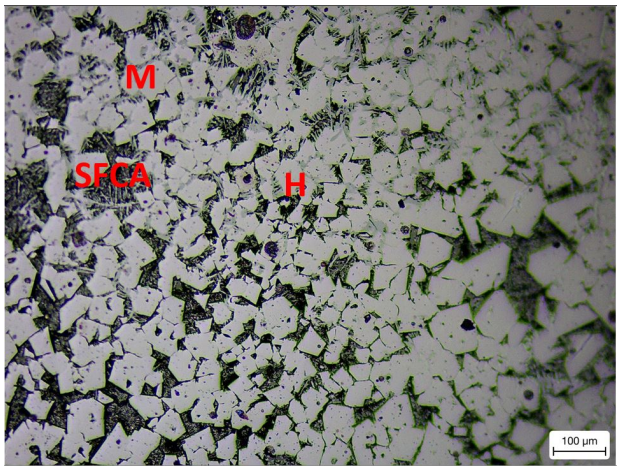

(c) sinter fuelled with breeze 1-2mm

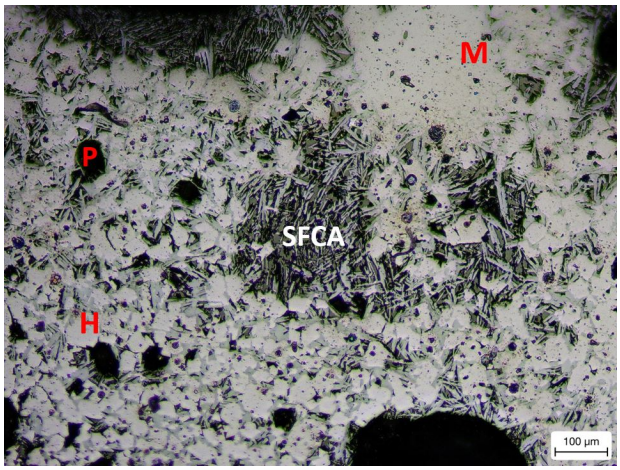

(d) Sinter fuelled with anthracite 1-2mm

Figure 98: Microstructures of sinter fuelled with breeze and anthracite. H - Hematite, M - magnetite, SFCA - silca-ferrites of calcium alumnium

5.2.5 Conclusion

i) This work can conclude that anthracite fuelled tests produce a more stable process with higher sinter quality across all particle sizes when compared to coke breeze with an optimum particle size found at 1-2mm.

ii) For comparable conditions, the anthracite fuelled tests produced slower sintering times and slower cooling rates.

5.3 Optimal Fuel Particle Size Distribution and Ratio

This section of the chapter will deep dive into investigating how the iron ore sintering process is impacted by introducing different fuel particle size distributions as well as different fuel ratios of breeze and anthracite whilst using these different fuel particle size distributions. The fuels in questions were breeze and anthracite. Please note anthracite A differs chemically to anthracite B. As mentioned previously, not enough information is in the scientific domain on how anthracite influences the flame front properties and how this impacts the quality of sinter. Furthermore, recent research suggests that all experimental work completed using alternative fuels such as anthracite have been on a fuel particle size of less than 3mm in diameter. Anthracite will in fact have a much larger average particle size when being used in a sinter plant. This paper aims to obtain an understanding of the sintering process when fuelling the small-scale sinter furnace with a large fuel particle size up to 5.00mm. The results would be beneficial in terms of plant operations as sinter plants may find it difficult to crush anthracite to such a small size on such a big scale. Small scale sinter furnace tests were conducted in order to investigate parameters such as sintering time, flame front speed, flame front width, max sintering temperature, off gas temperature and flow rates.

5.3.1 Introduction

As the literature suggests, there is little information in the domain on how displacing anthracite with breeze, whilst carefully controlling the particle size distribution input of the fuel particle, can impact the sintering process as well as quality of sinter produced. [67] This section aims to gain an increased understanding of the matter.

Furthermore, recent research suggests that all experimental work completed using alternative fuels such as anthracite have been on a fuel particle size of less than 3mm in diameter, and the particle size distribution not controlled [67]. Anthracite will have a much larger average particle size when being used in a sinter plant. This paper aims to obtain an understanding of the sintering process when fuelling the small-scale sinter furnace with a large fuel particle size up to 5.00mm. The results will be beneficial in terms of scientific input as the particle size of the fuel is essentially too large for the process in the pot which will give valuable information on over sized fuel particles in iron sintering. The investigation will also be beneficial to plant operations as sinter plants may find it difficult to crush anthracite to a small size on such a big scale. It can be noted here that when the sinter plant in Port Talbot attempted to crush and screen large amounts of anthracite, it had clogged up the

screens deeming the screening equipment none-operational. Small scale sinter furnace tests were conducted in order to investigate parameters such as permeability, sintering time, flame front speed, flame front width, max sintering temperature, off gas temperature, flow rates as well as sinter quality such as chemical composition, RDI and phase mineralogy.

Industrial context:

Anthracite Coal was purchased with the intention to fuel the iron ore sintering process at the sinter plant in Port Talbot. Instabilities within the process resulted in the anthracite being taken out and subsequently set aside due to the negative impacts it was having on production. It was not fully understood why the instabilities occurred and as mentioned, there was not much information in the research domain on the matter. as such, the small scale sinter pot was deployed to investigate what impact this particular anthracite has on the sintering process compared to coke breeze, when displacing breeze in increments and controlling the particle size and particle size distribution.

5.3.2 Experimental procedure

This section sets out the different experiments conducted for this section. The experiments below were designed to investigate how the particle size distribution and ratios of anthracite coal to coke breeze can impact the iron ore sintering process. The expectations of this research is that the particle size distribution and ratios of anthracite coal to coke breeze, can negatively, as well as positively, impact the thermal properties and kinetics of the iron ore sintering process, and therefor, sinter quality.

Experiment 1 – Particle size less than 3.15 uncontrolled distribution

The first set of experiments were designed to compare sintering process parameters and sinter quality when the particle size distribution was not controlled apart from all fuel was less than 3.15mm. Testing included fuelling with 100% coke breeze and with 100% anthracite. Tests were repeated and conducted using experimental procedure outlined in chapter 3.

Experiment 2 – Controlled PSD less than 3.15mm

The second set of experiments were designed to compare sintering process parameters and sinter quality when using a controlled fuel particle size distribution. This being 80% of particles between 1-2mm, 15% of particles between 2-3mm and 5% between 0.5-1mm. Testing included fuelling with 100% coke breeze and 100% anthracite, 75% coke breeze, 50% coke

breeze and 25% coke breeze with the remaining balances being made up with anthracite. Tests were repeated and conducted using standard experimental procedure that can be found in chapter 3.

Experiment 3 – Stock PSD less than 5mm

The third set of experiments were designed to compare sintering process parameters and sinter quality when using an increased fuel particle size distribution which is more representative of plant operation. A 2kg sample of anthracite was taken and screened to sub 5mm and then sized. This sizing was then used as the specific particle size distribution for the sub 5mm tests. This can be seen in table 21. Testing included fuelling with 100% coke breeze and 100% anthracite, 75% coke breeze, 50% coke breeze and 25% coke breeze with the remaining balances being made up with anthracite. Tests were repeated and conducted using experimental procedure outlined in chapter 3. The breeze and anthracite was screened to the following particle size fractions seen in table 21. The breeze and anthracite was then added to each blend according to the ratio and desired particle size distribution as outlined above.

Table 21: Results of screening the samples of coke breeze and anthracite

Screen (mm)	mass of breeze (grams)	mass of anthracite (grams)
+3.15	52.3	117.2
+2	100.6	195.3
+1	177.6	275.3
+0.5	197.2	175.3
+0.25	251.3	117.9
-0.25	218.6	117.6
Total	997.6	998.6

Experimental parameter set points

The experimental procedure follows the same principles outlined at the end of the commissioning section. Fuel was always kept to 0.903kg. Moisture was kept to 6-6.5% and granulation time remained constant. The pressure drop set point was maintained at 100mbar. The ignition time was kept constant at 1 minute. Please see section 3.3 for sinter pot dimensions and experimental design. Please see formula sheet in section 3.3.5 for calculations used. Post analysis included sinter yield, chemical composition analysis via X-ray fluorescence analysis. RDI via reduction degradation index testing. Phase analysis via x-ray diffraction. Blend composition can be seen in table 22 below, ores will remain confidential:

Table 22: Blend composition

Blend material	kg	%
Sinter Fines	1.935	15.0
Sinter feed A	2.742	21.5
Sinter feed B	2.742	21.5
Sinter feed C	2.742	21.5
Sinter feed D	2.742	21.5
Limestone	2.194	17.0
Fuel	0.903	7.0

5.3.3 Results and Discussion - Experiment 1

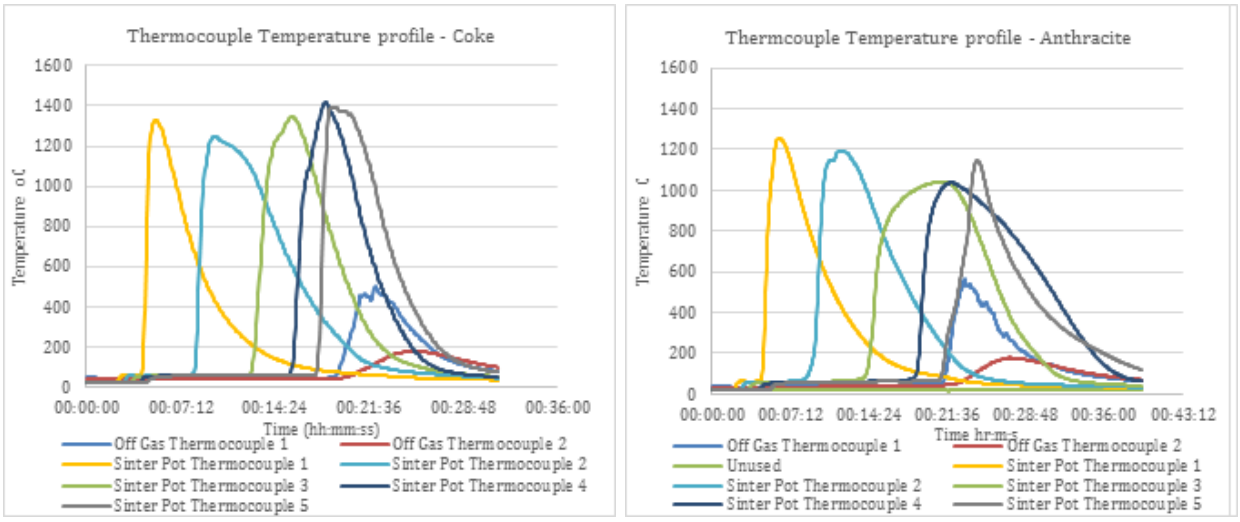

(a) Thermal profile fuelled with breeze

(b) Thermal profile fuelled with anthracite

Figure 99: Thermal profiles from experiment 1 in optimum fuel PSD and ratio study

Figure 99 above show the thermal profiles from the tests conducted with 100% breeze and 100% anthracite without controlling the fuel particle size distribution. Thermal profile with 100% breeze exhibited uniform traces, where each embedded thermocouple started to increase and peaked sequentially, one after the after. It can be seen that when fuelling with anthracite, a nonuniform profile was evident, indicating an unstable process with erratic flame front behaviour. This can be seen due to the thermocouple traces not peaking one after another as well as peaking after the off-gas thermocouples. This could also indicate that breeze is less sensitive to particle size distribution and this could be due to its more porous nature when compared to anthracite. This means that for a given PSD, breeze would have a higher surface area than when compared to anthracite. However, it must be noted here that the repeat conducted with 100% anthracite showed increased uniformity. This emphasises the importance of controlling the particle size distribution of fuel, as later seen in experiment 2 and 3.

Table 23: Process parameters from experiment 1 for uncontrolled fuel PSD study

	Coke	Anthracite	Units
Cold permeability flow rate	10.4	10.0	hr3/m
Hot permeability flow rate	7.2	6.9	hr3/m
Sintering time	00:19:45	00:21:05	hr:m:s
Max Thermocouple temperature	1417.0	1255.7	C
Thermocouple 1	1330.2	1255.7	C
Thermocouple 2	1248.2	1194.8	C
Thermocouple 3	1349.0	1042.3	C
Thermocouple 4	1417.0	1036.9	C
Thermocouple 5	1390.8	1148.6	C
Max off gas temperature 1	501.4	561.7	C
Max off gas temperature 2	177.0	177.6	C
Sintered air flow	56.8	47.8	hr3/m

Further analysis showed that on replacing breeze with anthracite, average cold flow rates decreased. This can be seen in the table above. It was also evident that average hot flow rates were decreased when replacing coke breeze with anthracite. It must be noted here that the increase in both cold and hot flow rates exceeded the standard deviation set out in the validation in section 2.3.2, table 6. This supports the original theory of increased surface area and porosity in coke breeze when compared to anthracite. The blend fuelled with anthracite is less porous thus not allowing as much gas flow to penetrate through the bed. Therefore, producing lower flow rates through the bed.

The table above shows maximum sintering temperatures as well as total sintering time. It could be seen that when fuelling with anthracite, a decrease in maximum sintering temperature was evident. This correlated with the thermogravimetric analysis conducted and discussed earlier in the chapter. It was also evident that sintering time was increased when

replacing breeze with anthracite. This also correlated with the thermogravimetric data discussed earlier, where it was said that anthracite had an increased total combustion time when compared to breeze. Therefore, increasing sintering time. This can also be seen when looking at flame front speed. As it takes anthracite longer to combust, a decreased flame front speed could be expected. This can be seen in the figure below.

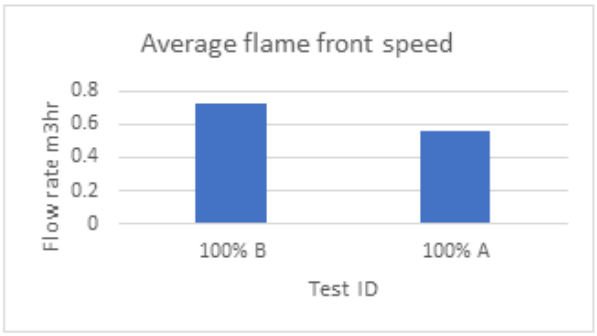

Figure 100: Average flame front speed per test

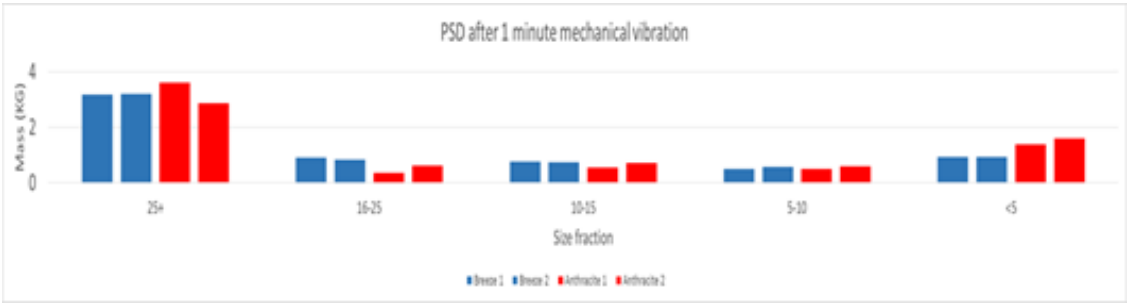

Figure 101: Sinter yield after 1 minute mechanical vibration in optimum fuel PSD and ratio study

Once sinter was discharged, it was subjected to 1 minute of mechanical vibration and screened into several size fractions. This can be seen in figure 101. It can be noted here that there was minimal variation across all size fractions. However, it was clear that the tests fuelled with 100% anthracite produced increased variation in the repeats as opposed to when repeating with 100% breeze. This could be due to the non-uniform profile and varied sintering temperatures exhibited when using anthracite as opposed to breeze, especially when not controlling the particle size distribution of the fuel being used. It is also worth noting here that return fines was increased on replacing breeze with anthracite. This was potentially

due to the decreased sintering temperatures exhibited when using anthracite. In conclusion, the increased porosity of coke breeze means that the surface area is increased which resulted in the coke breeze fuelled tests being less sensitive to the particle size distribution which is likely due to the impacts on the reactive surface area. This results in the anthracite fuelled tests exhibiting increased instability within the process.

Conclusion

On replacing coke breeze with anthracite and without controlling the particle size distribution of the fuel used, the following conclusions can be made:

1. Average cold flow rate and thus bed permeability decreased. This was due to the porosity of coke breeze and thus increase in surface area for a given PSD.
2. Maximum sintering temperature decreased. This was due to the higher calorific value of coke breeze compared to anthracite.
3. Average hot flow rate decreased and thus sintering time increased. This was due to the increased reactive surface if the coke breeze fuelled blends as a result of the increased porosity in coke breeze when compared to anthracite.
4. Average flame front speed decreased. This was due to the anthracite particles taking longer to combust. This was evident in the thermogravimentric analysis complete.
5. Sinter yield showed minimal variation with variation exhibited for the anthracite fuelled tests.

5.3.4 Results and Discussion - Experiment 2

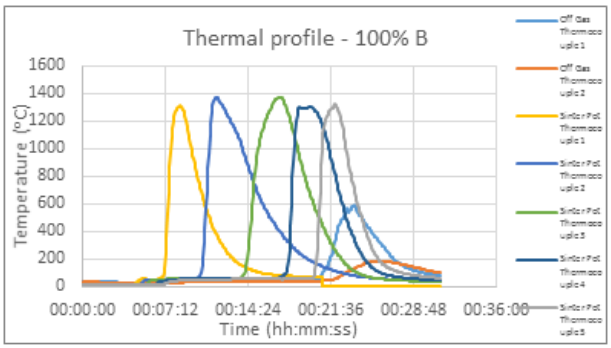

(a) Thermal profile from test with 100%breeze

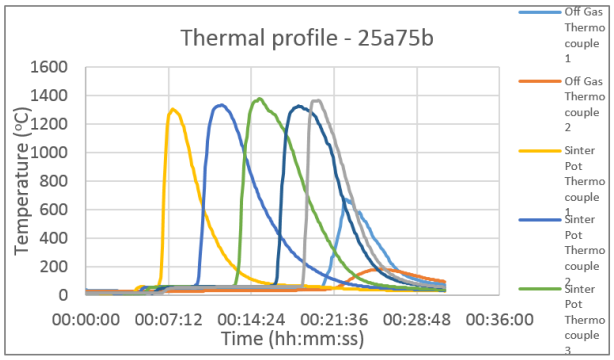

(b) Thermal profile from test with 25%anthracite 75%breeze

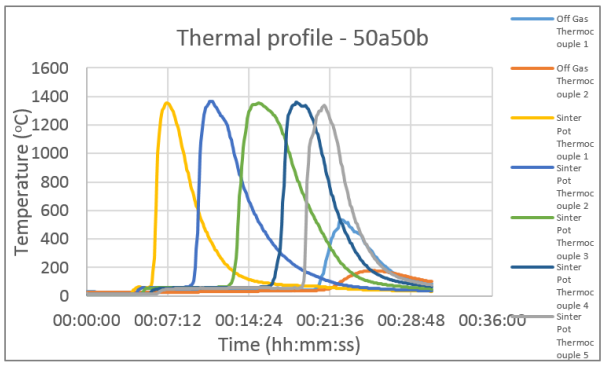

(c) Thermal profile from test with 50%anthracite50% breeze

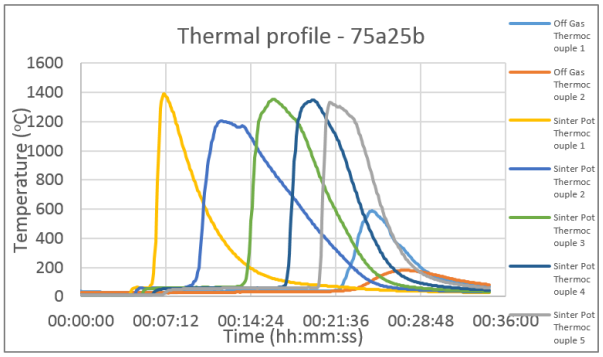

(d) Thermal profile from test with 25%anthracite 75%breeze

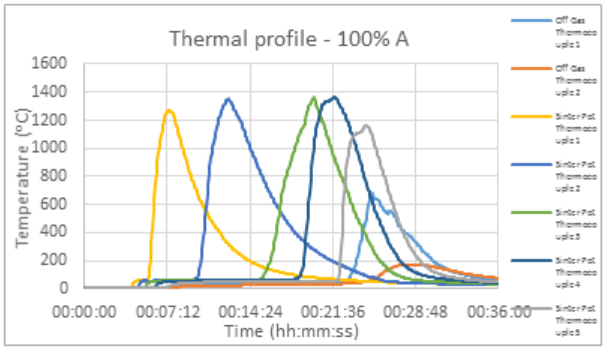

(e) Thermal profile from test with 100%anthracite

Figure 102: Thermal profiles from experiment 2 in optimum fuel PSD and ratio study

Figure 102 shows the thermal profiles from the tests conducted from 100% breeze to 100% anthracite by displacing breeze in 25% increments, whilst controlling the particle size distribution of both fuels. From visual inspections of the profiles, it was evident that all profiles exhibited relatively uniform and traces. Each embedded thermocouple trace started to increase and peak sequentially, one after the other. All off gas thermocouples also started to

increase and peak sequentially one after the other. This indicated that for all tests conducted, the flame front propagated down the pot in a stable manner right the way through to the flame front diminishing into the gas stream at the bottom of the pot. There was no evidence of the flame front reigniting or breaking apart for all tests conducted. When comparing these profiles to the profiles in experiment one where PSD was not controlled, it is clear on how important controlling the particle size of the fuel can be. This was especially true when analysing the tests conducted with 100% anthracite controlling the particle size distribution and comparing to the test conducted with 100% anthracite without controlling the particle size distribution of fuel.

Table 24: Process parameters from experiment 3 controlled psd less than 5mm with breeze and anthracite

Process parameters	100 b	25a75b	50a50b	75a25b	100 a	Units
Cold flow rate:	12.96	10.71269	11.01081	11.41905	12.72013	hr3/m
Hot flow rate:	8.17	7.528012	7.102796	7.314372	6.413532	hr3/m
Sintering time:	00:19:40	00:19:20	00:20:25	00:20:25	00:22:35	hr:m:s
Max sintering temp:	1316.19	1355.301	1303.783	1340.092	1367.091	C
Thermocouple 1	1231.82	1297.537	1124.796	1325.385	1262.941	C
Thermocouple 2	1282.01	1326.674	1008.087	1334.558	1084.446	C
Thermocouple 3	1098.91	1344.562	1213.484	1340.092	1246.009	C
Thermocouple 4	1250.70	1305.927	1303.783	1159.685	1319.425	C
Thermocouple 5	1316.19	1355.301	1300.03	1315.264	1367.091	C
Max off gas temp 1	672.75	597.5247	487.7718	663.7515	580.6323	C
Max off gas temp 2	179.88	180.7126	186.5181	183.0399	179.374	C
Sintered airflow	55.02	61.50766	53.01398	54.63391	56.71937	hr3/m

In the table above, average cold flow and average hot flow can be seen per test. It was evident that fuelling with 100% breeze with a controlled particle size distribution of the fuel produced the highest cold flow rates which is the flow rate prior to ignition. On increasing anthracite percentage by displacing coke breeze, it was evident that the cold flow rate decreased. This was also true for the average flow rate after ignition. As anthracite was increased, average hot flow rate decreased. As coke breeze is more porous with increased

surface area compared to anthracite then this fits well. The increased coke breeze allowed for more oxygen to permeate the bed and hence the increased flow rates. The table above also shows the maximum sintering temperature reached per test (A) as well as the maximum off-gas 2 temperature reached per test (B). There was minimal variation in maximum temperatures reached within the sinter pot across all tests. When analysing the maximum off gas temperatures, there was a slight trend in that increasing anthracite content produced decreased off gas temperatures, however the trend is not strong. The table above also shows total sintering time and average cooling rate of the sinter per test. On analysing the sintering time per test, there was a slight trend in that sintering time increased on displacing breeze with anthracite. It can be noted here that it took 18 minutes for sintering to complete when fuelling with 100% breeze compared to almost 21 minutes when fuelling with 100% anthracite. The sintering times correlated with the average flow rates mentioned earlier. If the flow rate is increased, in theory, the flame front propagates down the pot with an increased speed, speeding up the sintering process. This was true when comparing flame front speed for the test conducted with 100% breeze (with controlled psd) to the test conducted with 100% anthracite (with controlled psd). This can be seen below.

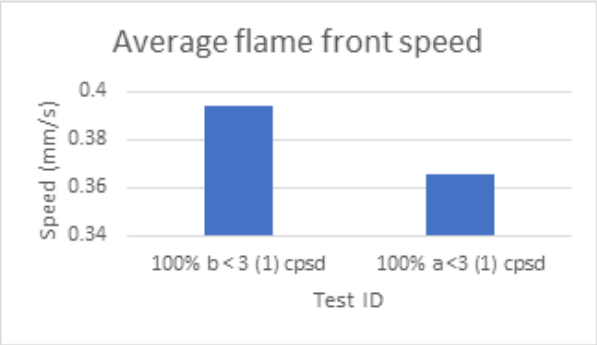

Figure 103: Average flame front speed per test in optimum fuel PSD and ratio study

As mentioned, once the sinter had been discharged, it was subjected to one minute of mechanical vibration and sized into several size fractions as seen in figure 104 below. There was minimal variation between the size fractions produced. However, there was a slight decrease in sinter produced above 25mm when using ratios as opposed to a 100% of either fuel. This can be seen below.

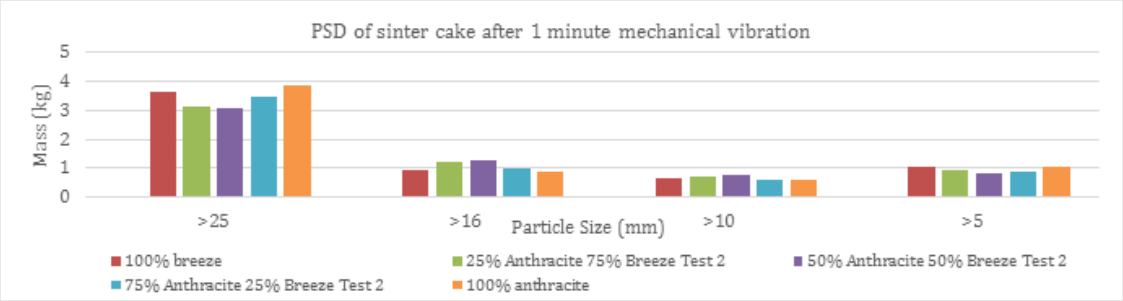

Figure 104: PSD of produced sinter in optimum fuel PSD and ratio study

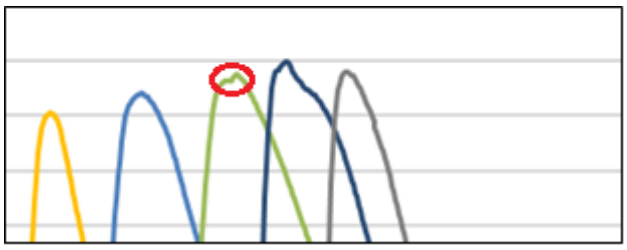

Figure 105: Indicates where sinter cake is sectioned for analysis

Before subjecting the sinter to one-minute mechanical vibration, a small amount of sinter was sampled from a specific location. Location was the area where thermocouple 3 was in contact with the sinter, and so the sinter within this area was sampled. This can be seen in figure 105 above. The sampled sections were then subjected to chemical analysis. This was done to correlate the data obtained from the chemical analysis to the data obtained from the thermal profile with pin-point accuracy. Chemical analysis included x-ray fluorescence testing and x-ray diffraction testing. This can be seen in table 25 and figure 106 below.

Table 25: XRF data from tests conducted with controlled psd with breeze and anthracite

XRF	100b	75b25a	50b50a	75a25b	100a
SiO_2	3.85	5.18	5.36	5.1	4.91
Al_2O_3	0.02	0.1	0.1	0.09	0.08
CaO	7.24	10.19	10.26	9.92	9.88
MgO	0.29	0.68	0.53	0.46	0.47
Fe	55.68	59.5	59.21	60.56	58.13
Fe_2O_3	65.18	70.47	70.58	71.52	71.27
FeO	9.12	13.14	12.67	13.56	10.66
P	0.029	0.039	0.041	0.036	0.035
Mn	0.11	0.14	0.12	0.14	0.15

On analysing the XRF data, it was evident that there was minimal variation in chemistry of the sinter. This proved that even though the fuel was being replaced with anthracite, as long as sufficient and adequate sintering temperatures were reached as well as being relatively consistent, similar chemical composition can be expected providing blend and process parameters remained constant. It must be noted here that the iron constituents in the sintered product fuelled with 100% breeze or 100% anthracite produced low results. This could mean that on mixing fuels it may introduce flamefronts fuelled by two different fuels that contain slightly different characteristics which may result in an increase in chemical variation of the sintered product. The iron oxides formation is highly dependent of the thermal conditions and this may be evident due to the small variation in sintering temperatures. With all this is mind, chemical analysis was in line with suitable sinter quality indices produced from the sinter plant.

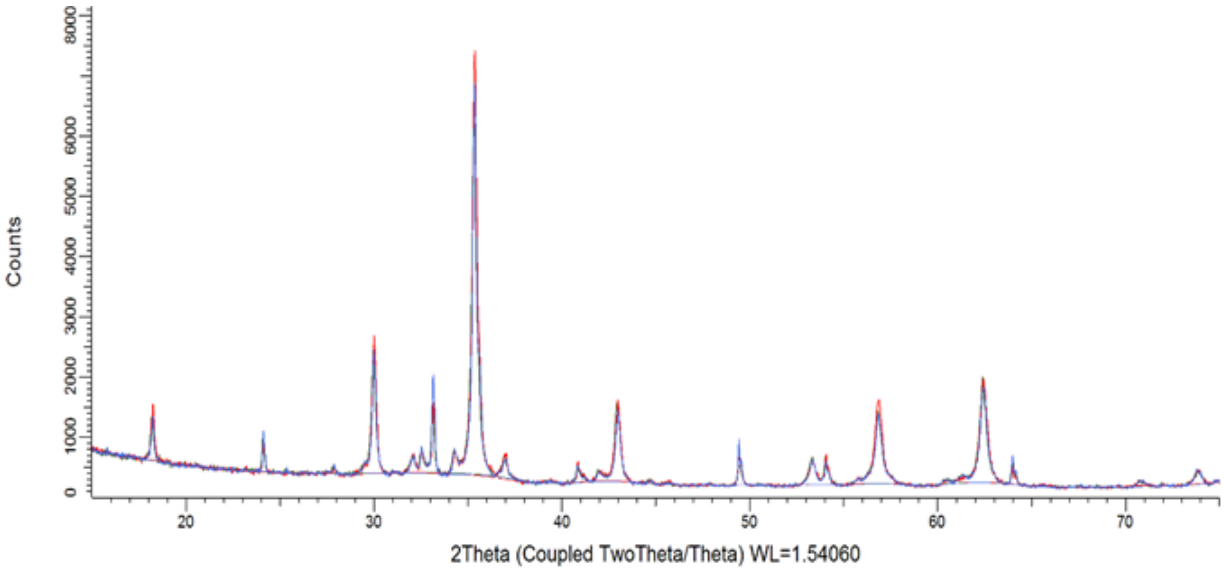

Figure 106: XRD spectrum of sinter sampled from TC3 fuelled with CPSD of 100% breeze and overlapped with 100% anthracite

Figure 106 above shows the x-ray diffraction spectra for the analysed sinter, layered on top of each other. It must be noted here that the main reason for this analysis was to investigate if there was any difference in peaks as well as peak intensities which would indicate different phases present as well as varying amounts of phases. It was evident from the layered spectra that variation was minimal and so we can conclude that the same phases were present in equal amounts. This clarifies the statement made earlier that providing the correct sintering temperatures are present within the process, similar chemical composition and thus phases could be expected, regardless of the fuel used.

Optical microscopy in optimum fuel PSD and ratio study

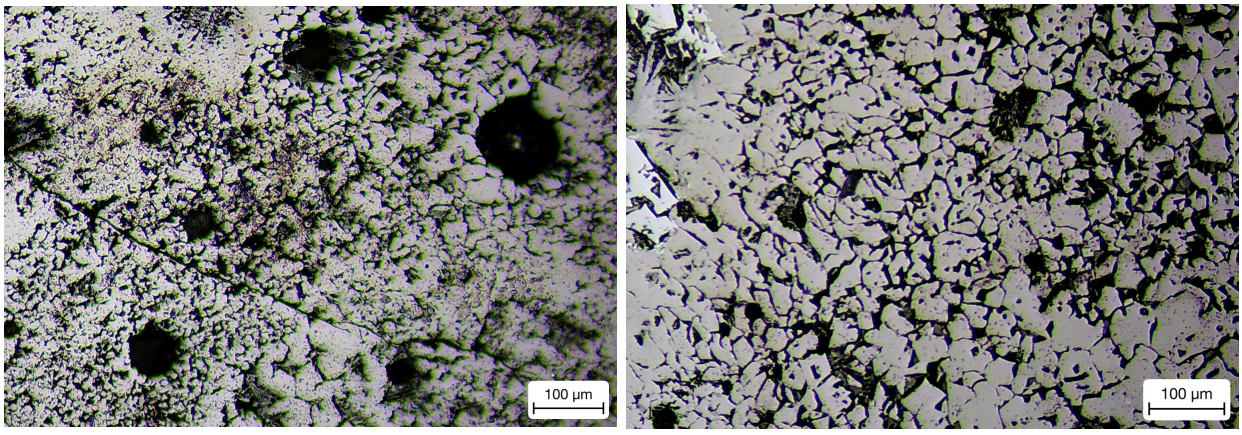

(a) 100 breeze cpsd x10

(b) 100 Anthracite cpsd x10

Figure 107: Fuelled with 100%breeze at a controlled particle size distribution vs Anthracite

On analysing figure 107 it was clear that both images feature a globular like structure with formations of SFCA's present. This was evident through out the samples. This was expected as the thermal characteristics were very similar in terms of sintering temperature.

Conclusion

In conclusion, when controlling fuel particle size and on increasing anthracite input the average cold and hot flow rates through the bed are decreased and as a result sintering time generally increased. This was due to the difference in porosity and available reactive surface energy of the coke breeze compared to anthracite. There was minimal variation in the amounts of sinter produced as well as in the various size fractions. The chemical composition of the sintered product, mainly Fe content, showed variation using either 100% breeze or anthracite. This was in line with the slightly varied sintering temperatures exhibited for the tests fuelled in ratios. The slightly varied temperatures could be due to the combination of two fuels with different combustion characteristics when mixing breeze with anthracite.

5.3.5 Results and Discussion - Experiment 3

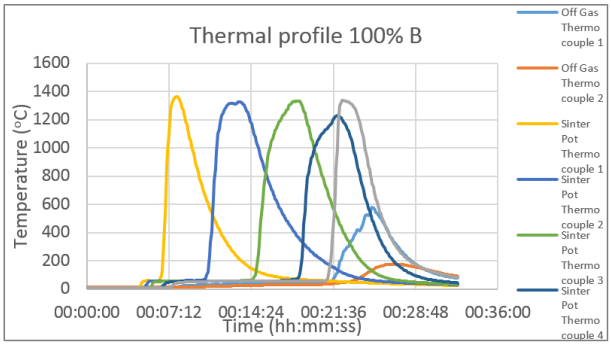

(a) Thermal profile from test with 100%breeze

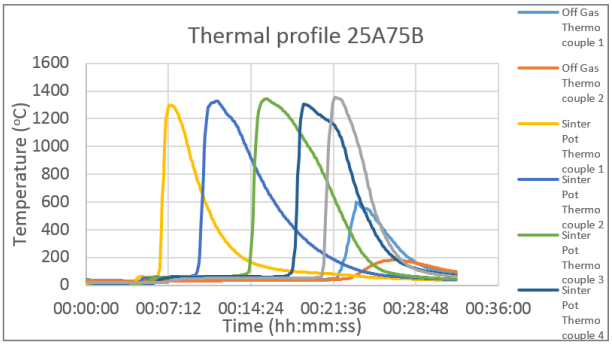

(b) Thermal profile from test with 25%anthracite 75%breeze

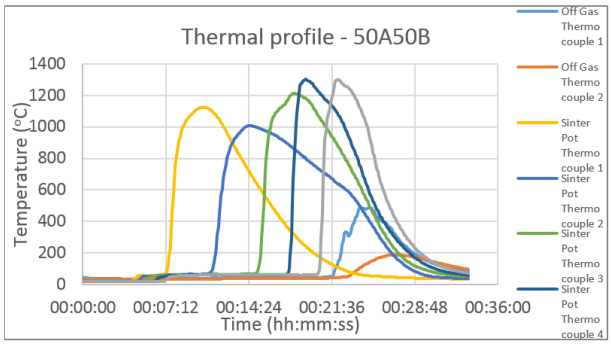

(c) Thermal profile from test with 50%anthracite50% breeze

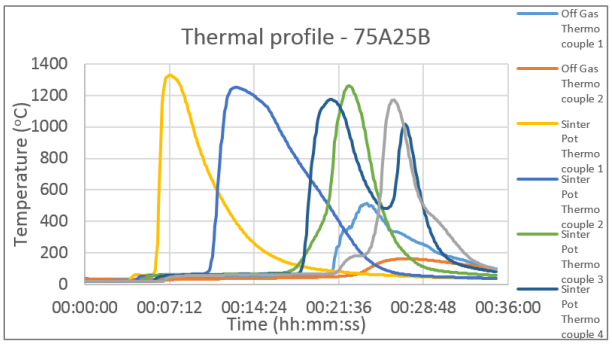

(d) Thermal profile from test with 25%anthracite 75%breeze

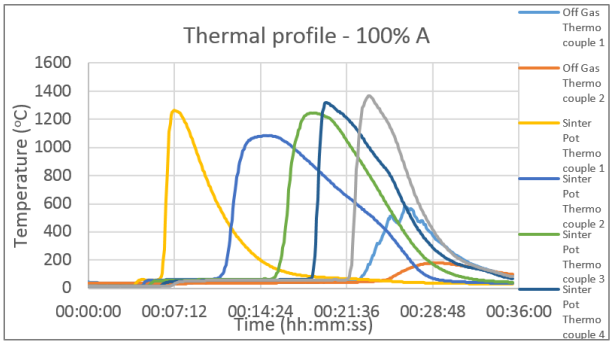

(e) Thermal profile from test with 100%anthracite

Figure 108: Thermal profiles from experiment 3 in optimum fuel PSD and ratio study

Figure 108 show the thermal profiles from tests conducted with 100% breeze with a stock-controlled particle size and then being displaced in 25% increments with anthracite with a stock-controlled particle size distribution. On initial visual inspection of the profiles and comparing them with the profiles in experiment 2, it was evident that the profiles were less uniform in appearance. However, profiles exhibited uniform characteristics evident from the stable profiles, albeit with slightly more variation than when controlling particle size

distribution. This was true for all thermal profiles apart from one, which was charged with 75% anthracite and 25% breeze. This profile exhibited a stable process up to thermocouple 4 but then the thermal traces started to increase in a nonuniform manner, also peaking in a nonuniform manner. This indicated the flame front broke apart and perhaps reignited at the lower half of the sinter pot. Off-gas thermocouple traces also peaked before the last embedded thermocouple trace, also indicating erratic flame front propagation. It must be noted here that the repeat for this test did not exhibited such erratic behaviour but main process parameters remained similar. The variation only emphasises the need to control the particle size distribution of fuel being used.

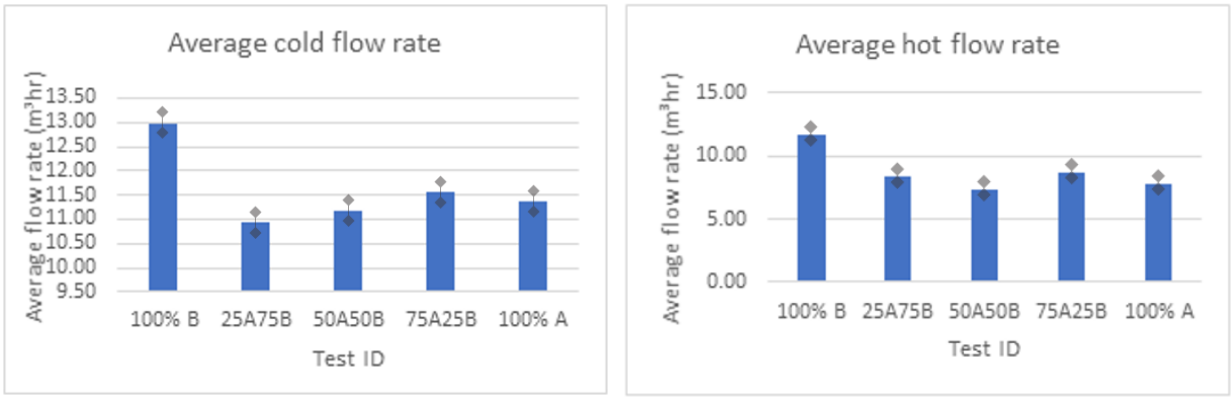

(a) Average cold flow rate per test

(b) Average hot flow rate per test

Figure 109: Average cold and hot flow rates from experiment 3 in optimum fuel PSD and ratio study

When analysing the calculated parameters some trends could be seen. Figures 109 a and b show average cold flow and average hot flow rates per test. Trends were not as clear when using the increased stock-controlled particle size distribution, adding to the need to control particle size distribution. However, a slight trend in decreasing flow rates in both average cold flow and average hot flow was present. This followed the clear trend in experiment 2. The reasons for decreased flow rate when increasing anthracite content follows the same in experiment 2 i.e. breeze being more permeable allowing for more oxygen to flow through.

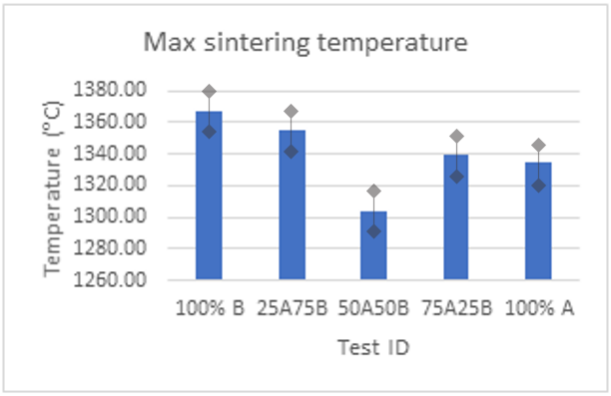

(a) Maximum sintering temperature per test

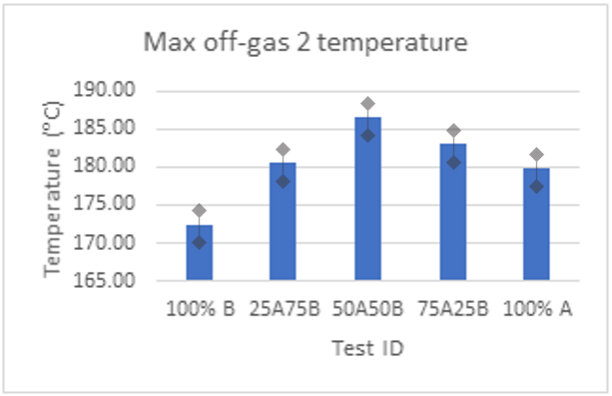

(b) Maximum off-gas temperature per test

Figure 110: Sintering temperatures from experiment 3 in optimum fuel PSD and ratio study

Figure 110 a and b show maximum sintering temperatures reached per test as well as maximum off-gas temperatures per test. It was seen from the graph displayed that no clear trend was evident, as opposed to the same parameter graphs displayed in experiment 2. However, adequate sintering temperatures were reached for all tests. It must be noted here that there was a slight trend in maximum sintering temperature in that the temperature decreased as anthracite content increased. This trend was not seen in experiment 2 however was evident for max off-gas temperatures. This variation further emphasises the need to control particle size distribution of the fuel being used.

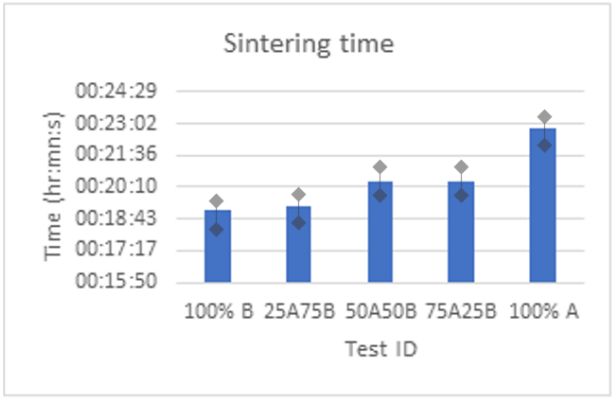

(a) Sintering time per test

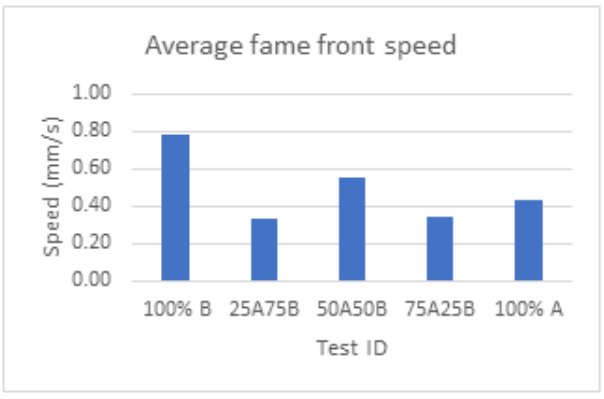

(b) Average cooling rate per test

Figure 111: Sintering time and flame front speeds from experiment 3 in optimum fuel PSD and ratio study

Figure 111 above shows total sintering time as well as average flame front speed per test. It was evident from analysing the graphs that sintering time increased as anthracite content was increased. The increased sintering time followed the same trend in experiment 2. Furthermore, when thermogravimetric analysis was conducted during the characterisation of the fuels, it was evident that anthracite had an increased combustion time when compared to coke breeze. This correlated with the increased sintering time when increasing anthracite content. It can be seen in figure 118 b that flame front speed generally decreased when increasing anthracite content. Average cooling rate of sinter can also be seen below, which generally decreased as anthracite content was increased. This was similar to the cooling rates seen in experiment 2. The flame front characteristics and cooling rates also correlated with the thermogravimetric analysis conducted during the characterisation.

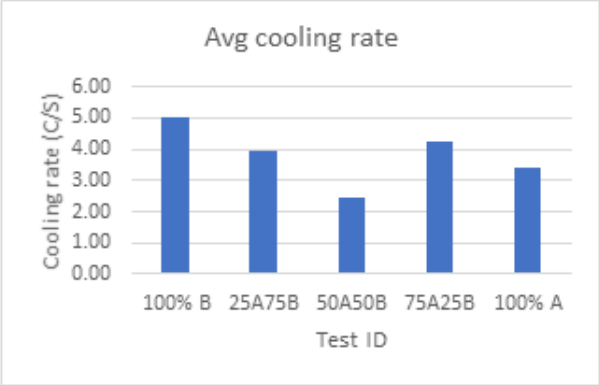

Figure 112: Average cooling rates speed per test in optimum fuel PSD and ratio study

As mentioned previously, once the sinter had been discharged it was subjected to 1 minute of mechanical vibration and screened into several size fractions. This can be seen in figure 113 below. It was evident that there was minimal variation in the size of the sinter produced across all tests in experiment 3. When comparing weights in each size fraction of sinter produced in experiment 3 to experiment 2, there was also minimal difference. This indicated that as long as adequate sintering temperatures are reached, difference in sinter yield would have minimal variation.

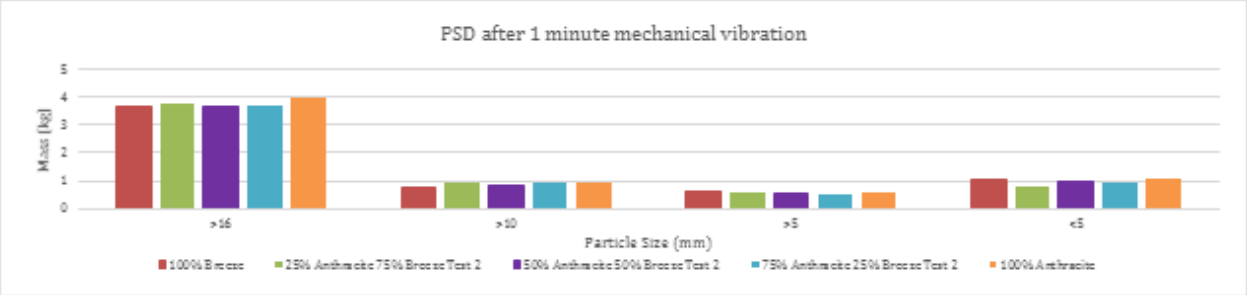

Figure 113: Sinter yield after 1 minute mechanical vibration in optimum fuel PSD and ratio study

As per experiment 2, sinter was sampled from the area in which thermocouple 3 was in contact with the sinter. The sinter was subjected to chemical analysis via XRF and phase analysis via XRD. These can be seen below in table 26.

Table 26: XRF from experiment 3 controlled psd 5mm with breeze and anthracite

XRF	100b	75b25a	50b50a	75a25b	100a
SiO_2	5.12	4.91	4.19	6.33	5.32
Al_2O_2	1.16	1.05	1.16	1.26	1.06
TiO_2	0.09	0.08	0.04	0.11	0.08
CaO	10.31	9.09	8.56	13.46	10.14
MgO	0.44	0.38	0.49	0.49	0.39
Fe	60.24	58.54	58.2	56.62	59.01
Fe_2O_3	77.36	72.89	68.23	67.85	74.38
FeO	7.9	9.73	9.62	11.8	9
P	0.037	0.038	0.041	0.045	0.036
Mn	0.15	0.17	0.13	0.17	0.16

From table 26, chemical composition can be seen. It can be noted that there was minimal

variation across all tests. Highest variation lied within the iron oxides which is highly dependent on thermal properties during the process. Due to the variation in thermal profiles this could be expected. When comparing chemical composition in experiment 3 to the chemical composition in experiment 2 it was evident there was more variation in experiment 3. This could be expected due to the increased amount of variation in thermal profiles exhibited in experiment 3, due to the increased particle size of fuel. This is also true for the phase analysis. This can be seen in figure 114 below. It was evident that even though similar peaks were present, increased variation was evident when comparing to the spectra from experiment 2.

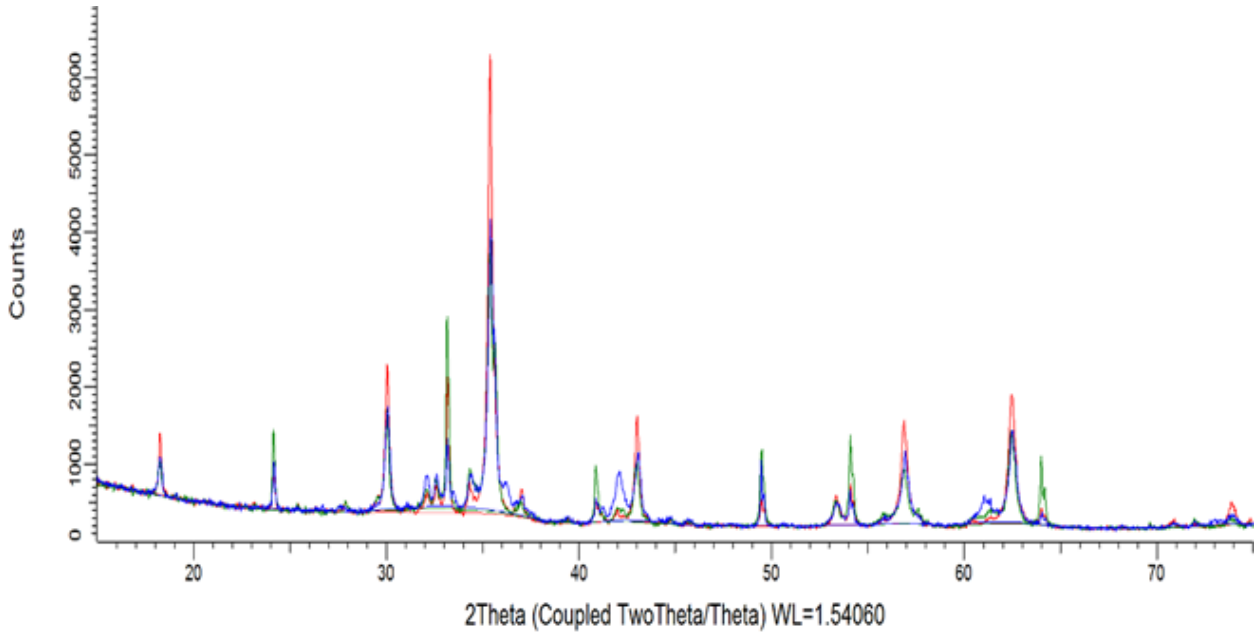

Figure 114: XRD overlay from tests conducted with anthracite and coke breeze controlled stock psd

Optical microscopy

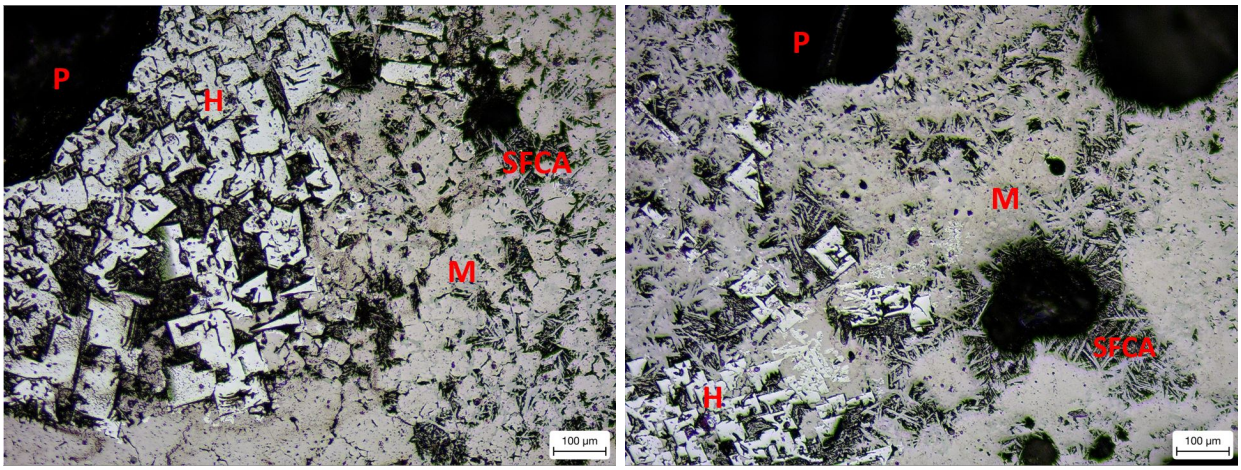

(a) 100 breeze 5mm x10

(b) 100 anthracite 5mm x10

Figure 115: Fuelled with 100%breeze at a stock-controlled particle size distribution vs Anthracite. H - hematite, M - magnetite, P - pore.

Figure 115 shows a representative microstructure from tests fuelled with 100% breeze and 100% anthracite when controlling the particle size distribution of fuel. A shows the microstructure of sinter fuelled with 100% breeze and B shows the microstructure of sintering fuelled with 100% anthracite both at a magnification of x10. Block-like hematite is evident in both sinter samples, along with SFCA's in the form of needle like accicular features. Due to the increased variation exhibited in the process when using the increased particle size, some variation could be expected in the resulting microstructure as the formation of the structures is highly dependant on the thermal characteristics exhibited in the process. This can be seen in the XRD spectrum in figure 114 which exhibits slightly more variation when comparing the spectra in figure 106. It must be noted that phase analysis was done to establish variation in peaks and peak intensity only, not to identify phases.

Conclusion

On displacing coke breeze with anthracite at a stock-controlled particle size distribution of less than 5mm, the following conclusions can be made. Both average cold and hot flow rates generally decreased as a result of the decreased porosity and reactive surface area of anthracite and as a result sintering time was generally decreased, thus decreasing productivity. Sinter yield was maintained with minimal variation which is an indication that cold strength was maintained through out the experiments. Chemical composition of sinter was maintained with minimal variation; however, variation was increased when compared to experiment 2. Phase mineralogy was maintained with minimal variation, however, variation was increased when compared to experiment 2.

5.3.6 Summary of conclusions

When comparing analysis from experiment 1 to experiment 2 the following conclusions can be made. When controlling particle size distribution of fuel:

1. Bed permeability is increased. This was due to being able to better control the particle size distribution of the input fuel. As mentioned, coke breeze is more porous so brings about increased cold flow rates and has an increased amount of reactive surface area and hence faster hot flow rates as well. As a result of this, sintering time is decreased.
2. Average cooling rate is increased and this was due to the increased permeability evident when being able to control the particle size distribution of the fuels.

When comparing analysis from experiment 2 to experiment 3 the following conclusions can be made. When using an increased particle size without controlling particle size distribution of fuel:

1. Increased process variation was evident and this was due to the increased variability in reactive surface area when dealing with increased particle sizes.
2. Average hot flow rate is generally decreased and this can be expected due to the increased particle size will take longer to combust and stays hot for a longer period of time when compared to a smaller size fraction. As a result of this, sintering times are generally increased.

3. Increased variation in sinter quality can be expected due to the increased process variation.

When comparing analysis from experiment 1 to experiment 3 the following conclusions can be made. When using an increased particle size and controlling the particle size distribution of fuel:

1. Increased process variation was evident and this was due to the increased variability in reactive surface area when dealing with increased particle sizes.

5.4 Optimal coke breeze in sinter pot

5.4.1 Introduction

The large amounts of fuel used in iron ore sintering means it is crucial to get optimal fuel rates correct, not only to be cost effective, but to try and lower the carbon footprint and keep an efficient and effective process, whilst maintaining product quantity and quality. The aim of this study is to investigate optimal fuel rate for the sinter pot through process and product analysis and find the correlation between chemical composition, reduction degradation index and process parameters such as fuel rate and sintering temperature. As mentioned in section 3.3.1, all pot tests up were conducted with 7% breeze as this was the initial fuel rate needed to ensure adequate sintering temperatures were met. Now, with a robust system and blend in place, it was decided to investigate what influence lowering the fuel rate in the pot would have on the sintering process and sinter quality. The research question being addressed here is what is the impact of decreasing fuel rate on sinter processing and quality. Research has been conducted on replacing fuel with various substitutions such as biomass, however, very little is on the optimum amount of coke breeze needed when fuelling a small scale sinter furnace. This may be due to the variation in dimensions as well as process stability in the different sinter pots available world wide.

5.4.2 Experimental procedure

In total, 4 blends were made up and 8 sinter pot tests were conducted for this set of experiments. Blend A contained 4% breeze, and this increased in increments of 1% up to 6% and then compared to a conventional fuelled test at 7%. Please see chapter 3 section 3.3 for full experimental procedure, sinter pot dimensions, formula sheet and post analysis procedure. Blends contained the following:

Table 27: Blend composition for optimum breeze content in pot

Material	Blend A	Blend B	Blend C	Blend D	kg
Sinter feed C	2.17	2.15	2.13	2.11	kg
Sinter feed E	2.17	2.15	2.13	2.1190	kg
Sinter feed AA	4.12	4.09	4.06	4.02	kg
Sinter feed B	2.38	2.36	2.34	2.33	kg
Sinter Fines	2.10	2.08	2.07	2.05	kg
Olivine	0.19	0.19	0.19	0.19	kg
Limestone	1.92	1.90	1.89	1.87	kg
Magstone	0.39	0.39	0.38	0.3850	kg
Coke Breeze	0.52	0.65	0.77	0.89	kg

5.4.3 Results

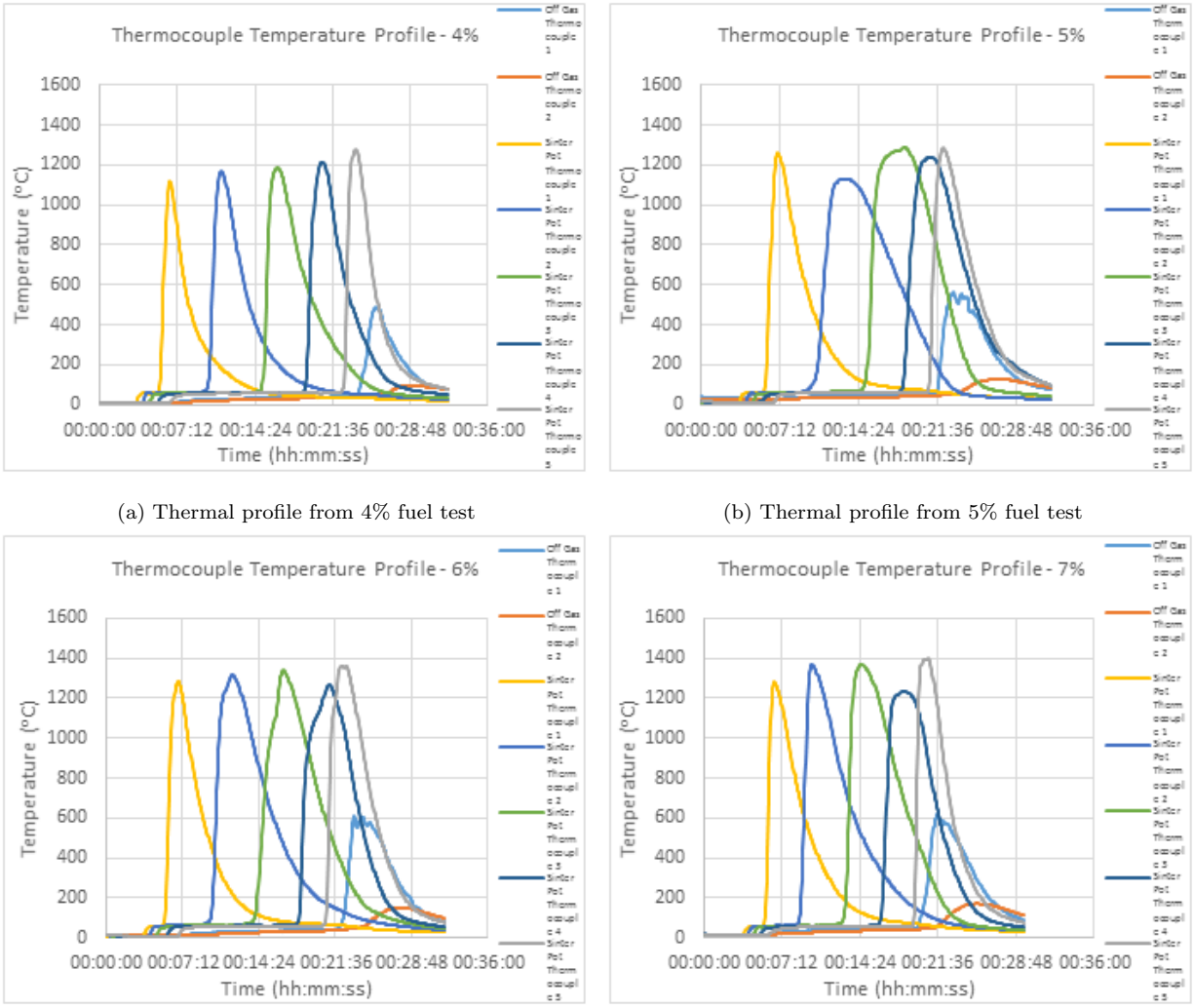

(a) Thermal profile from 4% fuel test

(b) Thermal profile from 5% fuel test

(c) Thermal profile from 6% fuel test

(d) Thermal profile from 7% fuel test

Figure 116: Thermal profiles from fuel content study

On analysing figure 116 above all thermal profiles were relatively uniform in appearance. All thermocouples traces start to increase and peak sequentially one after the other. Cooling rates also appeared relatively uniform. This indicated that all tests were completed with relatively stable and uniform flame front propagation. When referring to the research question, on reducing fuel, process stability is not impacted, however, maximum sintering temperatures is impacted greatly. It can be noted here that on appearance of the profiles, maximum sintering temperatures seemed to increase with increasing fuel content. This appears true for waste gas temperatures as well and can be clarified when looking at figure 118 below.

An increase in temperature was evident due to the increase in fuel content. It can be seen that hot flow rate is increased on increasing fuel content. As more oxygen is being passed through the bed, it reacts with the increased fuel input, and therefor increases temperatures.

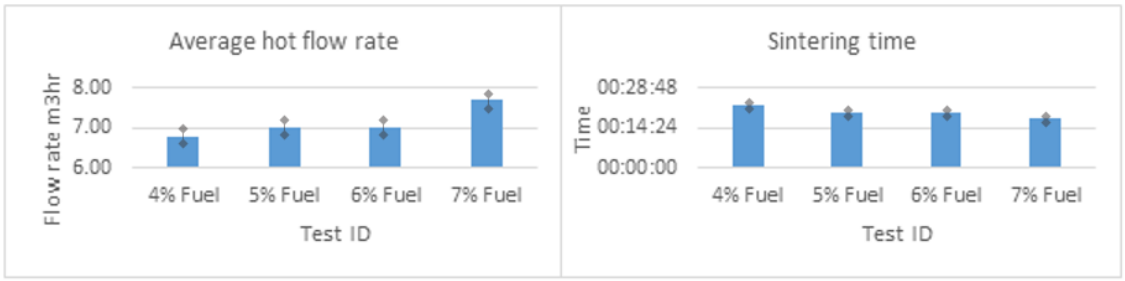

Figure 117: Average hot flow and sintering time from fuel content study

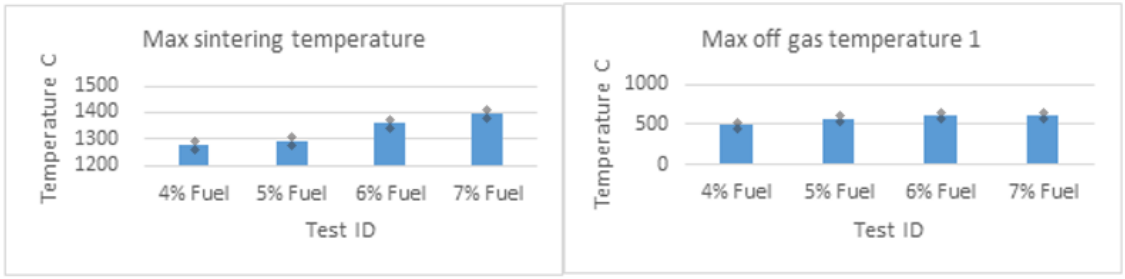

Figure 118: Sintering temperature and off-gas temperature from fuel content study

Figures 117-118 show graphs from the calculated process parameters across all tests. It can be noted here that the data indicated that the average hot flow rate increased with increasing fuel rate. This was due to the increased amount of fuel and thus increased reactive surface area. The increased fuel being combusted within the process, which requires it to react with oxygen and hence the flame front being more permeable, driving up the flow rate allowed to pass through. Maximum sintering temperature as well as off gas temperatures increased with increasing fuel. This was due to the reaction intensity being increased as a result of the increased reactive surface area of the fuel input. It can also be noted here that sintering time decreased with increasing fuel. This was also due to the increase in reaction rate caused by the increase in fuel content and flow rate through the bed, therefor increasing the speed of the process, thus, decreasing sintering time. On another note, the calorific value of the over all blends would increase as fuel is increased and therefor contributing to the increased temperatures and decreased sintering times.

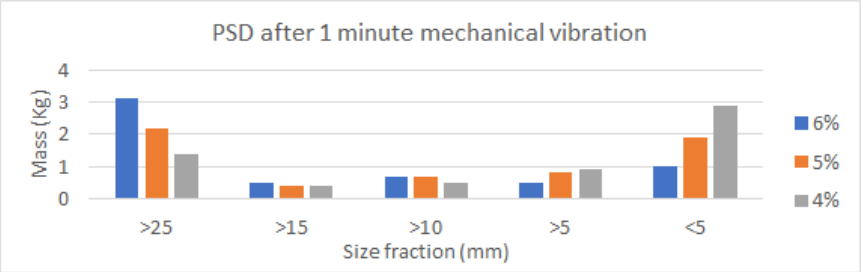

Figure 119: Particle size distribution of sinter after 1 minute mechanical vibration

Once the sintering process has been completed, the sinter cake produced was discharged and subjected to 1 minute of intense mechanical vibration where the sinter cake is broken up and screened into size fractions shown in figure 119. It can be seen that as fuel content was increased, stronger sinter was produced. As the fuel rate was increased, less return fines was produced. This correlated with the FeO and RDI data as can be seen in table 28 below.

Table 28: Sinter composition

XRF	4% fuel	5% fuel	6% fuel	7% fuel
SiO_2	6.31	6.41	6.46	5.7
Al_2O_3	1.21	1.41	1.25	1.61
TiO_2	0.084	0.083	0.086	0.11
CaO	9.82	9.63	9.59	10.2
MgO	1.85	1.95	1.84	1.65
Fe	57.95	57.88	56.92	57.88
Fe_2O_3	76.3	75	69.7	74.15
FeO	5.88	7.02	10.5	7.75
P	0.038	0.045	0.034	0.053
Mn	0.2	0.22	0.21	0.26
CaO/SiO_2	1.56	1.50	1.48	1.79
Al_2O_3/SiO_2 ratio	0.19	0.22	0.19	0.28

Sinter from each test between 10-15mm was subjected to x-ray fluorescence analysis and full elemental composition can be seen in table 25 above. Figures 121 and 122 are graphs showing elemental composition differences and RDI. On analysing table 28, FeO content increased per test as the fuel rate was increased up to a certain point. This could be due to the amount of time at temperatures above 1100C for each sintering process. This allowed more time for the reduction process to occur, thus, increasing FeO content. The same trend can seen when looking at the reducibility of sinter when increasing fuel content. RDI characteristics increased as fuel rate was increased i.e RDI value decreased. Further analysis can be seen below.

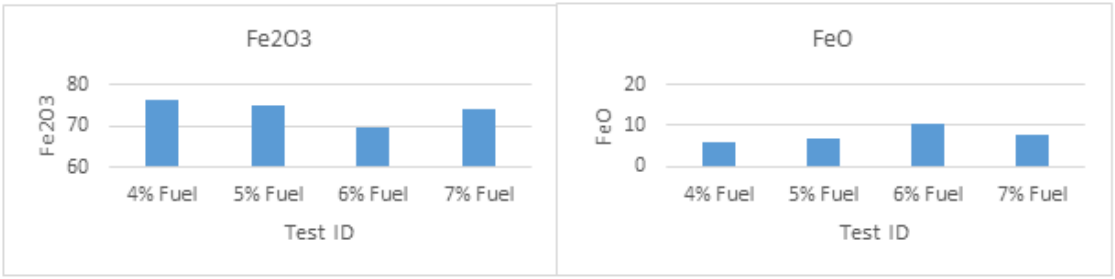

Figure 120: Sintering temperature and off-gas temperature from fuel content study

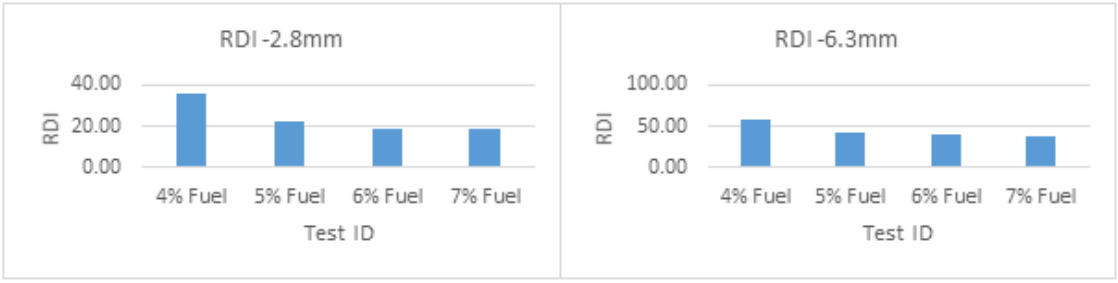

Figure 121: Average hot flow and sintering time from fuel content study

On analysing figure 122 below it was evident that there is a clear relationship between fuel content, RDI, peak temperature in the pot and FeO. It can be noted that when fuel increased, temperature and FeO increased but RDI decreased. It can be said that the FeO content in sinter is directly related to the RDI of the sinter. This correlation follows the trends discussed in the literature review in section 2.7.5. It was mentioned that studies showed that RDI value is decreased by 8 points for every 2% in FeO. [49] This was due to the increase in magnetite content on increasing FeO. A decrease in accicular calcium and ferrite phases and an increase in columnar ferrite phases was reported.

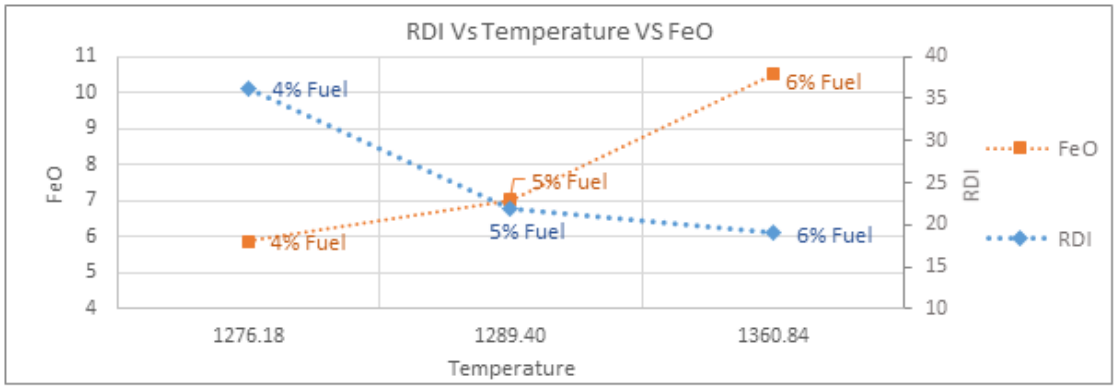

Figure 122: Relationship between peak sintering temperature, Fuel content, FeO and RDI

On the analysis of figure 123 below, it can be noted that there could also be a relationship between average hot flow rate, peak temperature in pot and FeO. On increasing fuel, it was evident that the average hot flow rates also increased along with FeO and peak temperature in the pot.

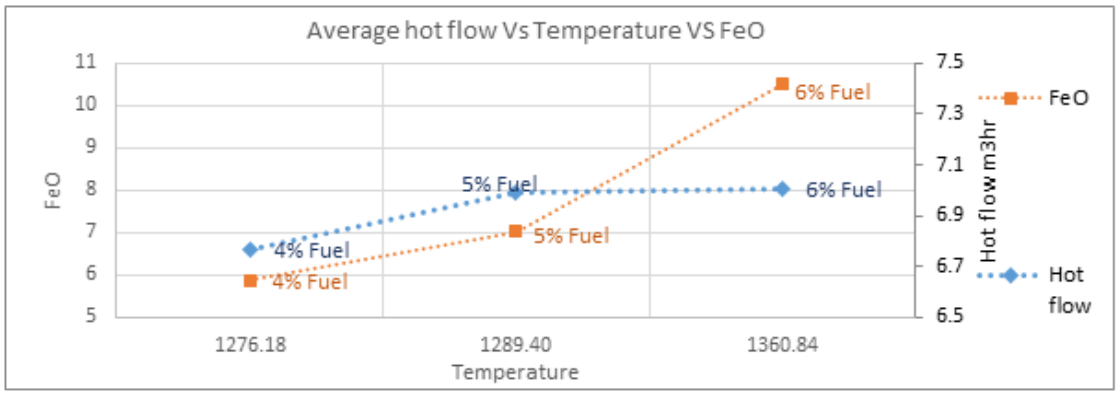

Figure 123: Relationship between peak sintering temperature, Fuel content, FeO and Average hot flow rate

On the analysis of the correlations in figure 124, it can be noted that flame front width at TC1-2 increased as the fuel increased. Flame front thickness across all thermocouples generally followed this trend and that can be seen in the graphs. It is worth noting here that flame front thickness increased with increasing temperature and FeO. It was seen that sintering time was decreased with increasing flame front thickness.

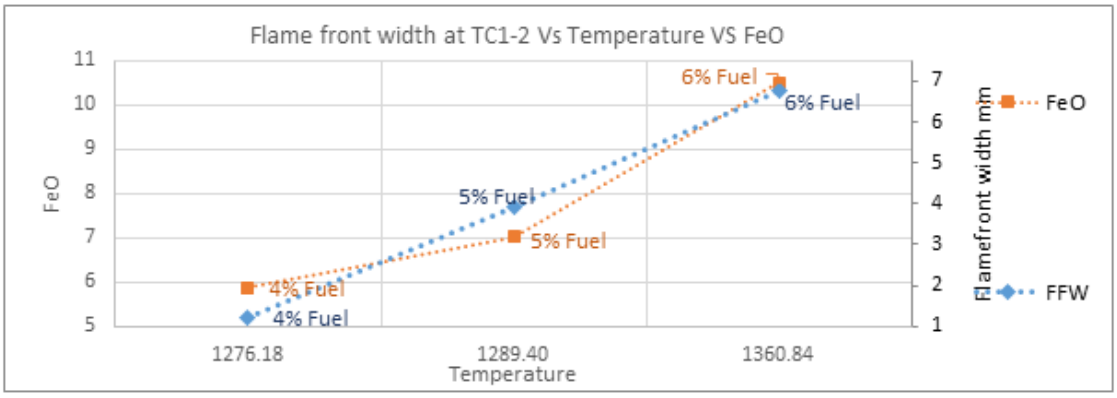

Figure 124: Relationship between peak sintering temperature, Fuel, FeO and flame front thickness

Optical microscopy

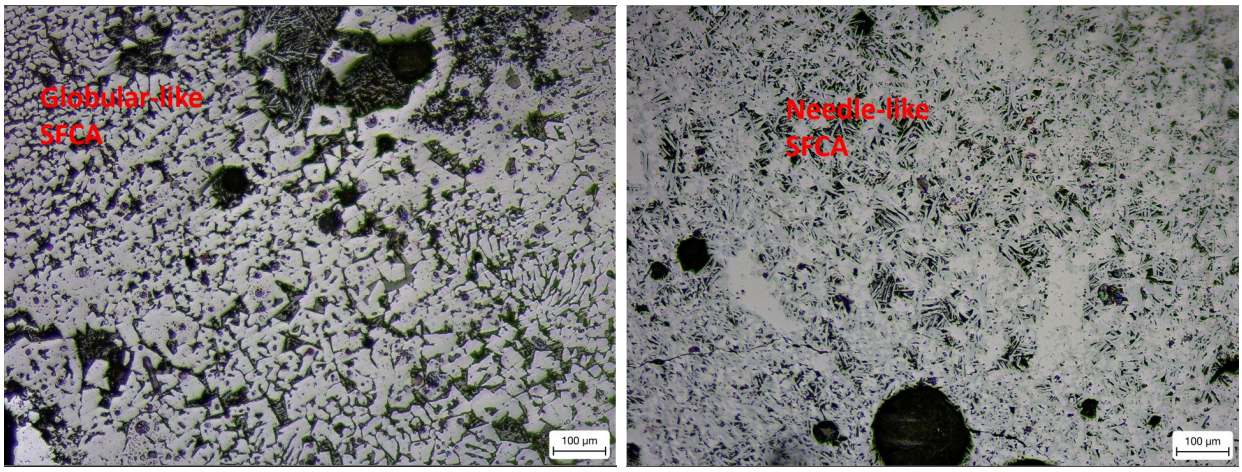

(a) Optical microstructure of sinter from 4% fuel test

(b) Optical microstructure of sinter from 6% fuel test

Figure 125: Micro structures of sinter produced from optimum breeze content study

Figure 125 shows the microstructures from the fuel content investigation. Samples were mounted and polished for optical microscopy. A shows the microstructure of sinter fuelled with with 4% breeze. B shows the microstructure of the sinter produced with 6% fuel. Both are under the same magnification and optical conditions. It was evident from analysing the microstructures fuelled with 4% fuel that a globular, dendritic structure was evident. Hematite and magnetite is evident in the microstructure, however, SFCA formation appears to take a more globular appearance. This was due to the temperatures reached during this test which were below 1200C and are not sufficient for partial melting to occur. This also corresponds to earlier studies as mentioned in the literature review [68]. When analysing the microstructure of the sinter produced when the fuel was increased to 6%, the resulting sinter microstructure exhibits a more needle like and accicular structure. Similarly, hematite and magentitie is evident, however, this time embedded in a needle like acciuluar formation of SFCA's. Most likely SFCA 1 rather than SFCA's according to literature [45]. SFCA's are associated with poor mechanical strength and poor reducibility when compared to SFCA 1's. This correlated with the results in this study when subjecting the sinter produced to reduction degradation index testing and analysing the sinter once subjected to 1 minute of mechanical vibration and comparing blend A to blend C.

Electron Dispersive X-ray Spectroscopy analysis

The sinter produced from the pot tests fuelled at 4% and 6% were subjected to electron dispersive x-ray spectroscopy analysis. Figure 126 below shows the layered images and spectra from both tests. The overall analysis confirms that Fe, O, Ca and Si are present in large quantities This indicates that iron oxides are present as well as silica-ferrites of calcium and aluminium. This confirms the descriptive analysis in the optical microscopy section above. The EDS analysis does not readily differentiate between hematite and magentite and hence why the optical microscopy is useful here.

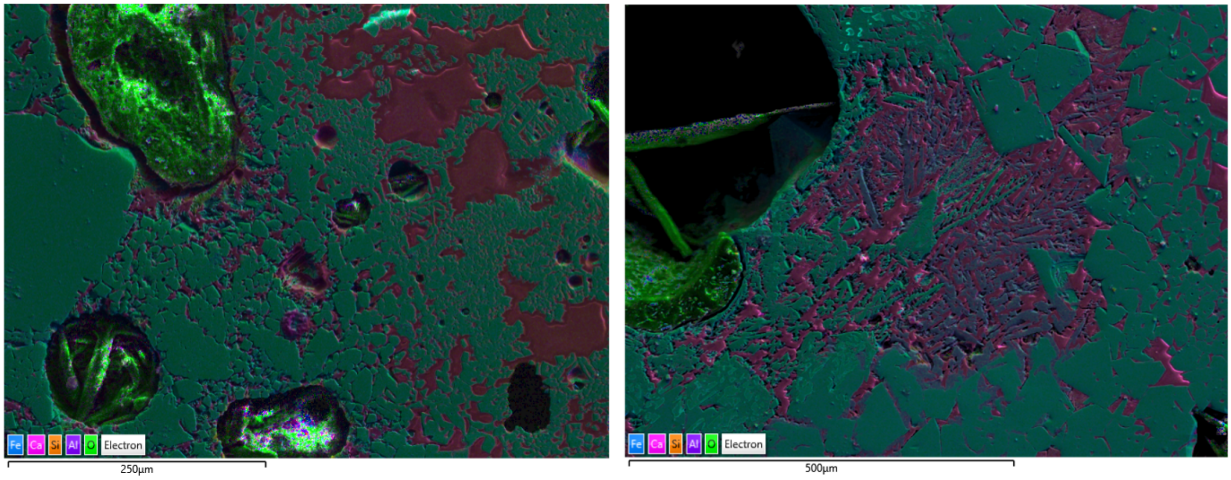

(a) Layered EDS image of sinter from 4% fuel test

(b) Layered EDS image of sinter from 6% fuel test

Figure 126: Micro structures of sinter produced from optimum breeze content study

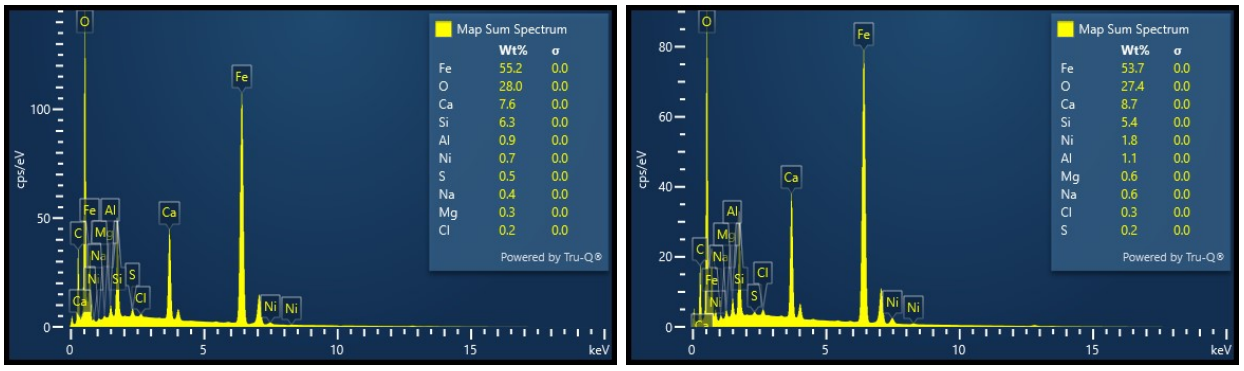

(a) EDS of sinter from 4% fuel test

(b) EDS of sinter from 6% fuel test

Figure 127: Micro structures of sinter produced from optimum breeze content study

5.4.4 Discussion

A number of trends and correlations can be drawn from the results above. The increase in average hot flow rate with increasing temperature can be explained due to the increase in fuel content. As average hot flow rate is an average of the flow rate from peak temperature at thermocouple 2 (i.e. centre of flame front) to the peak temperature at thermocouple 4, it gives an indication of flame front permeability. This was due to the following; the increase in fuel results in an increase reactive surface area and in calorific value which results in increased peak temperatures and flame front width. The increased combustion increased the hot flow rates through the bed via the exothermic oxidation reaction of the fuel which creates voids, thus increasing the gas flow through the bed. This can explain the increased average hot flow rates, peak temperatures and flame front width and can also explain the decreased sintering times. This study reports that when fuel content was increased, maximum sintering temperature increased, RDI decreased and FeO content increased. Sinter FeO is related to reduction of hematite and the oxidation of reduced phases during heating and cooling. It is known that the conversion of wustite is never completed as the kinetics of dissolution of oxygen to the melt can be expected to be very slow. [53] On increasing fuel content, temperature is increased which increases the rate of conversion. The solid-melt reaction determines the volume of melt produced and the amount of solids left un-reacted during the sintering process. The increased temperature allows higher liquid phase stability to exist in the system, i.e. in the flame front, and therefore allows for more superficial disintegration of hematite and therefor more FeO. Furthermore, conversion of Fe3+ to Fe2+ is favourable due to the evolution of oxygen from the melt, as appose to the reverse reaction due to the adverse kinetics involved. [48] It can be noted that this can be reflected in the sinter yield particle size distribution. An increased amount of larger sinter was made when increasing fuel content. This was due to a larger amount of acicular SFCA phases present due to the higher liquid phase stability in the flame front. Fine accicular sfca decreases the amount of large pores and crack initiation sites and therefor improves cold strength of sinter produced as well as RDI.

5.4.5 Conclusion

i) When investigating process stability and sinter quality on increasing fuel content, hot flow rate, sintering temperatures, off gas temperatures, flame front width and speed generally increased and sintering time decreased. This was explained due to the increased availability of fuel present which increased the reactive surface area and carbon

content for combustion to occur. The increased combustion resulted in an increase in the exothermic oxidation reaction of the fuel creating voids and higher liquid phase stability.

ii) This investigation can also conclude that on increasing fuel content, sinter size and FeO content increased and RDI value decreased. This could also be explained by the increase liquid phase stability allowing more superficial disintegration of hematite and therefor more FeO. The increase in FeO explains the increase in sinter size and decrease in RDI as mentioned previously.

6 Novel additions

The research and experimental work conducted up to now have proved that the pot can be used to accurately represent the industrial process. It has demonstrated that it can be used to optimise the utilisation of the conventional input materials and provide novel insight as to their value in use in terms of product quality and process stability. However, as a giant raw materials recycling / reprocessing unit in effect, the sinter plant offers up significant opportunity to explore the valorisation of other materials. This chapter explores at a level of indicative feasibility the potential for a diversification in feed stocks with the potential to reduce steel making waste and its carbon footprint through harnessing beneficial chemical properties of recycled materials.

The first section of this chapter focuses on increasing bed permeability via the addition of novel chemical composition of micro-pellets and investigate how this addition can have an impact on the sintering process and quality of the produced sinter when using a pilot line sinter pot. Chemical composition of the micro-pellets was mainly directly reduced iron ore fines which have been recycled from the production of directly reduced iron ore pellets. The DRI fines are a by-product of the process and are usually incorporated into a sinter blend but due to the fine nature of the particle size it is not advantageous for bed permeability. Thus, this section aims to prove that increasing the granule size of the directly reduced iron fines could increase bed permeability, in turn, increase flame front propagation speed and hence increase productivity - without having any negative consequences on the process and quality of sinter.

The second part of this chapter aimed to investigate and prove that specific novel materials can be recycled from various processes within the steel making plant and utilised in the iron ore sintering process. This investigation aimed to address the issue of sustainability and with proven concepts could help steer the iron ore sintering process to a more circular economy. The novel addition to the sintering process included used refractory brick that line ladles used in the steel making process at the basic oxygen steel making plant. After their time in service they are destined for land fill or sold on for a cheap price. The chemical composition of the crushed refractory brick has a high content of MgO and this study attempts to explain how it can be used in the sintering process as a MgO source.

6.1 Micro-pellets

6.1.1 Introduction

Directly reduced iron ore pellets are produced via a pelletization process ready to be directly charged into the blast furnace [69]. These are called DRI pellets. A by-product of this pelletizing process are fine particles of DRI. These are called DRI fines. The aim of this study was to investigate if there was any benefit to the sintering process when including micro pelletized DRI fines into a blend. The main reason for granulation is to reach adequate bed permeability to allow the flame front to travel at progressed speed. If the bed is not permeable, it would be difficult to create a suction and therefor the flame front would not propagate downwards, halting the sintering process [70] . Research has been done in the field on whether or not micro-pellets would be useful as a sintering addition and have concluded that permeability rates would increase if micro-pellets were used as opposed just iron ore fines [71] . However, there is not much evidence where sinter pot experiments have been performed to back this theory up. Hence this paper focusing directly on the impacts of including micro-pellets into the sintering process. There are numerous methods of agglomerating fines together [72]. However, the following study will focus on the micro-pelletized DRI fines made with a cement binder. It was apparent from an industrial point of view that these fines, due to the nature of their particle size, that can be somewhat be detrimental to a sintering bed's permeability. By the nature of the DRI fines, the amount of fines that can be used is limited. As the chemical make up of DRI is desirable, there is a need to increase the amount these fines being charged to a bed. By micro-pelletizing these fines and putting them into a blend at a 5% rate and subjecting the blend to a pilot line sinter pot facility, it hopes to give clarity and answer questions on how micro-pellets perform in a sintering rig. A conventional blend with 5% DRI fines was used to compare process parameters as well as sinter quality. The sinter pot was deployed for this study.

6.1.2 Experimental Procedure

In total, 2 blends were made up and 4 sinter pot tests were conducted. Micro-pellets were subjected to a sizing analysis and chemical composition analysis via XRF. Data was then used and incorporated into blend. Chemical composition of micro-pellets contained 6% cement binder and the rest DRI fines. Please see below table for XRF analysis of the micropellets and how this compares to the chemical make up of DRI fines. Blend A contained no micro-pellets and blend B contained 5% micro-pellets. The main difference per blend was the nuclei to

adhering ratio, NTLR, And this went from 1.14 to 1.27 on the addition of micropellets. The Si in the cement binder was negligible on a full blend basis. Please see below in table 26 for difference in NTLR. For full experimental procedure, sinter pot dimensions, formula sheet and post analysis procedure please see section 3.3. For the purpose of this experiment, blends were made up with 4% fuel to try and represent plant conditions as there was potential for full scale trials. Blends contained the following:

Table 29: Blend composition for micro-pellet study

Material	Blend A	Blend B	Units
Sinter feed C	2.063	2.063	Kg
Sinter feed E	2.063	2.063	Kg
Sinter feed AA	3.908	3.908	Kg
DRI	0.543	0.000	Kg
Sinter feed B	2.280	2.280	Kg
DRI-C Micro pellets	0.000	0.543	Kg
Sinter Fines	2.105	2.105	Kg
Olivine	0.197	0.197	Kg
Limestone	1.921	1.921	Kg
Magstone	0.395	0.395	Kg
Coke Breeze	0.526	0.526	Kg
NTLR	1.14	1.27	

Please note: Sinter pot tests were conducted at 4% fuel

6.1.3 Results and Discussion

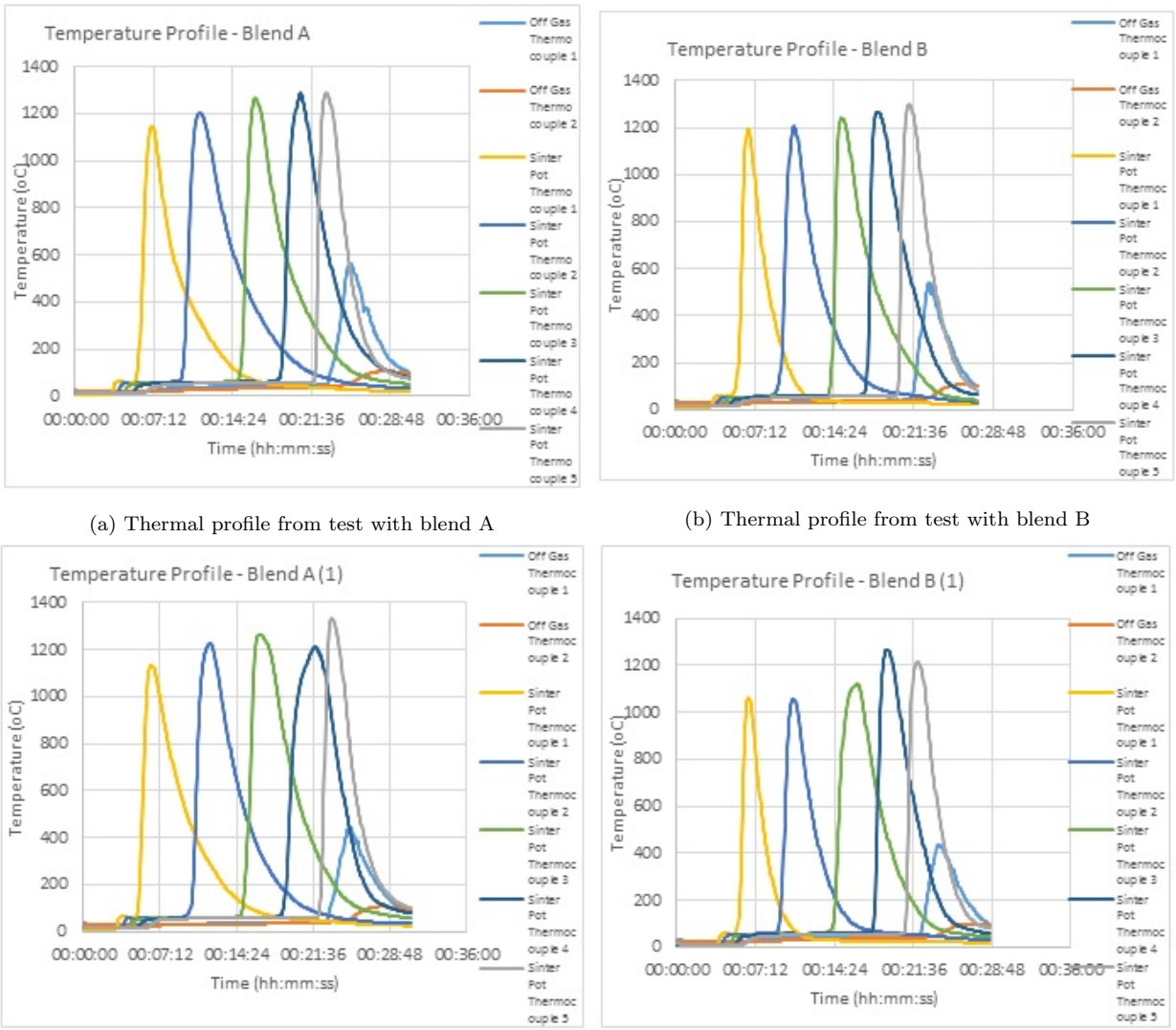

(a) Thermal profile from test with blend A

(b) Thermal profile from test with blend B

(c) Thermal profile from test with blend A repeat

(d) Thermal profile from test with blend B repeat

Figure 128: Thermal profiles from micro-pellet study

On analysing the thermal profiles in figure 128, it was evident that all the profiles were relatively uniform in appearance. It can be seen that the thermocouple traces peak sequentially indicating a stable process. However, it must be noted here that there is some variation between maximum temperatures reached, especially the lower temperatures exhibited for run 2 using blend B but all other parameters were within suitable sintering conditions.

Table 30: Process parameters for micropellet study

Parameters	Blend A	Blend A (r)	Blend B	Blend B (r)	Units
Pressure drop	100	100	100	100	mbar
Ignition time	01:00:00	01:00:00	01:00:00	01:00:00	m s
Cold flow rate	11.23	9.97	14.32	12.62	m3hr
Hot flow rate	6.34	6.37	7.53	7.51	m3hr
Sintering time	00:21:45	00:22:00	00:20:00	00:19:35	m s
Max sintering temp	1288.38	1338.38	1267.20	1299.59	C

Table 31: Process parameters for micropellet study

Parameters	Blend A	Blend A (r)	Blend B	Blend B (r)	Units
Flamefrontspeed					
TC1-2	0.26	0.21	0.29	0.28	mm/s
TC2-3	0.23	0.25	0.20	0.27	mm/s
TC3-4	0.29	0.23	0.45	0.35	mm/s
TC4-5	0.50	0.78	0.41	0.42	mm/s
Flamefront width					
TC1-2	2.64	3.18	N/A	2.80	mm
TC2-3	6.89	11.25	N/A	5.38	mm
TC3-4	8.57	7.90	13.55	7.00	mm
TC4-5	22.50	46.67	10.29	12.73	mm

The tables above shows parameters recorded to the computer panel during each sintering test. Full data set can be found in the appendices. On analysis, it was clear that sintering time decreased when using blend B. The decreased sintering time correlated with the

increased average flow rate through the bed and can be said to be due to the increase in overall average granule size of the bed. The increased average hot flow rate correlated with the higher average cold flow rate. Each micro pellet had a much larger particle diameter than particles in DRI fines, allowing for a much more permeable bed. The increased bed permeability allowed for more oxygen to be passed through which was evident from the increased average cold and hot flow rate readings. As more oxygen is able to pass through the bed, it increased the amount of oxidising agents and therefor increased the rate of the reactions taking place once the pot has been ignited – this was evident in the increased average hot flow as well as decreased sintering times. Flame front speed generally held this trend as well and this is evident on analysing the graphs in figure 136 (c). It must be noted here that the tests were fuelled with a 4% fuel rate. Further investigations would be ideal if the process could be fuelled at an increased rate. However, the above analysis backs up research [71] conducted in the past, as permeability is increased which is evident through the average hot flow rate and sintering times.

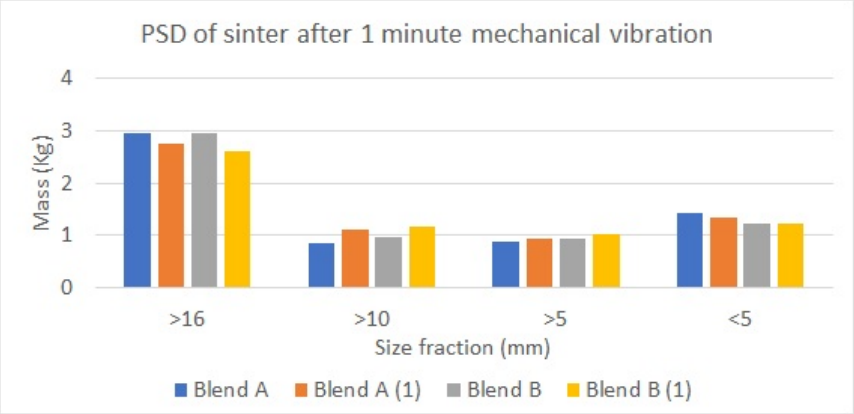

Figure 129: PSD of sinter after 1 minute of mechanical vibration

Figure 129 shows the yield in different size fractions of the sintered products. It can be noted that variation between the two sintered products was minimal. However, the sinter from blend B produced slightly less return fines. This is a promising sign for industry as return fines can be an issue and a sign of poor productivity. The increased amount of return fines could be due to the increased amount of fines within blend A as opposed to blend B. This suggest that the micro-pellets had good stabilising properties through out the sintering process. Sinter in the size fraction between 16-20mm was then taken for further analysis. Chemical analysis was complete by subjecting a small amount of sinter in this size fraction

to x-ray fluorescence testing. This can be seen in table 32. It was evident that there was minimal variation within chemistry between the two sintered products. This was another promising sign that DRI micro-pellets could be used and have an advantage over using DRI fines. Chemical composition from both sintered products were within range of suitable sinter plant sintering conditions ready for blast furnace charge.

Table 32: Sinter composition for micropellet study

XRF	Blend A	Blend B
FeO	6.89	7.01
SiO_2	5.76	5.62
Al_2O_3	1.35	1.29
TiO_2	0.07	0.1
CaO	9.42	10.35
MgO	1.76	2.02
Fe	54.67	56.65
Fe_2O_3	70.52	73.21
P	0.035	0.041
Mn	0.17	0.22

The sintered products from both tests were then subjected to a reduction degradation index testing. Only sinter in the region between 16-20mm in diameter was used. The results can be seen in figure 130. It was evident that RDI altered slightly between the two sintered products. This could be due to the increased reaction rate which results in less time for phase transformation to occur. However, this could be due to the lack of fuel within the system. As mentioned previously, further tests should be performed with an increased fuel rate in the sinter pot.

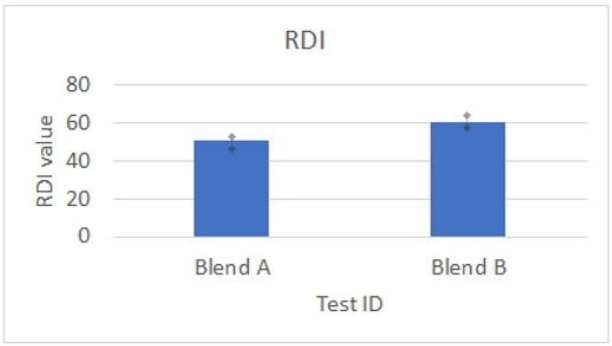

Figure 130: Reduction degradation index results of produced sinter

Optical microscopy

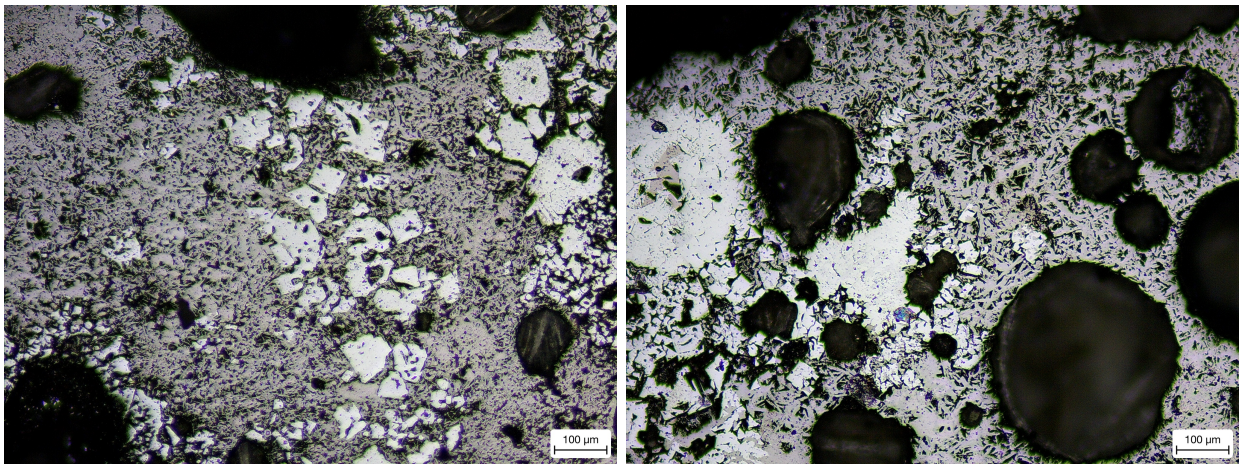

(a) No micropellets x10

(b) with 5% micropellets x10

Figure 131: Microstructures of the sinter produced with and without micro-pellets

Figure 131 shows the microstructures of sinter produced from the micro-pellet investigation. A shows the sinter microstructure without micro-pellets. B shows the microstructure of the sinter produced with micro-pellets. The main objective of the optical microscopy study was to ensure no major feature differences were evident within the microstructure. This could have given potential indication of the micro-pellets not fusing within the blend but this was not evident. Block-like hematite and magnetite evident in both samples. Needle like SFCA's were also evident.

6.1.4 Conclusion

i) Both blends produced a stable and uniform process and this was evident from the thermal profiles. This indicated that flame front propagated in a uniform and stable manner when replacing DRI fines with DRI micro-pellets.

ii) Sintering time was decreased by 5% when replacing DRI fines with DRI micro-pellets and flame front speed generally increased. Therefor, productivity was increased by 5% with no significant change in sinter quality.

iii) Sinter yield had minimal variation when replacing DRI fines with DRI micro-pellets, however, it must be noted that there was a slight decrease in returns fines when using DRI micro-pellets. Coupled with decreased sintering time this application could see potential for industrial use.

iv) Reduction degradation varies slightly between tests, showing an increase when DRI micro-pellets were used. This could be related to the increased reaction rate and less time for phase transformation to occur when using micropellets. This could be problematic when charged at the blast furnace. However, it must be suggested that further investigations must be complete before concluding as the sinter pot was only fuelled with a fuel rate of 4% and so high sintering temperatures was not evident through-out. Given the results of the previous fuel content study in section 5.4. RDI could potentially be rectified with a slight increase in fuel rate.

6.2 Alternative MgO source

Utilising by-products and recycled materials from all parts of a steelworks is of utmost importance in heading towards a more sustainable approach in the steel making process. The sinter plant operation is a pre-process of the steel making procedure and is known for utilising recycled products due to the nature of the sintering application. This section focused on a novel material to be used in sintering which had been recycled from the basic oxygen steel making plant. Spent refractory bricks were used in this study and in the set of experiments presented. This study aims to address whether the conventional MgO source in iron ore sintering can be replaced by novel means and how this novel sintering component can impact the sintering process and quality. The chemical composition of the used refractory brick was determined and was incorporated into a sinter blend. Process parameters were recorded with flame front characteristics analysed. The quality of sinter produced was investigated via analysis of chemical composition, reduction degradation index testing as well as optical microscopy. The alternative MgO proved a suitable MgO source for the sintering process with no sinter quality issue, however, some process issues still remain to be resolved. These issues are addressed in this section with possible rectifications.

6.2.1 Introduction

Fluxes generally lower the melting temperature of the compounds it is mixed with in iron ore sintering, promoting fluidity of the melt and allowing the sintering process to be conducted at lower temperatures [9]. This has great value for the sinter plant as it requires less energy input and hence improves efficiency and environmental performance. Some of the fluxes used are Magstone and Olivine which act as a Mgo and Si trim. The chemical composition of magstone and olivine can have roughly around 30 and 50% of MgO respectively. Olivine can have high concentrations of Si and so is used as a Si trim. In general, a steel works can spend over £1M on these fluxes every year as a suitable MgO or Si source. The magnesia based carbon bonded refractory bricks are used in the basic oxygen steel making plant to line their vessels and ladles. The bricks have a shelf life of just 1 year and are taken out of service regularly and replaced. The used refractory bricks are then either sold on for a very low price or sent to landfill. The chemical composition of the bricks once taken out of service can still be utilised due to it having a high content of MgO, over 70%. Better still, the alternative MgO source does not have an increased impurity level such as other fluxes used on plants especially when using reverts as a flux. This brings forward the argument of the alternative MgO source being an improved substitute than most fluxes with high impurities. Chemical

composition of the crushed refractory brick can be seen below. Impurities introduced in conventional fluxes result in slag quality / efficacy issues and if this could be minimised it would have an advantageous impact across the process [73]. Furthermore, there is a certain amount of carbon present within the refractory bricks which could have an impact on the sintering temperatures of the process. If utilised correctly, it can act as a fuel booster by allowing a reduction in the amount of coke breeze being used in a blend. These promising impacts could drive down energy input and prove not only cost effective but will steer towards a more sustainable and circular economy in iron making.

6.2.2 Experimental Procedure

In total, 2 blends were made up and 4 sinter pot tests conducted. Blend A did not contain any of the refractory brick and blend B contained crushed refractory brick. The refractory brick was crushed to less than 0.5mm for processing. A sample of the crushed refractory brick was pulverised and subjected to chemical analysis via x-ray fluorescence, this can be seen below. It can be seen that the brick contained around 70% MgO. That is 4x more than the MgO in magstone. The data was used accordingly to replace the magstone and olivine in blend B. It must be noted here the fluxes and ores were adjusted to maintain sinter chemistry. This was mainly extra limestone to make up for the CaO deficit when using the crushed refractory brick. All blends were made up under laboratory conditions. For full experimental procedure, formula sheet and post analysis procedure please refer back to chapter 3 section 3.7. Blends contained the following:

Table 33: Chemical composition of crushed refractory brick and conventional magstone

XRF	Crushed refractory brick	Conventional magstone
FeO	0.86	0
SiO_2	3.01	3.11
Al_2O_3	6.19	0.54
TiO_2	0.13	0
CaO	2.44	26.9
MgO	69.23	15.64
Fe	1.44	0
Fe_2O_3	1.1	1.49
P	0.017	0
Mn	0.17	0
C	13.48	-
Na_2O	0.055	0.253
K_2O	0.05	0.182
Zn	0.028	0.002

Table 34: Blend composition

Material	Blend A	Blend B	Units
Sinter feed C	2.0119	2.076	Kg
Sinter feed E	2.0119	2.076	Kg
Sinter feed AA	4.026	5.463	Kg
Sinter feed B	2.331	1.093	Kg
Refractory brick	0.000	0.219	Kg
Sinter Fines	2.055	2.081	Kg
Olivine	0.193	0.000	Kg
Limestone	1.875	2.081	Kg
Magstone	0.385	0.000	Kg
Breeze	0.899	0.911	Kg

6.2.3 Results and Discussion

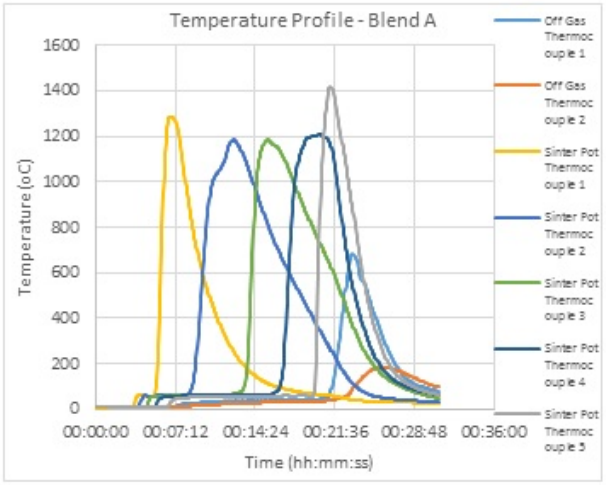

(a) Thermal profile from test with blend A

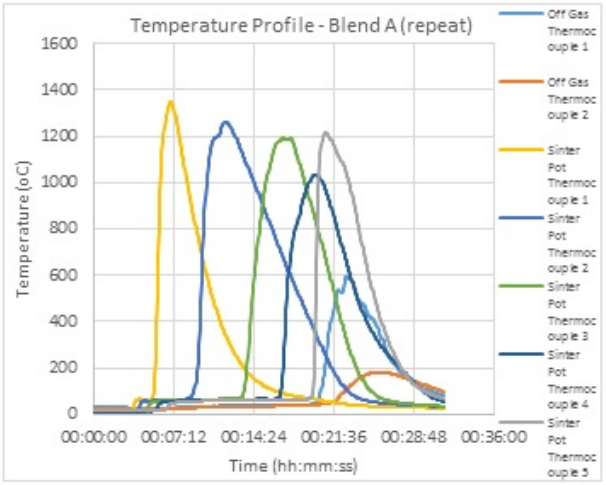

(b) Thermal profile from test with blend A

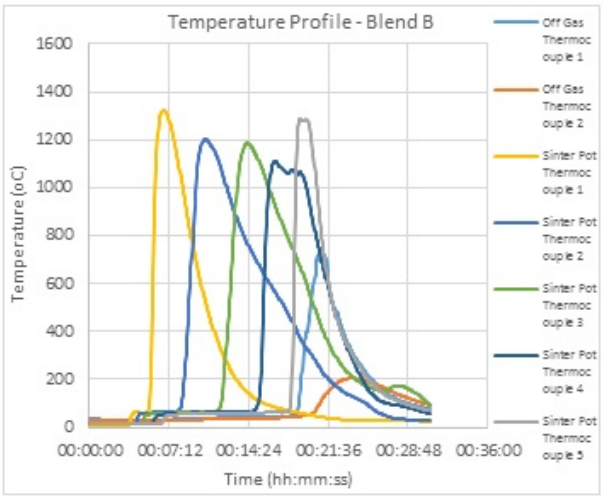

(c) Thermal profile from test with blend B

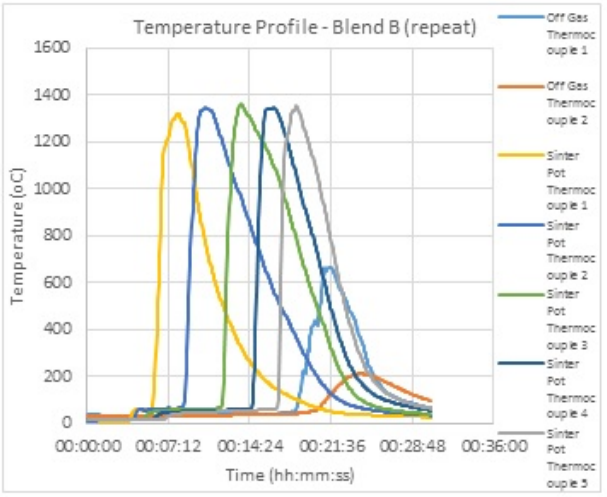

(d) Thermal profile from test with blend B repeat

Figure 132: Thermal profiles from MgO study

On analysing the thermal profiles in figure 132, it was evident that all the profiles exhibited uniform process stability. It must be noted here that there was slight variation in sintering temperatures when sintering with both blend A and blend B. It must be noted here that the carbon content of the crushed refractory brick was not taken into consideration when making up blends. Thus, this could be due to the fluctuation in carbon content in the crushed refractory brick as well as the discrepancies between materials used between the two blends. However, it must be noted that maximum sintering temperatures was within upper a lower limits 50°C which was within suitable variation as defined by the repeatability tests

outlined in section 3.2.3. The variation in sintering temperatures is very likely due to the extra carbon within the crushed refractory brick, further investigation must be complete to clarify this specifically. Regardless of this outcome, conclusions could still be drawn. The uniformity and stable process was the first tell tale sign that the alternative MgO source could be a suitable MgO trim for the sinter plant, providing that the extra carbon is taken into consideration when fuelling the process. The takeaway here was that all thermocouples started to peak sequentially which indicated that flame front travel was not impeded when including the crushed refractory brick.

Table 35: Process parameters for Alternative MgO source study

Parameters	Blend A	Blend A (r)	Blend B	Blend B (r)	Units
Pressure drop	100	100	100	100	mbar
Ignition time	01:00:00	01:00:00	01:00:00	01:00:00	m s
Cold permeability flow rate	10.62	11.10	11.90	10.64	M3 hr
Hot Permeability flow rate	6.97	6.82	7.72	7.48	M3 hr
Sintering time	00:19:45	00:19:15	00:17:15	00:17:35	hr:mn:s
Max sintering temp	1421.40	1348.36	1322.29	1358.94	C

Table 36: Process parameters for Alternative MgO source study

Parameters	Blend A	Blend A (r)	Blend B	Blend B (r)	Units
Flame front speed					
TC1-2	0.21	0.24	0.30	0.48	mm/s
TC2-3	0.38	0.23	0.31	0.37	mm/s
TC3-4	0.25	0.40	0.47	0.40	mm/s
TC4-5	1.27	1.17	0.52	0.58	mm/s
Cooling rate (1100C-600C)					
TC1	4.55	4.00	4.17	3.85	C/S
TC2	2.08	2.04	1.85	2.33	C/S
TC3	1.89	2.94	2.00	2.70	C/S
TC4	5.88	2.56	1.89	3.03	C/S

On analysing the table above, it was clear that sintering time was 2 minutes faster when using blend B. The faster sintering time correlated with the higher average hot flow rate when using blend B. The higher average hot flow rate correlated with the increased average cold flow rate. Reduced sintering times could be correlated with increased hot and cold flow rates. The increased cold a flow rate could be due to the changes in blend PSD brought about by substitution of flux for coarse ore due to the purity levels of MgO in the crushed refractory brick. Increased hot flow rate could be due to the extra carbon content in the crushed refractory brick resulted in a slight increase fuel rate. The difference in sintering time and cold flow rate falls within suitable variation limits and so no increase or decrease can be concluded. However, hot flow rate increase does not fall within suitable variation limits and therefor it could be concluded that on the addition of the crushed refractory brick an increase in hot flow could be expected. This could be a sign that the reduced sintering time could perhaps be due to the inclusion of the crushed refractory brick. Further investigation must be performed to give an accurate conclusion on this matter. It must be noted here that there was an increase in off gas temperatures when sintering blend B as opposed to A which can be seen in recorded parameters in the appendices. The increase in temperatures did not fall within the suitable variation limits and therefor it could be concluded that when using

crushed refractory brick, an increase in off gas temperature could be expected. This also correlated with the increased averaged hot flow rates as seen in table 35 as well as reduced sintering time when sintering with blend B. It must be noted that the increased off gas temperatures would be cause for concern at industry level due to the high temperatures the exhaust wind main would be subjected to. However, if fuel was adjusted to compensate for extra carbon within the refractory brick it could still be utilised. A further positive impact of using the crushed refractory brick would be that the fuel rate could be decreased resulting in cost savings.

In summary, on the addition of the MgO substitute, hot flow rate and flame front speed was increased and thus sintering time decreased. It can be said with confidence that this was due to the extra carbon within blend B.

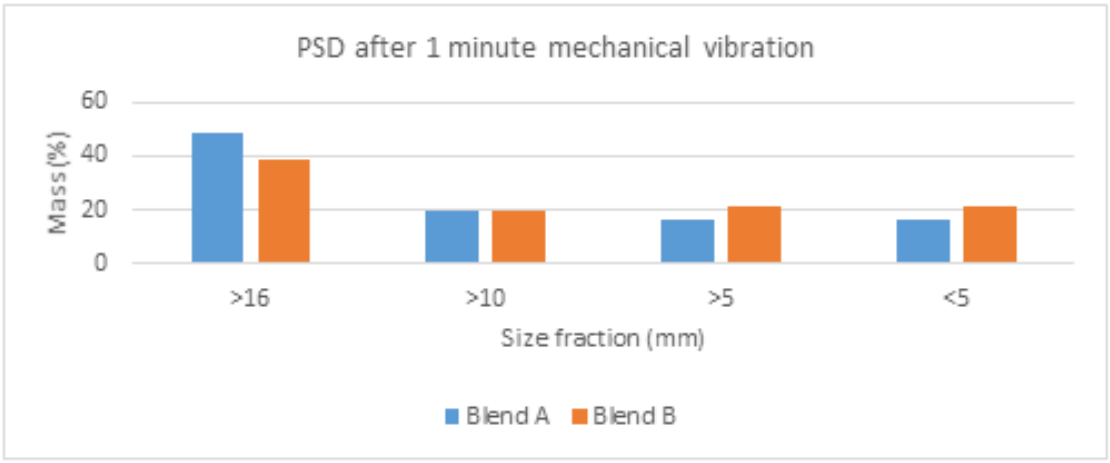

Figure 133: PSD after 1 minute mechanical vibration from MgO study

On analysing figure 133 there was little change in the amount of sinter made when sintering with blend A as opposed to blend B. Another positive sign that the alternative MgO source could be used as an alternative MgO trim. However, return fines seemed to increase slightly when sintering with blend B which correlated with the amount of sinter above 16mm it produced. This correlated with the decreased FeO in the sintered product using blend B. This could be due to the increased hot flow rate and flame front speed, resulting in less amount of time for reduction and agglomeration to occur. This could also be due to the particle size of the crushed refractory brick. Olivine and magstone are coarser in size and so this could be a direct result of replacing it with a finer material. Even though the variation in return fines is minimal (however, slightly above suitable variation limits) this

could have a negative impact at industrial level so further investigation should be performed to clarify this conclusion.

Table 37: Sinter composition

XRF	Blend A	Blend B
SiO_2	6.5	5.7
Al_2O_3	1.7	1.58
TiO_2	0.11	0.08
CaO	10.5	9.93
MgO	2.06	2.56
Fe	56.52	56.88
Fe_2O_3	52.29	59.89
FeO	25.66	19.29
P	0.042	0.038
Mn	0.25	0.18

The sintered product from both tests were subjected to a chemical analysis via x-ray fluorescence and results can be seen in table 37. When analysing table 30, the chemical composition did not vary from test to test, and the little variation evident may be classed as negligible as all were within a threshold of suitable sinter quality parameters outlined by sinter control operators. However, it is worth noting here that Fe_2O_3 content increased (which is slightly above the suitable variation limits) and thus FeO decreased when using blend B as opposed to A. This could be due to the difference in temperatures and flame front characteristics within the system when using the crushed refractory brick which could be due to the extra carbon within. It is also worth noting here that MgO levels were slightly increased, this could be due to the purity of crushed refractory brick, it must be ensured that the crushed refractory brick must be uniformly dispersed when mixing the green blend. This emphasises the purity of the crushed refractory brick and how little is needed in terms

of mass to maintain MgO levels, but great care is needed when mixing.

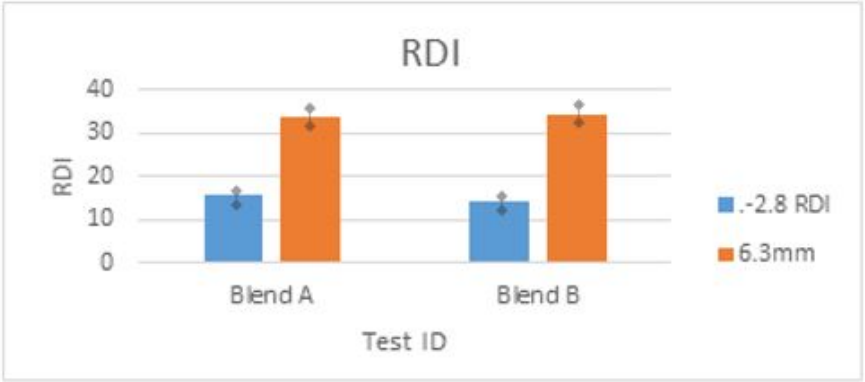

Figure 134: Reduction degradation index test

The sintered product from both tests was then subjected to a reduction degradation index testing. Only sinter in the region between 16-20mm in diameter was used. This followed normal sinter operations at the sinter plant, to ensure sinter is suitable for the blast furnace. The results can be seen in figure 134. It was evident that RDI does not alter significantly when using blend B as opposed to blend A. Both sintered products displayed sufficient RDI characteristics during the reduction degradation testing. This was another positive sign that the alternative MgO source could be used in the sinter plant.

It is worth noting here that due to there being additional carbon from the binder and graphite withing the refractory brick; as next steps in future work it would be ideal to conduct a thermo-gravimetric analysis comparison of conventional MgO source to the alternative MgO source to confirm extra carbon content and combustion characteristics so in further experiments fuel rates could be adjusted accordingly.

Optical microscopy and EDS analysis from MgO study

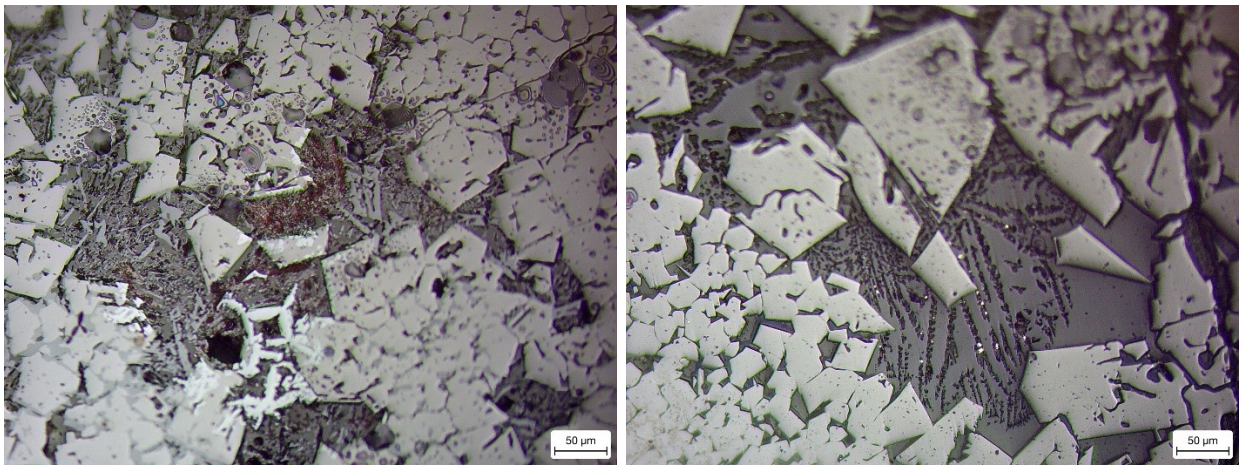

(a) Blend A (b) Blend B

Figure 135: Microstructure of sintered product using Blend A and Blend B from MgO study

Figure 135 shows the optical microscopy microstructures of the sintered products with and without the addition of the alternative MgO source. Figure 146 (a) shows the sinter that contains no MgO replacement. Figure 146 (b) shows the sinter that contains MgO replacement. From literature it can be said that the structures in the both microstructures exhibit block/plate-like features of hematite and magnetite surrounded by SFCA's [74]. There were no signs of alterations between the 2 sintered products when analysing with optical microscopy.

EDS was also deployed and the images in figure 136 below are the EDS layered images. It can be noted here that there was discrepancies in the colour differences. It must be noted here that the following EDS analysis was complete in order to support some of the qualitative characterisation of the microstructures exhibited above as well as investigate if there are any discrepancies picked up in MgO.

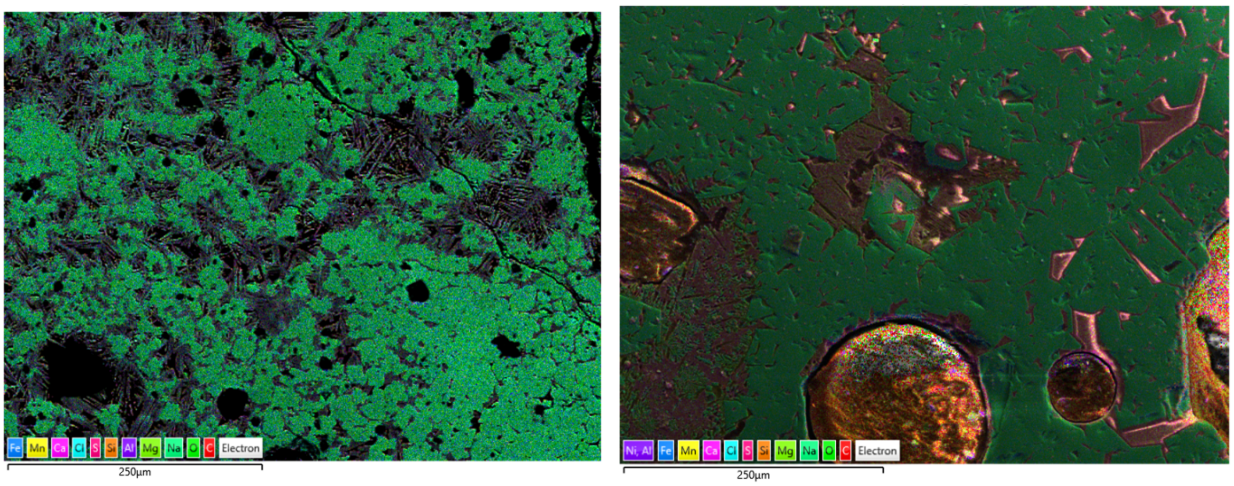

(a) Blend A

(b) Blend B

Figure 136: EDS layered images of sintered product using Blend A and Blend B from MgO study

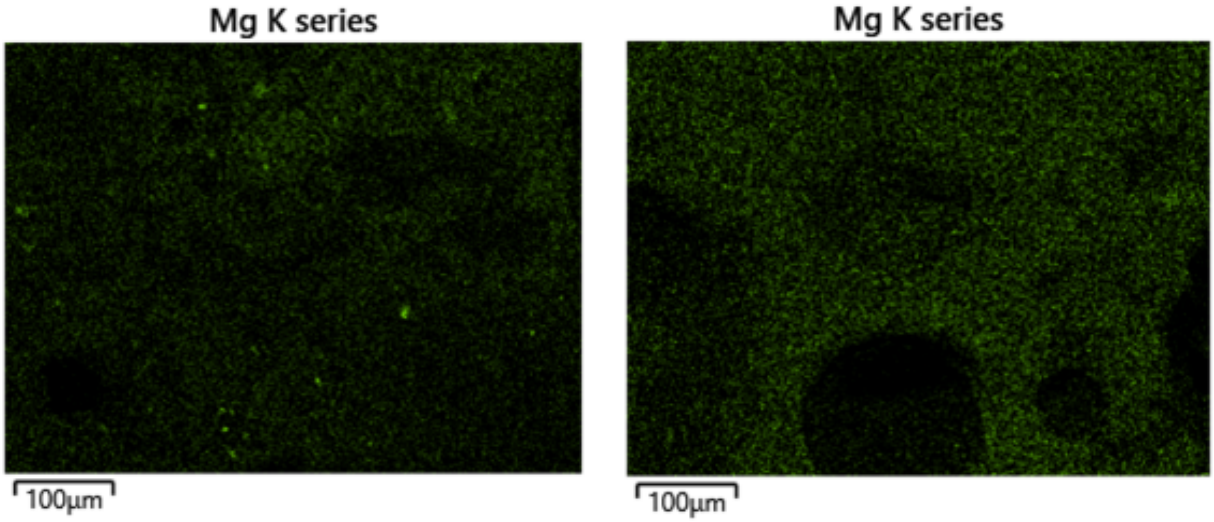

(a) Blend A

(b) Blend B

Figure 137: EDS Mg images of sintered product using Blend A and Blend B from MgO study

Figures 137 shows the EDS image associated with Mg levels. It can be noted that in image A the Mg seemed evenly distributed through out, however, exhibited a few localised areas of concentrated Mg. This could be due to the difference in particle size of the crushed

refractory brick compared to the conventional magstone. As the conventional magstone is coarser, it could lead to localised area rich in MgO. The spectra for the samples indicated that Na and Cl were noticeably higher when using the conventional magstone, however, only a qualitative judgement can be made. This can be seen in figure 138 below. The increase in Na could be due to the increased amount of sodium oxide in conventional magstone.

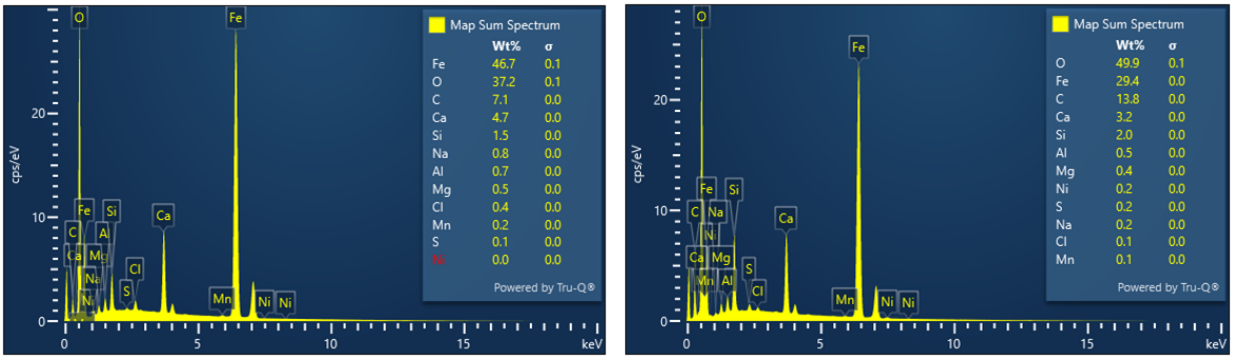

(a) Blend A

(b) Blend B

Figure 138: Spectra from EDS analysis images of sintered product using Blend A and Blend B from MgO study

Figure 139 and 140 shows the EDS image associated with Na as well as Cl. This can be seen below. When analysing the images, it was clear that more Na was evident in blend A when looking at the EDS images. As mentioned, the increased Na was due to the increased amounts of sodium oxide in conventional magstone when compared to the crushed refractory brick. Chloride analysis was not completed on the crushed refractory brick. However, the EDS images below suggest that there is more chloride in the sinter when using conventional magstone.

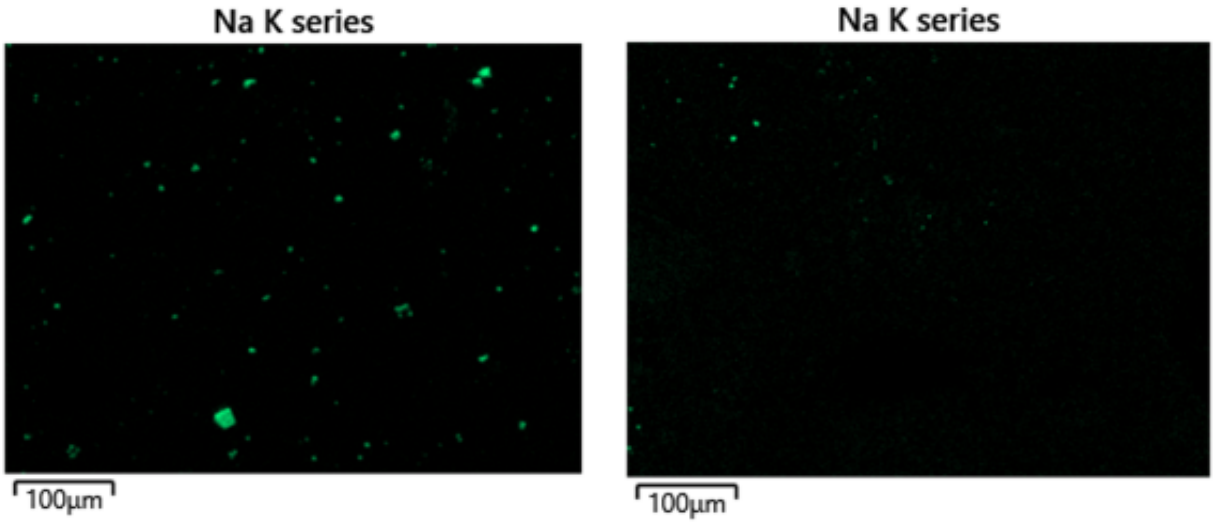

(a) Blend A

(b) Blend B

Figure 139: EDS Na images of sintered product using Blend A and Blend B from MgO study

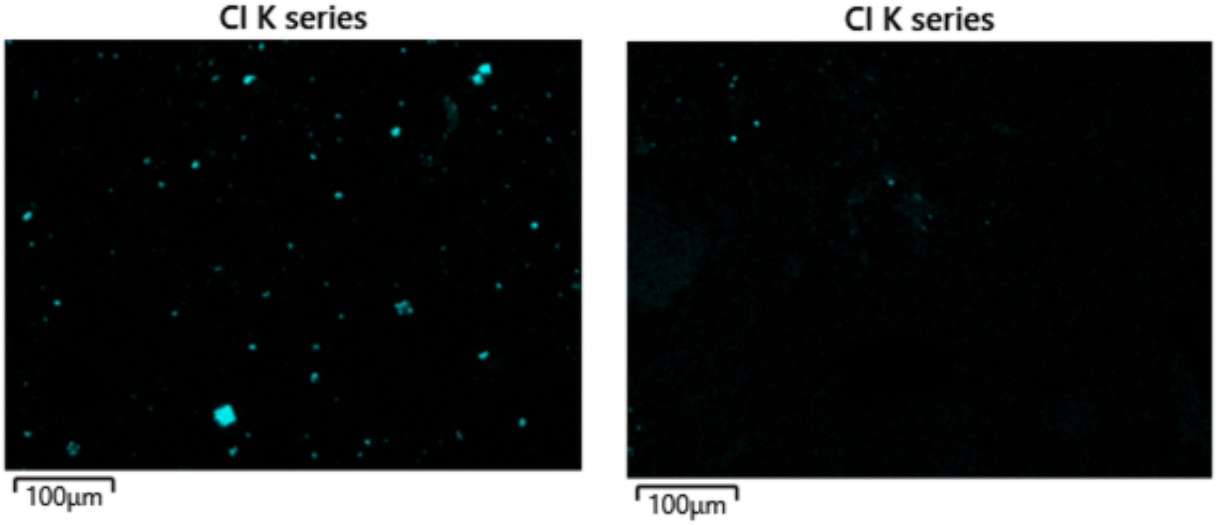

(a) Blend A

(b) Blend B

Figure 140: EDS Cl images of sintered product using Blend A and Blend B from MgO study

6.2.4 Conclusion

i) It was evident from the thermal profiles that both blends produced a relatively stable and uniform process with acceptable flame front propagation i.e. no broken flame front or extra flare ups.

ii) When sintering with the crushed refractory brick, an increase in off gas temperature could be expected. This could be due to the different volatile matter within the carbon of the crushed refractory brick.

iii) Sintering time was slightly reduced when using the crushed refractory brick, however, results were within suitable variation limits. Increased average hot flow rate and increased flame front speed naturally correlated with reduced sintering time. Further investigations are recommended to understand why the input of crushed refractory brick produced increased average hot flow rates and flame front speeds, thus decreasing sintering time.

iv) Return fines was slightly increased when when replacing magstone and olivine with crushed refractory brick.

v) Chemical composition of final sintered products did not vary apart from slight variation in Fe_2O_3 content and thus FeO content. This was a result of the difference in flame front characteristics which was a result of the increased and different carbon content in blend B. Regardless of this, all within suitable chemical composition of sinter ready for blast furnace operations.

vi) Reduction degradation index did not vary significantly between final sintered products between tests and both blends produced strong sinter with good RDI characteristics.

vii) This work can conclude that crushed refractory brick could be used as an alternative MgO source in iron ore sinter but may have some process impacts such as reduced sintering times and increased off gas temperature. This may be rectified by adjusting fuel content according to carbon content within the alternative MgO source.

viii) A sinter plant can use over 150,000 ton of magstone per year. If this was replaced with the crushed refractory brick, a total of 35,300 ton of crushed refractory brick would be needed to get the same MgO concentration, a 77% reduction.

7 Conclusion and future work

This chapter presents the summary of conclusions of the research described in the thesis. The aim and objectives of the research, outlined in chapter 1, are reviewed and their achievement addressed. Proposals for future work indicated by the research are suggested.

7.1 Conclusions

The objectives of this research are listed below. All of these objectives were completed as part of the research. Furthermore, the conclusions obtained as a direct result of meeting these objectives are addressed.

1. Can a 7kg pilot line sintering rig be utilised to adequately simulate the iron ore sintering process?

    - The research conducted can confidently state that a 7kg sinter pot can adequately simulate the iron ore sintering process. This has been accomplished via extensive validation experiments as well as identifying trends and correlations exhibited within the iron ore sintering process at an industrial scale.
    - The research proved that with careful selection of fuel rate as well as particle size distribution of the fuel particles, strong correlations were determined between the process behaviour and industrially produced sinter with comparatively low levels of variance for the key process parameters and product quality indices.
    - The capabilities that of the sintering rig had a substantial impact on industry. The sintering facility was incorporated into the systemic process of producing sintered iron. The sinterig rig was used for many purposes, from proving different theories in research, making process correlations to the production plant, to supporting cost effective decision making when purchasing different iron ores. The sintering rig clearly proved itself in industry as being a cost effectiver valuable tool to supoprt the sintering process.

2. What literature conducted by previous researchers in the field of iron ore sintering can be identified and built on further?

    - The literature review identified that further knowledge should be gained on the impact of fuel substitutions, mean fuel particle size and fuel particle size distribution on sinter product quality and process stability.

- Furthermore, the literature review conducted suggested that surplus research has been conducted on biomass, however, not enough research has been conducted on up-cycling materials and by-products from various parts of the iron and steel making process back into the sintering process.

3. Can such a small scale pilot line sinter pot be used to track optimum sintering characteristics varying different ferrous additions to sintering blend?

    - The sinter pot was used to determining optimum process characteristics and quality trends when varying different ferrous additions.
    - Optimum process characteristics include granulation time and speed, moisture content and pressure drop set points for various blends.
    - Optimum quality parameter trends include chemical composition and cold/hot strength characteristics such as sinter sizing and reduction degradation index testing.
    - Furthermore, optimum amounts were suggested and several observations noted when increasing certain ore percentages. Quality of sinter was analysed and an attempt made on optimising sinter quality indices via varying amounts of ore percentages.
    - This avenue of the project had impact in industry when selecting new ores that the plant had not seen before. Various iron ore pre-flight samples were processed by the sinter pot laboratory distributing valuable information supporting the raw material department when making multi million pound decisions when purchasing different iron ores.

4. What are the impacts of fuel particle size, and particle size distribution of the fuel used at 100% and in ratios of other fuels, have on the iron ore sintering process and sinter quality? Furthermore, what influence does this have on the kinetics of the process as well as how this has an impact on the quality of sinter produced?

    - Breeze and anthracite fuel was analysed. Furthermore, particle size and particle size distributions of the fuel used at 100% and in ratios was investigated. Research found that the particle size distribution of the fuels can play an important role in impacting the process and quality of sinter. Variation is increased in the process as well as quality of sinter when not controlling the particle size distribution of the fuels being used. The thermodynamic process is driven by the chemical

composition and temperature differences. For a given peak temperature, the particle size distribution impacts the kinetics, which is governed by the changes in the mechanism of a reaction defined by its thermodynamic potential.

- The research conducted proved that with precise control over fuel particle size and particle size distribution, increased stability was evident within the process. An optimum particle size distribution was identified as 80% 2-3mm, 15mm% 1-2mm and 5% 0-1mm and the impact of this was correlated to cold and hot permeability as well as flame front characteristics.
- It is worth noting here that the available literature does not state the origin of anthracite. Previously reported differences when using different anthracite sources results in variation within process parameters. This investigation found that anthracite properties vary by origin. Thus, thermal characteristics of anthracite will differ, varying its influence on the process.
- It was proven that the variation in particle size distribution of the various fuels used is of utmost importance when trying to achieve a cost effective and stable process. This had multi million pounds in savings across industry when selecting various fuels for the process and ensuring process stability.

5. What novel additions can be introduced to a sintering blend to create a more circular economy in iron and steel making without impeding the process nor quality of sinter? Can this be achieved by utilising the chemical composition of used by-products in the various iron and steel making plants?

    - It was determined that crushed refractory brick could be used as a substitute of conventional flux material with minimal negative impacts to the process. This has the potential to re-purpose up to a thousand tones of end of life refractory material used in steel making per year.
    - The carbon within the used crushed refractory brick could be utilised in lowering the fuel input for the iron ore sintering process, however, further investigation would be required to understand the impact on off gas temperatures.

6. What Novel additions can be introduced to a sintering blend to increase the productivity of the sintering process without negatively impacting the process and without impeding the quality of the sinter produced?

    - A novel micro-pellet was analysed by introducing it to a sintering blend. Directly reduced iron fines are a by-product of pelletizing directly reduced iron. Investigations concluded that directly reduced iron micro-pellets had an advantageous chemistry for sintering and increased the overall average particle size of the granulated blend. This increased bed permeability and thus increased flame front speed, reduced sintering time, reduced return fines and therefore increasing productivity by up to 5%.
    - This section of the project has great promise in industry. Business cases have been approved ready for full scale trials to commence at the production plant. This could potentially increase production rates inn a cost effective manner.

7.2 Industrial Impact

This project has established the sinter pot as a valuable tool in the iron making process. Not only has it impacted the industrial sector it has also played an important role in research and development. This section aims to set out the impacts of this project in terms of industrial applications.

1. The sinter pot is the only functioning pilot line rig in the whole of the UK. It is unique in many ways. Firstly it has the ability to turn over results in rapid time without effecting production. Secondly it has the ability to closely monitor flame front characteristics as well as many other parameters such as process and product quality. The rapid turn over in results has allowed the sinter plant to make rapid informed changes to the production process in good time based on sinter pot results. It has also allowed the sinter plant to evaluate the process impacts of raw materials to achieve optimum permeability and moisture before being reclaimed to the sinter plant. This project has also enabled the raw material team to evaluate the influence of materials before making any purchases. Although the savings incurred due to the above is classified it can be said to be in the region of hundreds of thousands of pounds on an annual basis.

2. An extensive study was performed on the sinter pot's ability to examine process conditions when incorporating and increasing ferrous additions to a blend. Although this was in the early stages of the project, it was a great success. The project impact with regards to ferrous additions allowed the sinter plant to fine tune their raw input blend according to optimum process characteristics acquired from the extensive sinter pot studies within this project. Recommendations were set out on the basis of optimum ore percentages within a blend. This allowed for increased process stability in the sinter plant as well as decreased variation in production quality.

3. The fuel particle size distribution study within this project has the potential to save over 1 million pounds annually. This was proved via a series of extensive sinter pot tests focusing on optimum particle size distribution of fuel within a sintering bed when using coke breeze and anthracite as the energy source. This allowed for a reduction in fuel consumption. Not only was there a benefit in cost savings, process stability increased and product quality increased. This resulted in further savings down the steel making process chain. This also has huge potential to have an environmental impact by decreasing the sinter plant's carbon foot print.

4. Incorporating micropellets into a sintering blend has huge potential for impact. Pot tests conducted in this project showed that by careful control over micropellet chemistry and size distribution, process stability can be maintained with an increase in speed of work. A main contributor to poor quality in output sinter is amount of return fines produced. This study proved that incorporating micropellets into a blend can reduce the total percentage of return fines produced. This resulted in a 5% increase in productivity. The result of this work would allow for finer raw material purchases to be made resulting in further cost savings. Business cases have now been written up to propose a trial of incorporating over 4000 tonne of micropellets into a sintering blend. If successful, and based on the outcome of the recommendations in this project, reverts will be incorporated into the micropellets with aims to reduce waste gas emissions. This would result in significant reduction in the environmental impact of the iron ore sintering process.

5. Minimising by-products and re-cycling waste products is key in achieving circular economy within the steel making industry. Thousands of tonne of end of life refractory brick are destined for land fill on a regular basis. This project has proved that by crushing and incorporating the refractory brick back into a sintering blend, it can be recycled within the sinter plant. Furthermore, the chemical composition of the refractory brick can be used as a flux within the sintering process. This can lead to reducing the need to purchase fluxing components resulting in substantial cost savings. The ability to recycle crushed refractory brick would have a positive impact in the aims of achieving circular economy in the steel making industry.

7.3 Recommendations for Future Work

The limitations the techniques developed and conclusions drawn from the research conducted have indicated the following areas as recommendations for further work.

1. The work conducted in this research included the commissioning of a small scale pilot line sinter pot. It is recommended that further analytical equipment be incorporated into the testing facility to include the capability for dust capture in the form of heavy and light particulates. A tray can be incorporated directly underneath the pot to analyse heavy dust particulates and a filter placed within the pipe work of the exhaust to analyse lighter dust particulates.

2. The work conducted in this research has demonstrated that there is the potential to increase efficiency through careful control over fuel particle size distributions. Further work should investigate the reductions in fuel rate by this method.

3. It can be recommended to further investigate the crushed refractory brick study with particular focus on whether the fuel rate can be reduced in order to compensate for the carbon content within the chemical composition of the used and crushed refractory brick. Full thermogravimetric analysis should be conducted on the crushed refractory brick and sinter pot tests performed with fuel rates adjusted accordingly.

4. The research in this work package showed the advantages of incorporating micropellets into a sintering blend. Using the sinter pot, the work demonstrated that productivity can be increased through increasing bed permeability. Further work should be carried out by incorporating reverts into the micropellet. This would prove that micropellets are an effective way of simultaneously maximising revert usage and increase productivity. This approach is recommended to maximise the utilisation of fine ferrous materials as well as by-products.

References

[1] M. Gan, Z. Ji, X. Fan, X. Chen, Y. Zhou, G. Wang, Y. Tian, and T. Jiang, "Clean recycle and utilization of hazardous iron-bearing waste in iron ore sintering process," *Journal of Hazardous Materials*, vol. 353, pp. 381–392, 7 2018.

[2] D. Fernández-González, I. Ruiz-Bustinza, J. Mochón, C. González-Gasca, and L. F. Verdeja, "Iron Ore Sintering: Raw Materials and Granulation," 1 2017.

[3] Y. Yang, K. Raipala, and L. Holappa, "Ironmaking," in *Treatise on Process Metallurgy*, vol. 3, pp. 2–88, Elsevier Ltd., 2014.

[4] R. N. Wright, "Relevant Aspects of Carbon and Low-Alloy Steel Metallurgy," in *Wire Technology*, pp. 201–233, Elsevier, 2016.

[5] D. Fernández-González, I. Ruiz-Bustinza, J. Mochón, C. González-Gasca, and L. F. Verdeja, "Iron Ore Sintering: Process," 7 2017.

[6] The Institute for Industrial Productivity, "Sinter Plant."

[7] X. C. M. W. Xiaoxia Chen, Jinhua She, "Modeling method of carbon efficiency in iron ore sintering process," *Engineering, Computer Science 2016 IEEE International Conference on Industrial Technology (ICIT)*, 2016.

[8] M. Ericsson, "Global Iron Ore Report: Iron Ore Prices Remain Relatively High," tech. rep., 2020.

[9] G. S. Feng, S. L. Wu, H. L. Han, L. W. Ma, W. Z. Jiang, and X. Q. Liu, "Sintering characteristics of fluxes and their structure optimization," *International Journal of Minerals, Metallurgy and Materials*, vol. 18, pp. 270–276, 6 2011.

[10] D. Fernández-González, I. Ruiz-Bustinza, J. Mochón, C. González-Gasca, and L. F. Verdeja, "Iron Ore Sintering: Quality Indices," 7 2017.

[11] K. Higuchi, Y. Takamoto, T. Orimoto, T. Sato, F. Koizumi, K. Shinagawa, and H. Furuta, "Quality Improvement of Sintered Ore in Relation to Blast Furnace Operation," tech. rep., 2006.

[12] T. Jiang, J.-Y. Hwang, P. Masset, O. Yucel, R. Padilla, G. Zhou, J. Fan, G. Qiu, Y. Guo, Y. Yang, and M. Cai, "STUDIES ON ALTERNATIVE BLAST FURNACE BURDEN STRUCTURE WITH HIGH PROPORTION SINTER," tech. rep.

[13] A. J. L. L. J. I. Palacios, J. M. and L. Iniesta, *La Fabricación del Acero,*. Madrid: UNESID,: Unión de Empresas Siderúrgicas., 1998.

[14] T. Umadevi, K. Nelson, P. C. Mahapatra, M. Prabhu, and M. Ranjan, "Influence of magnesia on iron ore sinter properties and productivity," *Ironmaking and Steelmaking*, vol. 36, pp. 515–520, 10 2009.

[15] S. Bölükbaşi, B. Tufan, T. Batar, and A. Altun, "The Influence of Raw Material Composition on the Quality of Sinter," Tech. Rep. 4, 2013.

[16] a. CaAl, "Investigation into how the magnesia, silica, and alumina contents magnesio-ferrite (Mg,Fe) 3 O 4 , silicoferrite of calcium and alumina (SFCA), with stoichiometries M 14 + 6n O 20 + 8n and M 25 O 36 , where n=0," tech. rep.

[17] W. Yang, S. Choi, E. S. Choi, D. W. Ri, and S. Kim, "Combustion characteristics in an iron ore sintering bed-evaluation of fuel substitution," *Combustion and Flame*, vol. 145, pp. 447–463, 5 2006.

[18] "Steel%27s+contribution+to+a+low+carbon+future,"

[19] G. Jha and S. Soren, "Study on applicability of biomass in iron ore sintering process," 2017.

[20] M. Zandi, M. Martinez-Pacheco, and T. A. Fray, "Biomass for iron ore sintering," *Minerals Engineering*, vol. 23, pp. 1139–1145, 11 2010.

[21] E. Mousa, C. Wang, J. Riesbeck, and M. Larsson, "Biomass applications in iron and steel industry: An overview of challenges and opportunities," 11 2016.

[22] D. W. Ri, B. J. Chung, and E. S. Choi, "Effects of anthracite replacing coke breeze on iron ore sintering," *Revue de Metallurgie. Cahiers D'Informations Techniques*, vol. 105, no. 5, pp. 248–254, 2008.

[23] S. S. Rath, D. S. Rao, S. K. Tripathy, and S. K. Biswal, "Characterization vis-á-vis utilization of blast furnace flue dust in the roast reduction of banded iron ore," *Process Safety and Environmental Protection*, vol. 117, pp. 232–244, 7 2018.

[24] "Transport Research Laboratory Creating the future of transport PUBLISHED PROJECT REPORT PPR647 BOS slag as a surface course aggregate Ten years of skid resistance monitoring A Dunford and P G Roe," tech. rep., 2010.

[25] S. A. Zareei, F. Ameri, N. Bahrami, P. Shoaei, H. R. Moosaei, and N. Salemi, "Performance of sustainable high strength concrete with basic oxygen steel-making (BOS)slag and nano-silica," *Journal of Building Engineering*, vol. 25, 9 2019.

[26] Z. Wang, D. Pinson, S. Chew, B. J. Monaghan, M. I. Pownceby, N. A. Webster, H. Rogers, and G. Zhang, "Effect of Addition of Mill Scale on Sintering of Iron Ores," *Metallurgical and Materials Transactions B: Process Metallurgy and Materials Processing Science*, vol. 47, pp. 2848–2860, 10 2016.

[27] T. K. Sandeep Kumar and S. Harsha Nistala, "Adhering behavior of Raw Material Fines on Granulation during Iron Ore Sintering," tech. rep.

[28] "KumarIronMaking2,"

[29] S. L. Wu, J. Zhu, J. C. Bei, G. L. Zhang, and X. B. Zhai, "Effects of particle characteristics on the granulation ability of iron ores during the sintering process," *International Journal of Minerals, Metallurgy and Materials*, vol. 22, pp. 907–916, 9 2015.

[30] A. A. Boateng, "Basic Description of Rotary Kiln Operation," in *Rotary Kilns*, pp. 13–26, Elsevier, 2016.

[31] M. R. Agrawal, S. Lecturer, M. K. L. Kar, M. S. Pathak, and M. P. Dani, "Importance of optimum moisture in Sinter raw mix to increase the Sinter strength," *International Journal Of Computer Science And Applications*, vol. 2, no. 1.

[32] X. W. Lv, C. G. Bai, C. Q. Zhou, H. Xie, and R. M. Shi, "New method to determine optimum water content for iron ore granulation," *Ironmaking and Steelmaking*, vol. 37, pp. 407–413, 8 2010.

[33] Ram Pravesh Bhagat, *Agglomeration of Iron Ores*. CRC Press, 1st edition ed., 2019.

[34] R. Murao, "Investigation on Reaction Schemes of Iron Ore Sintering Process by High Temperature in-situ X-ray Diffraction and Micro-texture Observation," tech. rep.

[35] Liming LuLiming LuTze Chean OoiTze Chean OoiX. Li, "Sintering emissions and their mitigation technologies," *Iron Ore - Mineralogy, Processing and Environmental Sustainability*, pp. 551–579, 2015.

[36] A. J. Purnell, "Application of the Fuller-Thompson equation in sinter blend design to increase sinter plant productivity," tech. rep., 2017.

[37] Hobart M. King, "Properties, uses and occurence of the most important ore of iron," 2005.

[38] D. Emerson, "Haematite: the Bloodstone," *Preview*, vol. 2017, pp. 43–53, 12 2017.

[39] T. C. Ooi, S. Campbell-Hardwick, D. Zhu, and J. Pan, "Sintering performance of magnetite-hematite-goethite and hematite-goethite iron ore blends and microstructure of products of sintering," *Mineral Processing and Extractive Metallurgy Review*, vol. 35, no. 4, pp. 266–281, 2014.

[40] P. R. Ame, M. Komatina, and H. W. Gudenau, "Association of Metallurgical Engineers Serbia and Montenegro THE STICKING PROBLEM DURING DIRECT REDUCTION OF FINE IRON ORE IN THE FLUIDIZED BED PROBLEM 'STIKINGA' TOKOM REDUKCIJE RUDE GVOŽA, MALIH DIMENZIJA ČESTICA U FLUIDIZOVANOM SLOJU," tech. rep.

[41] Professor Dr.-Ing. Heinrich Wilhelm Gudenau Professor Dr.-Ing. Jue Fang Dipl.-Ing. Takejuki Hirata Dipl.-Ing. Ulf Gebel, "Fluidized bed reduction as the prestep of smelting reduction," *Steel research international*, vol. 60, no. 3-4, pp. 138–144, 1989.

[42] . Y. G. . S. S. . N. S. Shinji YOSHIMURA, 1) Keiko KUROSAWA, , and Kunihiko NAKASHIMA3), "Penetration Behavior of Calcium Ferrite Melts into Hematite Substrate," *ISIJ International,*, vol. 49, no. 5, pp. 687–692, 2009.

[43] X. M. Mao, Z. X. You, Y. B. Zhang, Z. Y. Fan, G. H. Li, and T. Jiang, "Calcium ferrite formation characteristic during iron ore sintering with different oxygen atmospheres," *Journal of Central South University*, vol. 21, no. 8, pp. 3043–3048, 2014.

[44] T. Takayama and R. Murao, "Quantitative Analysis of Mineral Phases in Sinter Ore by XRD-Rietveld Method," tech. rep.

[45] N. A. Webster, M. I. Pownceby, I. C. Madsen, and J. A. Kimpton, "Silico-ferrite of calcium and aluminum (SFCA) iron ore sinter bonding phases: New insights into their formation during heating and cooling," *Metallurgical and Materials Transactions B: Process Metallurgy and Materials Processing Science*, vol. 43, pp. 1344–1357, 12 2012.

[46] J. C. W.G. Mumme and R. Gable, "Neues Jahrb. Miner," vol. 173, pp. 93–117, 1998.

[47] N. A. Webster, M. I. Pownceby, I. C. Madsen, A. J. Studer, J. R. Manuel, and J. A. Kimpton, "Fundamentals of Silico-Ferrite of Calcium and Aluminum (SFCA) and

SFCA-I Iron Ore Sinter Bonding Phase Formation: Effects of CaO:SiO2 Ratio," *Metallurgical and Materials Transactions B: Process Metallurgy and Materials Processing Science*, vol. 45, no. 6, pp. 2097–2105, 2014.

[48] J. Mochón, A. Cores, Ruiz-Bustinza, L. F. Verdeja, J. I. Robla, and F. Garcia-Carcedo, "sinterización de minerales de hierro parte 2. índices de calidad y productividad," *DYNA (Colombia)*, vol. 81, no. 183, pp. 168–177, 2014.

[49] G. J. Bristow, N. J. and A. G. Waters, "Influence of structural changes on the reducibility of iron ores," *Iron Steelmaker*, vol. 18, pp. 61–79, 1991.

[50] N. V. Scarlett, M. I. Pownceby, I. C. Madsen, and A. N. Christensen, "Reaction sequences in the formation of silico-ferrites of calcium and aluminum in iron ore sinter," *Metallurgical and Materials Transactions B: Process Metallurgy and Materials Processing Science*, vol. 35, no. 5, pp. 929–936, 2004.

[51] C. S. B. Nandy, B. and D. Ghosh, "Assessment of blast furnace behavior through softening-melting test," *Ironmaking and Steelmaking*, vol. 33, pp. 111–119, 2006.

[52] R. R. V. A. S. Kumar, C. U. and A. K. Das, "Quality of sínter in the light of blast furnace performance."," *Tata search*, pp. 20–25, 1995.

[53] T. Umadevi, P. Karthik, P. C. Mahapatra, M. Prabhu, and M. Ranjan, "Optimisation of FeO in iron ore sinter at JSW Steel Limited," *Ironmaking and Steelmaking*, vol. 39, pp. 180–189, 4 2012.

[54] M. K. Kalenga and A. M. Garbers-Craig, "Investigation into how the magnesia, silica, and alumina contents of iron ore sinter influence its mineralogy and properties," *The Journal of the Southern African Institute of Mining and Metallurgy*, vol. 110, pp. 447–455, 2010.

[55] H. Zhou, Z. Liu, M. Cheng, R. Liu, and K. Cen, "Effect of flame-front speed on the pisolite-ore sintering process," *Applied Thermal Engineering*, vol. 75, pp. 307–314, 1 2015.

[56] H. Li, D. J. Zhou BlueScope Steel Limited David Pinson, P. Zulli, and L. Lu, "Sintering of Iron Ores in a Millipot in Comparison with Tablet Testing and Sintering of Iron Ores in a Millipot in Comparison with Tablet Testing and Industrial Process Industrial Process Recommended Citation Recommended Citation," tech. rep.

[57] P. A. Markwordt, "A Study of Emission during Iron Ore Sintering," tech. rep., 2013.

[58] H. Zhao, W. Zhong, G. Zhou, Y. Shao, T. Wang, F. Liu, and B. S. Jin, "Experimental research on utilization of steel rolling sludge in sintering process," *International Journal of Chemical Reactor Engineering*, vol. 11, 6 2013.

[59] R. Fisher, D. R. Anderson, D. T. Wilson, E. Aries, D. Hemfrey, and T. A. T. Fray, "EFFECT OF CHLORIDE ON THE FORMATION OF PCDD/Fs AND WHO-12 PCBs IN IRON ORE SINTERING," tech. rep., 2004.

[60] D. Shindu and T. Oikawa, "4. Energy Dispersive X-ray Spectroscopy," tech. rep., 2002.

[61] T. K. Sandeep Kumar and S. Harsha Nistala, "Adhering behavior of Raw Material Fines on Granulation during Iron Ore Sintering," tech. rep.

[62] M. Zhou, Z. Yu, P. Wang, H. Xie, Y. Wen, and J. Li, "Thermodynamic analysis of iron ore sintering process based on biomass carbon," *Energies*, vol. 13, 11 2020.

[63] D. C. Goldring, "Iron ore categorisation for the iron and steel industry," *Transactions of the Institution of Mining and Metallurgy, Section B: Applied Earth Science*, vol. 112, pp. 5–17, 4 2003.

[64] V. Smil, "Modern Ironmaking and Steelmaking," in *Still the Iron Age*, pp. 87–114, Elsevier, 2016.

[65] B. Anameric and S. K. Kawatra, "Properties and features of direct reduced iron," *Mineral Processing and Extractive Metallurgy Review*, vol. 28, pp. 59–116, 1 2007.

[66] L.D Michaud, "Beneficiation-iron-ore," 4 2016.

[67] Z. Cheng, J. Yang, L. Zhou, Y. Liu, Z. Guo, and Q. Wang, "Experimental study of commercial charcoal as alternative fuel for coke breeze in iron ore sintering process," *Energy Conversion and Management*, vol. 125, pp. 254–263, 10 2016.

[68] E. Donskoi, A. Poliakov, and J. R. Manuel, "Automated optical image analysis of natural and sintered iron ore," in *Iron Ore: Mineralogy, Processing and Environmental Sustainability*, pp. 102–159, Elsevier Inc., 8 2015.

[69] T. Battle, U. Srivastava, J. Kopfle, R. Hunter, and J. McClelland, "The Direct Reduction of Iron," in *Treatise on Process Metallurgy*, vol. 3, pp. 89–176, Elsevier Ltd., 2014.

[70] V. Roshan, K. Kumar, R. Kumar, and G. V. Nageswara Rao, "Preparation of Iron Ore Micro-pellets and Their Effect on Sinter Bed Permeability," *Transactions of the Indian Institute of Metals*, vol. 71, pp. 2157–2164, 9 2018.

[71] J. Pal, S. Ghorai, P. Venkatesh, M. C. Goswami, D. Bandyopadhyay, and S. Ghosh, "Development of fluxed micropellets for sintering utilising iron oxide waste fines," *Ironmaking and Steelmaking*, vol. 40, pp. 498–504, 10 2013.

[72] D. Fernández-González, J. Piñuela-Noval, and L. F. Verdeja, "Iron Ore Agglomeration Technologies," in *Iron Ores and Iron Oxide Materials*, InTech, 7 2018.

[73] H. R. Kokal and M. G. Ranade, "METALLURGICAL USES FLUXES FOR METALLURGY," tech. rep.

[74] T. Umadevi, R. Sah, and P. C. Mahapatra, "Influence of sinter basicity (CaO/SiO2) on low and high alumina iron ore sinter quality," *Transactions of the Institutions of Mining and Metallurgy, Section C: Mineral Processing and Extractive Metallurgy*, vol. 123, no. 2, pp. 75–85, 2014.

Appendices

.1 Safe operating procedure

Appendix A

Safe Operating Procedure for Sinter Pot

4. Safety Equipment

PPE Requirements:	Safety Glasses Fire Proof Gloves Proban Workwear
Photo(Optional):	Dust mask Chrome leather gloves

ALL YOUR PPE MUST FIT and YOU MUST ENSURE THAT IT IS MAINTAINED CORRECTLY
DO NOT WEAR DAMAGED PPE

Additional Safety Equipment: Personal gas monitor

5. Tools to Complete the Task

Tools and equipment:

Scope

The sinter pot is a laboratory scaled sintering furnace. It can produce iron ore sinter in 7kg batches.

This pot mimics the process conditions of the sinter plant at a laboratory scale in order to investigate and optimize the process.

Principle

The furnace is filled with iron ores, coke breeze and limestone. The top is ignited via burner head and air is then drawn through from the bottom of the furnace, drawing the flame front downwards. This allows combustion to occur throughout the mixture, finishing the agglomeration process.

Warnings and Precautions

Safety precautions are taken in line with the risk assessment above.
Handling samples, Full PPE is to be worn as stated above in the risk assessment.
PPE to be worn at all times, also a 4 in 1 gas monitor to be placed in the laboratory and switched on during all testing. Manual handling procedures are to be followed at all times.
Operation of equipment – only trained and competent employees are to use this equipment. Extreme care should be taken when undergoing analysis due to the hazards outlined in the risk assessment above.
Extraction system to be used during testing process.

For use of the cement mixer please ensure the following precautions are taken:

Constrain loose clothing and long hair.
Keep hands/fingers away from rotating drum and drive system.
Avoid creating dust when loading drum
Do NOT place shovel in drum when rotating.
Do NOT leave the machine running unattended.
Ensure lid is fastened to cement mixer to avoid dust spilling out.
Report all machine faults and hazards.
Make sure all tools and other equipment are removed from the cement mixer prior to turning it on.
Do not overload mixer. An overload could damage the mixer.
Do not move the cement mixer during operation. The mixer could tip over or the motor could be damaged.
When transporting the mixer, disconnect the power and make sure the drum is empty of all material/
Ensure lid is secure on cement mixer during use.

Reagents

Compressed air
Natural gas

Apparatus

Galvanised Bucket
Sample trays
3001-320-0600-0008-0047 Pickstone oven.
Riffle box.
Moisture balance
Granulation drum
Sinter pot
Burner head
Gas rig
Type R Thermocouples X 5
Type K Thermocouples X 3
Sieves
Drying oven
Cement Mixer
Scoop
Ceramic sleeves
Weighing Balance

Preparation of Test Sample
If a previously mixed blend is provided from the sinter plant ensure mechanical noise is minimised to avoid compaction. Please not where the sample has been taken from. If prior to granulation drum, trimmings are to be added. If the sample has been provided from roll feeder it can be charged directly into the pot. If the sample has not been provided by the sinter plant, the operator will need to use the blend model spreadsheet to develop a new blend.

Drying and storage of sample material.

Ensure care is taken when handling hot trays, Chrome leather gloves are to be worn when handling hot trays. Ensure care is taken when sizing samples due to vibration

All samples are collected and dried for at least 24 hours at 105˚C.

1) Fill galvanised buckets or sample trays with individual iron ores

2) Using the pickstone oven located in the samplers building, place the buckets/trays in the oven and leave for a minimal of 24 hours.
3) Retrieve the samples after 24 hours wearing chrome leather heat protective gloves and long sleeves as bucket/trays will be hot.

Screening

1) Iron ores <5 mm to be screened out using round 5 mm sieves. Screen out process can be done manually or by using the vibrating sieve plate.
2) Coke breeze <3 mm to be screened out using round 3 mm sieves. Screen out process can be done manually or by using the vibrating sieve plate.
3) Flux <3 mm to be screened out using round 3 mm sieves. Screen out process can be done manually or by using the vibrating sieve plate.

Operating the vibrating sieve plate

1) Pour full contents of dried sample into sieve stack.
2) Turn on sieve shaker and allow to shake for 4 minutes.
3) Switch off sieve shaker and allow to settle.
4) Pour contents of the <5mm (or <3 mm if screening fuel or flux) sieve in designated sample bins and discard >5mm (or 3mm if screening fuel or flux)

Fig 1 – sample storage bins

Preparing blend.

Using the blend model spreadsheet provided, the user can construct a blend with predicted chemistry. Please ensure to use dry, screened material.

1) Once correct weights are obtained, proceed to stored samples in storage facility and collect individual constituents i.e. iron ore, flux, fuel
2) Using the weight balance, weigh out the correct amounts stated in the blend model spreadsheet and place into a bucket.
3) Once all material has been weighed out into signle bucket, content of bucket can be poured into cement mixer.
4) Ensure cement mixer is fastened at 30 degrees.
5) Ensure lid is fastened to cement mixer.
6) Turn the green switch on and allow the cement mixer to rotate for 2 minutes to obtain dry homogenous mixture.
7) Turn the red switch to stop.
8) Unclamp the lid and slide the mixed blend into a bucket ready for granulation.

Moisture test

The sample can now be brought back into the sinterpot lab. A moisture test is carried out using the moisture balance.

1) Turn on moisture control balance via plug socket
2) Wait approximately 30 seconds and open the lid.
3) Ensure the correct metallic dish provided is clean and in the correct position.
4) Close the lid of the moisture control balance and wait until the mass can be seen on the digital screen.
5) Re-open the lid, place 20g of sample in the metallic dish when prompted on the digital screen.
6) Close the lid (reading will start to be taken, do not open the lid when in operation) The device will sound once complete. Take 3 readings for accuracy.

Fig 2 – Moisture balance

Granulation

Prepare water spray can before starting the granulation drum. Providing the blend is dry - 1.1 litres of water is placed in the spray can to achieve a 5-6.5% moisture reading in the blend.

1) Fill pressurized spray can with 1.1litre of water.
2) Pressurize the spray can with 100 pumps
3) When using the spray can, an automatic switch on the nozzle can be used.

Fig 3 – spray can

The granulation drum must be clean and free of debris before using. Remove any debris from the drum and surrounding surfaces to ensure a smooth rotation.

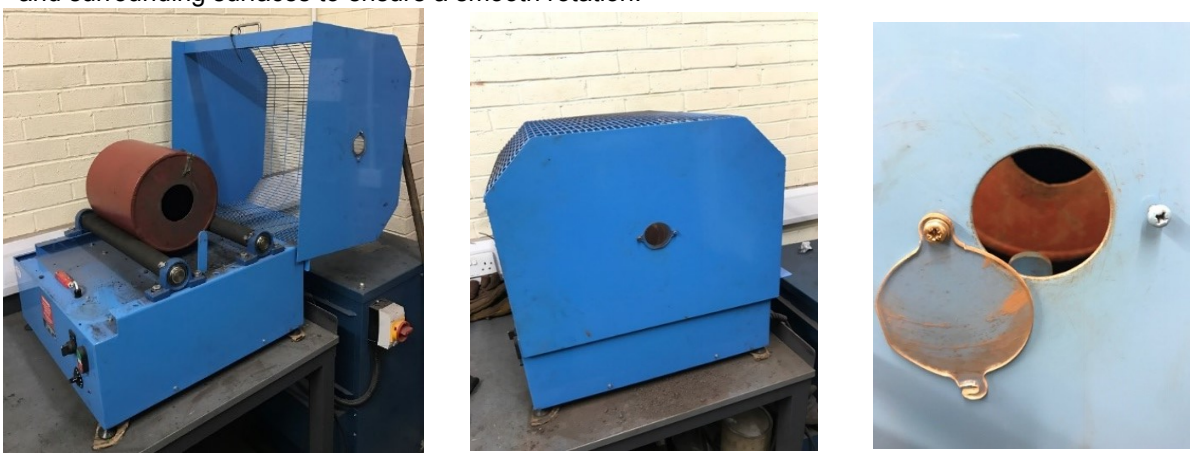

Fig 4 – granulation drum

1) Open cage and pour contents of bucket into granulation drum. Tilt granulation drum for ease.
2) Ensure lid is fastened to granulation drum.
3) Pull down the safety cage and ensure it is magnetically interlocked, set the granulation speed to 0.
4) Turn on the granulation drum by pressing the green button then turn the dial from off to on.
5) Once the drum starts to rotate, the nozzle of the spray can be carefully placed into the hole in the cage and into the drum.
6) Spray all the water into the rotating granulation drum with a back and forth motion to ensure the water is evenly spread across the blend. (this process takes approximately 4 minutes).
7) Once all the water is deposited in the granulation drum, leave the drum rotate for a further 5 minutes.
8) Stop the granulation drum after the 5 minutes by pressing the red stop button and turning the dial from on to off.

Once granulation has completed, the blend can be split into 2 8kg samples using the riffle box. 7kg is used to fill up the reaction vessel and 1 kg is left for further analysis. Ensure the riffle box is free of debris as well as the trays are aligned underneath. Ensure the trays are properly aligned.

1) Safely remove the granulation drum and empty the contents into the clean, closed riffle box. – be cautious that the granulation drum can be heavy.
2) Spread the blend evenly across the riffle box. – ensure even split minimising mechanical noise i.e. not to disrupt particle size or packing.
3) Pull the leaver on the side and allow the mixture to fall evenly into the underneath trays. Each tray is enough for 1 furnace run + 1kg for analysis.

Fig 5 – Riffle box

Computer Set Up

1) Turn the computer system on by switch. (sinter pot control interface should be displayed)
2) Ensure there is a USB drive in the port when switching on the computer as it will not be recognised after this point and computer system will have to be restarted if USB is needed.
3) Open desktop shortcut ‘Sinter Pot’.
4) Input ‘sample name’ and ‘sample ID’ (‘time start’ and ‘time end’ will input automatically when test starts and ends)

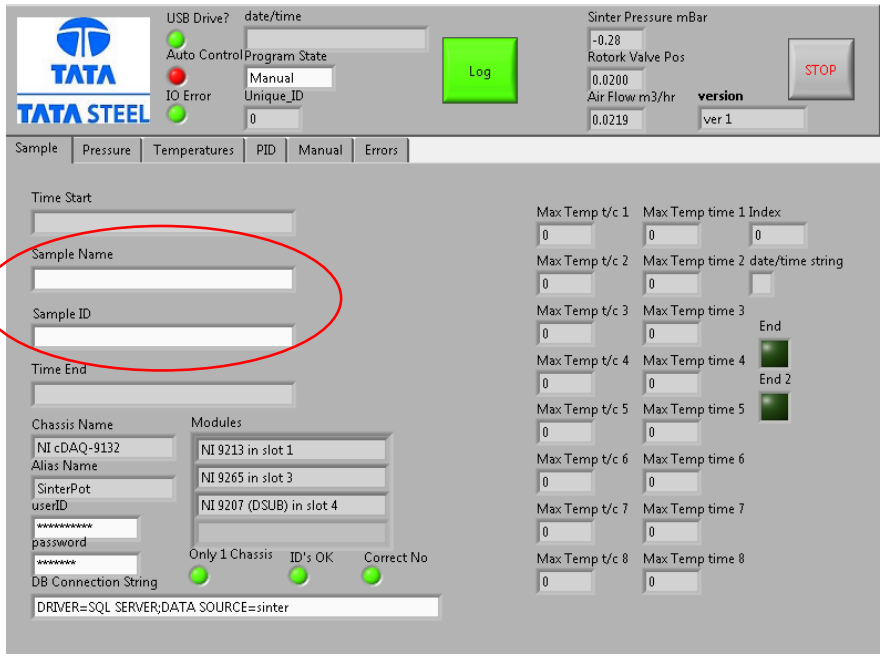

Fig 6 – computer program set up

Analysis Procedure

Once the 16kg blend mixture is split equally in the riffle box the sinter pot is ready to be charged.

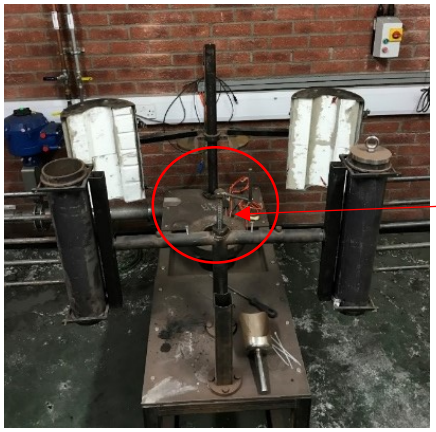

Fig 7 – sinter pots and leaver circled

1) Using the leaver in the middle of the two sinter pots, rotate in a clockwise movement to higher the sinter pots to enable the operator to rotate the desired sinter potl 180˚ over the wheel barrow in a vertical position.
2) Using a metal rod, carefully push into each thermocouple entrance to ensure there are no blockages.
3) Ensure metal mesh is placed at bottom of sinter pot, held up by bolts.
4) A layer of 400g of hearth layer at a size portion of 10-15mm is evenly spread across the bottom, on top of the metal mesh. (this prevents the blend binding to the mesh)
5) Scoop by scoop place the 7kg blend into the sinter pot ensuring each scoop is rotated in a different position to prevent preferential packing. (To prevent big particles falling to one side – which can cause channelling). Fill to the top of the furnace and level off with a ruler to ensure a flat surface minimising packing.

6) Rotate the reaction vessel 180˚still at a vertical position very carefully not to hit the vessel when positioning back in place. (Be aware of trapping points at the bottom of the vessel when positioning).
7) Extreme care should be taken when lowering the reaction furnace into place by turning the middle leaver in a clockwise position.
8) Ensure mechanical noise is kept to a minimum when positioning sinter pot with blend inside.

Fig 8 – charging the sinter pot

Cold Permeability Test

1) On the computer system open 'PID' tab. Set a set point depending on parameters. Usually set at 100mbar.
2) Carefully fasten flow meter over the top of the reaction vessel and lower using top leaver turn

Top Leaver to use when moving between flow meter head and burner head.

clockwise. (be aware of trapping point between flow meter head and reaction vessel when positioning the flow meter into place)

3) Plug all the steel thermocouple tubes with rubber seals.
4) Set the computer system to manual and press the 'log' button. (light will turn from green to red when logging data)
5) Ensure yellow dial is turned on
6) A red line and white line will appear on screen, when the lines meet, the extraction can then be turned on by pressing the green 'on' extraction button.

Pressure drop parameters set at

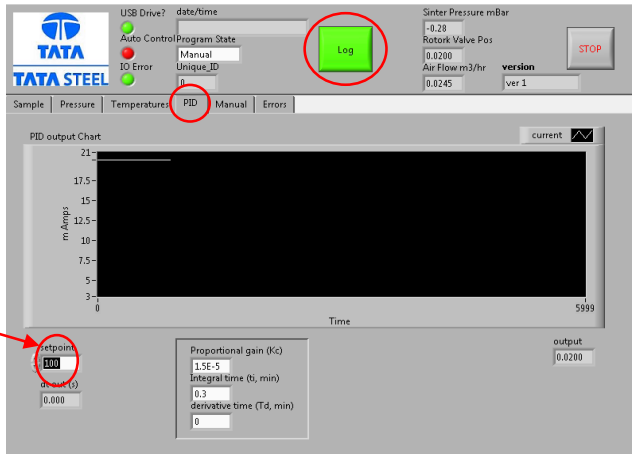

Fig 9 – Flow meter with leaver circled Extraction 'on' and 'off' and control panel for pressure drop

7) Allow the cold permeability test to run for 5 minutes before stopping the recording by repressing the 'log' button and press stop.
8) Close the page down and set up new logging data ready for sintering.

Note: The white line on the screen indicates the pressure drop. The red line indicates the flow rate. The cold permeability test gives the operator an indication of how permeability the blend is.

Sintering Process

1) Unfasten the flow meter head by rotating the top leaver anticlockwise. Rotate the dial to set the burner head in position. (use extreme care not to hit the furnace and disturb the mixture. Be aware of trapping point when positioning burner head). Lower the burner head into position carefully, the ignition pipe should be resting on the edge. (1inch above the sinter pot).
2) Unplug rubber seals and poke a measured hole using metal rod into the steel tube and into the bed for thermocouple to sit into.
3) Plug thermocouples with ceramic sleeves
4) Insert thermocouple (with ceramic sleeve) into steel tubes and into blend ensuring the thermocouples should be at the same depth into the blend.
5) If not all thermocouples are in use be sure to plug the steel thermocouple entrances with rubber corks.

Ceramic sleeves

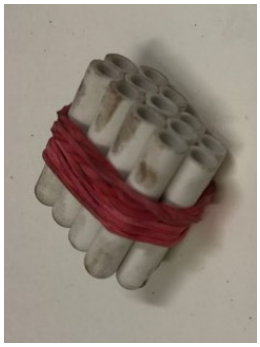

Fig 11 – ceramic sleeves

Thermocouples

Fig 12 – thermocouples in position

6) Ensure the burner head is fastened into place. (1 inch above the sinter pot).

The sinter pot is not set up ready to ignite.

7) Start recording data by switching to automatic control, then click the green log button (will turn red when recording).

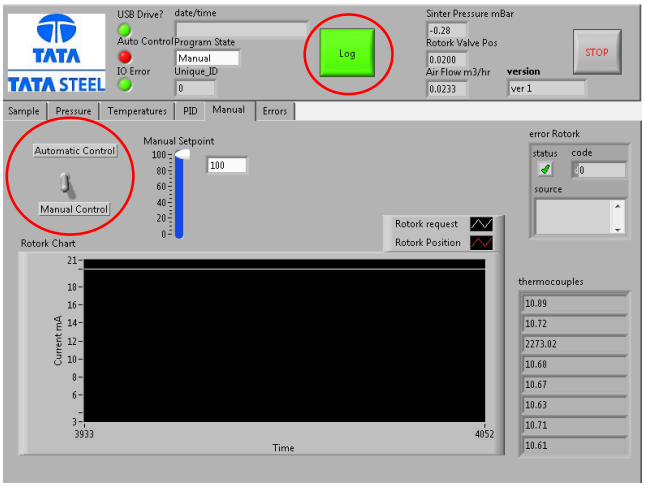

Fig 13 – computer program set up

8) Once recording turn the extraction fan on immediately by turning yellow dial to ‘on’ position and pressing the green button.
9) Wait for pressure to get to 99/100mbar before igniting the burner head.

10) Ensure all gas valves and air supply valves are open apart from the final valves. Once pressure drop reaches 99/100mbar, the final gas and air valves can be opened and the red button pressed to start the ignition process.
11) After 1 minute of ignition, immediately close the gas and air supply valves to turn off ignition.
12) Unfasten the burner head using the top leaver and turning it anticlockwise. **Extreme care should be taken and heat resistant gloves must be worn.**
13) Fasten the flow meter back on.
14) Allow sintering process to complete. (~30minutes)
15) Stop test when all 7 thermocouples read <100˚C. This can be seen in the Temperature tab as well as manual tab.
16) Stop test by switching back to 'manual control', press the red 'logging' button to stop recording (will turn green) and then press 'stop', all on the computer program. The red bottom to stop extraction fan can then be pressed immediately after data has stopped recording.
17) Raw data recorded to memory stick and can be exported to sinter pot test spreadsheet.

After each test the program must be shut down and re-opened to run a new test.

Discharging of Sinter pot

PPE to be worn throughout. I.e. glasses, overalls and heat resistant gloves.

1) Once all thermocouples read <100˚C they are safe to be removed. Remove all thermocouples and place in designated area. (if stuck tip the pot horizontally and knock slightly to release the thermocouples. Note: may need assistance if thermocouples are stuck, beware of hot sinter/sinter pot)
2) Unfasten the flow meter by rotating the top leaver anticlockwise.
3) Unclamp the ceramic insulation.
4) Using the leaver positioned in the middle, turn anticlockwise enabling the operator to move the reaction vessel 180˚. Rotate the reaction vessel 180˚ and securely position over the provided wheelbarrow.
5) Tilt the reaction vessel 180˚ vertically so that it is upside down.
6) Using a metal rod gently push out the sinter into wheel barrow. Please ensure PPE is worn.
7) Place content of wheelbarrow into bucket ready for post analysis.

Post Sinter Prep

Sieves to be used +40mm/+25mm/+16mm/+10mm/+5mm/-5mm.

Fig 14 – mechanical sieve

Sinter should be allowed to cool to room temperature (hour) before sizing analysis takes place. The large sieve shaker shall be used for the size analysis. The various screen sizes shall be set in descending order largest screen at top +40mm down to smallest screen at bottom -5mm.

1) Tip contents of 1 pot test worth into top sieve
2) The large top lid is placed onto the screens and secured in placed using threaded bolts, which locks onto the top plate, ensure the bolts are tight.
3) The mechanical sieve is turned on via green button and allowed to break the sinter apart for 2 minutes.
4) The mechanical sieve must not be touched when it is in use, after time has elapsed, the machine must be stopped by depressing the emergency stop button.
5) Once the mechanical sieve has completed, the top plate is removed.
6) Sieve by sieve, the content in each size fraction can be weighed out and noted.
7) 300/500g of the 16-25mm sample is kept for RDI test. Can be submitted via single source.
8) 50g of sinter between 16-25mm kept for chemical analysis. Can be submitted via single source.

Please refer back to the 'manual' provided for further information regarding equipment described in this safe operating procedure.

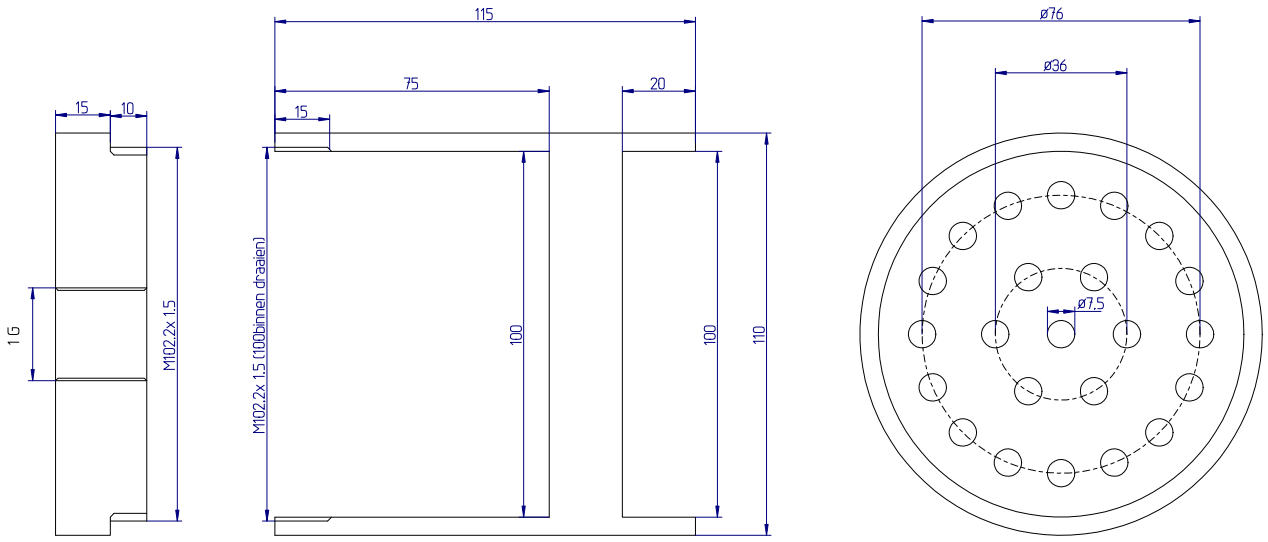

MATERIAAL	SCHAAL : 1:1	GETEKEND : D. Prins	OPMERKINGEN:
RVS 310	MAATEENHEID : MM	ONTWERP : CRDT PRC MIE PRO	
PROJECTIE	RUWHEID : 0,8	DATUM : 25-04-14	
	TOLERANTIE : 0,1	VERSIE : 1.0	
	TENZIJ ANDERS AANGEGEVEN	VERSIE DATUM : 25-04-14	
TATA STEEL	BENAMING: [redacted]		NUMMER: 462

.2 Alternative Si trim investigation

Introduction

Iron ore materials with a high content in silica are an important constituent in iron making and sintering as they are used as a flux, promoting the chemical reactions taking place. It was decided that an alternative material, high in silica would be trialled in order to act as an additional Si trim. The trim was relevant to Tatasteel in Port Talbot and sourced in house by a third party. The sinter pot was deployed to investigate if the alternative Si trim would have any process issues and to investigate the sintered product when being used in a blend. In order to test the new alternative Si trim, it was added to a blend and process parameters compared against a conventional base blend.

Experimental procedure

In total, 2 blends were made up and 4 sinter pot tests conducted. A sample of the alternative Si trim was subjected to a sizing analysis and chemical analysis via x-ray fluorescence and data was used accordingly to incorporate create a new blend. For full experimental procedure, formula sheet and post analysis procedure please see chapter 3 section 3.7. Blends contained the following:

Table 38: Blend composition

Material	Blend A	Blend B	Units
Sinter feed C	3.321	3.257	Kg
Sinter feed E	2.307	2.262	kg
DRI	1.303	1.278	Kg
Sinter feed S	2.595	2.545	Kg
Sinter feed G	1.153	1.131	Kg
SiO_2 Fines	0.000	0.084	Kg
Sinter Fines	2.382	2.355	Kg
Dunnite	0.172	0.170	Kg
Limestone	1.601	1.792	Kg
Magstone	0.503	0.471	Kg
Coke Breeze	0.662	0.654	Kg

Please note: Sinter pot tests were conducted at 5% fuel

A) **First Experiment:**

x2 pot test with base blend A at 100mbar

B) **Second Experiment:**

x2 pot test with blend B incorporating small amounts of Si trim at 100mbar

Results

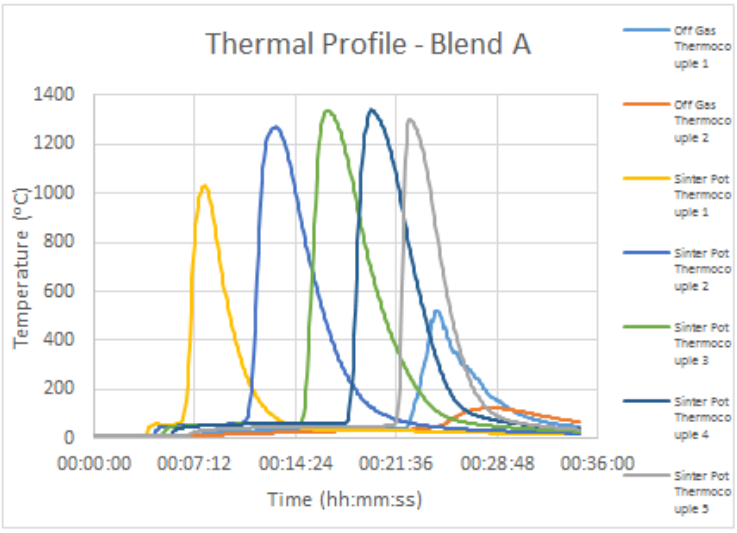

Figure 141: Thermal profile for blend A alternative Si study

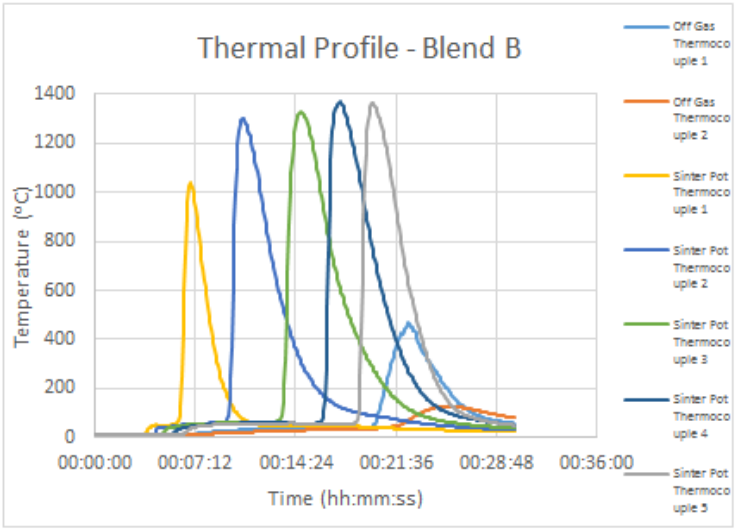

Figure 142: Thermal profile for blend B alternative Si study

Discussion and Conclusion

When analysing the thermal profiles in figure 152-153 the following can be determined. Each of the thermocouple traces start to rise and peak sequentially one after another, and decreases in a uniform manner. the off-gas thermocouple also start to rise after all embedded thermocouples. this indicates that a uniform and stable process was evident with uniform and steady flame front propagation down the sinter pot. It is worth noting here that the first thermocouple does not reach as high of temperatures as previous sinter pot experiments. This was due to it being decided to run the discussed sinter pot tests in this experiment at 5% fuel rate. This was done to try and replicate plant conditions. The only thing to note from visual inspection of the thermal profiles was that blend A exhibited a wider trace than blend B. Perhaps indicating an increased sintering time than that of blend B.This is then backed up when looking at the recorded parameters in table 44. It can be seen that sintering time was decreased when using Blend B. This could be from the nature of the particle size of the alternative Si trim, however, only small amounts was added. More so, this could be due to the slight decrease in finer ores when replacing with the alternative Si trim. It must be noted here that all other recorded parameters exhibited very minimal variation, this being the first indication that the alternative Si trim could be a suitable material for iron ore sintering. The wider trace and increased sintering time can be backed up when looking at calculated flame front characteristics in table consisting of recorded process parameters (appendices) as well as the graphs in figure 154 below. It can be seen that flame front speed is generally higher per thermocouple for blend B, which correlates with the decrease in sintering time. It can also be seen that flame front thickness is generally higher per thermocouple point which correlates to the wider profile.

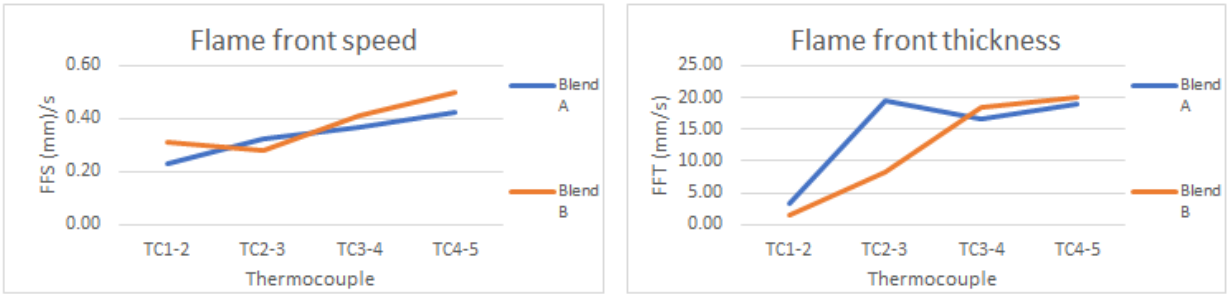

(a) Flame front speed

(b) Flame front thickness

Figure 143: Flame front characteristics from alternative Si trim study

As per normal operations, the sinter cake was subjected to 1 minute of mechanical vibrations in order to give sinter yield. It is worth noting here this also gives an indication of cold strength but can only be compared to a series of tests within an experiment. This was done due to not being able to use a tumbler as a tumble index experiment requires more sinter than the sinter pot can make, at a specific size fraction. Sinter yield can be seen below in figure 155. It is worth noting here, return fines have increased and size fraction greater than 16mm decreases which could be cause for concern. This could be a result of the increased sintering time but further investigation required to concisely conclude on the matter.

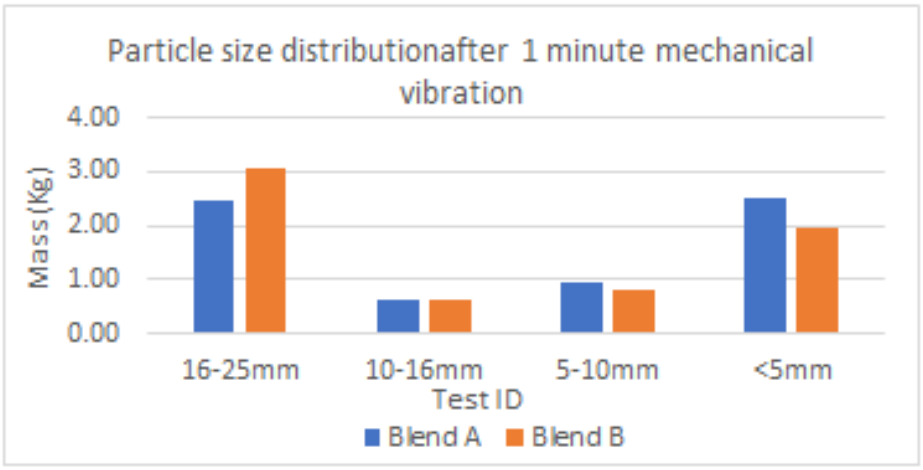

Figure 144: PSD after 1 minute mechanical vibration

The sinter in size fraction between 16-26 was then subjected to reduction degradation testing in order to investigative reducability of produced sinter. A small amount of sinter in this size fraction was also taken for x-ray diffraction testing in order to investigate sinter chemical composition analysis. These can be seen in figure 156 and table 32 below. On analysing the figure 156, it was evident that the sinter produced with both blends A and B had good RDI which comply with normal sinter plant operations ready for the blast furnace. Chemical composition can be seen in table 47, and it was evident that minimal variation was witnessed between the two sintered products. This is emphasised when looking at figure 156 (b) which looks at basicity, which Si influences and minimal variation was evident.

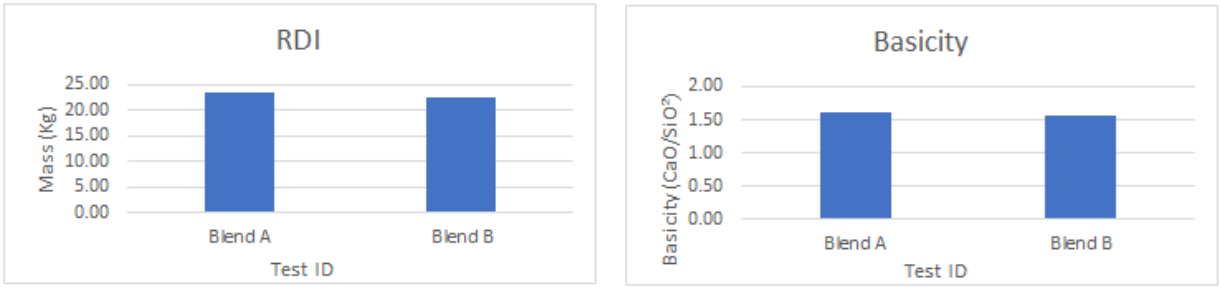

(a) Reduction degradation index

(b) Basicity

Figure 145: RDI and basicity of sintered products from blend A and B

Table 39: Sinter composition

XRF	Blend A	Blend B
SiO_2	5.83	5.89
Al_2O_3	0.83	0.89
TiO_2	0.07	0.08
CaO	9.44	9.22
MgO	1.88	1.67
Fe	57.50	57.34
Fe_2O_3	76.13	75.88
FeO	5.48	5.50
P	0.03	0.03
Mn	0.15	0.15

Conclusion

i) Both blends produced a relatively stable and uniform process evident from the sequential peaks in the thermocouple traces as well as all embedded thermocouples peaking before the off-gas thermocouples. This indicated that flame front travelled in a uniform and stable manner when sintering both base blend and blend B containing the alternative Si trim. No process issues were found.

ii) It must be noted here, when using alternative Si trim, sintering time was decreased.

iii) Significant variation seen in the yield of final sintered products when comparing PSD of sinters produced with Blend a and Blend B. Notable the return fines increased when using blend B could be cause of concern.

iv) Chemical composition of final sintered products did not vary.

v) Reduction degradation index did not vary significantly between final sintered products between tests and both blends produced strong sinter.

vi) This paper can conclude that the alternative Si trim can be used as an alternative Si source in iron ore sintering but further investigations must be performed to understand why returns fines increased. This would be cause for concern when scaling up to industry scale

vii) All post analysis variation is minimal and within acceptable process conditions for normal sinter plant operations.

Appendix B

.3 Recorded process parameters

Chapter 4

Table 40: Process parameters for increasing sinter feed A study

Parameters	0% sinter feed A	8.5% sinter feed A	17% sinter feed A	25.5% sinter feed A
Sintering time	00:24:15	00:23:20	00:20:00	00:20:25
Cold flow rate	8.4	8.5	8.8	8.7
Hot flow rate	5.9	6.2	6.8	5.8
Max sintering temp	1304	1310	1081	1310
Peak temperatures				
Thermocouple 1	1221	987	1062	1240
Thermocouple 2	1112	1228	1020	1245
Thermocouple 3	1244	1259	1058	1310
Thermocouple 4	1304	1310	1081	1284

Table 41: Process parameters for increasing DRI study

Parameters	0% DRI	10% DRI	20% DRI	30% DRI
Avg cold flow rate	8.90	10.30	7.88	8.11
Avg Hot flow rate	6.26	7.00	6.03	6.18
Sintering time	00:20:30	00:18:20	00:19:25	00:19:25
Sintering temperature	1334.06	1394.27	1335.18	1348.59
Peak temperatures				
TC 1	1164.01	1220.12	1107.52	1191.64
TC 2	1249.74	1368.29	1315.31	1348.59
TC 3	1334.06	1394.27	1328.88	1347.82
TC 4	1306.94	1352.59	1335.18	1328.28

Table 42: Process parameters for Sinter feed B investigation

	0%Sinter feed B	5%Sinter feed B	15%Sinter feed B	25%Sinter feed B	35%Sinter feed B	45%Sinter feed B	55%Sinter feed B	
Pressure drop	100	100	100	100	100	100	100	mbar
Ignition time	01:00:00	01:00:00	01:00:00	01:00:00	01:00:00	01:00:00	01:00:00	m s
Cold flow	9.14	10.57	9.87	9.13	9.27	10.48	9.73	m3hr
Hot flow	7.59	7.97	7.31	7.87	7.80	8.55	8.02	m3hr
Sintering time	00:20:35	00:19:25	00:22:00	00:19:10	00:19:50	00:18:05	00:20:05	m s
Sintering temp	1375.66	1345.86	1367.82	1376.97	1341.69	1392.64	1342.66	C
Peak temperatures								
TC1	1279.92	1203.68	1200.42	906.00	1237.67	1310.42	1239.28	C
TC2	1244.87	1261.74	1226.48	1279.23	1151.08	1366.05	1342.66	C
TC3	1005.40	1340.87	1339.87	1251.74	1341.69	1346.23	1309.87	C
TC4	1317.58	1321.14	1367.82	1376.97	1305.42	1324.72	1279.92	C
TC5	1375.66	1345.86	1243.93	1228.77	1294.56	1392.64	1334.60	C
Off-gas temp 1	415.62	548.50	535.85	386.23	399.50	419.80	389.57	C
Off-gas temp 2	162.64	173.72	174.63	174.87	178.35	174.50	172.80	C
sintered airflow	45.53	55.39	43.25	48.52	58.03	62.21	44.38	m3hr
Time above 1000C								
TC1	02:30:00	03:40:00	02:35:00	00:00:00	02:55:00	02:15:00	02:05:00	mm:s
TC2	04:10:00	03:35:00	04:25:00	03:25:00	03:40:00	02:55:00	04:05:00	mm:s
TC3	01:20:00	04:50:00	04:20:00	04:55:00	05:10:00	04:00:00	04:25:00	mm:s
TC4	04:15:00	03:25:00	03:55:00	04:05:00	04:20:00	04:00:00	04:05:00	mm:s
TC5	03:05:00	03:40:00	04:05:00	02:30:00	02:30:00	02:35:00	03:30:00	mm:s

Table 43: Blend composition for Sinter feed B investigation

	0%TSMC	5%TSMC	15%TSMC	25%Sinter feed B	35%Sinter feed B	45%Sinter feed B	55%Sinter feed B	
Flamefrontspeed								
TC1-2	0.19	0.26	0.17	0.32	0.26	0.29	0.25	mm/s
TC2-3	0.15	0.32	0.44	0.26	0.61	0.39	0.26	mm/s
TC3-4	-0.36	0.36	0.28	0.52	0.40	0.39	0.70	mm/s
TC4-5	0.29	0.54	1.40	0.54	0.56	0.88	0.54	mm/s
Flamefront width								
TC1-2	5.60	15.56	5.19	N/A	22.04	16.04	7.37	mm
TC2-3	13.08	35.00	61.25	25.09	39.57	23.33	17.17	mm
TC3-4	N/A	52.05	28.00	59.63	22.00	25.28	66.50	mm
TC4-5	4.37	48.46	154.00	64.62	39.20	56.87	18.85	mm
Flamefront Cooling rate								
TC1	7.55	6.35	8.01	DIV/0!	12.75	12.92	10.65	C s
TC2	5.61	9.45	9.64	9.06	8.48	9.58	5.12	C s
TC3	DIV/0!	6.74	6.73	5.67	3.45	5.15	5.07	C s
TC4	3.68	8.48	9.03	8.18	4.86	5.00	5.04	C s
TC5	6.46	9.94	3.48	13.97	8.68	6.89	4.90	C s

Table 44: Process parameters for Sinter feed C concentrates investigation

	0% Sinter feed C (1)	0% Sinter feed C (2)	32% Sinter feed C (1)	32% Sinter feed C (2)	units
Pressure drop	100	100	100	100	mbar
Ignition time	01:00:00	01:00:00	01:00:00	01:00:00	m s
Cold flow rate	8.30	7.30	9.55	9.08	m3hr
Hot flow rate	5.76	5.35	6.48	7.04	m3hr
Sintering time	00:27:20	00:32:05	00:24:25	00:22:10	m s
Max sintering temp	1167.58	1066.40	1281.36	1299.22	C
Peak temperatures					
TC 1	809.67	626.86	1097.04	1215.40	C
TC 2	932.24	443.85	1197.03	1207.10	C
TC 3	697.91	1061.55	1186.21	1217.74	C
TC 4	1167.59	894.37	1130.20	1299.23	C
TC 5	449.86	1066.40	1281.36	1154.06	C
Max off gas temp 1	475.61	443.42	501.32	509.19	cm/s
Max off gas temp 2	132.25	117.64	158.29	179.36	s
Sintered airflow	29.98	20.88	36.04	43.62	m3hr
Time above 1000C					
TC 1	00:00:00	00:00:00	01:45:00	03:15:00	mm:s
TC 2	00:00:00	00:00:00	03:50:00	03:10:00	mm:s
TC 3	00:00:00	02:55:00	05:10:00	04:00:00	mm:s
TC 4	01:50:00	00:00:00	03:35:00	03:50:00	mm:s
TC 5	00:00:00	01:05:00	02:45:00	01:45:00	mm:s

Table 45: Calculated parameters for Sinter feed C investigation

	0% Sinter feed C (1)	0% Sinter feed C (2)	32% Sinter feed C (1)	32% Sinter feed C (2)	units
Flamefront speed					
TC1-2	0.39	0.07	0.28	0.26	mm/s
TC2-3	0.10	-14.00	0.23	0.23	mm/s
TC3-4	-0.82	0.23	0.20	0.27	mm/s
TC4-5	0.16	2.80	0.54	0.56	mm/s
Flamefront width					
TC1-2	N/A	N/A	N/A	16.85	mm
TC2-3	N/A	N/A	9.33	9.03	mm
TC3-4	N/A	N/A	15.22	24.23	mm
TC4-5	4.77	N/A	32.31	72.80	mm
Flamefront Cooling rate					
TC1	DIV/0!	DIV/0!	DIV/0!	7.69	C s
TC2	DIV/0!	DIV/0!	5.69	7.14	C s
TC3	DIV/0!	DIV/0!	4.34	7.27	C s
TC4	14.19	DIV/0!	10.60	9.99	C s
TC5	DIV/0!	DIV/0!	9.73	11.08	C s
Reduction degradation index					
RDI	29.89	30.08	21.11	22.10	

Table 46: Process parameters for fuel particle size

Parameters	0-1 cb	0-1 wa	1-2 cb	1-2 wa	2-3 cb	2-3 wa	3-4 cb	3-4 wa	units
Cold_{flow}									
rate	10.46	10.88	13.09	12.07	13.14	14.05	11.52	15.15	m3/hr
Hot flow									
rate	6.37	6.03	8.32	8.15	8.74	8.66	9.31	8.23	m3/hr
Sintering									
time	00:21:35	00:20:55	00:19:35	00:20:35	00:26:35	00:22:10	N/A	00:19:35	hr:mn:s
Max temp	1286.49	1248.11	1359.33	1369.65	1342.80	1399.67	1183.39	1359.33	
Peak temp									
Tc 1	1286.49	1248.11	1271.39	1293.00	972.56	1152.04	451.08	1271.39	C
Tc 2	1068.05	1219.34	1343.99	1299.39	1032.40	1269.12	1032.79	1343.99	C
Tc 3	973.71	828.44	1359.33	1322.21	1110.32	1376.59	1121.44	1359.33	C
Tc 4	1018.52	1222.92	1339.43	1302.10	1342.80	1386.71	1183.39	1339.43	C
Tc 5	1132.61	840.41	1230.84	1369.65	1328.36	1399.67	379.93	1230.84	C
Off-gas T 1	483.34	493.64	619.46	483.77	346.07	626.41	26.96	619.46	C
Off-gas T 2	147.98	146.36	178.18	191.52	103.60	180.09	25.55	178.18	C
Sintered									
airflow	43.28	45.93	60.70	59.18	22.79	45.54	10.65	60.70	m3/hr
Time above									
1000C									
TC 1	01:30:00	01:50:00	01:20:00	01:30:00	00:00:00	01:25:00	00:00:00	01:20:00	hr:mn:s
TC 2	03:30:00	04:05:00	02:30:00	03:05:00	00:30:00	02:30:00	01:15:00	02:30:00	hr:mn:s
TC 3	00:00:00	00:00:00	03:30:00	03:20:00	01:10:00	04:00:00	01:55:00	03:30:00	hr:mn:s
TC 4	00:40:00	01:50:00	03:00:00	03:50:00	01:50:00	03:45:00	01:05:00	03:00:00	hr:mn:s
TC 5	01:55:00	00:00:00	02:50:00	03:15:00	02:00:00	03:45:00	00:00:00	02:50:00	hr:mn:s

Table 47: Flamefront width

TC	Welsh anthracite	Coke breeze	Units
TC1-2	0.25	0.26	mm/s
TC2-3	0.48	0.22	mm/s
TC3-4	0.35	0.37	mm/s
TC4-5	0.48	0.58	mm/s

Table 48: Flamefront speed

Table 49: Cooling rate

TC	Welsh anthracite	Coke breeze	Units
TC1-2	17.82	18.15	mm
TC2-3	62.76	28.00	mm
TC3-4	47.25	49.74	mm
TC4-5	77.24	93.33	mm

TC	Welsh anthracite	Coke breeze	Units
TC1	5.56	5.88	c/s
TC2	3.57	3.70	c/s
TC3	2.86	3.70	c/s
TC4	3.23	5.26	c/s
TC5	3.33	4.76	c/s

Table 50: Process parameters from experiment 1 for uncontrolled fuel PSD study

	Coke	Anthracite	Units
Cold permeability flow rate	10.46894814	10.02187906	hr3/m
Hot permeability flow rate	7.266651505	6.985231396	hr3/m
Sintering time	00:19:45	00:21:05	hr:m:s
Max Thermocouple temperature	1417.07233	1255.707082	C
Thermocouple 1	1330.222292	1255.707082	C
Thermocouple 2	1248.242943	1194.815584	C
Thermocouple 3	1349.036422	1042.375704	C
Thermocouple 4	1417.07233	1036.907821	C
Thermocouple 5	1390.85380	1 1148.611976	C
Max off gas temperature 1	501.483271	561.720057	C
Max off gas temperature 2	177.06119	177.647238	C
Sintered air flow	56.889681	47.80022	hr3/m

Table 51: Process parameters for from experiment 2 for controlled psd less than 3mm

Process parameters	100b	25a75b	50a50b	75a25b	100a	Units
Thermocouple 1	1277.66	1301.33	1357.13	1388.07	1198.21	C
Thermocouple 2	1300.83	1331.07	1367.43	1204.22	1315.80	C
Thermocouple 3	1336.62	1376.05	1353.38	1354.53	1124.69	C
Thermocouple 4	1285.49	1322.87	1359.45	1350.37	1253.21	C
Thermocouple 5	1360.79	1363.12	1338.48	1330.68	1215.46	C
Max off gas temp 1	552.21	672.79	533.79	587.95	589.56	C
Max off gas temp 2	185.87	180.46	177.58	180.64	172.90	C
Sintered airflow	54.42	57.31	53.89	57.04	47.80	hr3/m

Table 52: Process parameters from experiment 3 controlled psd less than 5mm with breeze and anthracite

Process parameters	100 b	25a75b	50a50b	75a25b	100 a	Units
Cold flow rate:	12.96	10.71269	11.01081	11.41905	12.72013	hr3/m
Hot flow rate:	8.17	7.528012	7.102796	7.314372	6.413532	hr3/m
Sintering time:	00:19:40	00:19:20	00:20:25	00:20:25	00:22:35	hr:m:s
Max sintering temp:	1316.19	1355.301	1303.783	1340.092	1367.091	C
Thermocouple 1	1231.82	1297.537	1124.796	1325.385	1262.941	C
Thermocouple 2	1282.01	1326.674	1008.087	1334.558	1084.446	C
Thermocouple 3	1098.91	1344.562	1213.484	1340.092	1246.009	C
Thermocouple 4	1250.70	1305.927	1303.783	1159.685	1319.425	C
Thermocouple 5	1316.19	1355.301	1300.03	1315.264	1367.091	C
Max off gas temp 1	672.75	597.5247	487.7718	663.7515	580.6323	C
Max off gas temp 2	179.88	180.7126	186.5181	183.0399	179.374	C
Sintered airflow	55.02	61.50766	53.01398	54.63391	56.71937	hr3/m

Table 53: Process parameters for optimum fuel content in pot study

Parameters	Blend A	Blend B	Blend C	Blend D	Units
Pressure drop	100	100	100	100	Mbar
Ignition time	01:00	01:00	01:00	01:00	S
Cold flow rate	10.31	11.06	10.00	12.16	M hr
Hot flow rate	6.77	6.99	7.01	7.72	M hr
Sintering time	00:22:10	00:19:40	00:19:45	00:17:50	hr:mn:s
sintering temp	1276.18	1289.40	1360.84	1398.17	C
Peak temperatures					
Thermocouple 1	1118.43	1258.89	1282.92	1279.68	C
Thermocouple 2	1168.59	1129.46	1314.74	1370.57	C
Thermocouple 3	1184.15	1289.40	1339.10	1368.46	C
Thermocouple 4	1215.28	1238.35	1268.33	1234.37	C
Thermocouple 5	1276.18	1287.46	1360.84	1398.17	C
Max off gas temp 1	490.17	560.83	609.26	621.78	C
Max off gas temp 2	92.84	127.14	150.33	169.68	C
Sintered airflow	32.66	46.69	52.39	53.51	M hr
Time above 1000C					
Thermocouple 1	00:45:00	01:30:00	01:35:00	01:40:00	mn:s
Thermocouple 2	01:15:00	03:30:00	03:10:00	02:30:00	mn:s
Thermocouple 3	01:45:00	04:40:00	03:10:00	03:20:00	mn:s
Thermocouple 4	01:40:00	03:10:00	03:20:00	03:10:00	mn:s
Thermocouple 5	01:30:00	02:05:00	02:50:00	02:10:00	mn:s

Table 54: Process parameters for optimum fuel content

Parameters	Blend A	Blend B	Blend C	Blend D	Units
Flamefrontspeed					
TC1-2	0.25	0.20	0.23	0.33	mm/s
TC2-3	0.22	0.21	0.25	0.25	mm/s
TC3-4	0.28	0.50	0.27	0.31	mm/s
TC4-5	0.38	0.93	1.00	0.48	mm/s
Flamefront width					
TC1-2	1.23	3.94	6.77	5.00	mm
TC2-3	3.33	7.21	15.96	6.36	mm
TC3-4	8.40	72.50	10.77	17.11	mm
TC4-5	13.24	60.67	70.00	31.38	mm
Cooling rate max - 600					
TC1	6.10	4.25	4.71	4.00	C/S
TC2	4.37	1.65	3.04	3.28	C/S
TC3	3.54	3.06	3.08	2.90	C/S
TC4	4.56	2.84	3.71	3.09	C/S
TC5	6.44	3.72	3.90	5.91	C/S
Cooling rate max - 1100C					
TC1	34.56	13.18	15.18	11.33	C s
TC2	18.95	6.23	7.94	7.71	C s
TC3	14.60	6.89	7.39	6.15	C s
TC4	15.38	6.38	8.91	6.34	C s
TC5	16.90	10.58	8.01	13.30	C s

Table 55: Process parameters for micropellet study

Parameters	Blend A	Blend A (r)	Blend B	Blend B (r)	Units
Pressure drop	100	100	100	100	mbar
Ignition time	01:00:00	01:00:00	01:00:00	01:00:00	m s
Cold flow rate	11.23	9.97	14.32	12.62	m3hr
Hot flow rate	6.34	6.37	7.53	7.51	m3hr
Sintering time	00:21:45	00:22:00	00:20:00	00:19:35	m s
Max sintering temp	1288.38	1338.38	1267.20	1299.59	C
Peak temperatures					
Thermocouple 1	1148.76	1135.96	1065.42	1194.18	C
Thermocouple 2	1205.32	1228.97	1059.11	1204.80	C
Thermocouple 3	1265.57	1266.29	1120.97	1239.78	C
Thermocouple 4	1288.24	1210.83	1267.20	1266.45	C
Thermocouple 5	1288.38	1338.38	1212.46	1299.59	C
Max off gas temp 1	564.51	441.47	435.58	544.09	C
Max off gas temp 2	106.25	106.62	99.90	106.31	C
Sintered airflow	35.31	33.03	32.66	34.55	m3hr
Time above 1000C					
Thermocouple 1	01:05:00	01:15:00	00:30:00	00:50:00	mm:s
Thermocouple 2	01:55:00	02:00:00	00:45:00	01:10:00	mm:s
Thermocouple 3	01:50:00	02:25:00	01:40:00	01:30:00	mm:s
Thermocouple 4	02:05:00	02:50:00	01:50:00	01:50:00	mm:s
Thermocouple 5	01:40:00	01:45:00	01:30:00	01:35:00	mm:s

Table 56: Process parameters for micropellet study

Parameters	Blend A	Blend A (r)	Blend B	Blend B (r)	Units
Flamefrontspeed					
TC1-2	0.26	0.21	0.29	0.28	mm/s
TC2-3	0.23	0.25	0.20	0.27	mm/s
TC3-4	0.29	0.23	0.45	0.35	mm/s
TC4-5	0.50	0.78	0.41	0.42	mm/s
Flamefront width					
TC1-2	2.64	3.18	N/A	2.80	mm
TC2-3	6.89	11.25	N/A	5.38	mm
TC3-4	8.57	7.90	13.55	7.00	mm
TC4-5	22.50	46.67	10.29	12.73	mm
Cooling rate max - 600					
TC1	4.57	3.35	6.65	6.25	c/s
TC2	3.27	3.81	4.83	4.84	c/s
TC3	4.03	3.17	4.34	4.00	c/s
TC4	4.44	3.82	4.30	4.04	c/s
TC5	5.51	5.27	5.33	5.38	c/s
Cooling rate max - 1100					
TC1	27.44	26.80	DIV/0!	23.77	c/s
TC2	12.11	13.98	DIV/0!	17.28	c/s
TC3	13.31	7.84	34.73	14.22	c/s
TC4	13.76	10.18	11.12	12.12	c/s
TC5	12.52	10.55	15.31	12.72	c/s

Table 57: Process parameters for Alternative MgO source study

Parameters	Blend A	Blend A (r)	Blend B	Blend B (r)	Units
Pressure drop	100	100	100	100	mbar
Ignition time	01:00:00	01:00:00	01:00:00	01:00:00	m s
Cold permeability flow rate	10.62	11.10	11.90	10.64	M3 hr
Hot Permeability flow rate	6.97	6.82	7.72	7.48	M3 hr
Sintering time	00:19:45	00:19:15	00:17:15	00:17:35	hr:mn:s
Max sintering temp	1421.40	1348.36	1322.29	1358.94	C
Peak temperatures					
Thermocouple 1	1287.23	1348.36	1322.29	1319.88	C
Thermocouple 2	1184.05	1263.22	1203.06	1345.37	C
Thermocouple 3	1185.22	1192.37	1184.87	1358.94	C
Thermocouple 4	1209.45	1035.16	1111.19	1347.23	C
Thermocouple 5	1421.40	1215.29	1286.69	1350.54	C
Max off gas temp 1	682.65	596.61	741.12	666.59	C
Max off gas temp 2	184.67	181.46	203.61	210.20	C
Sintered airflow	70.68	61.10	73.24	73.62	M3 hr
Time above 1000C					
Thermocouple 1	02:00	02:25	02:30	02:55	mn:s
Thermocouple 2	03:40	04:15	02:45	03:55	mn:s
Thermocouple 3	03:20	03:25	02:55	04:30	mn:s
Thermocouple 4	03:45	01:15	03:25	03:30	mn:s
Thermocouple 5	02:30	02:40	01:55	03:20	mn:s

Table 58: Process parameters for Alternative MgO source study

Parameters	Blend A	Blend A (r)	Blend B	Blend B (r)	Units
Flame front speed					
TC1-2	0.21	0.24	0.30	0.48	mm/s
TC2-3	0.38	0.23	0.31	0.37	mm/s
TC3-4	0.25	0.40	0.47	0.40	mm/s
TC4-5	1.27	1.17	0.52	0.58	mm/s
Flame front width					
TC1-2	6.18	10.68	10.65	36.21	mm
TC2-3	15.14	19.19	12.44	18.42	mm
TC3-4	9.82	24.00	16.33	18.00	mm
TC4-5	140.00	N/A	5.19	37.92	mm
Cooling rate (1100C-600C)					
TC1	4.55	4.00	4.17	3.85	C/S
TC2	2.08	2.04	1.85	2.33	C/S
TC3	1.89	2.94	2.00	2.70	C/S
TC4	5.88	2.56	1.89	3.03	C/S
TC5	5.26	3.33	6.25	3.85	C/S
Cooling rate (max – 600C)					
TC1	3.93	3.74	3.52	3.51	C/S
TC2	1.91	1.87	1.72	2.13	C/S
TC3	1.63	2.28	1.80	2.08	C/S
TC4	3.69	2.23	1.79	2.72	C/S
TC5	4.56	2.62	4.29	3.19	C/S

Table 59: Process parameters for Alternative Si source study

Parameters	Blend A	Blend B	Units
Pressure drop	100	100	mbar
Ignition time	01:00:00	01:00:00	m s
Cold permeability flow rate	10.47	11.14	m3hr
Hot Permeability flow rate	7.61	8.63	m3hr
Sintering time	00:20:45	00:18:45	hr:mn:s
Max sintering temp:	1339.78	1368.71	C
Peak temperatures			
Thermocouple 1	1030.08	1037.25	C
Thermocouple 2	1269.51	1299.08	C
Thermocouple 3	1337.87	1327.59	C
Thermocouple 4	1339.78	1368.71	C
Thermocouple 5	1303.01	1361.47	C
Max off gas temp 1	519.99	468.93	C
Max off gas temp 2	123.46	125.82	C
sintered airflow	37.59	44.64	cm/s

Table 60: Process parameters for Alternative Si source study

Parameters	Blend A	Blend B	Units
Flame front speed			
TC1-2	0.23	0.31	mm/s
TC2-3	0.33	0.28	mm/s
TC3-4	0.37	0.41	mm/s
TC4-5	0.42	0.50	mm/s
Flame front width			
TC1-2	3.44	1.56	mm
TC2-3	19.53	8.40	mm
TC3-4	16.58	18.53	mm
TC4-5	19.09	20.00	mm
Cooling rate (Max -1100)			
TC1	n/a	n/a	C s
TC2	10.30	10.76	C s
TC3	7.38	10.39	C s
TC4	7.40	9.61	C s
TC5	9.37	10.15	C s
Cooling rate (1100-600)			
TC1	5.56	7.14	C s
TC2	4.35	5.56	C s
TC3	4.35	4.76	C s
TC4	4.76	5.00	C s
TC5	5.88	5.56	C s